

Identification of *cis*-regulatory modules in mouse embryonic limb buds and heart using endogenous epitope-tagged transcription factors

Inauguraldissertation

zur

Erlangung der Würde eines Doktors der Philosophie
vorgelegt der
Philosophisch-Naturwissenschaftlichen Fakultät
der Universität Basel

von

Frédéric Laurent

aus Fey, VD

Basel, 2014

Genehmigt von der Philosophisch-Naturwissenschaftlichen Fakultät
auf Antrag von
Prof. Dr. Rolf Zeller (Dissertationsleiter und Fakultätsverantwortlicher),
Prof. Dr. Verdon Taylor (Korreferent)

Basel, den 16. September 2014

Prof. Dr. Jörg Schibler
Dekan

1. Table of contents

1. Table of contents	3
2. Summary	7
3. List of Abbreviations	9
4. Introduction	11
4.1. <i>Cis</i> -regulatory modules and transcriptional control of embryonic development	11
4.2. Morphogenesis of the Heart	16
4.2.1. Composition and function of the adult mammalian heart	16
4.2.2. Overview of the main steps of cardiac development in the mouse	19
4.2.3. From cardiogenic mesoderm to the myocardium and endocardium: determination of the cardiac lineages	21
4.2.4. Patterning and differentiation of the second heart field	23
4.2.5. The T-box genes family and the development of the atrioventricular canal and atrioventricular node	26
4.2.6. Formation of the cardiac valves: from endothelial-mesenchymal transition to the cardiac cushions	29
4.2.7. <i>Hand2</i> is a crucial regulator for the development of second heart field derived structures	32
4.3. The BMP signaling pathway during limb bud development and the <i>Grem1 cis</i> -regulatory landscape	38
5. Aims of the Thesis	41
6. Results	43
6.1. From <i>cis</i> -regulatory modules to <i>trans</i> -acting factors: control of <i>Grem1</i> genomic landscape during limb bud development and generation of <i>Smad4</i> ^{3xFLAG} mice by homologous recombination	43
6.1.1. Paper 1: “ <i>Smad4</i> is required to induce digit ray primordia and to initiate the aggregation and differentiation of chondrogenic progenitors in mouse limb buds”	43
6.1.2. Paper 2: “Conserved <i>cis</i> -regulatory regions in a large genomic landscape control SHH and BMP-regulated <i>Gremlin1</i> expression in mouse limb buds”	55
6.1.3. The <i>Grem1 cis</i> -regulatory landscape integrates several signaling inputs from multiple CRMs	77
6.1.4. Identification of SMAD4 target CRMs during limb bud development: the need for a new tool	79
6.1.5. Generation of <i>Smad4</i> ^{3xFLAG} mice by homologous recombination	80
6.2. From <i>trans</i> -acting factor to <i>cis</i> -regulatory modules: identification of the direct transcriptional targets of HAND2 during heart morphogenesis	85

6.2.1. The <i>Hand2</i> ^{3xFLAG} allele is a new genetic tool to study HAND2 distribution during heart development.....	85
6.2.2. ChIP-Seq analysis using pooled <i>Hand2</i> expressing tissues identifies the genome-wide HAND2 target regions in association with tissue-specific gene functions.....	87
6.2.3. HAND2 controls the expression of genes involved in early second heart field morphogenesis.....	91
6.2.4. HAND2 controls the expression of genes associated with known cardiac-specific enhancers.....	93
6.2.5. <i>Hand2</i> -deficient mouse embryos lack the delaminated endocardial cells in the atrioventricular canal	96
6.2.6. HAND2 directly regulates <i>Has2</i> -mediated extracellular matrix deposition in the cardiac jelly.....	97
6.2.7. <i>Twist1</i> but not <i>Sox9</i> is a direct transcriptional target of HAND2 during cardiac cushion formation	99
6.2.8. <i>Snai1</i> -dependent initiation of endothelial-mesenchymal transition in the atrioventricular canal is regulated by HAND2.....	102
6.2.9. The <i>Hand2</i> loss-of-function affects the EndMT upstream signaling but not the patterning of the myocardium.....	104
6.2.10. <i>Tbx2</i> and <i>Tbx3</i> are direct targets of HAND2 during cardiac development	106
7. Discussion	113
7.1. Identification of HAND2 target gene networks that function during heart morphogenesis.....	113
7.1.1. Genome-wide identification of cardiac CRMs.....	113
7.1.2. HAND2 and its target CRMs in the heart: direct and indirect DNA-binding interactions	114
7.1.3. HAND2 target genes in the progenitors of the second heart field	115
7.1.4. <i>Furin</i> and <i>Myocd</i> are direct transcriptional targets of HAND2	116
7.1.5. A causal link between atrioventricular canal defects and embryonic lethality in <i>Hand2</i> -deficient embryos?	117
7.2. Gene networks controlling endothelial-mesenchymal transition in the atrioventricular canal are directly regulated by HAND2.....	119
7.2.1. <i>Hand2</i> participates in extracellular matrix deposition within the cardiac jelly	119
7.2.2. HAND2 directly regulates <i>Twist1</i> and <i>Snai1</i> expression during formation of the AVC cardiac cushions	120
7.2.3. HAND2 is an intermediate factor in the myocardial/endocardial signaling events that induce the EndMT	124
7.2.4. A role for <i>Hand2</i> in cardiac valves maturation and remodeling?.....	126
7.3. The paralogous <i>Tbx2</i> and <i>Tbx3</i> genomic landscapes encode heart and limb bud specific CRMs bound by HAND2 chromatin complexes	126
8. Conclusions and Outlook.....	129

9. Materials and Methods	131
9.1. Genetic engineering of plasmids	131
9.1.1. General cloning procedures	131
9.1.2. Construction of pBSK <i>Smad4</i> ^{3xFLAG} targeting vector for Homologous Recombination	132
9.2. Cell culture	133
9.2.1. Embryonic Fibroblasts (EMFs) culture	133
9.2.2. Embryonic Stem (ES) cell culture	134
9.2.3. ES cells electroporation and selection	135
9.2.4. ES cell clones screening by Southern Blot	136
9.3. Mice husbandry and experiments with embryos	138
9.3.1. Ethic statement	138
9.3.2. Mouse strains	138
9.3.3. Generation of <i>LacZ</i> reporter transgenic embryos	138
9.3.4. Whole-mount <i>LacZ</i> staining of mouse embryos	139
9.3.5. Whole-mount <i>in situ</i> hybridization (WISH)	139
9.3.6. Preparation of digoxigenin-labelled RNA riboprobe	140
9.4. Molecular Biology	141
9.4.1. Immunocytochemistry	141
9.4.2. Protein detection by Western Blot (WB)	141
9.4.3. Immunoprecipitation (IP)	143
9.4.4. Chromatin Immunoprecipitation (ChIP)	144
9.4.5. Extraction of RNA and cDNA synthesis	147
9.4.6. Real-time quantitative PCR (RT-qPCR)	148
9.5. Histology	149
9.5.1. Paraffin embedding procedure	149
9.5.2. Preparation of frozen sections	150
9.5.3. Immunohistochemistry	150
9.5.4. TUNEL assay	151
9.5.5. Hematoxylin/Eosin staining	152
9.5.6. Alcian Blue staining	152
9.5.7. <i>In situ</i> hybridization on sections	152
9.6. Genomics online resources	154
9.7. Tables	154
9.7.1. Antibodies tables	154
9.7.2. Primers tables	155

10. Acknowledgments	159
11. Bibliography	161
12. Appendixes.....	187
12.1. Generation of <i>Smad4</i> ^{3xFLAG} mice using dRMCE.....	187
12.1.1. Testing three epitope-tagged versions of SMAD4 in ES cells	187
12.1.2. Embryonic lethality of <i>Smad4</i> ^{3xFLAG} homozygous embryos	191
12.2. Additional methods relative to the dRMCE targeting.....	194
12.2.1. Construction of the pcDNA3 <i>Smad4</i> ^{3xTag} expression vectors	194
12.2.2. Construction of the pDREV <i>S4</i> ^{3xTag} targeting vectors for dRMCE	195
12.2.3. Transfection of HEK-293T cells.....	196
12.2.4. dRMCE: ES cells electroporation, selection and screening	197
12.2.5. Differentiation of ES cells to embryoid bodies	197
12.2.6. dRMCE primers table	198
12.3. Manuscripts in preparation.....	199
12.4. Curriculum vitae	201

2. Summary

The genes that control mouse embryonic development are tightly regulated spatially and temporally by the integration of various signaling pathways. The interaction of downstream transcription factors with *cis*-regulatory modules located in the genomic landscapes of their target genes is crucial to control gene expression and enable the growth and patterning of embryonic tissues. However, in most of the cases, the genome wide range of target regions bound by a given *trans*-acting factor in a tissue-specific manner is not known. In this thesis, I have taken advantage of epitope-tagging essential transcriptional regulators such as SMAD4 and HAND2 to gain mechanistic insight into their functions during limb and heart development.

In particular, the morphogenesis of the limb bud depends on a self-regulatory system of signaling feedback loops in the core of which the BMP antagonist GREMLIN1 plays a critical role. We analyzed the *cis*-regulatory landscape of *Gremlin1* and identified a conserved region that recapitulates several aspects of the dynamic expression of *Gremlin1* during limb bud development and requires the BMP signal transducer SMAD4 to be expanded in the distal anterior part of the limb bud. To investigate the *Gremlin1* *cis*-regulatory modules that directly interact with SMAD4-containing chromatin complexes, I have generated a new mouse line that expresses a 3xFLAG epitope-tagged version of SMAD4 from its endogenous locus, with which we will perform ChIP-Seq analysis from developing embryonic tissues, including limb buds.

Following a similar rationale, I have used ChIP-Seq data from a mouse line expressing a *Hand2*^{3xFLAG} allele to provide the first identification of the HAND2 target gene networks that function during cardiogenesis, which is severely impaired in the absence of HAND2. This analysis indicates that HAND2 directly controls the expression of the paralogous genes *Tbx2* and *Tbx3* in the progenitors of the second heart field that give rise to the outflow tract and right ventricle. This regulation is mediated by the interaction of HAND2 with tissue-specific *cis*-regulatory modules located in *Tbx2* and *Tbx3* genomic landscapes. Furthermore, we observed in *Hand2*-

deficient embryos that the cells of the atrioventricular canal do not undergo the endothelial-mesenchymal transition that normally initiates the formation of the cardiac cushions, which are the precursors of the cardiac valves. We established that the expression of *Snai1*, *Twist1* and *Has2*, which are key genes in this process, are directly controlled by HAND2-containing chromatin complexes. Epitope-tagging of transcription factors is thus a powerful tool to identify the range of *cis*-regulatory modules they bind to, which allows to uncover the transcriptional networks they control during embryonic development.

3. List of Abbreviations

AER	Apical Ectodermal Ridge	GREM1	Gremlin1
AVC	Atrioventricular Canal	GRS1	Gremlin Regulatory Sequence 1
AVN	Atrioventricular Node	HA	Hyaluronic Acid
BAC	Bacterial Artificial Chromosome	HA-tag	Hemagglutinin tag
bHLH	basic Helix-Loop-Helix	HAND2	Heart, Autonomic nervous system and Neural crest Derivatives 2
BMP	Bone Morphogenetic Protein	HAS2	Hyaluronan Synthase 2
BRE	BMP Responsive Element	HCN4	Hyperpolarization-activated Cyclic Nucleotide-gated potassium channel 4
BSA	Bovine Serum Albumin	HEK	Human Embryonic Kidney cell
CHD	Congenital Heart Disease	HEY	Hairy/Enhancer-of-split related with YRPW motif
ChIP	Chromatin Immunoprecipitation	HMCO	Human Mouse Chicken Opossum
CMV	Cytomegalovirus	HR	Homologous Recombination
cNCC	cardiac Neural Crest Cells	HRP	Horseradish Peroxidase
Cq	Quantification Cycle	ICC	Immunocytochemistry
CRM	<i>Cis</i> -Regulatory Module	ID1	Inhibitor of Differentiation 1
CS	Coding Sequence	IHC	Immunohistochemistry
CTCF	CCCTC-binding Factor	IKMC	International Knockout Mouse Consortium
Cx40	Connexin 40	IPP	Immunoprecipitation
DBH	Dopamine Beta-Hydroxylase	ISL1	Islet LIM homeobox 1
DEPC	Diethylpyrocarbonate	LA	Left Atrium
DIG	Digoxigenin	LIF	Leukemia Inhibitory Factor
DMSO	Dimethyl Sulfoxide	LV	Left Ventricle
DNase HS	DNase I Hypersensitive Site	MCP	Multipotent Cardiac Progenitors
dRMCE	dual Recombinase-Mediated Cassette Exchange	MEF2C	Myocyte Enhancer Factor 2C
E	Embryonic day	MESP1	Mesoderm Posterior 1 homolog
ECM	Extracellular Matrix	MET	Mesenchymal-Epithelial Transition
EMFI	Embryonic Mouse Fibroblast	MSX1	Msh homeobox 1
EMT	Epithelial-Mesenchymal Transition	MYOCD	Myocardin
EndMT	Endothelial-Mesenchymal Transition	NDR	Nuclear Dbf2-Related kinases
ES cell	Embryonic Stem cell	Neo	Neomycin
EUCOMM	European Conditional Mouse Mutagenesis program	NFATC1	Nuclear Factor of Activated T-cells, Cytoplasmic 1
FBS	Fetal Bovine Serum	NPPA	Natriuretic Peptide A
FCS	Fetal Calf Serum	O.C.T	Optimum Cutting Temperature
FGF	Fibroblast Growth Factor	OFT	Outflow Tract
FLK1	Fetal Liver Kinase 1	PBS	Phosphate Buffered Saline
FMN1	Formin1	PBT	PBS with 0.1% Tween 20
GBR	GLI binding region	PEO	Proepicardial Organ
GFP	Green Fluorescent Protein	PFA	Paraformaldehyde
GO	Gene Ontology	PHF	Primary Heart Field
GRE1	GLI Responsive Element 1	polyA	Polyadenylation
GREAT	Genomic Regions Enrichment Annotation Tool	PRX1	Paired Related homeobox 1
		Puro	Puromycin

RA	Right Atrium
RPL19	Ribosomal Protein L19
rpm	Revolutions per minute
RT	Room Temperature
RV	Right Ventricle
SAN	Sinoatrial Node
SB	Southern Blot
SDS	Sodium Dodecyl Sulfate
SHF	Second Heart Field
SHH	Sonic Hedgehog
SNAI1	Snail family zinc finger 1
SOX9	SRY (sex determining region Y)-box 9
SV40	Simian Virus 40
TF	Transcription Factor
TGFβ2	Transforming Growth Factor Beta 2
TSS	Transcriptional Start Site
TUNEL	Terminal deoxynucleotidyl transferase dUTP nick end labeling
UCSC	University of California Santa Cruz
UTR	Untranslated Region
V5-tag	Simian Virus 5 tag
VE-Cad	Vascular Endothelial Cadherin
VEC	Valve Endothelial Cell
VEGF	Vascular Endothelial Growth Factor
VIC	Valve Interstitial Cell
VIM	Vimentin
WB	Western Blot
WISH	Whole-mount <i>in situ</i> Hybridization
WNT	Wingless-type MMTV integration site
WT	Wild-Type
βglob	β-globin

4. Introduction

4.1. *Cis*-regulatory modules and transcriptional control of embryonic development

The question of how complex, multicellular-types tissues and organs arise from undifferentiated progenitor cells during embryonic development is fascinating. Cell fates are controlled by robust spatio-temporal and tissue-specific gene expressions, which progressively shape the body plan of the developing embryo. Growth and patterning are regulated by combinatorial interactions between transcription factors and multiple genetic *cis*-regulatory modules, whose integrated action determines the quantitative transcriptional output of a given protein-coding gene.

Cis-regulatory modules (CRMs) are composed of clusters of binding sites for multiple transcription factors (TFs) and can act as enhancers, silencers or insulators (Fig.1A). An enhancer is able to activate transcription independently of its location or orientation relative to a promoter, often in a tissue-specific manner (Bulger and Groudine, 2011; Ong and Corces, 2011; Levine, 2010) while a silencer will have the opposite effect and repress the expression of a target gene (Petrykowska et al., 2008). Insulators are CRMs that can either block the action of others CRMs on a promoter when located between them, or create barriers to prevent the spreading of heterochromatin compaction (Gaszner and Felsenfeld, 2006). Insulators are typically interacting with the ubiquitously expressed CTCF zinc-finger protein (Bell et al., 1999; Ong and Corces, 2014). Functional redundancy between CRMs acting on the same gene can occur, which confers phenotypic robustness (“shadow enhancers”, (Barolo, 2012; Frankel et al., 2010). CRMs can be intergenic, embedded in introns of unrelated neighboring genes, or located in gene deserts (Zeller and Zuniga, 2007; Nobrega et al., 2003). In addition to CRMs proximal to the promoter of their target gene, CRMs usually operate over distances shorter than 50kb but can occasionally act over considerably longer distances (up to 2-3Mb, (Krivega and Dean, 2012)). They are often scattered in large genomic landscapes, or archipelagos, and cooperate to synergistically act on their target genes (Montavon et al., 2011; Marinic et al., 2013).

The physical contact between distant-acting CRMs and the basal transcriptional machinery at the promoter depends on the three-dimensional architecture of the genome and higher-order chromatin interactions, with regions of open euchromatin forming loops that bring together multiple genomic elements (Fig.1B). The formation of these loops can be initiated *de novo* following an instructive process or be preformed in a ground state, and depends on CRMs-TFs interactions (de Laat and Duboule, 2013).

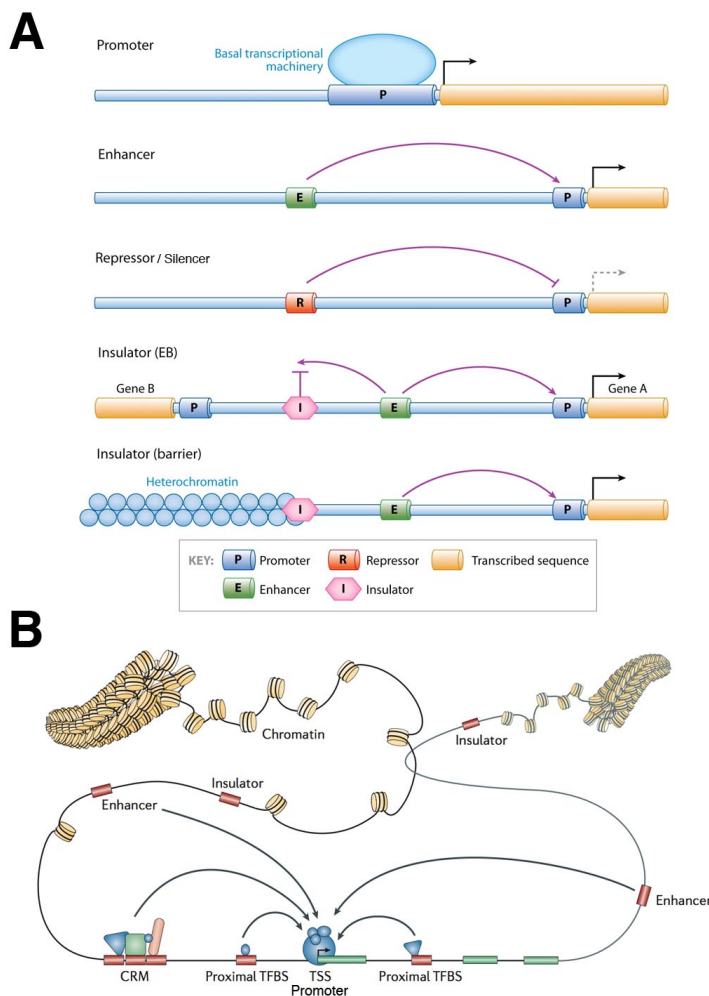


Figure 1. *Cis*-regulatory modules and genomic architecture

(A) Categories of *cis*-regulatory modules. From top to bottom: basal transcriptional machinery (RNA polymerase II and general transcription factors) bound to the promoter of a gene. Enhancer and silencer sequences mediate positive and negative effects on the transcription of a target gene. Insulator blocks the activity of an enhancer of gene A on gene B. Barrier insulator prevents the spread of chromatin condensation. Adapted from (Noonan and McCallion, 2010).

(B) Schematic representation of the *cis*-regulatory landscape of a gene. The chromatin is composed of DNA wrapped around histones to form nucleosomes and can be in different compaction states. Open chromatin loops to bring CRMs in physical contact with the promoter and basal transcriptional machinery. Adapted from (Lenhard et al., 2012).

The accessibility of CRMs to TFs during developmental progression depends on the state of chromatin compaction. Active CRMs are located in regions of open chromatin and are therefore sensitive to digestion by DNA nucleases (Crawford et al., 2006). They are also bound by the ubiquitously expressed p300 histone acetyltransferase (Visel et al., 2009a). Indeed, the chromatin signature of active CRMs can also be determined by the presence of specific post-translational modifications on the

histones tails in the nucleosomes flanking these CRMs (Calo and Wysocka, 2013; Spitz and Furlong, 2012). The acetylation of the lysine 27 of Histone 3 (H3K27ac), a high H3K4me1/H3K4me3 ratio and the absence of the repressive H3K27me3 are all typically associated with active CRMs, high levels of H3K4me3 being observed at actively transcribed promoters (Fig.2A) (Heintzman et al., 2007; Bonn et al., 2012; Creyghton et al., 2010; Rada-Iglesias et al., 2011; Djebali et al., 2012).

The best technique to assess the interactions between a TF of interest and its target CRMs is chromatin immunoprecipitation (ChIP, Fig.2B). ChIP relies on the chemical crosslinking of proteins and DNA interactions within a tissue or a living cell population (typically $\sim 10^7$ cells), followed by shearing the chromatin into small fragments (200-300bp) by sonication. An antibody recognizing the TF of interest is then used to selectively immunoprecipitate the chromatin complexes in which this TF is contained. The associated DNA fragments are finally purified and can be used for deep sequencing to identify genome-wide target CRMs (ChIP-Seq, (Park, 2009), or for qPCR to confirm a specific TF-CRM interaction (ChIP-qPCR).

Based on these observations, several methods exist to identify CRMs within the genome that can be applied to specific tissues or developmental stages (Hardison and Taylor, 2012). DNase hypersensitivity profiling and ChIP-Seq using an antibody recognizing p300, H3K27ac or H3K4me1 can all identify candidate CRMs genome-wide (Cotney et al., 2012; May et al., 2012; Blow et al., 2010; Visel et al., 2009a; Shu et al., 2011). Chromosome conformation capture (3C) and derivatives (4C, Hi-C...) can identify all potential chromatin-chromatin interactions and thus all the CRMs that contact a specific promoter (Dekker et al., 2013). In addition to these experimental approaches, *in silico* comparative genomics can identify conserved non-coding elements between different species, even if sequence conservation does not always implies that the CRM function is conserved (Nelson and Wardle, 2013). Finally, computational approaches to identify the occurrence of TF binding motifs can also identify candidate CRMs (Narlikar et al., 2010).

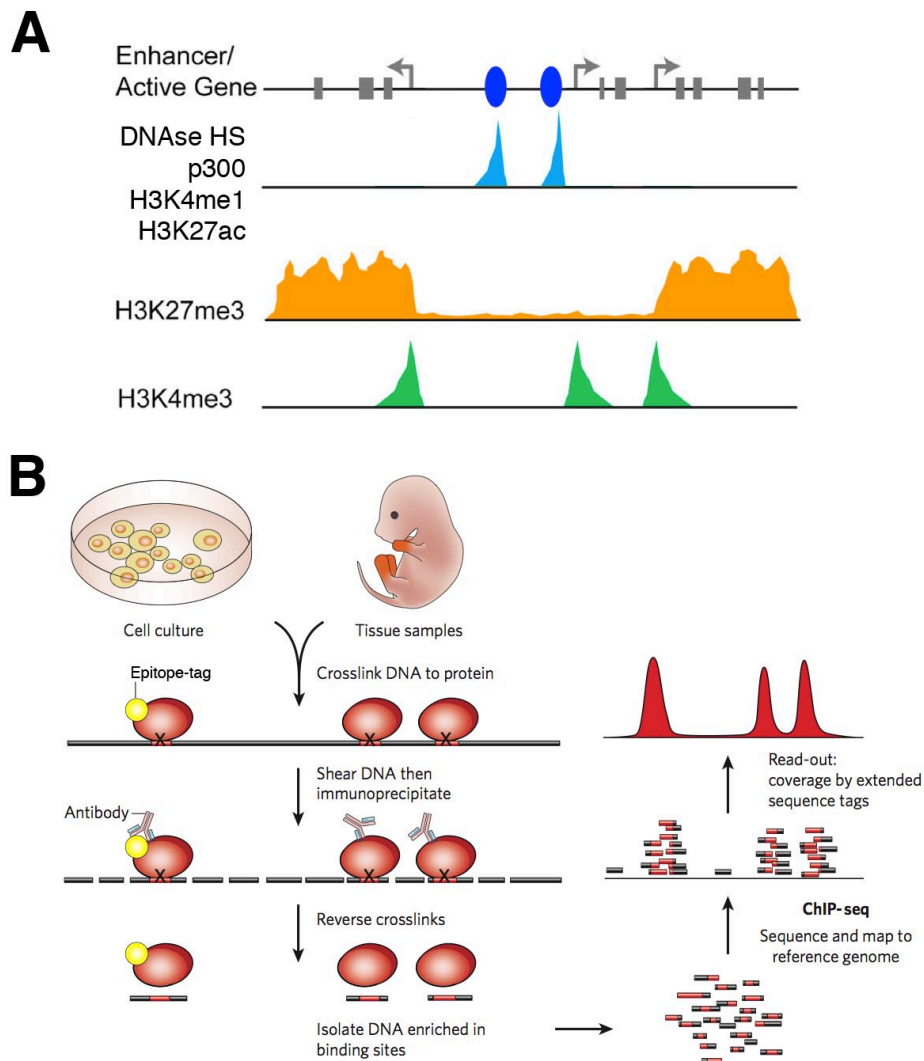


Figure 2. Chromatin marks and ChIP-Seq procedure

(A) Representation of genome-wide chromatin signatures for a hypothetical *cis*-regulatory genomic landscape. From top to bottom: transcriptional start sites and exons of active genes (grey arrows and boxes) and associated CRMs (blue ovals). Blue: active CRMs are hypersensitive to DNase and are marked by p300 binding, H3K4me1 and H3K27ac. Orange: repressive H3K27me3 mark. Green: promoter-enriched H3K4me3 mark. Adapted from (Phillips-Cremins and Corces, 2013). (B) Main steps of ChIP-Seq procedure. DNA and interacting proteins from cultured cells or embryonic tissues are crosslinked and sheared in small chromatin fragments. Immunoprecipitation of the protein of interest (red) is achieved using either an antibody recognizing it directly (right) or recognizing an epitope tag (left, yellow circle). Following reverse crosslinking, the purified DNA fragments are sequenced and mapped to a reference genome. Adapted from (Visel et al., 2009b).

Transcription factors usually recognize small degenerate sequence-specific binding motifs of 6-12bp (Loots and Ovcharenko, 2004). The binding motifs of several different TFs can be observed within a CRM, leading to possible combinatorial binding of various TFs at different developmental time points and in different tissues at the same CRM. Furthermore, the binding of a specific TF can be a prerequisite for

the recruitment of additional TFs, cofactors and/or chromatin remodeling complexes that will modulate their function. Together, the cooperative and/or additive interactions between these TFs, or between TFs interacting with different CRMs, will determine the transcriptional output of their target genes (Wilczynski and Furlong, 2010; Yanez-Cuna et al., 2012; Spitz and Furlong, 2012; Farnham, 2009; MacQuarrie et al., 2011). Electrophoretic Mobility Shift Assay (EMSA) is traditionally used to assess the interaction between a TF and a CRM, but ChIP-qPCR is becoming more frequently used. To study the function and spatiotemporal expression pattern driven by a candidate CRM, the standard method is a reporter assays in which the candidate CRM is used to drive the expression of a reporter gene (*LacZ*, GFP, Luciferase...) in transgenic embryos or transfected cells. Finally, combining reporter assays with the mutation of TFs binding sites within a given CRM allows analyzing the requirement of specific TFs regarding the functionality and enhancing capacity of the considered CRM.

Genome-wide identification of CRMs interacting with a specific TF using ChIP-Seq analysis requires high quality antibodies. Tagging TFs with established epitope-tags represents an alternative to commercial antibodies that often lack specificity for their target protein (Fig.2B). For this, conventional genome editing techniques by homologous recombination or cassette exchange in mouse ES cells allow the introduction of an epitope tag in the endogenous locus coding for a specific TF. Targeting the endogenous locus maintains its transcriptional regulation by native promoter and CRMs. It allows studying the spatio-temporal distribution of the TF and the identification of its target genes in a physiological context, without off-target effects coming from overexpression (Zhang et al., 2008a; Conway et al., 2010).

While most of the identified mutations associated with congenital developmental malformations are mapped to coding sequences, only a few have been located in CRMs (Gordon and Lyonnet, 2014; Smemo et al., 2012; Uslu et al., 2014; Lettice et al., 2003). The identification and mapping of CRMs is thus crucial for potential diagnosis of congenital malformations, and to understand how complex gene patterns are regulated during embryonic development.

4.2. Morphogenesis of the Heart

4.2.1. Composition and function of the adult mammalian heart

The heart is the first organ to form during embryonic development. Unlike other embryonic structures and organs, the heart and associated structures of the cardiovascular system are essential for the survival of the embryo. Perturbations in the complex gene regulatory networks controlling the formation of the cardiac structures can lead to various types of congenital heart diseases (CHD), which can be observed in 6 to 75 per 1000 live births and are one of the major cause of mortality in infants and adults (Bruneau, 2008; Khoshnood et al., 2012; Ishikawa et al., 2011; Wren et al., 2012; Brickner et al., 2000). The adult mammalian heart is a muscular organ composed of four distinct chambers, two atria and two ventricles, separated by cardiac valves. Its rhythmic and coordinated contractions driven by the conduction system pump blood to the organs of the body via the blood vessels, a function crucial to maintain the homeostasis of the organism (Fig.3A). The anatomy of the heart has significantly changed over the course of evolution. From a simple linear tube subjected to peristaltic contractions in primitive chordates, through a single atrium and single ventricle in fishes, the vertebrate heart evolved to a more powerful and complex pump by successive additions of new cardiac structures that likely occurred through the acquisition of new regulatory inputs and by gene duplications (Olson, 2006; Jensen et al., 2013). The cardiac chambers are mainly composed of three concentric tissue layers with different developmental origins: the endocardium is the endothelial lining of the heart and is in contact with the blood. The myocardium consists mainly of a muscular layer of contractile cardiomyocytes and conductive cells. Finally, the epicardium is a specialized epithelium mostly composed of connective tissues that envelop and protect the heart (Fig.3A). During embryogenesis, the endocardium is separated from the myocardium by a layer of extracellular matrix, the cardiac jelly. The cells of the myocardium are derived from two different lineages: the primary heart field and the second heart field (Buckingham et al., 2005).

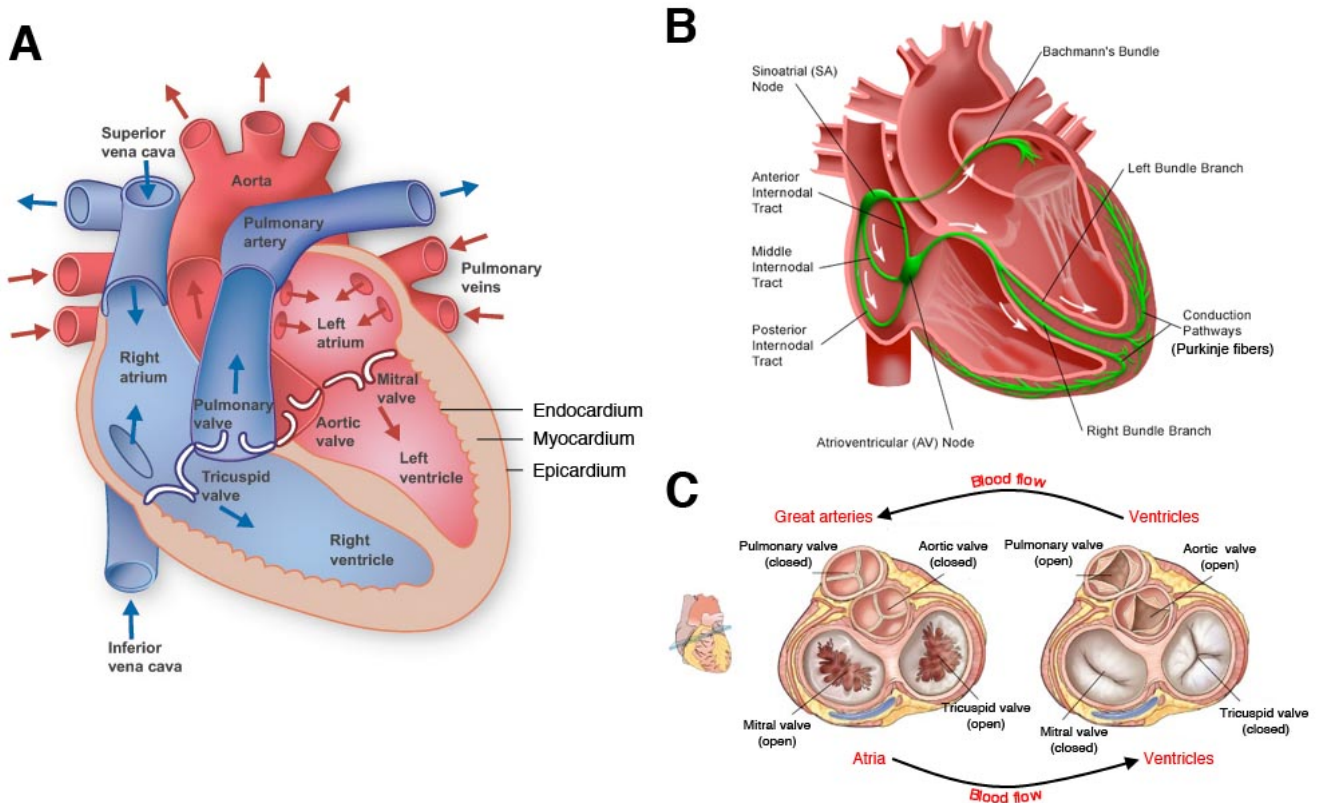


Figure 3. Anatomy of the adult mammalian heart

(A) Blood circulation inside the heart (direction indicated by arrows). Deoxygenated blood (blue) returning from the body through the superior and inferior vena cava enters the right atrium, where cardiac contractions pumps it out through the tricuspid valve into the right ventricle. Delayed contractions pumps the blood into the pulmonary arteries through the pulmonary valve. Left and right pulmonary arteries are connected to the lungs, where the blood gets oxygenated (red) before returning to the heart via the pulmonary veins. The blood enters the left atrium, is pumped through the mitral valve into the left ventricle, and pumped out in the aorta through the aortic valve to be distributed to the remainder of the organism. Image modified from the Texas Heart Institute website. (B) Cardiac conduction system. The electrical impulse is generated in the sinoatrial node and contracts the atria. It is transmitted to the atrioventricular node, which propagates it with a delay to the bundle of His (right and left branches) along the interventricular septum. From the heart apex, the impulse is transmitted to the fast conducting Purkinje fibers, which contracts the ventricles. From Main Line Health website (<http://www.mainlinehealth.org/oth/Page.asp?pageID= OTH005458>). (C) Above view of a transverse heart section showing the opening and closure of the cardiac valves following cardiac contractions. The mitral (bicuspid) and tricuspid valves are composed of two and three leaflets, respectively. The pulmonary and aortic (semilunar) valves are composed of three leaflets called cusps. Adapted from (http://www.tokresource.org/tok_classes/biobiobio/biomenu/transport_system/index.htm).

The cardiac contractions depend on an electrical impulse generated in the pacemaker cells of the sinoatrial node. This impulse is transmitted through the myocardium of the atria, leading to their simultaneous contraction, to the atrioventricular node and further to the ventricles to contract them (Fig.3B). A delay in the propagation of the impulse from the atrioventricular node allows non-simultaneous contractions between the two atria and the two ventricles, necessary

for unidirectional blood flow. The heart functions therefore as two serially working atrial and ventricular pumps (Christoffels and Moorman, 2009). In the mouse, this whole cardiac cycle takes less than 200ms for an average of 500 beats per minute (bpm) (Berul et al., 1996; Ho et al., 2011), which is much faster than the average human cardiac rhythm of 70bpm and reflects the effects of the size of an organism on the speed of its metabolism (Kleiber, 1947). Congenital malformations and aging can cause dysfunctions of the pacemaker tissues, resulting in arrhythmias. If the primary pacemaker in the sinoatrial node is impaired or if the electrical impulse is not propagated, the atrioventricular node can act as an accessory pacemaker and initiate an electrical impulse (Christoffels et al., 2010).

The cardiac valves are essential to avoid blood regurgitation between the chambers, and open and close over 700'000 times per day in the mouse. The adult heart contains two atrioventricular valves separating atria and ventricles (tricuspid and mitral (or bicuspid) valves), and two semilunar valves located between the ventricles and the great arteries (pulmonary and aortic valves) (Fig.3A). After the blood is pumped from the atria to the ventricles, the atrioventricular valves close and the semilunar valves open (Fig.3C). The inverse takes place following blood expulsion into the great arteries. Each valve consists of 2-3 leaflets, composed of an outer layer of valve endothelial cells (VEC) enveloping three stratified layers of extracellular matrix (collagen, proteoglycan and elastin) interspersed with valve interstitial cells (VIC). The composition of these extracellular matrix layers is essential for the biomechanical properties of the leaflets to open and close, and the VIC and VEC plays additional roles in their homeostasis (Hinton et al., 2006; Tao et al., 2012). Indeed, in valves diseases the leaflets lose this stratification, leading to improper valve closure, backward blood flow and cardiac insufficiencies (Hinton et al., 2006). Congenital valve diseases are observed in 5% of live human births, accounting for 25-30% of all cardiovascular malformations and are a major cause of mortality in adults (Armstrong and Bischoff, 2004; Combs and Yutzey, 2009). The most common valve diseases (2-4% of the human population) include bicuspid aortic valve (only two leaflets), mitral valve prolapse (increased deposition of extracellular matrix) and valve calcification (osteogenic process leading to extracellular matrix mineralization) (Rajamannan et al., 2003; Tao et al., 2012).

4.2.2. Overview of the main steps of cardiac development in the mouse

The heart of the mouse embryo can first be observed in a crescent-shape structure at embryonic day 7.5 (E7.5) (Fig.4A). The cardiac crescent is composed of myocardial progenitors from both the primary heart field and the second heart field lineages, which will contribute to different structures in the adult heart. These progenitors fuse across the embryo midline, forming a linear tube that starts beating at around E8.0. This heart tube is mainly composed of cells from the primary heart field and serves as a scaffold for second heart field cells that migrate from adjacent splanchnic pharyngeal mesoderm to both the venous and arterial poles of the tube (Fig.4A). The venous pole, located caudally, is the entry point of the blood in the heart tube (inflow tract, prospective atrial chambers). The arterial pole, located cranially, is where the blood exits the heart tube (prospective outflow tract). The outflow tract is a transient structure that connects the right ventricle to the aortic sac, from which the aortic arches arteries arise in the branchial (pharyngeal) arches. At E8.5, the heart undergoes a rightward looping that breaks its bilateral symmetry and progressively moves the venous pole cranially. Myocardial cells rapidly proliferate and expand to shape the future cardiac chambers (Fig.4A). The primary heart field (PHF), marked by the expression of *Nkx2.5*, contributes mainly to the prospective left ventricle and to both atria, and partially to the prospective right ventricle. In contrast, the cells of the second heart field (SHF), marked by the expression of *Isl1*, contribute mainly to the prospective right ventricle, outflow tract and prospective atria.

From E9.0-E9.5, cardiac neural crest cells delaminate from the dorsal ectoderm of the neural tube and migrate through the branchial arches to the outflow tract (Fig.4B) (Jiang et al., 2000). The developing heart is in the meantime invaded by another population of extracardiac cells: from E8.5-E9.0, cells from the transient proepicardial organ located at the venous pole detach and migrate to form both the epicardium that envelop the heart and the coronary vasculature that will provide blood supply to the heart itself (Fig.4B) (Reese et al., 2002; Männer et al., 2001).

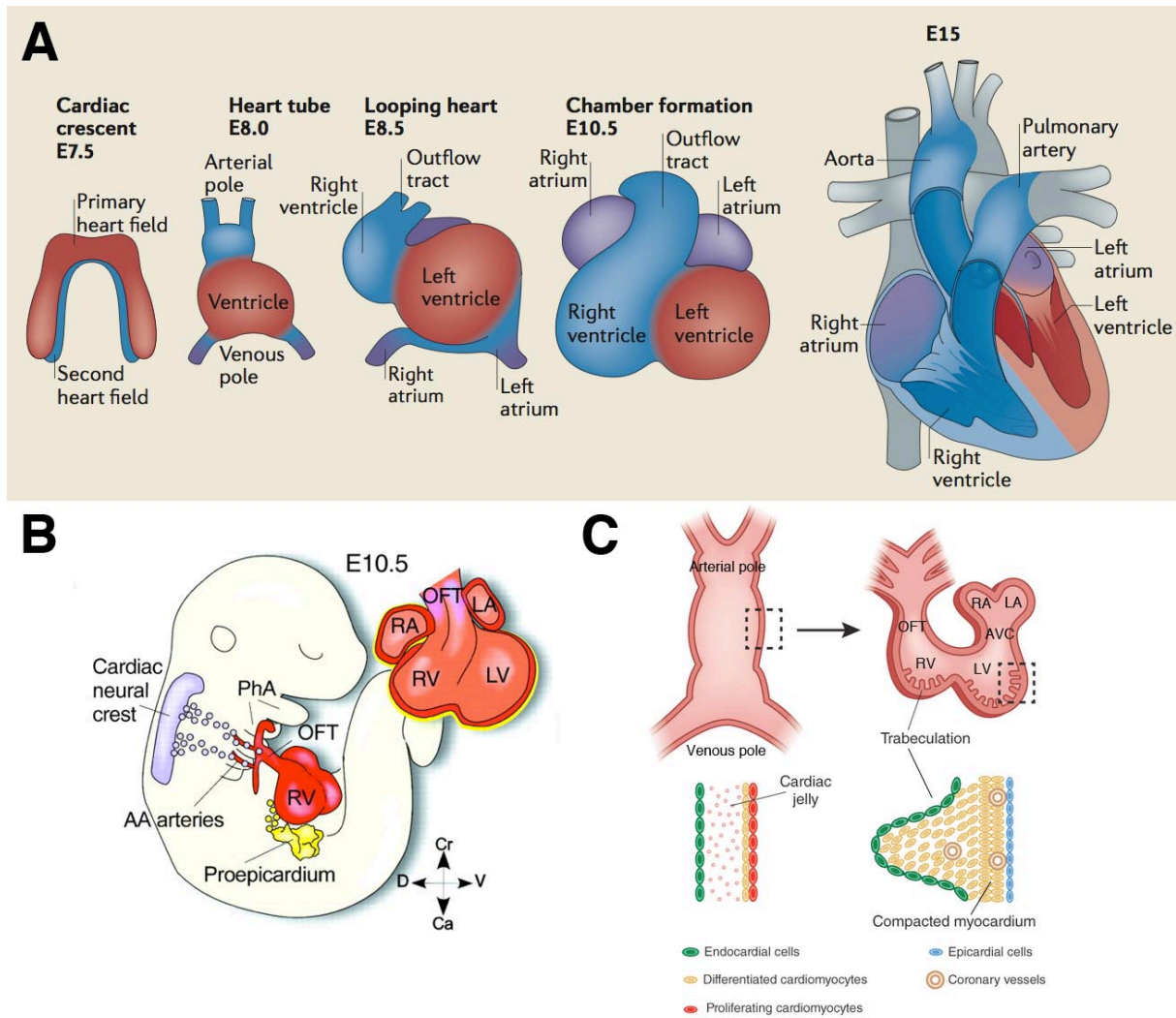


Figure 4. Main steps of mouse heart development

(A) Cardiac development in the mouse. See details in main text. From left to right: cardiac crescent stage (E7.5), heart tube stage (E8.0), looping heart (E8.5), formation of the chambers (E10.5) and functional four chambers heart (E15.0). Red indicates the primary heart field (PHF) and blue the second heart the field (SHF) and their derivative structures. Adapted from (Xin et al., 2013). (B) Contribution of extracardiac cell populations to the developing heart at ~E10.5. In purple, cardiac neural crest cells (cNCC) migrate from the neural tube through the pharyngeal arches (PhA) and invade the outflow tract. In yellow, cells from the proepicardial organ migrate to cover the heart and form the epicardium and coronary vasculature. Adapted from (Laugwitz et al., 2008). (C) Formation of the compact zone and trabeculations in the ventricular myocardium at ~E.10.5. OFT: outflow tract. RV: right ventricle. LV: left ventricle. AVC: atrioventricular canal. RA: right atrium. LA: left atrium. Cell types in the bottom panel are indicated. Adapted from (Misra and Garg, 2013).

Between E10.5 and E12, the proliferation of the cardiomyocytes in the myocardium of the ventricular chambers leads to the formation of a multilayered compact zone that increases the thickness of the ventricular wall to ensure powerful contractions. Some of these cells migrate towards the interior of the ventricles and form finger-like protrusions called trabeculations, which increases the surface of the myocardium to

ensure sufficient oxygenation before the establishment of a functional coronary circulation within the myocardium (Fig.4C) (Martin-Puig et al., 2008). The conduction system and the cardiac valves are formed during this period of chambers formation (see below) (Christoffels et al., 2010; Combs and Yutzey, 2009). The cardiac valves develop both in the outflow tract and in the atrioventricular canal, which connects the left ventricle to the common atria before they are separated (Fig.4C). Together with the formation of these valves, the formation of the interventricular, interatrial and atrioventricular septa divide the heart into four functional chambers (Lin et al., 2012). Along with chambers septation, the cardiac neural crest cells contribute to divide the outflow tract into the pulmonary trunk and the aorta that are finally connected to the right and left ventricles, respectively.

4.2.3. From cardiogenic mesoderm to the myocardium and endocardium: determination of the cardiac lineages

The different structures composing the mammalian embryonic heart are derived from progenitor cells of three developmentally distinct origins: the cardiogenic mesoderm, the cardiac neural crest cells (cNCC) and the proepicardial organ (PEO) (Laugwitz et al., 2008). These multipotent progenitors differentiate into several cardiac cell types through a complex lineage diversification involving multiple intermediate progenitor states (Martin-Puig et al., 2008; Vincent and Buckingham, 2010; Lescroart and Meilhac, 2012).

The cardiogenic mesoderm contains the progenitors that will contribute to the earliest cardiac structures derived from both the PHF and SHF (Fig.5). It is marked by the transient expression of *Mesp1*, and can first be detected in the anterior part of the primitive streak at the onset of gastrulation (E6.5) (Bondue and Blanpain, 2010). Following gastrulation, these progenitors migrate away from the primitive streak (PS) to anterior-lateral positions under the head folds, forming two groups of expanding lateral plate mesoderm cells on both side of the midline (Fig.5). At E7.0-7.5, these heart-forming regions extend across the embryo midline and fuse to form the cardiac crescent. Paracrine signals from adjacent tissues contribute to activate the expression of cardiac transcription factors in *Mesp1*⁺ cells of the cardiac crescent (Rana et al., 2013; Harvey, 2002; Zaffran and Frasch, 2002).

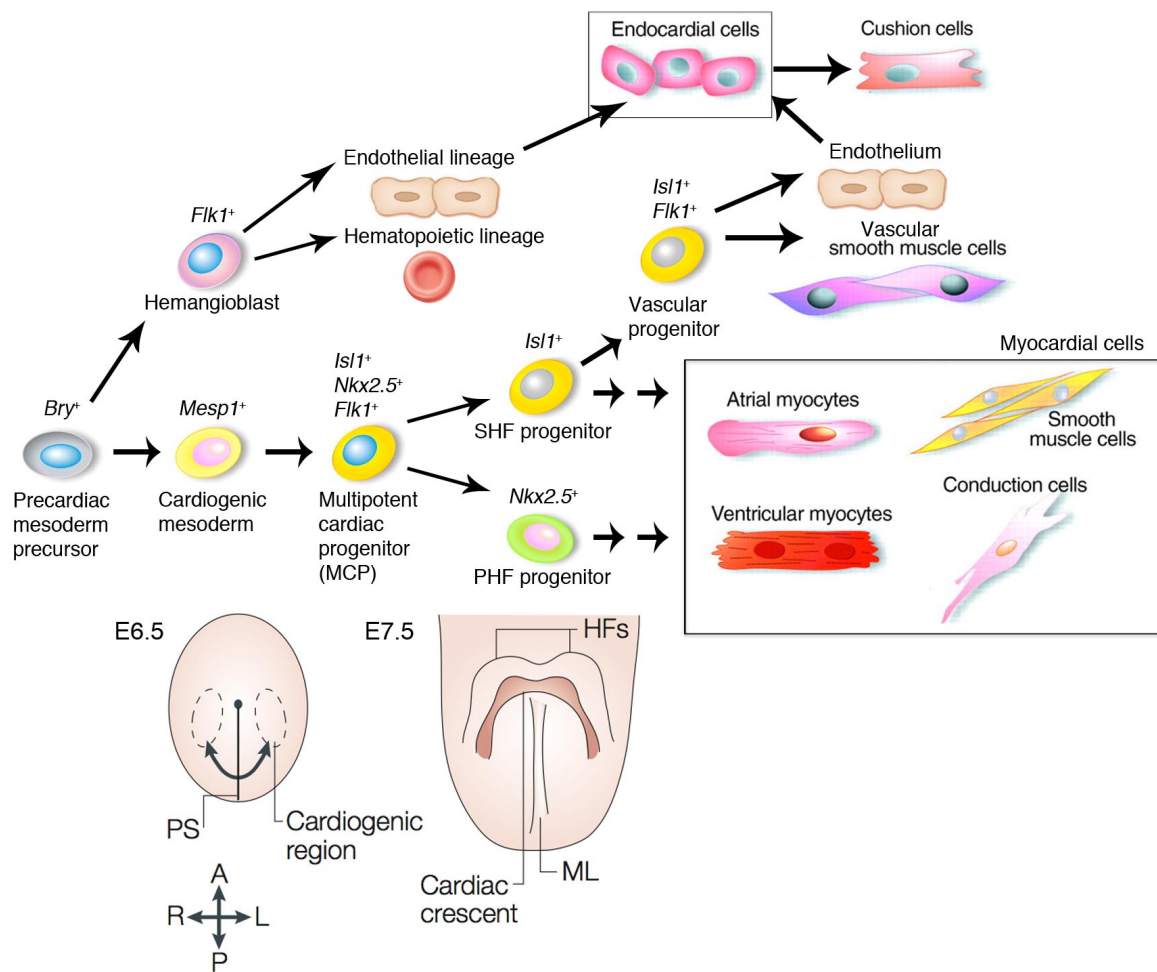


Figure 5. Lineage tree of the myocardial and endocardial progenitors

Representation of the main cellular hierarchies and lineages relationships of the cardiac cells with associated genetic marker(s). *Brachyury* (*Bry*⁺) precursors give rise both to the cardiogenic mesoderm expressing *Mesp1* and the hemangioblast cells that are the progenitors of the hematopoietic and endothelial cell lineages. The primary and second heart fields derive from *Isl1*⁺/*Nkx2.5*⁺/*Flk1*⁺ multipotent cardiac progenitors (MCP). Following successive transient progenitor states, they give rise to the cardiomyocytes of the atria and ventricles, the cells of the conduction system and smooth muscle cells. The endocardial cells derive from both *Isl1*⁺ SHF progenitors and vascular progenitors unrelated with the myocardium. The post-gastrulation stages at which the cardiogenic mesoderm and subsequent cardiac crescent can be observed are represented under the corresponding cells they contain. PS: primitive streak. HF: head folds. ML: midline (adapted from (Buckingham et al., 2005)). This scheme is not exhaustive and is adapted from (Laugwitz et al., 2008), with additional data based mainly on (Martin-Puig et al., 2008; Misfeldt et al., 2009; Milgrom-Hoffman et al., 2011).

The multipotent cardiac progenitor cells (MCP) that further express *Isl1*, *Nkx2.5* and *Flk1* are able to differentiate into all major cell types of the heart: cardiomyocytes, smooth muscle cells, endothelial cells and cells of the conduction system (Fig.5) (Moretti et al., 2006; Wu et al., 2006; Sun et al., 2007; Martin-Puig et al., 2008). The two myocardial lineages are determined at the cardiac crescent stage from these MCP cells. Due to their common origin and close proximity in the cardiac crescent,

the distinction between the progenitors of the two lineages is mainly due to the timing of their differentiation (Meilhac et al., 2004; Meilhac et al., 2003; Dyer and Kirby, 2009). The PHF cells, embedded in the lateral plate mesoderm, are the first ones to differentiate and will form the early heart tube and derived left ventricle (LV). The SHF cells, coming from splanchnic pharyngeal mesoderm in the dorsal wall of the pericardial cavity, differentiate later and are progressively added to the elongating heart tube from both poles to contribute to the outflow tract (OFT), right ventricle (RV) and atria (Cai et al., 2003; Zaffran et al., 2004; Meilhac et al., 2004) (Fig.4A). PHF cells are marked mainly by the expression of *Nkx2.5*, but also of *Tbx5* and *Hand1*. In contrast, *Isl1* expression marks the cells of the SHF, which also express *Gata4*, *Foxh1*, *Tbx1*, *Fgf8*, *Fgf10*, *Mef2c*, *Hand2* and *Nkx2.5* (Buckingham et al., 2005; Laugwitz et al., 2008).

The developmental origin of the endocardium has been controversial regarding the stage at which it segregates from the progenitors of the myocardial lineages (Harris and Black, 2010; Lescroart and Meilhac, 2012; Puceat, 2013). Two distinct sources of endocardial progenitors have been identified (Fig.5). The first population derives from the *Isl1*⁺ SHF and shares a common precursor with the myocardium (Ferdous et al., 2009; Misfeldt et al., 2009). The second population is composed of *Flk1*⁺ vascular endothelial cells unrelated with the myocardium. This endocardial population migrates from a medial position to the cardiac crescent and enters the heart from the arterial pole (Milgrom-Hoffman et al., 2011). The endocardial cells in the outflow tract and in the atrioventricular canal give rise to the cardiac cushions that are the precursors of the cardiac valves (see below) (Puceat, 2013; von Gise and Pu, 2012). Furthermore, ventricular endocardial cells invade the myocardium in the compact zone and form the endothelium of the coronary arteries between E11.5 and E13.5 (Wu et al., 2012).

4.2.4. Patterning and differentiation of the second heart field

The *Isl1*⁺ second heart field is located in the dorsal pericardial wall and is patterned along the embryo antero-posterior (cranio-caudal) axis, with cells coming from distinct but clonally related regions taking different migratory routes for different developmental outcomes (Kelly, 2012; Lescroart and Meilhac, 2012; Lescroart et al.,

2012). This patterning requires retinoic acid upstream of a graded expression of *Hox* genes, but the boundary between the anterior and the posterior SHF is not clearly defined (Ryckebusch et al., 2008; Bertrand et al., 2011; Kelly, 2012).

The cells in the anterior SHF are closely linked to the mesodermal core of the branchial arches (Tzahor and Evans, 2011). They are mainly characterized by the expression of *Fgf10*, *Fgf8* and *Tbx1*, and migrate through the arterial pole to contribute to the OFT and RV myocardium (Fig.6A) (Kelly et al., 2001; Mjaatvedt et al., 2001; Xu et al., 2004; Lescroart et al., 2010). The anterior SHF cells are clonally related to the skeletal head muscles, with lateral regionalization that links the progenitors of the aorta and pulmonary trunk to the progenitors of the right and left facial expression muscles, respectively (Lescroart et al., 2010). The anterior SHF should not be mixed up with the “secondary” heart field, which was identified in the chicken and originates from a subdomain of the anterior SHF that gives rise only to the OFT distal myocardium (Waldo et al., 2001; Dyer and Kirby, 2009). In contrast to the anterior SHF, the posterior SHF contributes to the venous pole of the heart with clonal relationship between the cells of the superior vena cava, pulmonary vein and of both atria (Lescroart et al., 2012). Furthermore, the atria are clonally related to the AVC myocardium, and their left/right identity is further determined by asymmetric expression of *Pitx2* (Domínguez et al., 2012; Galli et al., 2008).

Two major properties discriminate the SHF from the PHF cells: their sustained proliferation and their differentiation delay, controlled by paracrine Sonic Hedgehog (SHH), Wnt, Fibroblast Growth Factors (FGFs), Bone Morphogenetic Proteins (BMPs) and Notch signaling from the surrounding pharyngeal ectoderm and endoderm and by autocrine signaling from the pharyngeal mesoderm itself (Fig.6B) (Rochais et al., 2009b; Vincent and Buckingham, 2010; Francou et al., 2013). Indeed, SHF cells remain in an undifferentiated progenitor state in the pharyngeal mesoderm at the time the PHF cells form the heart tube and differentiate into cardiomyocytes. It is only after their migration and addition to the heart tube that the exposure to new signaling factors differentiate SHF cells into cardiomyocytes or smooth muscle cells, associated with downregulation of their early markers *Fgf8*, *Fgf10*, *Tbx1* and *Isl1* and

activation of the expression of *Nkx2.5*, *Gata4*, *Mef2c* and *Hand2* (Dyer and Kirby, 2009; Kelly, 2012).

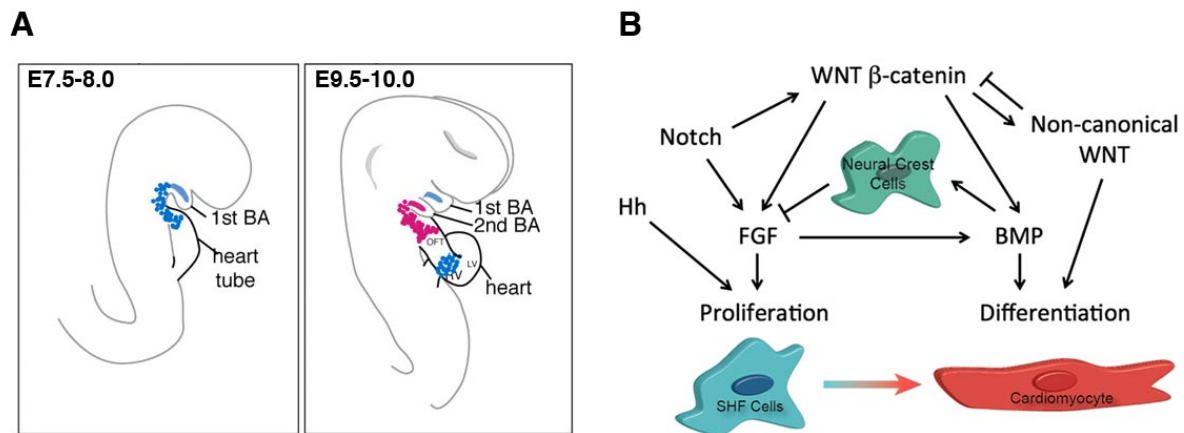


Figure 6. Migration and differentiation of second heart field progenitors

(A) Migration of anterior second heart field progenitors from the pharyngeal mesoderm of the branchial arches (BA) towards the heart tube. Blue: sub-lineage originating in the 1st BA and contributing to the RV myocardium and to the masticatory muscles. Pink: sub-lineage originating in the 2nd BA and giving rise to the OFT myocardium and to the facial expression muscles. From (Lescroart et al., 2010). (B) Signaling interactions controlling the balance between FGF-induced proliferation and BMP-induced differentiation of second heart field progenitors towards cardiomyocytes. See details in main text. From (Francou et al., 2013).

The balance between proliferation and differentiation of SHF cells depends mainly on opposite effects of FGF and BMP signaling (Fig.6B) (Hutson et al., 2010). *Fgf10* and *Fgf8* functionally overlap and control the survival and progenitor state maintenance of the SHF cells that will contribute to the OFT and RV (Ilagan et al., 2006; Park et al., 2006; Watanabe et al., 2010). The expression of *Fgf10* in these progenitors depends on a CRM located in its proximal promoter, which is mainly activated by TBX1 and ISL1 and repressed by NKX2.5 upon myocardium differentiation (Watanabe et al., 2012). In addition, FGF signaling is also activated by Wnt/ β catenin in the anterior SHF (Cohen et al., 2007). In contrast, the non-canonical *Wnt11* later promotes differentiation of SHF cells (Cohen et al., 2012; Pandur et al., 2002). BMP signaling from the distal prospective OFT antagonizes the proliferative FGF signals through the activation of *Msx1* and *Msx2* in the invading cNCC, but the mechanism by which these BMP targets further downregulate FGF ligands and decreases the proliferation of SHF progenitors is unclear (Tirosh-Finkel et al., 2010; Hutson et al., 2006). BMP4

is required for the septation of the OFT and the formation of the cardiac cushions, and its expression in the pharyngeal mesoderm and in the OFT is activated by Wnt signaling (McCulley et al., 2008; Ai et al., 2007). Furthermore, autocrine pharyngeal mesodermal FGF8 signaling is also required for *Bmp4* expression (Park et al., 2008). Finally, both *Tbx2* and *Tbx3* are necessary to activate BMP signaling in the distal OFT (Mesbah et al., 2012). These regulatory crosstalks between proliferative FGF and differentiating BMP signals suggest that their expression levels are critical to reach a signaling threshold necessary to affect cell fate (Vincent and Buckingham, 2010). The differentiation of SHF-derived structures (OFT, RV) depends further on a network of various transcription factors, among which *Hand2* plays an essential role (see below).

4.2.5. The T-box genes family and the development of the atrioventricular canal and atrioventricular node

The first signs of an electrical activity in the developing heart can be observed at the heart tube stage, with pacemaker activity at the venous pole generating slow peristaltic contractions (Christoffels and Moorman, 2009; Christoffels et al., 2010). This pacemaker activity, both at early and late stage of cardiac development, depends on the expression of the potassium/sodium channel *Hcn4* (Stieber et al., 2003). When cardiac chambers start to differentiate, the transmission of the electrical impulse depends on rapid conduction through Cx40/Cx43 gap-junction channels in atria and ventricles myocardium and on slow conduction through Cx45/Cx30.2 gap-junctions channels in the AVC and OFT, providing a contraction delay in these two compartments (de Jong et al., 1992; Moorman and Christoffels, 2003; Christoffels and Moorman, 2009). The primordia that form later the definitive components of the conduction system start to differentiate around E9.0-E9.5, and can originate both from transdifferentiation of cardiomyocytes or from pre-specified cardiac progenitors (Munshi, 2012; Christoffels and Moorman, 2009).

Several members of the T-box family of transcriptional regulators play an essential role during cardiac development and in the formation of the conduction system in particular, functions that are conserved among vertebrates (Stennard and Harvey,

2005; Hoogaars et al., 2007a; Greulich et al., 2011). This family is characterized by a highly conserved “T-box” DNA binding domain and consists of at least 17 members in mammals. Based on sequence homology, two main subfamilies can be identified: the first one contains *Tbx1*, *Tbx18* and *Tbx20*, while the second contains *Tbx2*, *Tbx3*, *Tbx4* and *Tbx5* (Plageman and Yutzey, 2005). The members of this second subfamily are closely related, as they evolved by two rounds of gene duplications from a single ancestral gene that resulted in two separate paralogous gene clusters: the *Tbx3/Tbx5* and *Tbx2/Tbx4* landscapes (Agulnik et al., 1996). *Tbx1* is involved in the proliferation of anterior SHF progenitors (Xu et al., 2004; Watanabe et al., 2012), *Tbx5* is a marker of the PHF involved in the differentiation of cardiomyocytes (Bruneau et al., 1999; Bruneau et al., 2001), *Tbx18* is important for the formation of the epicardium (Wu et al., 2013; Cai et al., 2008), and *Tbx4* is not involved in cardiogenesis. The main T-box genes involved in the formation of the conduction system are the transcriptional repressors *Tbx2* and *Tbx3*. *Tbx2* has been implicated mainly in the formation of the atrioventricular node (AVN) (Aanhaanen et al., 2011; Aanhaanen et al., 2009), while *Tbx3* marks the entire cardiac conduction system with highest expression in the developing and mature sinoatrial node (SAN), AVN and bundle of His (Hoogaars et al., 2004; Hoogaars et al., 2007b; Bakker et al., 2008; Horsthuis et al., 2009). *Tbx2* and *Tbx3* are expressed in the myocardium of the AVC and OFT, but not in the atrial and ventricular chambers. Their patterning and morphogenesis effect on these compartments occurs by repression of the chamber myocardial differentiation gene program, mainly through the direct repression of the differentiation marker *Nppa* (ANF, Atrial Natriuretic Factor) (Habets et al., 2002; Christoffels et al., 2004; Harrelson et al., 2004; Dupays et al., 2009; Mesbah et al., 2008). The AVC and OFT thus retain a low proliferation rate and slow conduction mode in comparison to the differentiating chambers. This progressively replaces the peristaltic contractions of the heart tube by a pattern of serial contractions combining alternate slow conducting and poorly contracted myocardium in AVC and OFT with fast conducting and contracting myocardium in the chambers (Moorman and Christoffels, 2003; Christoffels et al., 2010).

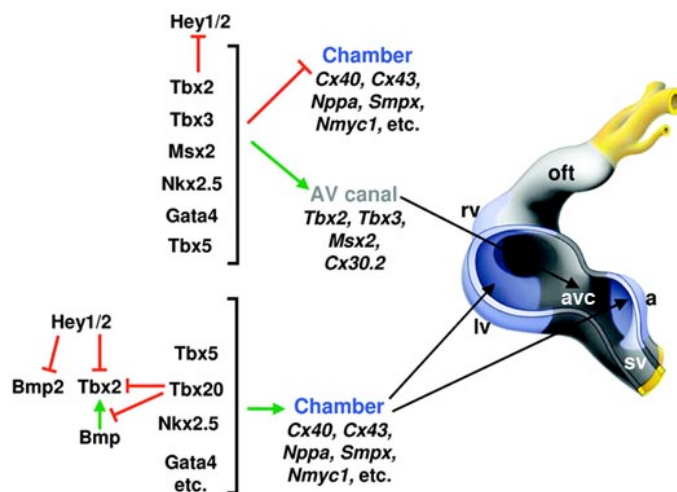


Figure 7. Atrioventricular canal and node formation

Molecular pathways regulating the development of the atrioventricular canal (avc) and the establishment of the boundary with the adjacent chambers myocardium. See details in main text. Adapted from (Christoffels et al., 2010).

The atrioventricular node (AVN) starts to differentiate at E9.5 from the myocardium of the AVC, which originates from both the PHF and posterior SHF (Aanhaanen et al., 2009; Domínguez et al., 2012). The AVC is specified by the expression of *Bmp2* in the myocardium, which mediates the induction of *Tbx2* expression to repress the chamber differentiation genes *Cx40*, *Cx43* and *Nppa* (Fig.7) (Yamada et al., 2000; Ma et al., 2005; Harrelson et al., 2004; Christoffels et al., 2004; Habets et al., 2002). In the cardiomyocytes of the neighboring chambers, Notch signaling activates *Hey1* and *Hey2*, which suppress *Tbx2* expression thereby restricting it to the AVC myocardium and creating the boundaries between the AVC and the heart chambers (Rutenberg et al., 2006; Kokubo et al., 2007). Furthermore, *Tbx2* expression in chambers myocardium is also repressed by *TBX20* (Singh et al., 2005; Cai et al., 2005; Stennard et al., 2005). This repression is not direct but is mediated by interfering with BMP2 signal transduction: *TBX20* binds to *SMAD1/5* and prevents their interaction with *SMAD4*, which in turn prevent them to bind to *Tbx2* proximal promoter (Fig.7 and Fig.10B) (Singh et al., 2009; Singh and Kispert, 2010). *Tbx3* is also expressed in the myocardium of the AVC, where it functions together with *Tbx2* to inhibit precocious chamber differentiation (Hoogaars et al., 2004; Singh et al., 2012). These two genes also have non-redundant functions, *Tbx2* being more important in the regulation of AVC patterning and *Tbx3* in the formation of the AVN itself by controlling the expression of the pacemaker gene program (Munshi, 2012; Frank et al., 2012; Aanhaanen et al., 2011; Horsthuis et al., 2009). By E13.5, the *Tbx3/Hcn4/Cx30.2/Cx45* positive cells of the AVN will extend into the left ventricle

and connect with both the fast conducting *Cx40/Cx43* positive trabeculations and the interventricular septum to form the bundle of His (Christoffels et al., 2010).

4.2.6. Formation of the cardiac valves: from endothelial-mesenchymal transition to the cardiac cushions

Epithelial-mesenchymal transition (EMT) is a common developmental mechanism by which epithelial cells are converted into mesenchymal cells by the loss of cell-cell adhesion and cellular polarity, and the gain of motile and invasive characteristics (Fig.8A). For instance, EMT is crucial for the formation of the mesoderm during gastrulation, the delamination of the cNCC from the neural tube, and the formation of the epicardium (Sauka-Spengler and Bronner-Fraser, 2008; Männer et al., 2001; Olivey and Svensson, 2010; von Gise and Pu, 2012). Successive waves of EMT and MET (mesenchymal-epithelial transition) are typically required for the formation of organs (Thiery et al., 2009; Lim and Thiery, 2012; Kovacic et al., 2012).

The formation of the cardiac valves is initiated in the endocardium at E9.5 in the AVC and E10.5 in the OFT by endothelial-mesenchymal transition (EndMT), a particular type of EMT. In response to signals coming from the myocardium, endocardial cells delaminate, transform into mesenchymal cells (Fig.8A,B) and migrate into the cardiac jelly between the two cellular layers, where they proliferate to form the cardiac cushions (Fig.8B). Following proliferative expansion and increased production of ECM, the cardiac cushions are remodeled into cardiac valves primordia (von Gise and Pu, 2012). The formation of the semilunar valves in the OFT also involves the cNCC. After their migration through the branchial arches, these cells invade the mesenchyme of the OFT cardiac cushions and contribute to their fusion to form the aorticopulmonary septum that divides the OFT into aorta and pulmonary trunk, and the associated semilunar valves (Lin et al., 2012). Alterations in the formation of the cardiac cushions or in their fusion with the cardiac septa can lead to atrial-septal and atrioventricular-septal defects, two frequent types of valves-associated CHDs.

In the AVC, the EndMT is initiated by a crosstalk between myocardium and endocardium involving multiple signaling pathways (Fig.8C). Myocardial *Bmp2* is crucial for both myocardium patterning (see above) and endocardial EndMT (Ma et

al., 2005; Rivera-Feliciano and Tabin, 2006). BMP2 paracrine signaling induces the expression of *Msx1* in the endocardium, which functions to maintain *Notch1* expression (Ma et al., 2005; Chen et al., 2008). Then, Notch1 endocardial signaling promotes the EndMT through the indirect non-cell autonomous activation of myocardial *Tgfβ2* (Timmerman et al., 2004). Furthermore, BMP2, Notch1 and TGFβ2 all converge to synergically activate *Snai1* expression in the endocardium (Timmerman et al., 2004; Niessen et al., 2008; Luna-Zurita et al., 2010). In addition, endocardial Notch1 signaling upregulates myocardial *Bmp2* expression via paracrine Wnt4, and BMP2 signaling also induces *Tgfβ2* expression in the myocardium via *Tbx2* (Wang et al., 2013; Ma et al., 2005; Shirai et al., 2009). This complex integration of BMP2/Notch1/TGFβ2 signaling between myocardium and endocardium drives and restricts the EndMT to the AVC (Garside et al., 2013).

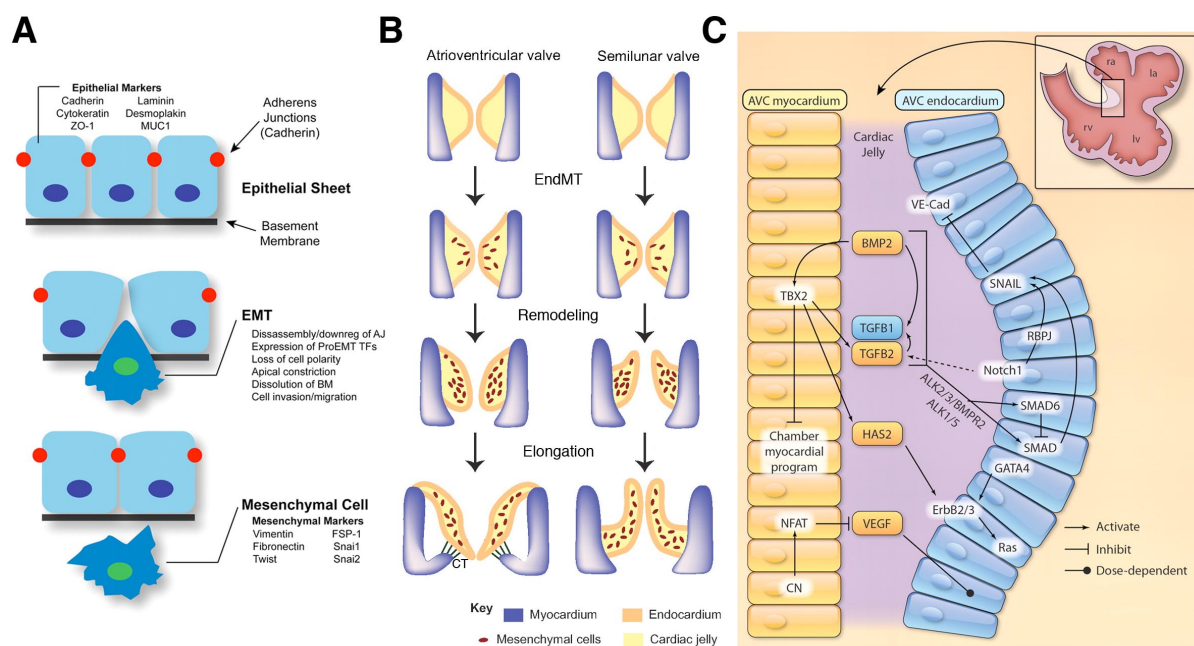


Figure 8. Formation of the cardiac valves by endothelial-mesenchymal transition

(A) Mechanism of epithelial-mesenchymal transition (EMT). During EMT, a cell in an epithelial sheet loses its adherent junctions and polarity while gaining migratory and invasive phenotypes. It delaminates or ingresses depending on the tissue and becomes a mesenchymal cell. From (von Gise and Pu, 2012). (B) Main steps of endothelial-mesenchymal transition (EndMT) in atrioventricular (left panel) and semilunar (right panel) valves. The atrioventricular valve leaflets are attached to the papillary muscles in the ventricles by chordae tendinae (CT). Adapted from (Lin et al., 2012). (C) AVC gene regulatory network controlling EndMT. See details in main text. Adapted from (von Gise and Pu, 2012).

Furthermore, myocardial TBX20 is also important to pattern the AVC upstream of the EndMT by regulating *Bmp2* expression (Cai et al., 2011). In contrast, endocardial TBX20 is not required to initiate the EndMT, but is essential later for cardiac cushion maturation and valves elongation by altering Wnt/ β -catenin signaling (Cai et al., 2013). Finally, signaling through the endocardial ErbB3 tyrosine kinase receptor is also necessary to induce EndMT (Camenisch et al., 2002), and requires upstream activation of *ErbB3* by GATA4 (Rivera-Feliciano et al., 2006).

Snai1 and the related gene *Snai2* are key mediators of EMT in a variety of developmental processes and disease states, such as the initiation of cancer metastasis (Barrallo-Gimeno and Nieto, 2005; Carver et al., 2001). During normal cardiac cushion development, endocardial Notch signaling induces the expression of *Snai1*, which in turn directly downregulates the expression of the adherent junction marker *VE-Cadherin* (*VE-Cad*) and hence disrupts cell contacts in the endocardium (Timmerman et al., 2004; Luna-Zurita et al., 2010). In addition, *Snai1* upregulates the expression of the intermediate filament Vimentin (VIM) to reorganize the cytoskeleton and gain cellular motility (Cano et al., 2000), and activates the expression of matrix metalloproteinases such as MMP15 that degrade the basal surface of endocardial cells to facilitate their delamination and migration into the cardiac jelly (Tao et al., 2011; Song et al., 2000).

One of the main components of the cardiac jelly ECM is hyaluronic acid (HA). HA interacts with other ECM components such as the proteoglycans aggrecan and versican, thereby contributing to the architecture of the ECM in the cardiac jelly to provide a support for the migration of the cardiac cushion progenitors (Bernanke and Markwald, 1979). HA also participates in ErbB3 tyrosine kinase receptor-mediated signaling transduction, which activates *Ras* that is required for AVC morphogenesis (Camenisch et al., 2000; Camenisch et al., 2002; Lakkis and Epstein, 1998). HA is mainly produced by the enzyme Hyaluronan Synthase 2 (HAS2). *Has2* expression in the myocardium depends of *Bmp2* (Ma et al., 2005), and it is also expressed by the endocardium and the migrating cardiac cushion mesenchymal progenitors (Fig.8C).

Has2-deficient embryos die by E10.0 due to hypoplastic OFT and RV and lack of ventricular trabeculation and cardiac cushions (Camenisch et al., 2000).

In the AVC, the transcriptional regulator *Twist1* controls the migration, proliferation and differentiation of cardiac cushion cells and the subsequent remodeling of the cardiac valves (Shelton and Yutzey, 2008; Lee and Yutzey, 2011; Vrljicak et al., 2012; Chakraborty et al., 2010). One target of *Twist1* in the cardiac cushions is *Sox9* (Vrljicak et al., 2012). *Sox9* is not required to initiate the EndMT and migration, but is activated following delamination and regulates cardiac jelly invasion and proliferation of cardiac cushion progenitors (Akiyama et al., 2004). *Sox9* is also required at later stages for proper distribution of ECM molecules during valves remodeling (Lincoln et al., 2007), and its downregulation leads to valve calcification phenotypes (Peacock et al., 2010).

Calcineurin/NFATc signaling is also critical for cardiac cushion formation, together with VEGF. *Nfatc1* is expressed specifically in endothelial cells of the endocardium but not the remainder of the vasculature, and is required for the formation of the semilunar valves but not for EndMT (Ranger et al., 1998; de la Pompa et al., 1998). At E9.0, Calcineurin/NFATc signaling in the AVC myocardium reduces the production of VEGF, as low levels of VEGF are required for EndMT. Accumulated levels of VEGF ultimately terminate EndMT at E10.5, and a second wave of Calcineurin/NFATc signaling in the endocardium directs valves elongation and remodeling from E11.0 (Chang et al., 2004; Lambrechts and Carmeliet, 2004). During valves remodeling, *Nfatc1* prevents a fraction of endocardial cell to undergo EndMT, which maintains them in a proliferative state (Wu et al., 2011).

4.2.7. *Hand2* is a crucial regulator for the development of second heart field derived structures

Hand2 and its closely related gene *Hand1* encode basic helix-loop-helix (bHLH) proteins belonging to the Twist-family of transcriptional regulators. These proteins are composed of a basic domain followed by two amphiphatic α -helices that are separated by a loop of variable length. While the helix-loop-helix motif (HLH)

mediates protein-protein interactions, the basic domain is responsible for DNA interactions through canonical E-box motifs (CANNTG). *In vitro*, HAND2 interacts with the highest affinity with the CATCTG E-box motif (Dai and Cserjesi, 2002). The dimerization of two bHLH proteins via their HLH domain is crucial for E-box recognition by two juxtaposed basic domains, and the choice of binding partner directly dictates the function and specificity of the bHLH transcriptional complex (Massari and Murre, 2000; Conway et al., 2010; Vincentz et al., 2011). The phosphorylation status of HAND2 and others Twist-family members at conserved Threonine and Serine residues in helix 1 alters their dimerization affinity for others bHLH proteins and consequently affects their DNA binding specificity (Firulli et al., 2005; Firulli et al., 2007; Barnes and Firulli, 2009).

Hand2 (or *dHand*) is expressed in the deciduum, heart, autonomic nervous system and neural crest derivatives and is crucial for the morphogenesis of these embryonic structures. In the sympathetic nervous system, *Hand2* regulates the expression of the norepinephrine biosynthetic enzymes that impact on the cardiac rhythm (Morikawa et al., 2007; Hendershot et al., 2008; Morikawa and Cserjesi, 2008; VanDusen et al., 2014). In addition, *Hand2* also regulates the formation of craniofacial structures derived from neural crest cells (Charité et al., 2001; Yanagisawa et al., 2003; Funato et al., 2009; Barron et al., 2011; Xiong et al., 2009). *Hand2* is also essential to activate *Shh* expression in the posterior forelimb and hindlimb bud mesenchyme, necessary for antero-posterior patterning of the limb (Charité et al., 2000; te Welscher et al., 2002; Galli et al., 2010).

The *Hand2* genomic sequence, expression pattern and functions are highly conserved among vertebrate species (Angelo et al., 2000; Srivastava, 1995; Yelon et al., 2000). During mouse cardiac development, *Hand2* expression is first detected in SHF progenitors at the cardiac crescent stage (E7.5). It is further maintained in the whole heart tube before being progressively restricted to the RV and OFT myocardium during cardiac looping, with remaining expression in the LV to a lesser extent (E8.5). From the heart tube stage, *Hand2* expression can also be detected in the endocardium and in the splanchnic pharyngeal mesoderm in the dorsal pericardial wall. From E9.5, *Hand2* is also expressed in the proepicardial organ and

derived epicardium, in the branchial arches and in the migrating cNCC that invade them, and in the developing vasculature. Its expression is gradually restricted during cardiac chambers remodeling to be detected only in the atria by birth (Fig.9A) (Srivastava, 1995; Srivastava et al., 1997; Biben and Harvey, 1997; Barnes et al., 2011; Dirkx et al., 2013). In contrast, *Hand1* is expressed mainly in PHF derived structures and becomes restricted to the LV when cardiac looping occurs (Fig.9A) (Srivastava et al., 1997; Biben and Harvey, 1997). HAND2 and HAND1 can form heterodimers, and they function redundantly and in a gene dosage-dependent manner for the differentiation of the PHF-derived LV, while *Hand1* does not play a role in the formation of the SHF-derived RV (Firulli et al., 2000; Firulli et al., 2010; McFadden et al., 2005).

Embryos deficient for *Hand2* display severe cardiac defects leading to growth retardation and embryonic lethality by E10.5 (Srivastava et al., 1997). The heart of these embryos appears morphologically normal until cardiac looping, but then displays several malformations: an hypoplastic RV that results in an abrupt connection between the OFT and LV, a thin myocardium without trabeculation, a dilated aortic sac, an absence of the aortic arches arteries, and hypoplastic branchial arches (Fig.9B) (Srivastava et al., 1997; Togi et al., 2006). In these mutant embryos, *Hand1* expression is not affected (Srivastava et al., 1997).

The conditional inactivation of *Hand2* in the epicardial lineage using both *Hand1-Cre* and *Wt1-CreERT2* disrupts the secondary epicardial EMT and the formation of the coronary vasculature, showing that *Hand2* is also required for the formation and differentiation of these cardiac structures (Barnes et al., 2011). Furthermore, *Hand2* conditional deletion in SHF progenitors using *Isl1-Cre* leads to a hypoplastic RV and to increased cell death in SHF progenitors in the pharyngeal mesoderm, impairing their subsequent migration towards the OFT. This establishes that *Hand2* is crucial for the survival of the SHF progenitors and for the subsequent formation of the RV (Tsuchihashi et al., 2011). Conditional inactivation of *Hand2* in cNCC using *Wnt1-Cre* results in misspattered aortic arches arteries, hypertrabeculation, enlarged RV, septation defects in both the ventricles and the OFT, and double-outlet right ventricle (DORV) in which both the aorta and the pulmonary trunk are connected to the right

ventricle (Holler et al., 2010; Morikawa and Cserjesi, 2008). Interestingly, cNCC-specific deletion of *Hand2* also showed that *Hand2* controls the expression of several genes involved in the proliferation and differentiation of both cNCC and SHF-derived cells in the RV trabecular myocardium (Holler et al., 2010; Morikawa and Cserjesi, 2008). Indeed, the marker of myocardial chamber differentiation *Nppa* is downregulated in these conditional mutant embryos, which, together with their enlarged RV and hypertrabeculation, points to a defect in the control of SHF proliferation. This occurs through an interaction between cNCC and SHF progenitors that takes place before their migration into the PHF heart tube (Morikawa and Cserjesi, 2008; Houweling et al., 2005; Yelbuz et al., 2002).

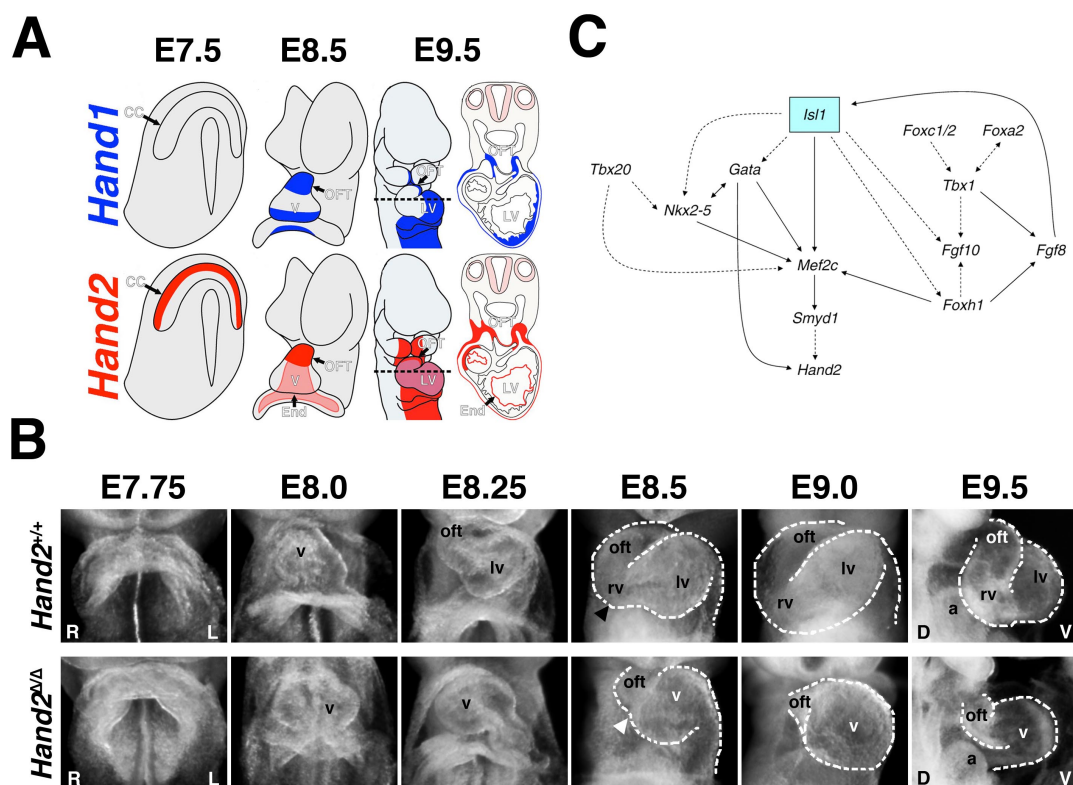


Figure 9. *Hand2* is a crucial regulator for second heart field differentiation

(A) Schematic representation of the expression of *Hand1* (top panel, blue) and *Hand2* (lower panel, red) during cardiac development. CC: cardiac crescent. V: ventricle. End: endocardium. OFT: outflow tract. LV: left ventricle. See details in main text. Adapted from (Vincentz et al., 2011). (B) Morphology of the developing heart in wild-type (top panels) and *Hand2*-deficient embryos (lower panel). Differences can be observed from the stage of cardiac looping (E8.25). From E8.5, the absence of the right ventricle (rv, black arrowhead in *Hand2*^{+/+}) is obvious in *Hand2*^{Δ/Δ} embryos (white arrowhead). a: atria. R/L: right/left. D/V: dorsal/ventral. (C) Model of the transcriptional network active in the second heart field that controls the development of the right ventricle and outflow tract. Solid lines: direct *in vivo* interactions. Dotted lines: genetic or *in vitro* interactions. From (Laugwitz et al., 2008).

The proliferative role of *Hand2* was shown in zebrafish embryos as well, in which it can promote the proliferation of SHF-derived cardiomyocytes. *Hand2* is also re-expressed in adult zebrafish heart following cardiac injury, where it increases cardiomyocytes proliferation thereby enhancing their cardiac regenerative capacities (Schindler et al., 2014; Wills et al., 2008). Similarly, *Hand2* expression is reactivated in the postnatal mouse heart following cardiac stress, leading to cardiomyocytes hypertrophy, cardiac dilation and eventually heart failure (Dirkx et al., 2013). This re-expression is mediated by the transcriptional inhibition of the microRNA miR-125 by Calcineurin/NFATc, as otherwise miR-125 inhibits *Hand2* translation by interacting with its 3'UTR (Dirkx et al., 2013). Negative regulation of *Hand2* translation is also mediated by interactions between its 3'UTR and the microRNAs miR-1 and miR-133a, which originate from the same bicistronic precursor (Zhao et al., 2005; Vo et al., 2010). Overexpression of miR-1 leads to defects in the proliferation of the cardiomyocytes, which also points to a role of *Hand2* controlling the proliferation of SHF myocardial cells (Zhao et al., 2005).

The RV-specific expression of *Hand2* is controlled by a GATA factors-dependent enhancer located in the *Hand2* proximal promoter (McFadden et al., 2000). In *Gata4*-deficient embryo, the precardiogenic mesoderm fails to fuse to form a heart tube (cardia bifida) (Kuo et al., 1997; Molkentin et al., 1997). In these mutant embryos, the RV-specific CRM of *Hand2* is still able to drive *LacZ* reporter expression in the two primitive hearts with highest intensity in the right one, suggesting that GATA5 or GATA6 could compensate for the loss of GATA4 to regulate *Hand2* expression in the RV (McFadden et al., 2000). Furthermore, GATA factors also regulate the expression of the PHF marker *Nkx2.5* in the RV through specific CRMs (Searcy et al., 1998; Lien et al., 1999; Reecy et al., 1999). Embryos deficient for *Nkx2.5* form a heart tube but fail to undergo cardiac looping. They show a severe reduction of the expression of cardiac differentiation markers, but not of *Hand2* (Lyons et al., 1995; Biben and Harvey, 1997; Yamagishi et al., 2001). Furthermore, the heart of embryos lacking both *Nkx2.5* and *Hand2* do not form any ventricles but only a single atrium, likely originating from the posterior SHF (Yamagishi et al., 2001; Lescroart et al., 2012; Srivastava, 2006).

The differentiation of the RV from anterior SHF progenitors is also impaired in embryos lacking *Isl1*, the early marker of this lineage (Cai et al., 2003). RV hypoplasia can also be observed in embryos deficient for *Mef2c*, which downregulates *Hand2* expression (Lin, 1997). *Mef2c* is a target of several key SHF transcription factors including ISL1, GATA4 and FOXH1 (Dodou et al., 2004; von Both et al., 2004). Furthermore, MEF2C directly activates the expression of the histone methyltransferase *Smyd1* (*Bop1*), which inactivation leads as well to RV hypoplasia and *Hand2* downregulation (Phan et al., 2005; Gottlieb et al., 2002). These and other genetic interactions determine a cascade of transcription factors crucial for the development of the right ventricle and the outflow tract (Fig.9C). *In vitro*, HAND2 directly activates the transcription of *Nppa* synergically with MEF2C, GATA4 or NKX2.5 (Zang et al., 2004; Dai et al., 2002; Thattaliyath et al., 2002), but no direct endogenous target gene of HAND2 in the second heart field or in other cardiac lineages have been identified so far (Vincentz et al., 2011).

4.3. The BMP signaling pathway during limb bud development and the *Grem1* cis-regulatory landscape

The developing tetrapod limb bud has been extensively used as a model to study the interactions between signaling networks and their effects on gene regulation (Zeller et al., 2009). It also provides an excellent system to analyze *cis*-regulatory landscapes and the role of individual CRMs using transgenic approaches (Zeller and Zuniga, 2007; Spitz and Duboule, 2008).

The tetrapod limb buds originate, as the cardiovascular system, from the lateral plate mesoderm and emerge as pockets of mesenchymal cells surrounded by a monolayer of ectodermal cells. Mouse limb buds outgrowth and patterning along the proximo-distal and antero-posterior axis are controlled by two signaling centers: the zone of polarizing activity (ZPA) and the apical ectodermal ridge (AER), which interact in a self-regulatory feedback system involving SHH, BMPs, FGFs and the BMP antagonist GREMLIN1 (GREM1) (Fig.10A) (Panman et al., 2006; Benazet et al., 2009; Zeller et al., 2009).

The BMP signaling pathway occupies a central role during mouse limb bud development (reviewed in (Pignatti et al., 2014)). It is involved in limb bud initiation, outgrowth and patterning and is important for the chondrogenic differentiation of the limb skeletal elements (Kobayashi et al., 2005). BMP ligands belong to the TGF β superfamily. In the developing limb bud, BMP2, BMP4 and BMP7 are expressed in specific spatio-temporal patterns, and their activity is modulated by various extracellular antagonists. The binding of BMP ligand dimers to serine/threonine receptors triggers the phosphorylation of receptor-associated SMADs (R-SMADs, or SMAD1,5,8), which mediate canonical BMP signal transduction by associating with SMAD4 (co-SMAD). The resulting transcriptional complex is translocated to the nucleus, where it interacts with BMP responsive elements (BRE) in the *cis*-regulatory landscapes of target genes (*Id1*, *Msx2*...) and activates their expression (Fig.10B). SMAD4 is an essential mediator for both BMP and TGF β signal transduction in the development of various tissues. It is composed of two evolutionary conserved MAD homology domains (MH) separated by a linker.

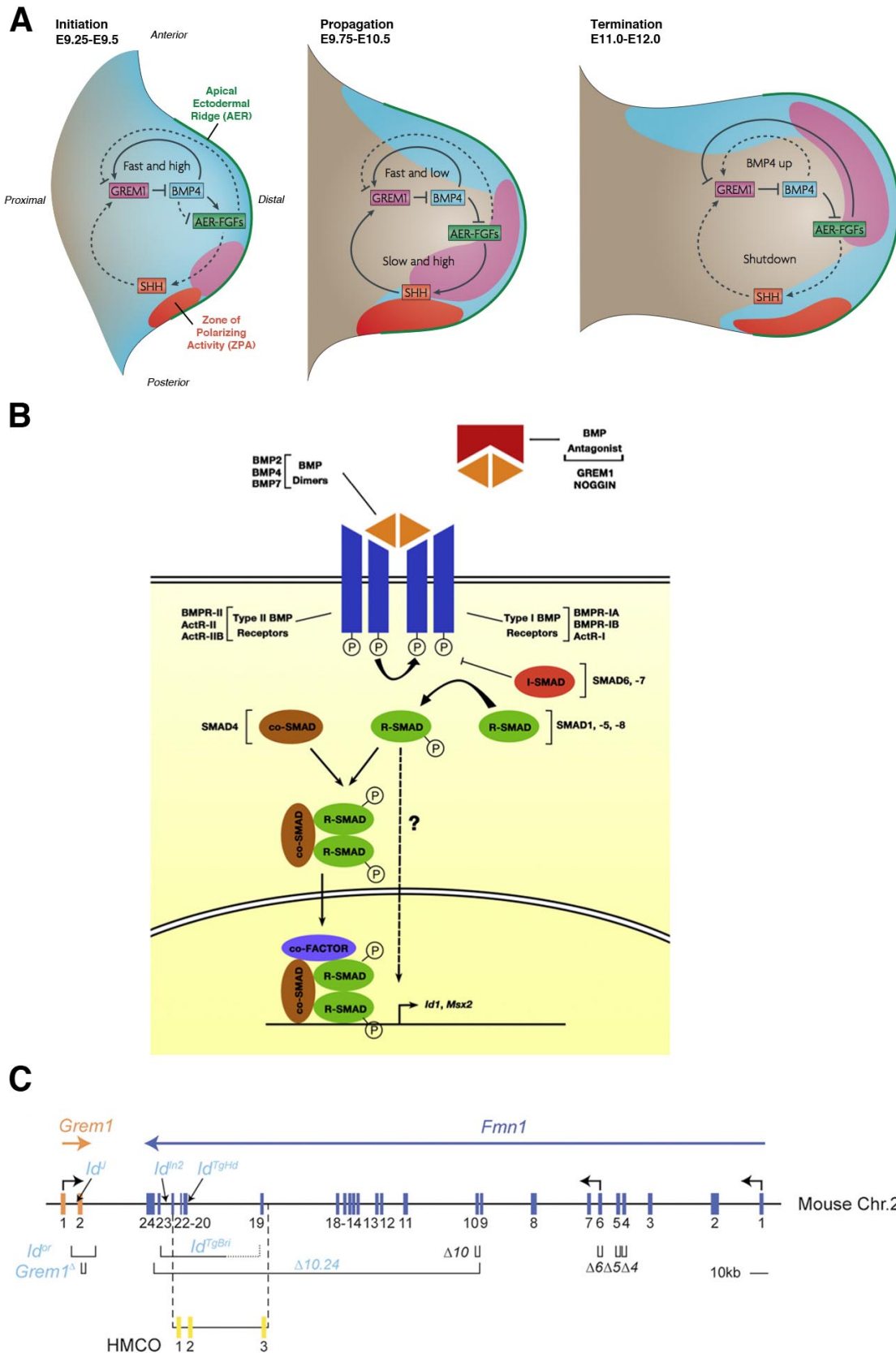


Figure 10. Limb bud development and BMP signaling pathway

(A). Interlinked signaling feedback loops control limb bud outgrowth. During the initiation phase, high BMP4 (blue) levels in the mesenchyme maintain AER-FGFs (green) and activate the expression of the BMP antagonist *Grem1* (purple). During the propagation phase, increasing GREM1 levels antagonize

BMP4 signaling, which enables FGF signaling from the AER to the underlying mesenchyme for proliferative outgrowth and to the ZPA to maintain *Shh* expression (red). The SHH/GREM1/AER-FGFs epithelial-mesenchymal feedback loop is self-terminated as *Grem1* is repressed by AER-FGFs and as the expanding population of *Shh*-expressing descendant cells becomes refractory to *Grem1* expression, generating a gap that brings the *Grem1* expression domain out of reach of long range SHH signaling. This results in an increase in BMP activity, initiating chondrogenic differentiation of mesenchymal progenitors. From (Zeller et al., 2009). (B) BMP signaling pathway. See main text for details. From (Pignatti et al., 2014). (C) The *Grem1-Fmn1* cis-regulatory landscape. Point mutations, deletions (Δ), inversions and transgene insertions are indicated above or below the landscape. Mutations indicated in pale blue cause the *limb deformity (ld)* phenotype due to disruption of *Grem1* cis-regulation. The three yellow boxes indicate the location of the conserved HMCOs elements. Adapted from (Zeller and Zuniga, 2007).

The N-terminal MH1 domain binds to DNA, mediates protein-protein interactions and contains the nuclear localization signal. The C-terminal MH2 domain is phosphorylated by type I BMP receptors and mediates heterodimerization with R-SMADs. Embryos deficient for *Smad4* die before E7.5 due to gastrulation defects, which preclude the analysis of its specific role during limb bud development (Sirard et al., 1998).

Grem1 is a crucial node during limb bud morphogenesis, as its dynamic expression is controlled by BMP, SHH and FGF signaling pathways during limb bud initiation, expansion and termination, respectively (Fig.10A) (Zuniga et al., 1999; Capdevila et al., 1999; Scherz et al., 2004; Verheyden and Sun, 2008; Benazet et al., 2009). *Grem1*-deficient mice lack kidneys and ureters and die shortly after birth. They also display limb skeleton patterning defects such as fused ulna and radius and reduction in digit number (Michos et al., 2004; Khokha et al., 2003). *Grem1* expression in limb buds depends on a large cis-regulatory landscape that extends at least in the neighboring *Formin1* (*Fmn1*) gene. This region is able to activate reporter expression in the limb bud similarly to *Grem1* endogenous expression, and contains three regions highly conserved between Human, Mouse, Chicken and Opossum (HMCOs), that can potentially act as CRMs (Fig.10C) (Zuniga et al., 2004).

5. Aims of the Thesis

During embryonic development, genomic *cis*-regulatory landscapes integrate inputs from multiple signaling pathways to control cell specification, determination and differentiation. Understanding the spatio-temporal and tissue-specific control of genes expression involves the identification of the *cis*-regulatory modules necessary for their activity and of the *trans*-acting factors required to activate or repress these genes.

In my PhD project I became interested in transcriptional gene regulation during mouse limb bud and heart morphogenesis. The first part of this thesis focuses on limb bud development and more specifically on components of the Bone Morphogenetic Protein (BMP) signaling pathway. The aims of this first part were: (1) to analyze the role of the BMP signal transducer SMAD4 during limb bud chondrogenesis using *in vitro* differentiation systems; (2) to study the role of a highly conserved region in the *cis*-regulatory landscape of *Grem1* by analyzing its reporter activity in transgenic wild-type and mutant embryos (the publications that include the results from these two projects are directly presented in this thesis in their published version); (3) to globally dissect the transcriptional networks regulated by SMAD4 during chondrogenesis and to identify the *cis*-regulatory modules interacting with SMAD4 in the *Grem1* genomic landscape. Due to the lack of suitable anti-SMAD4 antibodies for ChIP-Seq, I used cassette exchange and homologous recombination approaches in embryonic stem cells to generate a new mouse line that expresses an epitope-tagged SMAD4 protein from its endogenous locus.

In the second part of this thesis, my aim was to identify the direct transcriptional targets of the essential transcription factor HAND2 during heart development. Towards this aim I analyzed ChIP-Seq data previously generated in the laboratory using a mouse endogenously expressing an epitope-tagged HAND2 protein. By combining gene and protein expression analysis with cellular resolution, ChIP-qPCR and transgenic reporter studies, I was able to define the regulatory network controlled by HAND2 during second heart field development and in the formation of the cardiac cushions.

6. Results

6.1. From *cis*-regulatory modules to *trans*-acting factors: control of *Grem1* genomic landscape during limb bud development and generation of *Smad4*^{3xFLAG} mice by homologous recombination

6.1.1. Paper 1: “*Smad4* is required to induce digit ray primordia and to initiate the aggregation and differentiation of chondrogenic progenitors in mouse limb buds”

This publication focuses on the conditional deletion of *Smad4* from the limb buds mesenchyme using *Prx1-Cre* mice. I carried out the analysis of the high-density *in-vitro* limb mesenchymal cell cultures isolated from wild-type and *Smad4*-deficient limb buds shown in Figure 6.

Smad4 is required to induce digit ray primordia and to initiate the aggregation and differentiation of chondrogenic progenitors in mouse limb buds

Jean-Denis Bénazet^{1,*‡}, Emanuele Pignatti^{1,‡}, Ashleigh Nugent¹, Erkan Unal^{1,2}, Frédéric Laurent¹ and Rolf Zeller^{1,§}

SUMMARY

SMAD4 is an essential mediator of canonical TGF β /BMP signal transduction and we inactivated *Smad4* in mouse limb buds from early stages onward to study its functions in the mesenchyme. While this *Smad4* inactivation did not alter the early *Sox9* distribution, prefiguring the chondrogenic primordia of the stylopod and zeugopod, it disrupted formation of all *Sox9*-positive digit ray primordia. Specific inactivation of *Smad4* during handplate development pointed to its differential requirement for posterior and anterior digit ray primordia. At the cellular level, *Smad4* deficiency blocked the aggregation of *Sox9*-positive progenitors, thereby preventing chondrogenic differentiation as revealed by absence of collagen type II. The progressive loss of SOX9 due to disrupting digit ray primordia and chondrogenesis was paralleled by alterations in genes marking other lineages. This pointed to a general loss of tissue organization and diversion of mutant cells toward non-specific connective tissue. Conditional inactivation of *Bmp2* and *Bmp4* indicated that the loss of digit ray primordia and increase in connective tissue were predominantly a consequence of disrupting SMAD4-mediated BMP signal transduction. In summary, our analysis reveals that SMAD4 is required to initiate: (1) formation of the *Sox9*-positive digit ray primordia; and (2) aggregation and chondrogenic differentiation of all limb skeletal elements.

KEY WORDS: BMP signaling, Limb bud, Mouse

INTRODUCTION

Bone morphogenetic proteins (BMPs) are ligands belonging to the transforming growth factor beta (TGF β) superfamily, which control inductive processes in early embryos and during organogenesis (reviewed by Zakin and De Robertis, 2010) and are required for chondrogenesis, growth and ossification of bones in vertebrates (reviewed by Wu et al., 2007). BMP ligands interact with two types of BMP receptors (BMPRI and BMPRII), which in turn trigger intracellular signal transduction by phosphorylation of the receptor-associated SMAD1, -5 and -8 proteins. These in turn form a complex with SMAD4, an essential mediator of both canonical BMP and TGF β signal transduction (Yang et al., 2002). These SMAD complexes translocate to the nucleus and regulate the expression of target genes in concert with other transcriptional regulators (Feng and Derynck, 2005). Genetic and functional analysis of mouse and chicken limb bud development has uncovered important morphoregulatory functions of the BMP pathway in the establishment and functioning of the two limb bud signaling centers, namely sonic hedgehog (SHH) signaling by the posterior mesenchymal organizer and fibroblast growth factor (FGF) signaling by the apical ectodermal ridge (AER).

During limb bud outgrowth, BMPs and the BMP antagonist gremlin 1 (GREM1) control the epithelial-mesenchymal signaling

interactions that coordinate outgrowth with patterning and determination of digit identities (reviewed by Zeller et al., 2009). During the onset of limb bud development, BMP4 is first required in the mesenchyme and BMPRII in the ectoderm for formation of the AER, as inactivation of these molecules disrupts establishment of the AER-FGF signaling centre, which results in limb truncations and loss of dorsoventral polarity (Ahn et al., 2001; Pizette et al., 2001; Pajni-Underwood et al., 2007; Bénazet et al., 2009). During initiation of limb bud outgrowth, the SHH signaling centre is established and restricted to the posterior mesenchyme under the influence of BMP signaling (Bastida et al., 2004). Concurrently, BMP4 triggers expression of the BMP antagonist *Grem1* in the posterior limb bud mesenchyme, which causes rapid lowering of mesenchymal BMP activity (Nissim et al., 2006; Bénazet et al., 2009). The subsequent distal-anterior expansion of the *Grem1* expression domain depends largely on its positive regulation by AER-FGF and SHH signaling. This self-regulatory SHH/GREM1/AER-FGF feedback loop coordinates anteroposterior (AP) with proximodistal (PD) limb bud outgrowth and patterning (Zúñiga et al., 1999; Michos et al., 2004; Panman et al., 2006; Bénazet et al., 2009; Probst et al., 2011).

During limb bud outgrowth, low mesenchymal BMP activity is required to restrict the length of the AER, as inactivation of *Bmp4* during this developmental period results in extended AER-FGF signaling and digit polydactyly (Selever et al., 2004; Bénazet et al., 2009). As inactivation of *Bmpr1a* in the mesenchyme also disrupts limb bud outgrowth (Ovchinnikov et al., 2006), tight control of BMP activity is required for normal progression of limb development (reviewed by Zeller et al., 2009).

These signaling interactions are terminated as the SHH/GREM1/AER-FGF feedback signaling system breaks down owing to progressive inhibition of *Grem1* expression by high AER-FGF levels and the increasing separation of the *Shh* and *Grem1*

¹Developmental Genetics, Department of Biomedicine, University of Basel, Mattenstrasse 28, CH-4058 Basel, Switzerland. ²Department of Biosystems Science and Engineering (D-BSSE), ETH Zurich, Mattenstrasse 26, CH-4058 Basel, Switzerland.

*Present address: Broad Center for Regenerative Medicine and Stem Cell Research, University of Southern California, 1425 San Pablo Street, Los Angeles, CA 90089, USA

[‡]These authors contributed equally to this work

[§]Author for correspondence (rolf.zeller@unibas.ch)

expression domains (Scherz et al., 2004; Verheyden and Sun, 2008). This termination results in a renewed increase in BMP activity during development of the digit ray primordia (giving rise to metacarpals and phalanges) (Bénazet et al., 2009), which probably serves two purposes: first, to control digit identity by signaling from the interdigit mesenchyme to the distal phalanx-forming region (PFR) (Dahn and Fallon, 2000; Suzuki et al., 2008; Witte et al., 2010), and second, to induce apoptosis of the interdigit mesenchyme (Bandyopadhyay et al., 2006; Pajni-Underwood et al., 2007; Maatouk et al., 2009; Wong et al., 2012). In agreement with these dynamic changes in BMP activity, BMPs inhibit chondrogenic differentiation of early limb bud mesenchymal progenitors while promoting chondrogenesis at late stages (Karamboulas et al., 2010). Noggin-mediated BMP antagonism under experimental conditions showed that BMPs are required to initiate compaction and chondrogenic differentiation of *Sox9*-positive mesenchymal progenitors (Brunet et al., 1998; Pizette and Niswander, 2000; Barna and Niswander, 2007). Genetic inactivation of both *Bmp2* and *Bmp4* in the limb bud mesenchyme disrupted formation of the two posterior-most digit primordia and the ulna (Bandyopadhyay et al., 2006). Experimental evidence indicated that BMPs participate in activating *Sox9* expression in prechondrogenic progenitors, and *Sox9* not only marks the chondrogenic lineage but is essential to initiate chondrogenesis during formation of skeletal elements (Bi et al., 1999; Akiyama et al., 2005; Pan et al., 2008).

Genetic analysis of the BMP pathway during chondrogenesis established that BMP signaling and antagonism are required recurrently for the proliferation of prechondrogenic progenitors, chondrocyte differentiation, shaping the skeletal primordia and formation of the endochondral growth plate (Brunet et al., 1998; Kobayashi et al., 2005; Yoon et al., 2005). In parallel, mesenchymal cells receiving different signals are specified as tendons, ligaments and connective tissues. For example, chondrogenic differentiation is inhibited and mesenchymal cells remain in a proliferative, undifferentiated state when they are exposed to both ectodermal WNT and AER-FGF signaling, whereas WNT signaling alone promotes the development of non-specific connective tissue (ten Berge et al., 2008; Gros et al., 2010).

TGF β ligands are expressed from early limb bud stages onward, and inhibition of TGF β signal transduction in cultured mesenchymal cells provided evidence that TGF β signaling functions in early limb buds to alleviate the inhibitory effects of BMPs on initiation of chondrogenic differentiation (Karamboulas et al., 2010). Therefore, brief exposure of mesenchymal progenitors to TGF β signaling seems necessary to allow subsequent induction of chondrogenesis by BMPs (Roark and Greer, 1994; Karamboulas et al., 2010). Furthermore, implantation of TGF β 1-loaded beads into the interdigit mesenchyme of chicken limb buds is able to induce formation of ectopic digit phalanges, i.e. trigger ectopic chondrogenesis (Merino et al., 1999; Lorda-Diez et al., 2011). Genetic analysis of TGF β ligands and receptors in mouse embryos has revealed their essential roles during limb long bone, joint and tendon morphogenesis (Sanford et al., 1997; Seo and Serra, 2007). Although this genetic analysis revealed essential functions during limb skeletal development, it is possible that earlier functions in initiating chondrogenesis were masked by functional complementation among TGF β and/or BMP ligands and receptors (see e.g. Karamboulas et al., 2010).

As *Smad4*-deficient (*Smad4*^Δ) embryos die during gastrulation (Chu et al., 2004), we used a conditional loss-of-function allele (Yang et al., 2002) to study its requirement in the limb bud mesenchyme. *Prx1*-Cre-mediated conditional inactivation of

Smad4 in limb bud mesenchyme resulted in the clearance of SMAD4 protein during early limb bud outgrowth, and the distribution of *Sox9* transcript and SOX9 protein was normal until at least embryonic day (E) 11.0 in the proximal mesenchyme. By contrast, *Sox9* expression was not activated in the distal *Smad4*-deficient limb bud mesenchyme that would normally give rise to the digit ray primordia. The analysis of SOX9 also indicated that with the exception of a small proximal aggregate, the aggregation and condensation of all mesenchymal progenitors to form the cartilage elements was disrupted in *Smad4*-deficient limb buds. Mutant cells failed to deposit extracellular collagen type II (COL type II) fibres, a hallmark of chondrogenesis, and progressively lost SOX9, i.e. chondrogenic lineage. In parallel, the expression of markers for other mesenchymal lineages was upregulated in *Smad4*-deficient limb buds without their normal spatial restriction, which provided evidence for a diversion of *Smad4*-deficient progenitors toward non-specific connective tissue.

MATERIALS AND METHODS

Ethics statement concerning animal experiments and mouse strains

Animal experiments were approved by the legally required regional commission in strict accordance with Swiss law. All studies were classified as grade zero, which implies minimal suffering. The 3R and Basel Declaration principles were implemented. The *Prx1*-Cre was used to conditionally inactivate *Smad4* (*Smad4*^{fllox}) (Yang et al., 2002) in the mesenchyme from early limb bud stages onward (Logan et al., 2002), and the *Hoxa13*^{Cre/+} knock-in allele was used for autopod specific inactivation (Lopez-Rios et al., 2012; Scotti and Kmita, 2012). *Prx1*-Cre-mediated inactivation of *Bmp2* and *Bmp4* was done as described (Bandyopadhyay et al., 2006).

In situ hybridization and skeletal preparations

Whole-mount in situ hybridization was performed using standard protocols. Control and experimental embryos were age-matched by counting somites. To assess the clearance of *Smad4* transcript in *Smad4*-deficient limb buds, a probe against the deleted region, coding exon 8 (Yang et al., 2002) was used for hybridization. Depending on the analysis, *Smad4*^{+/+}, *Smad4*^{+fllox}, *Smad4*^{fllox/fllox} or *Smad4*^{ΔM/+} *Prx1*-Cre^{tg/+} or *Hoxa13*^{Cre/+} heterozygous embryos were used as controls and collectively referred to as 'wild-type controls'. Alcian Blue and Alizarin Red were used to reveal cartilage and bone.

Optical projection tomography

Optical projection tomography (OPT) imaging (Sharpe et al., 2002) was used to acquire 3D images and prepare optical sections. RNA hybrids were detected using nitro-blue tetrazolium and 5-bromo-4-chloro-3'-indolylphosphate (NBT/BCIP, Roche). Whole-mount immunofluorescence analysis was done as follows: embryos were permeabilized in cold acetone (15-30 minutes) and then incubated in blocking solution (PBT with 1% bovine serum albumin, 1% dimethyl sulfoxide and 5% inactivated bovine serum) for 20 minutes. SMAD4 was detected using rabbit monoclonal anti-SMAD4 antibodies, 1:50 in blocking solution (Abcam; 12 hour incubation at 4°C). Samples were washed extensively and incubated with secondary antibodies Alexa Fluor 594-conjugated anti-rabbit antibody, 1:250 (Invitrogen; overnight at 4°C). Subsequently, samples were embedded in 1% low melting point agarose (Sigma), dehydrated in 100% methanol and cleared in BABB. Samples were scanned either at high (1024×1024 pixels) or intermediate resolution (512×512 pixels) in the Bioptonics OPT scanner using Skyscan software (Bioptonics, MRC Technology). The GFP1 filter (425/40 nm, 475 nm LP) was used to detect sample anatomy. No filter (bright field) or the TXR filter (560/40 nm, 610 nm LP) was used to image NBT/BCIP signals or fluorescently labeled samples, respectively. OPT scans were reconstructed using NRecon software (SkyScan) and analysed using the Bioptonics Viewer. Rendering images were taken using the maximum intensity projection function. For generation of iso-surfaces, the iso-surface editor of the Bioptonics viewer program was used at 25%

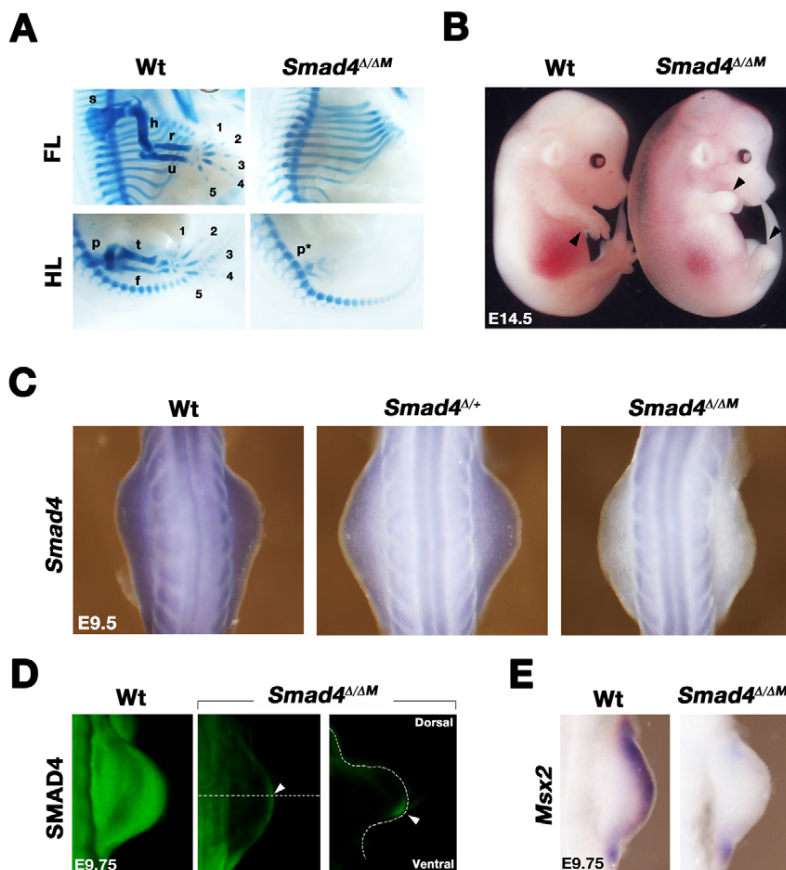


Fig. 1. *Prx1*-Cre-mediated inactivation of *Smad4* in mouse forelimb bud mesenchyme. (A) Skeletal preparations at embryonic day E14.5. Note the absence of all skeletal elements including the scapula in *Smad4*^{Δ/ΔM} forelimbs (FL) and formation of only a rudimentary pelvic girdle in mutant hindlimbs (HL). (B) Brightfield images of wild-type and *Smad4*^{Δ/ΔM} embryos at E14.5 to reveal the paddle-like limb morphology. (C) *Smad4* transcript distribution (blue-purple staining) in wild-type, *Smad4*^{Δ/+} and *Smad4*^{Δ/ΔM} forelimb buds at E9.5 (23–24 somites). *Smad4* transcript levels are reduced in *Smad4*^{Δ/+} forelimb buds and cleared in *Smad4*^{Δ/ΔM} forelimb buds. (D) Detection of SMAD4 protein (green fluorescence) by whole-mount antibody staining in wild-type (29 somites) and *Smad4*^{Δ/ΔM} forelimb buds at E9.75 (27 somites). SMAD4 levels are also reduced along the primary axis, as only one *Smad4* allele is functional in *Smad4*^{Δ/ΔM} embryos. The broken line indicates the approximate position of the virtual OPT section shown in the right-most panel. SMAD4 is lost from the mutant mesenchyme, whereas AER expression remains (arrowheads). (E) *Msx2*, a direct transcriptional target of BMP signaling, is downregulated in *Smad4*^{Δ/ΔM} forelimb buds by E9.75 (26 somites). 1–5: digits 1–5; f, femur; h, humerus; p, pelvis; p*, rudimentary pelvis; r, radius; s, scapula; t, tibia; u, ulna.

iso-surface quality and 50% Gaussian smoothing parameters. Iso-surface values were determined and compared with the strength and distribution of the original signal to exclude aberrant iso-surfaces.

Quantification of transcript levels by quantitative real-time PCR

Forelimbs were isolated at E10.5 (35–39 somites) and E11.75 (51–53 somites) and analysed (Bénazet et al., 2009) using the primers listed in supplementary material Table S1. At least eight samples per stage and genotype were analysed. All results shown are mean±SD; each dot represents one sample, and the significance of all differences was verified using the two-tailed non-parametric Mann-Whitney U-test.

Immunofluorescence analysis

Embryos or forelimb buds were isolated and fixed in 4% PFA overnight at 4°C. Samples were dehydrated stepwise into 100% ethanol, then transferred to xylene. Subsequently, samples were embedded in Paraplast wax (Sigma) and sectioned following standard procedures. For most antibodies, antigen retrieval was achieved by heating the dewaxed sections at 121°C in 1 atm for 6 minutes in a desktop autoclave. The COL type II antigen was retrieved by digesting sections with pepsin (1 mg/ml in 10 mM HCl, pH 2.0) for 15 minutes (37°C). Sections were blocked using PBS containing 0.3% Triton X-100 and 1% BSA (blocking solution; 1 hour at room temperature). Following pre-treatment, sections were incubated with primary antibodies (blocking solution overnight at 4°C). The following primary antibodies were used: rabbit polyclonal anti-Ki67 1:200 (Millipore); rabbit polyclonal anti-Sox9 1:500 (Millipore); mouse monoclonal anti-collagen type-II 1:100 (Thermo Scientific); rabbit polyclonal anti-collagen type-I 1:500 (Abcam). Immunocomplexes were detected using the following secondary antibodies (1 hour at room temperature): goat anti-rabbit Alexa Fluor 594 1:500 (Invitrogen), goat anti-mouse Alexa Fluor 488 1:200 (Invitrogen). Apoptotic cells were detected by whole-mount Lysotracker analysis (Invitrogen) as previously described (Benazet et al., 2009).

Limb mesenchymal cell culture and immunofluorescence

Forelimbs were dissected in ice-cold PBS, and 2% trypsin digestion (25 minutes at 4°C) in combination with gently pipetting resulted in single cell preparations of mesenchymal cells that were plated in DMEM/F12 medium (supplemented with 0.5% penicillin/streptomycin and 10% FBS, Gibco-BRL) at 7.5×10^5 cells/300 μ l in eight-well chamber slides (Ibidi). After 48 hours' culturing, samples were washed in PBS and fixed in 4% PFA (30 minutes at room temperature) before permeabilization and antigen detection as described above. BMP signaling was specifically inhibited by adding 10 μ M dorsomorphin (Yu et al., 2008) and TGF β signaling was inhibited by adding 10 μ M SB431542 (Inman et al., 2002) in 0.1% DMSO (final concentration in medium). Control cells were cultured in medium containing 0.1% DMSO. Media were refreshed every 24 hours. The results shown are representative of eight independent experiments (supplementary material Fig. S5). Inhibition of p38, which is involved in non-canonical BMP signal transduction, had no effect on cell aggregation and the onset of chondrogenic differentiation (data not shown).

RESULTS

Requirement of mesenchymal *Smad4* for propagation of the SHH/GREM1/AER-FGF feedback loop during mouse limb bud development

Prx1-Cre-mediated conditional inactivation of *Smad4* in the mesenchyme (*Smad4*^{Δ/ΔM}) resulted in fore- and hindlimbs lacking skeletal elements (Fig. 1A). Stunted paddles replaced the autopod with digits at embryonic day E14.5 (Fig. 1B, arrowheads). As this initial analysis pointed to a late onset phenotype, the clearance of *Smad4* gene products was assessed (Fig. 1C,D; supplementary material Fig. S1A). Mesenchymal transcripts were undetectable by ~E9.5 (Fig. 1C) and proteins from ~E9.75 onward in *Smad4*^{Δ/ΔM} forelimb buds (Fig. 1D). As the *Prx1*-Cre transgene is activated in

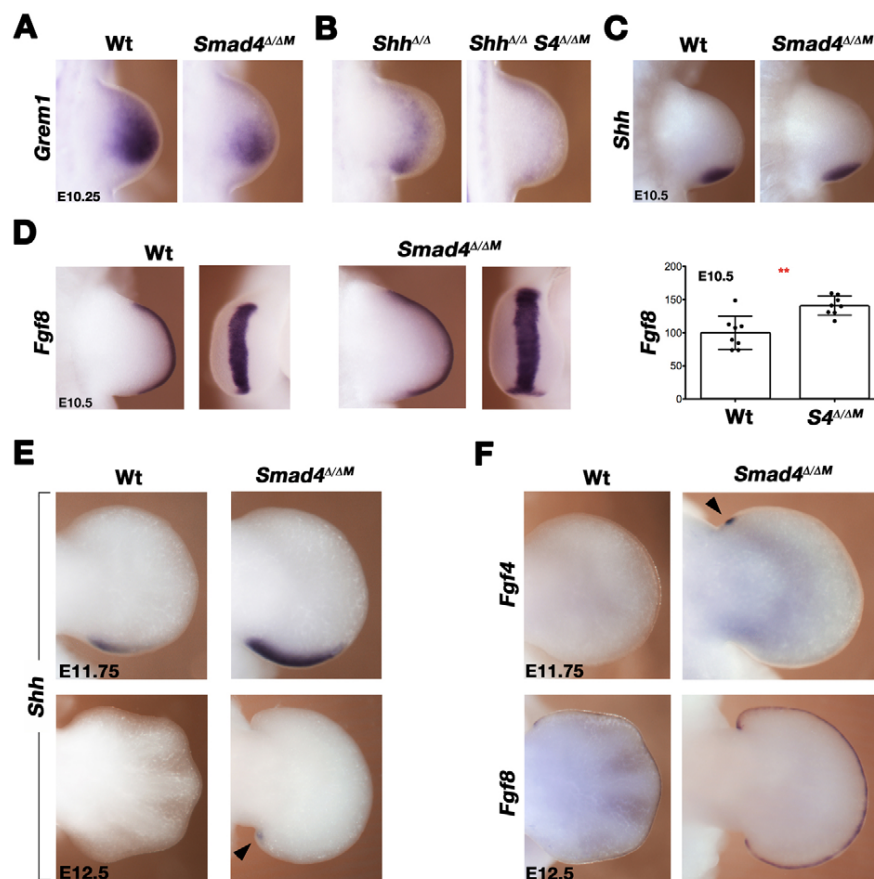


Fig. 2. Effect of mesenchymal *Smad4* deficiency on the SHH/GREM1/AER-FGF feedback loop. (A,B) *Grem1* expression in wild-type, *Smad4^{Δ/ΔM}*, *Shh^{Δ/Δ}* and *Shh^{Δ/Δ} Smad4^{Δ/ΔM}* forelimbs at E10.25 (31–32 somites). **(C)** *Shh* expression is not significantly altered in *Smad4^{Δ/ΔM}* forelimb buds at E10.5 (35 somites). **(D)** Expression of *Fgf8* in wild-type and *Smad4^{Δ/ΔM}* forelimb buds at E10.5 (35 somites). Right panel: qPCR-based quantification of *Fgf8* levels in forelimb buds at E10.5. Expression is significantly higher in *Smad4^{Δ/ΔM}* than wild-type forelimbs ($P \leq 0.01$). Data are shown as mean \pm SD. **(E,F)** Termination of *Shh* (E) and AER-*Fgf* (F) expression is delayed in *Smad4^{Δ/ΔM}* forelimb buds. The black arrowheads indicate the prolonged *Shh* (E11.75, 50 somites and E12.5, 60 somites) and anterior AER-*Fgf* expression (at E11.75, 50 somites) in mutant limb buds.

the forelimb bud territory before E9.0 (Logan et al., 2002), the complete functional inactivation of *Smad4* in forelimb buds required ~18 hours. In agreement with these inactivation kinetics, the expression of the BMP target *Msx2* was reduced from ~E9.75 onward (Fig. 1E; supplementary material Fig. S1B). By contrast, the three main *Bmp* ligands were either unchanged or slightly increased in mutant limb buds (supplementary material Fig. S2).

Previous analysis provided evidence that activation and initial upregulation of *Grem1* expression in the limb bud mesenchyme depended on BMP4 signaling (Nissim et al., 2006; Bénazet et al., 2009). In *Smad4^{Δ/ΔM}* forelimb buds, *Grem1* expression was reduced, but its posterior domain was maintained at E10.25 (Fig. 2A). To discriminate between SMAD4-independent regulation and the well-characterized positive regulation of *Grem1* expression by SHH signaling (Zúñiga et al., 1999; Panman et al., 2006), forelimb buds lacking both *Shh* and *Smad4* were analysed. In contrast to the low expression in *Shh^{Δ/Δ}* forelimb buds (Fig. 2B, left panel), *Grem1* expression was lost from *Shh^{Δ/Δ} Smad4^{Δ/ΔM}* forelimb buds (Fig. 2B, right panel). These results showed that *Grem1* expression in the limb bud mesenchyme is positively regulated by both SHH and SMAD4-mediated signal transduction. Contrary to *Grem1*, *Shh* expression and signal transduction appeared normal (Fig. 2C and data not shown), whereas the AER-*Fgf8* expression domain was broadened and levels increased from ~E10.5 onward in *Smad4^{Δ/ΔM}* forelimb buds (Fig. 2D). This analysis showed that mesenchymal *Smad4* is either not required, or its functional inactivation occurred too late to disrupt establishment of the AER-*Fgf8* expression domain (Bénazet et al., 2009), in contrast to its direct requirement in the AER (Bénazet

and Zeller, unpublished). As the SHH/GREM1/AER-FGF signaling system terminated in wild-type limb buds, the expression of both *Shh* (Fig. 2E) and AER-*Fgfs* (Fig. 2F) persisted in *Smad4^{Δ/ΔM}* forelimb buds. Rather unexpected from previous analysis (Scherz et al., 2004; Verheyden and Sun, 2008), these results reveal that mesenchymal *Smad4* is required for correct termination of the epithelial-mesenchymal feedback signaling system. In agreement with the initially normal progression of limb bud development, no striking alterations in cell proliferation were apparent in *Smad4^{Δ/ΔM}* forelimb buds (supplementary material Fig. S3A). However, apoptosis of core mesenchymal cells was increased up to ~E11.5, whereas apoptosis in mutant handplates was suppressed because of the absence of the interdigit mesenchyme (supplementary material Fig. S3B; Fig. 3).

The spatiotemporal expression of the 5'-most *HoxD* and *HoxA* genes, which regulate limb bud patterning and outgrowth (reviewed by Zakany and Duboule, 2007) was not significantly altered up to E11.5 (data not shown). Fig. 3 shows the expression of select markers for the autopod, digit and interdigit territories. *Hoxa13* correctly delineated the presumptive autopod territory in mutant limb buds, but none of the putative digit primordia were outlined (Fig. 3A). *Cyp26b1* is normally expressed in the distal part of all digit primordia including the PFRs (Fig. 3B) (Yashiro et al., 2004). *Smad4^{Δ/ΔM}* forelimb buds lacked these PFR-like expression domains and *Cyp26b1* was largely confined to the anterior and posterior margins (Fig. 3B). *Dlx5* is normally expressed by the AER and interdigit mesenchyme in wild-type limb buds (Robledo et al., 2002), but its expression was confined largely to the AER in *Smad4^{Δ/ΔM}* forelimb buds (Fig. 3C). These results indicated that

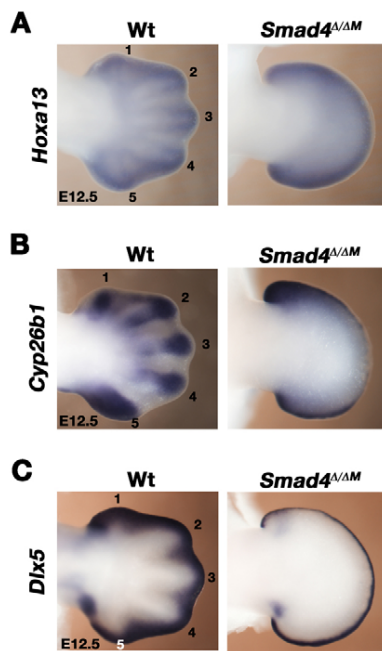


Fig. 3. Mesenchymal *Smad4* inactivation disrupts the spatial distribution of genes that mark specific autopod territories.

(A) *Hoxa13* expression at E12.5 (60 somites). In wild-type forelimb buds, the distal parts of the developing digits and perichondria express the highest levels of *Hoxa13* transcript. In *Smad4*^{Δ/ΔM} forelimb buds, *Hoxa13* expression is distally restricted but not localized to specific structures. (B) *Cyp26b1* marks the PFRs of all developing digit primordia in wild type, whereas no differential expression is apparent in *Smad4*^{Δ/ΔM} forelimb buds. (C) *Dix5* is expressed by the AER, subectodermal mesenchyme, and the interdigit mesenchyme in wild type, which is lacking in *Smad4*^{Δ/ΔM} forelimb buds. The wild-type digit ray primordia are labelled 1 (thumb) to 5 (little finger).

separation of the mutant mesenchyme into digit ray primordia and interdigit mesenchyme was disrupted in *Smad4*^{Δ/ΔM} autopods.

***Smad4* is required to induce formation of the *Sox9*-positive digit ray primordia**

Sox9 marks prechondrogenic progenitors from early limb bud stages onward. As *Sox9* prefigures the formation of all mesenchymal condensations that initiate chondrogenesis and give rise to the skeletal primordia (Bi et al., 1999; Akiyama et al., 2005), its expression was assessed (Fig. 4). Despite the early mesenchymal loss of *Smad4* and disruption of BMP signal transduction (Fig. 1B-D), the *Sox9* transcript distribution remained comparable to wild-type controls until at least E11.0 (Fig. 4A, left panels). These results indicated that SMAD4 is not required for activation and patterning of *Sox9* during the developmental period characterized by low BMP activity (Bénazet et al., 2009). The *Sox9*-positive progenitors in the proximal mesenchyme normally give rise to the cartilage elements of the scapula, stylopod (humerus) and zeugopod (radius and ulna). In wild-type forelimb buds, the *Sox9*-positive progenitors giving rise to the carpals and digit rays (metacarpals and phalanges) were apparent by ~E11.5, and the *Sox9*-positive digit ray primordia of all except digit 1 had formed by ~E12.25 (Fig. 4A, upper right panels) (Zhu et al., 2008). In *Smad4*^{Δ/ΔM} limb buds, the distalmost zone of *Sox9*-negative mesenchyme expanded (Fig. 4A, brackets) and *Sox9* expression

was progressively lowered (Fig. 4A, right-most lower panel). This downregulation was paralleled by a complete loss of the *Sox9*-positive primordia corresponding to carpals and digit rays (Fig. 4A,B). By E12.25, the characteristic *Sox9*-positive domains prefiguring all of the chondrogenic limb skeletal elements were largely lost from *Smad4*^{Δ/ΔM} limb buds (Fig. 4A, right-most panels). By E13.5, only very low *Sox9* expression remained in *Smad4*^{Δ/ΔM} limb buds, whereas *Sox9* was abundant in the PFRs and phalanges of all wild-type digits (supplementary material Fig. S4A). To gain further insight, OPT (Sharpe et al., 2002) was used in combination with iso-surface rendering for comparative analysis of the *Sox9* transcript distribution in wild-type and *Smad4*^{Δ/ΔM} forelimb buds. This analysis revealed thinning of the distal arch of *Sox9*-positive cells (Fig. 4B, brackets), whereas the proximal domain was enlarged in *Smad4*^{Δ/ΔM} forelimb buds (Fig. 4B, arrowheads; better seen in supplementary material Movie 1).

The requirement of *Smad4* for formation of the *Sox9*-positive digit rays could be transient, as evidenced by the kinetics of *Hoxa13*^{Cre/+}-mediated conditional inactivation of either one (*Smad4*^{Δ/ΔA13}) or both *Smad4* alleles (Fig. 4C, *Smad4*^{ΔA13/ΔA13}, supplementary material Fig. S4). Inactivation of *Smad4* using the *Hoxa13*^{Cre/+} knock-in allele (Scotti and Kmita, 2012) resulted in the progressive clearance of *Smad4* transcripts during autopod development and specific agenesis of the autopod skeleton (supplementary material Fig. S4B,C). The functional loss of *Smad4* should be faster in *Smad4*^{Δ/ΔA13} than *Smad4*^{ΔA13/ΔA13} forelimb buds, as two conditional alleles have to be inactivated and twice as much SMAD4 proteins cleared in the latter (Bénazet et al., 2009). As only one *Hoxa13* allele is functional in mouse embryos carrying the *Hoxa13*^{Cre/+} knock-in, we first established that formation of digit ray primordia was not altered in *Hoxa13*^{Cre/+} and *Hoxa13*^{Cre/+}*Smad4*^{ΔA13/+} forelimb buds (Fig. 4C). However, only the two posteriormost digit ray primordia were apparent in *Smad4*^{Δ/ΔA13} forelimb buds, whereas the primordia of digit rays 2-5 formed in all *Smad4*^{ΔA13/ΔA13} forelimb buds (Fig. 4D). These results indicated that morphogenesis of anterior digit ray primordia could require *Smad4* for longer or at a later stage than posterior primordia.

SOX9-positive mesenchymal progenitors fail to aggregate and initiate chondrogenic differentiation of all cartilage elements in *Smad4*^{Δ/ΔM} limb buds

As whole-mount RNA in situ hybridization analysis did not provide cellular resolution, the SOX9 protein distribution was analysed on serial sections of forelimb buds (Fig. 5, red fluorescence). At E10.5, scattered SOX9-positive mesenchymal cells were detected mainly in the core of both wild-type and *Smad4*^{Δ/ΔM} forelimb buds (Fig. 5A,B). By E11.75, SOX9-positive progenitors condensed to initiate formation of the cartilage elements of the humerus and the ulna/radius and the posterior digit 4 in wild-type limb buds (Fig. 5C) (Zhu et al., 2008). In *Smad4*^{Δ/ΔM} forelimb buds, a small proximal condensation was apparent (Fig. 5D, arrowhead), but most SOX9-positive cells remained loose and in a pattern reminiscent of the *Sox9*-positive distal arch (compare Fig. 5D and Fig. 4A). During subsequent development, no organized mesenchymal condensations and cartilage elements formed in *Smad4*^{Δ/ΔM} forelimb buds (Fig. 5E-H). Rather, the small proximal condensation disappeared and SOX9-positive cells dispersed throughout the distal mesenchyme (Fig. 5F,H). Taken together, this analysis indicated that aggregation of the SOX9-positive progenitors to initiate chondrogenic differentiation and

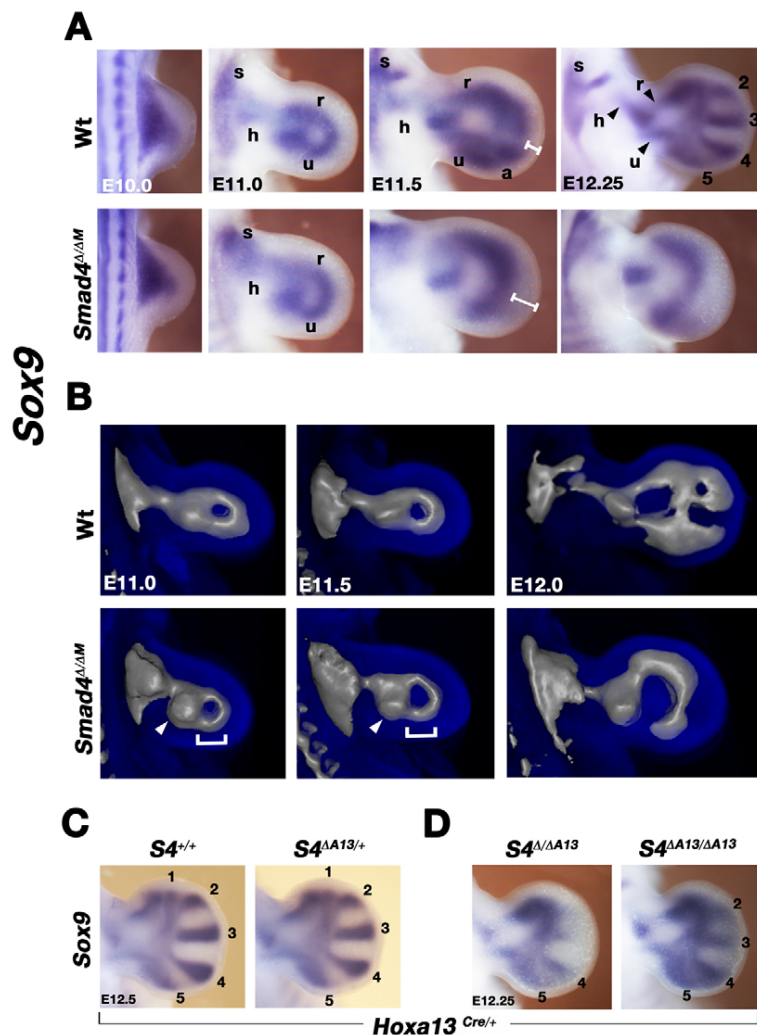


Fig. 4. Induction of Sox9-positive digit progenitors and maintenance of Sox9 expression are disrupted in *Smad4*^{Δ/ΔM} forelimb buds. (A) Spatial distribution of Sox9 transcript in wild-type (upper panels) and *Smad4*-deficient forelimb buds. (B) Iso-surface rendering of the Sox9 expression domains by OPT analysis. This reveals the progressive thinning of the distal arch (white brackets) and absence of Sox9-positive digit primordia in *Smad4*-deficient forelimb buds. By contrast, the Sox9 expression domain probably corresponding to the zeugopod appears thickened (white arrowheads). (C) Heterozygosity for the *Hoxa13*^{Cre/+} allele alone (*S4*^{+/+}) or in combination with inactivation of one *Smad4* allele (*S4*^{ΔA13/+}) has no effect on Sox9-positive digit ray primordia. (D) *Hoxa13*^{Cre/+}-mediated conditional inactivation of either one (*S4*^{ΔA13}) or both *Smad4* alleles (*S4*^{ΔA13/ΔA13}) during autopod development reveals the differential effects on posterior and anterior digit ray primordia. E10.0: 30-32 somites; E11.0: 41 somites; E11.5: 44 somites; E12.0: 50 somites. E12.25-12.5: 53-57 somites. Primordia are indicated as follows: 1-5, primordia of digit rays 1-5; a, autopod; h, humerus; r, radius; s, scapula; u, ulna;

formation of cartilage elements was disrupted in *Smad4*-deficient forelimb buds.

To gain further insight into the underlying cellular defects, wild-type and mutant mesenchymal cells were dissociated from limb buds at E11.5 and high-density cultures were used to assess their chondrogenic differential potential (Barna and Niswander, 2007). A hallmark of chondrogenic differentiation is the transcriptional activation of *Col2a1*, a direct transcriptional target of SOX9 that encodes the pro-alpha1(II) chain of COL type II, which is cartilage-specific (Bell et al., 1997; Lefebvre et al., 1997). In wild-type mesenchymal cultures, cells aggregated and compacted to form the typical cell-dense condensations often paralleled by reduced SOX9 expression, and the onset of chondrogenesis was revealed by abundant COL type II (Fig. 6A). By contrast, no COL type II was detected in areas of less densely packed cells (Fig. 6A, enlargements), which revealed that chondrogenesis was initiated in regions with high mesenchymal cell density, i.e. after cells had aggregated. By contrast, slightly lower levels of SOX9 were consistently detected in mesenchymal cells isolated from *Smad4*^{Δ/ΔM} forelimb buds, which failed to aggregate and produce COL type II fibres (Fig. 6B). This failure of *Smad4*-deficient mesenchymal cells to aggregate appeared more severe than the effects of Noggin-mediated inhibition of BMP activity in limb bud mesenchymal

cells, which aggregate but fail to undergo subsequent compaction and initiation of chondrogenesis (Barna and Niswander, 2007). To gain further insight, we selectively inhibited BMP type I receptors and thereby BMP signal transduction using Dorsomorphin (Yu et al., 2008), which disrupted condensation and COL type II expression of wild-type cells similar to *Smad4*^{Δ/ΔM} cells (compare supplementary material Fig. S5B and Fig. 6B). Inhibiting TGFβ receptors with the selective antagonist SB431542 (Inman et al., 2002) blocked cell aggregation and COL type II deposition to a similar extent (supplementary material Fig. S5B) (Karamboulas et al., 2010). These results indicated that BMP and TGFβ signal transduction were both required for initiating chondrogenesis of mesenchymal progenitors in culture.

As these experiments revealed striking effects on deposition of extracellular COL type II fibres, the extent to which *Col2a1* expression might be altered in *Smad4*^{Δ/ΔM} forelimb buds was determined (Fig. 7A). At E11.5, the *Col2a1* transcript distributions in wild-type and mutant forelimb buds were similar and comparable to *Sox9* at this stage (compare Fig. 7A, left panels and Fig. 4A). As autopod development progressed, *Col2a1* was expressed abundantly by all skeletal elements including digit rays in wild-type limb buds (Fig. 7A, upper panels). By contrast, *Col2a1* expression remained diffuse and was progressively lost

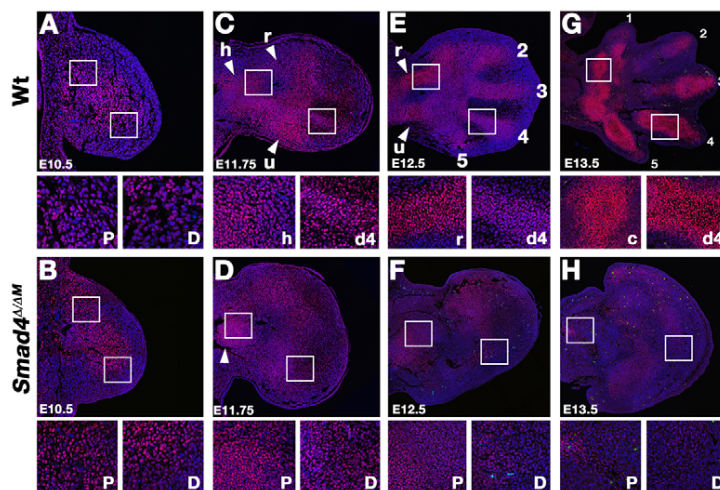


Fig. 5. SOX9 protein distribution in wild-type and *Smad4*^{Δ/ΔM} forelimb buds. (A-H) The distribution of nuclear SOX9 protein (red) was determined on serial histological sections of limb buds from E10.5 to E13.5. Nuclei were counterstained using the DNA dye Hoechst (blue). (A,C,E,G) Wild-type forelimb buds. (B,D,F,H) In *Smad4*^{Δ/ΔM} forelimb buds, the SOX9-positive cells fail to aggregate and initiate mesenchymal condensations. Only a small but transient proximal condensation is formed (arrowhead in D). White rectangles indicate the positions of the enlargements shown below. 1-5, digit ray primordia 1-5; c, carpal primordia; D, distal; d4, digit 4; h, humerus; P, proximal; r, radius; u, ulna.

from *Smad4*^{Δ/ΔM} forelimb buds (Fig. 7A, lower panels). Indeed, high levels of COL type II protein were detected in all chondrogenic primordia of the skeletal elements in wild-type limb buds, whereas only few scattered positive clusters were detected in *Smad4*^{Δ/ΔM} limb buds (Fig. 7B). Taken together, this analysis (Figs 5-7) revealed the disruption of chondrogenesis and absence of all cartilage elements prefiguring the limb skeleton in *Smad4*^{Δ/ΔM} forelimb buds.

To determine the extent to which *Smad4*-deficient mesenchymal cells might acquire non-chondrogenic fates, genes marking other mesenchymal lineages were analysed. Collagen type I (COL type I) is expressed by diverse connective tissues such as skin, tendons, ligaments and bones, and muscle-associated connective tissues (see e.g. ten Berge et al., 2008). In wild-type limb buds, *Colla2* was detected first in the proximal mesenchyme (Fig. 7C, E11.5). At later stages, *Colla2* outlined the forming perichondria and tendons (Fig. 7C, arrowheads). In *Smad4*^{Δ/ΔM} forelimb buds, *Colla2* transcript and protein were detected throughout the mesenchyme (Fig. 7C,D, lower panels). COL type I localized to the perichondrium and developing dermis in wild type (Fig. 7D, upper panels), whereas its expression appeared more widespread and disorganized in *Smad4*^{Δ/ΔM} forelimb buds (Fig. 7D, lower panels). As decorin (*Dcn*) regulates the assembly of collagen fibres (Danielson et al., 1997), its expression was analysed. In wild-type limb buds, the initially rather diffuse *Dcn* expression became excluded from the chondrogenic cores of all developing cartilage elements including digit rays (Fig. 8A, upper panels and data not shown). By contrast, *Dcn* expression was enhanced and persisted throughout the mesenchyme of *Smad4*^{Δ/ΔM} forelimb buds (Fig. 8A, lower panels; supplementary material Fig. S6A). Possible effects on *Dcn* expression were also assessed in forelimb buds lacking both mesenchymal *Bmp2* and *Bmp4*, as the two posteriormost digit ray primordia are not formed (Fig. 8B) (Bandyopadhyay et al., 2006). Analogous to the *Smad4* deficiency (Fig. 8A), the absence of these two digit ray primordia results in uniformly increased expression of *Dcn* in the posterior mesenchyme of limb buds lacking both *Bmps* (Fig. 8B, posterior region indicated by a bracket). The striking similarity of these alterations indicates that formation of the posterior *Sox9*-positive digit ray primordia and restriction of *Dcn* expression depends on BMP signal transduction that is mediated by SMAD4.

In addition, the expression of the transcriptional regulator scleraxis (*Scx*, marking tendon and ligament progenitors)

(Schweitzer et al., 2001) was also increased in *Smad4*^{Δ/ΔM} forelimb buds (supplementary material Fig. S6B). While *Scx* marked both dorsal and ventral tendons in wild-type limb buds (Fig. 8C, upper panels), its expression was upregulated and diffuse in *Smad4*^{Δ/ΔM} forelimb buds (Fig. 8C, lower panels). This was paralleled by widespread and diffuse expression of *Fjx1*, which normally marks the attachment points of the forming tendons and the developing joints (Rock et al., 2005), in *Smad4*-deficient forelimb buds (supplementary material Fig. S6C). In addition to tendons and ligaments, limb skeletal muscles form in concert with the limb skeletal elements. Analysis of the *MyoD* distribution (marking all limb muscle primordia) (Francis-West et al., 2003) showed that dysplastic skeletal muscles were present in the flank and proximal part of *Smad4*-deficient forelimb buds, whereas the distal mesenchyme was devoid of *MyoD*-expressing cells (supplementary

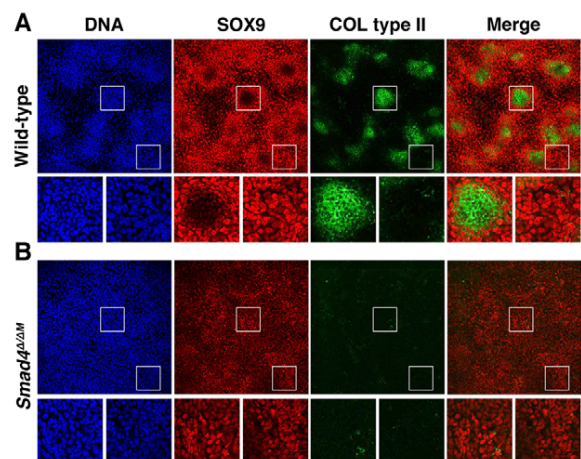


Fig. 6. Chondrogenic potential of wild-type and *Smad4*-deficient mesenchymal cells. (A) Wild-type limb bud mesenchymal cells (isolated at E11.5) form chondrogenic condensations after 48 hours in high-density culture. The peripheral cells of the chondrogenic condensations express the highest levels of SOX9 (red fluorescence). Cells in the core often express lower levels of SOX9 and produce COL type II (green fluorescence). (B) By contrast, *Smad4*^{Δ/ΔM} mesenchymal cells fail to aggregate and produce COL type II. Cell nuclei were labelled by Hoechst (blue fluorescence). White rectangles indicate the positions of the enlargements shown below.

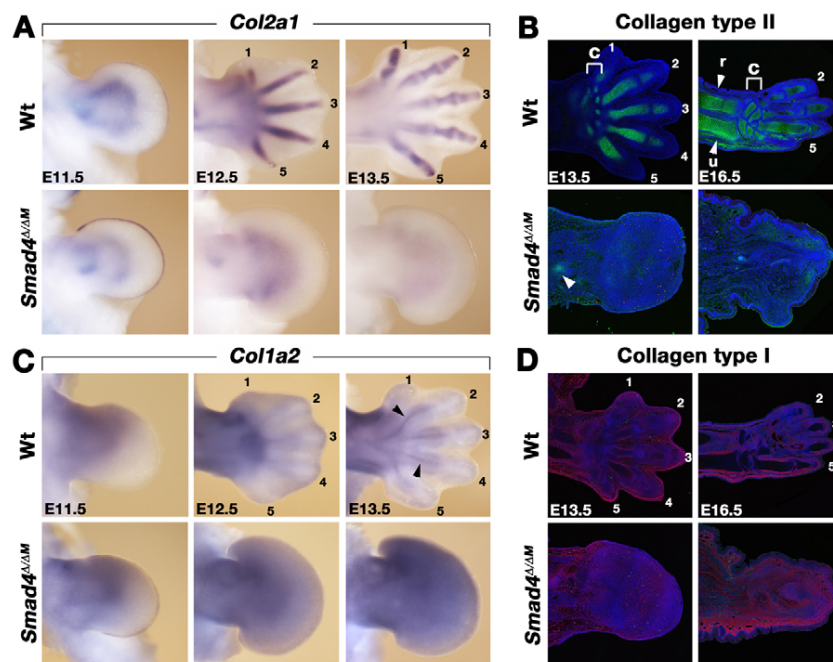


Fig. 7. Loss of cartilage-specific and increase of connective tissue-type collagens in *Smad4*^{Δ/ΔM} forelimb buds. (A) *Col2a1* transcript distribution in wild-type and *Smad4*^{Δ/ΔM} forelimb buds. In *Smad4*^{Δ/ΔM} forelimb buds, mesenchymal *Col2a1* expression in the mesenchyme is similar to that of wild type up to E11.5, but is lost during subsequent stages. The *Col2a1* upregulation in the AER of *Smad4*^{Δ/ΔM} forelimb buds was reproducibly detected at E11.5. (B) The COL type II distribution (green fluorescence) was assessed on serial histological sections. At E16.5, COL type II marks all developing limb skeletal elements. In *Smad4*^{Δ/ΔM} forelimb buds, a small but transient cluster positive for COL type II was always detected (arrowheads). (C) *Col1a2* expression in wild-type forelimb buds marks connective tissue, perichondria and developing tendons (arrowheads, upper-right panel). In *Smad4*^{Δ/ΔM} forelimb buds, *Col1a2* expression becomes increasingly widespread and diffuse (lower panels). (D) The COL type I distribution (red fluorescence) was assessed on serial histological sections. In wild-type forelimb buds, COL type I outlines the perichondria and dermis. The developing dorsal and ventral tendons are not apparent, as sections through the core mesenchyme are shown. In *Smad4*^{Δ/ΔM} forelimb buds, most mesenchyme expresses this connective tissue-type collagen by E16.5. Labelling of primordia: 2-5, digit rays c, carpal; h, humerus; r, radius; u, ulna.

material Fig. S6D). Taken together, this analysis revealed the rather diffuse expression of genes marking diverse non-chondrogenic lineages and general disruption of tissue organization in *Smad4*^{Δ/ΔM} forelimb buds, which pointed to diversion of chondrogenic to loose and non-specific connective tissue (Fig. 8D).

DISCUSSION

Our genetic analysis of mesenchymal *Smad4* during mouse limb bud development uncovers its dual requirement for initiating: (1) formation of the *Sox9*-positive digit ray primordia; and (2) aggregation and chondrogenic differentiation of all *Sox9*-positive prechondrogenic progenitors that give rise to the cartilage elements of the future limb skeleton (Fig. 8D). SMAD4 is essential to induce chondrogenesis because cell aggregation, which is the first step toward chondrogenic differentiation, is disrupted and mutant progenitors remain scattered in *Smad4*^{Δ/ΔM} forelimb buds (Fig. 8D) (see also Pizette and Niswander, 2000; Barna and Niswander, 2007). By contrast, the expression of *Sox9*, which prefigures the primordia of the stylopod and zeugopod, is normal up to at least E11.0 in *Smad4*^{Δ/ΔM} forelimb buds. A role of SMAD4 in activation of *Sox9* expression in early limb buds cannot be formally excluded, as the protein is only cleared around the time *Sox9* is activated in *Smad4*^{Δ/ΔM} forelimb buds. Nevertheless, the *Smad4*-independent phase of *Sox9* expression coincides well with the period of low BMP activity in mouse limb buds (Bénazet et al., 2009), which

corroborates the proposal that the spatiotemporal regulation of *Sox9* expression does not require SMAD4-mediated signal transduction before handplate formation (this study). Indeed, it has been proposed that BMPs inhibit *Sox9* expression and initiation of chondrogenic differentiation in the mesenchyme of early limb buds; an effect that can be alleviated by short-term exposure to TGFβ signaling in culture (Karamboulas et al., 2010). However, inhibition of BMP or TGFβ signal transduction in vitro disrupted chondrogenesis in a similar way to the genetic *Smad4* deficiency, but did not cause complete loss of SOX9 (this study).

In addition to *Sox9*, the mesenchymal expression of the early chondrocyte marker *Col2a1* is activated normally in *Smad4*^{Δ/ΔM} forelimb buds. During distal progression of limb bud development, *Col2a1* expression is lost concurrent with the failure to refine SOX9 protein distribution, as expected from direct transcriptional regulation of *Col2a1* by SOX9 (Bell et al., 1997; Lefebvre et al., 1997). In *Smad4*^{Δ/ΔM} forelimb buds, the progressive loss of *Sox9* and *Col2a1* was paralleled by widespread and diffuse expression of markers for other lineages and a general absence of tissue organization and differentiation. Therefore, SMAD4 appears to function in signaling networks that restrict non-chondrogenic progenitors and connective tissue lineages. In agreement with the diffuse *Scx* expression in *Smad4*^{Δ/ΔM} forelimb buds, inhibition of BMP signaling results in ectopic *Scx* expression without the formation of additional tendons (Schweitzer et al., 2001). However,

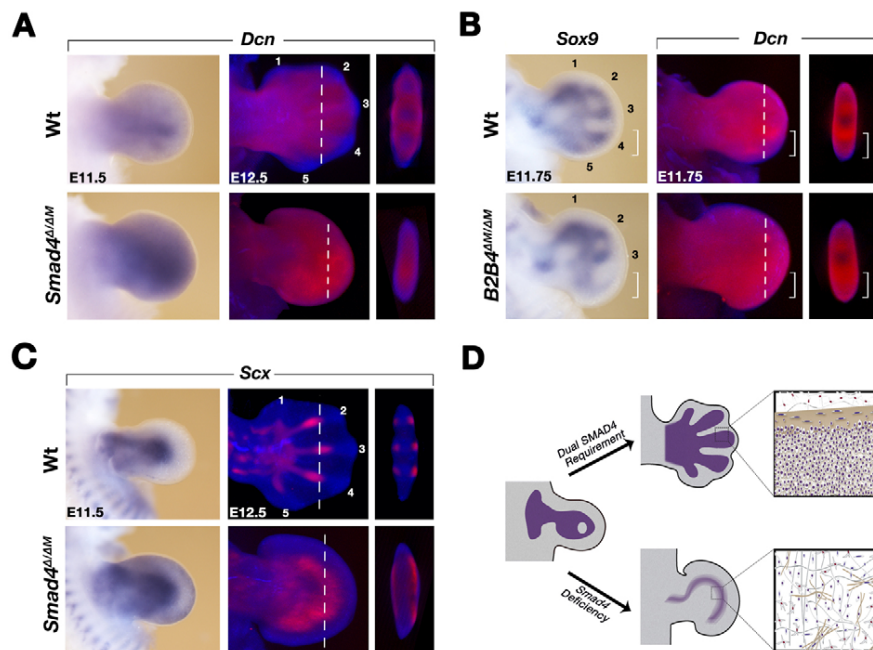


Fig. 8. General loss of tissue organization results in diversion towards fascia-like connective tissue in *Smad4*^{Δ/ΔM} limb buds. (A) *Dcn* transcript distribution in wild-type and *Smad4*-deficient forelimb buds visualized by brightfield microscopy (left) and OPT analysis (right panels). The positions of the virtual OPT cross-sections are indicated by the broken white lines in the middle panels. (B) *Prx1*-Cre mediated inactivation of *Bmp2* and *Bmp4* in the forelimb bud mesenchyme (*B2B4*^{ΔM/ΔM}). Left panels show *Sox9* expression at E11.75 (51 somites). Middle and right panels show OPT analysis of *Dcn* distribution at E11.75. White brackets mark the relevant posterior part of *B2B4*^{ΔM/ΔM} and wild-type forelimb buds. (C) *Scx* transcript distribution in wild-type and *Smad4*-deficient forelimb buds, which becomes normally restricted to the forming tendons by E12.5. OPT analysis reveals the diffuse *Scx* expression extending into the core mesenchyme of *Smad4*^{Δ/ΔM} forelimb buds. (D) SMAD4 is required: (1) for digit ray formation in the distal mesenchyme; and (2) to induce aggregation and chondrogenic differentiation of all *Sox9*-positive mesenchymal progenitors. In *Smad4*^{Δ/ΔM} limb buds, mutant mesenchymal cells remain loose and divert toward non-specific connective tissue lineages.

as both *Colla1* and *Colla2* are positively regulated by SCX (Cserjesi et al., 1995), the ectopic *Scx* expression in *Smad4*^{Δ/ΔM} forelimb buds could contribute to the increased COL type I expression (this study). These molecular changes and the complete lack of tissue organization in *Smad4*-deficient limb buds (Fig. 8D) indicate that SMAD4 functions in the morphoregulatory networks that pattern diverse limb bud mesenchymal lineages and/or orchestrate coordinated tissue differentiation. Taken together, these studies uncover the recurrent differential requirement of SMAD4-mediated canonical BMP/TGFβ signal transduction during specification and aggregation of SOX9-positive prechondrogenic progenitors and initiation of their chondrogenic differentiation (Fig. 8D).

Although formation of the *Sox9*-positive primordia of the stylopod and zeugopod appears *Smad4*-independent, the induction of the *Sox9*-positive digit ray primordia depends critically on *Smad4* and increased BMP activity (Bandyopadhyay et al., 2006; Bénazet et al., 2009; Lopez-Rios et al., 2012; this study). As the proximal *Sox9*-positive domains are enlarged, the mutant prechondrogenic cells may contribute preferentially to proximal primordia as evidenced by thinning of the distal arch in *Smad4*^{Δ/ΔM} forelimb buds (this study). Such a differential requirement of *Smad4* might be of evolutionary relevance as the autopod and digits of tetrapod limbs are so-called neomorphic structures, whose development may have relied on co-opting novel gene-regulatory networks (reviewed by Woltering and Duboule, 2010). Our analysis indicates that limb bud development and formation of

Sox9-positive digit ray primordia become *Smad4* dependent as BMP activity rises owing to self-termination of the SHH/Grem1/AER-FGF signaling system (Scherz et al., 2004; Verheyden and Sun, 2008; Benazet et al., 2009). During this developmental period, differential BMP signaling appears to determine digit identities in both chicken and mouse (Dahn and Fallon, 2000; Suzuki et al., 2008; Witte et al., 2010). As extensive genetic analysis of TGFβ signaling in mouse embryos has not produced similar phenotypes (see e.g. Sanford et al., 1997; Seo and Serra, 2007), SMAD4-mediated BMP signal transduction is likely to be predominant during these advanced stages of digit ray primordia growth and patterning. It has been proposed that the progenitors giving rise to the digit ray primordia are recruited from the distal limb bud mesenchyme (Suzuki et al., 2008), which is defective in *Smad4*^{Δ/ΔM} forelimb buds as revealed by the increasing gap of *Sox9*-negative cells in the distal mesenchyme (this study). In addition, temporally controlled *Smad4* inactivation in the autopod provided evidence for its possible differential requirement for posterior and anterior digit ray primordia. A region free of the BMP antagonist GREM1 is generated within the posterior limb bud mesenchyme by the population of *Shh* descendants, which is refractory to *Grem1* expression and increases as limb bud development progresses (Scherz et al., 2004). These results together with the differential requirement observed in this study indicate that BMP activity might first rise in the posterior mesenchyme, where *Bmp2* and *Bmp4* are co-expressed and required for digit ray formation (Bandyopadhyay et al., 2006). The

mechanism that controls BMP-dependent formation of the digit ray primordia was recently uncovered (Lopez-Rios et al., 2012). Inactivation of *Gli3* in the developing autopod promoted cell cycle entry and delayed the exit of digit progenitors to chondrogenesis due to prolonged GREM1-mediated BMP-antagonism in the anterior limb bud mesenchyme. Taken together, this indicates that two distinct mechanisms regulate digit ray formation in the posterior and anterior handplate via BMP-dependent SMAD4-mediated signal transduction. The spatiotemporal requirements of BMPs and SMAD4 for posterior and anterior digit ray primordia (Bandyopadhyay et al., 2006; Lopez-Rios et al., 2012; this study) is apparently at odds with the genetic analysis of the temporal requirement of *Shh* during mouse limb bud development (Zhu et al., 2008). This analysis showed that digit ray primordia form with alternating posterior to anterior sequence (starting with d4, d2, d5 and ending with d3), while digit 1 forms in a SHH-independent manner. However, these apparent discrepancies are resolved if BMPs and SMAD4 were transiently required to initiate a posterior and anterior mesenchymal condensation that would subsequently give rise to the primordia of digits 4 and 5 and digits 2 and 3, respectively, following the sequence defined by Zhu et al. (Zhu et al., 2008).

Finally, BMPs are widely used to induce chondrogenesis in ex vivo models of cartilage and bone engineering, but outcomes are often conflicting (Jiang et al., 2010; Sanchez-Adams and Athanasiou, 2012). In light of the complex regulation of chondrogenesis during limb bud development, ex vivo developmental engineering of cartilage and endochondral bone (Scotti et al., 2010) will probably require activation and inhibition of BMP signal transduction in a spatiotemporally controlled manner as revealed by the present study. In particular, this study highlights the temporal kinetics of the SMAD4 requirement during formation of the *Sox9*-positive digit ray primordia and its more general role in inducing aggregation of the mesenchymal progenitors during the onset of chondrogenesis, which is key to developmentally engineering cartilage and bone.

Acknowledgements

We are grateful to Chuxia Deng for providing us with the *Smad4* conditional allele and to Georg Holländer for colony founder mice, to Marie Kmita and Martina Scotti for providing us with the *Hoxa13*-Cre knock-in mouse strain, and to Philippa Francis-West and Manfred Gesser for providing plasmids for RNA in situ hybridization probes. We are grateful to Angelika Offinger and Cornelia Meyer for excellent mouse care and to Chris Müller-Thompson for help in preparing this manuscript. Group members are thanked for helpful input into the manuscript.

Funding

This study was made possible by grants from the Swiss National Science Foundation [31003A-130803 to R.Z.], a EU Marie Curie International Incoming Fellowship [273304 to A.N.], a SystemsX.ch iPhD grant [20101078 to E.U. and R.Z.] and support by the University of Basel.

Competing interests statement

The authors declare no competing financial interests.

Supplementary material

Supplementary material available online at <http://dev.biologists.org/lookup/suppl/doi:10.1242/dev.084822/-DC1>

References

Ahn, K., Mishina, Y., Hanks, M. C., Behringer, R. R. and Crenshaw, E. B., 3rd (2001). BMP-1A signaling is required for the formation of the apical ectodermal ridge and dorsal-ventral patterning of the limb. *Development* **128**, 4449-4461.

Akiyama, H., Kim, J. E., Nakashima, K., Balmes, G., Iwai, N., Deng, J. M., Zhang, Z., Martin, J. F., Behringer, R. R., Nakamura, T. et al. (2005). Osteochondroprogenitor cells are derived from *Sox9* expressing precursors. *Proc. Natl. Acad. Sci. USA* **102**, 14665-14670.

Bandyopadhyay, A., Tsuji, K., Cox, K., Harfe, B. D., Rosen, V. and Tabin, C. J. (2006). Genetic analysis of the roles of BMP2, BMP4, and BMP7 in limb patterning and skeletogenesis. *PLoS Genet.* **2**, e216.

Barna, M. and Niswander, L. (2007). Visualization of cartilage formation: insight into cellular properties of skeletal progenitors and chondrodysplasia syndromes. *Dev. Cell* **12**, 931-941.

Bastida, M. F., Delgado, M. D., Wang, B., Fallon, J. F., Fernandez-Teran, M. and Ros, M. A. (2004). Levels of *Gli3* repressor correlate with *Bmp4* expression and apoptosis during limb development. *Dev. Dyn.* **231**, 148-160.

Bell, D. M., Leung, K. K., Wheatley, S. C., Ng, L. J., Zhou, S., Ling, K. W., Sham, M. H., Koopman, P., Tam, P. P. and Cheah, K. S. (1997). *Sox9* directly regulates the type-II collagen gene. *Nat. Genet.* **16**, 174-178.

Bénazet, J. D., Bischofberger, M., Tiecke, E., Gonçalves, A., Martin, J. F., Zuniga, A., Naef, F. and Zeller, R. (2009). A self-regulatory system of interlinked signaling feedback loops controls mouse limb patterning. *Science* **323**, 1050-1053.

Bi, W., Deng, J. M., Zhang, Z., Behringer, R. R. and de Crombrughe, B. (1999). *Sox9* is required for cartilage formation. *Nat. Genet.* **22**, 85-89.

Brunet, L. J., McMahon, J. A., McMahon, A. P. and Harland, R. M. (1998). Noggin, cartilage morphogenesis, and joint formation in the mammalian skeleton. *Science* **280**, 1455-1457.

Chu, G. C., Dunn, N. R., Anderson, D. C., Oxburgh, L. and Robertson, E. J. (2004). Differential requirements for *Smad4* in TGFbeta-dependent patterning of the early mouse embryo. *Development* **131**, 3501-3512.

Cserjesi, P., Brown, D., Ligon, K. L., Lyons, G. E., Copeland, N. G., Gilbert, D. J., Jenkins, N. A. and Olson, E. N. (1995). Scleraxis: a basic helix-loop-helix protein that prefigures skeletal formation during mouse embryogenesis. *Development* **121**, 1099-1110.

Dahn, R. D. and Fallon, J. F. (2000). Interdigital regulation of digit identity and homeotic transformation by modulated BMP signaling. *Science* **289**, 438-441.

Danielson, K. G., Baribault, H., Holmes, D. F., Graham, H., Kadler, K. E. and Iozzo, R. V. (1997). Targeted disruption of decorin leads to abnormal collagen fibril morphology and skin fragility. *J. Cell Biol.* **136**, 729-743.

Feng, X. H. and Derynck, R. (2005). Specificity and versatility in tgfbeta signaling through Smads. *Annu. Rev. Cell Dev. Biol.* **21**, 659-693.

Francis-West, P. H., Antoni, L. and Anakwe, K. (2003). Regulation of myogenic differentiation in the developing limb bud. *J. Anat.* **202**, 69-81.

Gros, J., Hu, J. K., Vinegoni, C., Feruglio, P. F., Weissleder, R. and Tabin, C. J. (2010). WNT5A/JNK and FGF/MAPK pathways regulate the cellular events shaping the vertebrate limb bud. *Curr. Biol.* **20**, 1993-2002.

Inman, G. J., Nicolás, F. J., Callahan, J. F., Harling, J. D., Gaster, L. M., Reith, A. D., Laping, N. J. and Hill, C. S. (2002). SB-431542 is a potent and specific inhibitor of transforming growth factor-beta superfamily type I activin receptor-like kinase (ALK) receptors ALK4, ALK5, and ALK7. *Mol. Pharmacol.* **62**, 65-74.

Jiang, Y., Chen, L. K., Zhu, D. C., Zhang, G. R., Guo, C., Qi, Y. Y. and Ouyang, H. W. (2010). The inductive effect of bone morphogenetic protein-4 on chondral-lineage differentiation and in situ cartilage repair. *Tissue Eng. Part A* **16**, 1621-1632.

Karamboulas, K., Dranse, H. J. and Underhill, T. M. (2010). Regulation of BMP-dependent chondrogenesis in early limb mesenchyme by TGFbeta signals. *J. Cell Sci.* **123**, 2068-2076.

Kobayashi, T., Lyons, K. M., McMahon, A. P. and Kronenberg, H. M. (2005). BMP signaling stimulates cellular differentiation at multiple steps during cartilage development. *Proc. Natl. Acad. Sci. USA* **102**, 18023-18027.

Lefebvre, V., Huang, W., Harley, V. R., Goodfellow, P. N. and de Crombrughe, B. (1997). *Sox9* is a potent activator of the chondrocyte-specific enhancer of the pro alpha1(I) collagen gene. *Mol. Cell Biol.* **17**, 2336-2346.

Logan, M., Martin, J. F., Nagy, A., Lobe, C., Olson, E. N. and Tabin, C. J. (2002). Expression of Cre Recombinase in the developing mouse limb bud driven by a *Prlx* enhancer. *Genesis* **33**, 77-80.

Lopez-Rios, J., Speziale, D., Robay, D., Scotti, M., Osterwalder, M., Nusspaumer, G., Galli, A., Holländer, G. A., Kmita, M. and Zeller, R. (2012). *GLI3* constrains digit number by controlling both progenitor proliferation and BMP-dependent exit to chondrogenesis. *Dev. Cell* **22**, 837-848.

Lorda-Diez, C. I., Montero, J. A., Diaz-Mendoza, M. J., Garcia-Porrero, J. A. and Hurlé, J. M. (2011). Defining the earliest transcriptional steps of chondrogenic progenitor specification during the formation of the digits in the embryonic limb. *PLoS ONE* **6**, e24546.

Maatouk, D. M., Choi, K. S., Bouldin, C. M. and Harfe, B. D. (2009). In the limb AER *Bmp2* and *Bmp4* are required for dorsal-ventral patterning and interdigital cell death but not limb outgrowth. *Dev. Biol.* **327**, 516-523.

Merino, R., Macías, D., Gañan, Y., Rodríguez-Leon, J., Economides, A. N., Rodríguez-Esteban, C., Izpisua-Belmonte, J. C. and Hurlé, J. M. (1999). Control of digit formation by activin signaling. *Development* **126**, 2161-2170.

Michos, O., Panman, L., Vintersten, K., Beier, K., Zeller, R. and Zuniga, A. (2004). Gremlin-mediated BMP antagonism induces the epithelial-mesenchymal feedback signaling controlling metanephric kidney and limb organogenesis. *Development* **131**, 3401-3410.

Nissim, S., Hasso, S. M., Fallon, J. F. and Tabin, C. J. (2006). Regulation of Gremlin expression in the posterior limb bud. *Dev. Biol.* **299**, 12-21.

- Ovchinnikov, D. A., Selever, J., Wang, Y., Chen, Y. T., Mishina, Y., Martin, J. F. and Behringer, R. R. (2006). BMP receptor type IA in limb bud mesenchyme regulates distal outgrowth and patterning. *Dev. Biol.* **295**, 103-115.
- Pajni-Underwood, S., Wilson, C. P., Elder, C., Mishina, Y. and Lewandoski, M. (2007). BMP signals control limb bud interdigital programmed cell death by regulating FGF signaling. *Development* **134**, 2359-2368.
- Pan, Q., Yu, Y., Chen, Q., Li, C., Wu, H., Wan, Y., Ma, J. and Sun, F. (2008). Sox9, a key transcription factor of bone morphogenetic protein-2-induced chondrogenesis, is activated through BMP pathway and a CCAAT box in the proximal promoter. *J. Cell. Physiol.* **217**, 228-241.
- Panman, L., Galli, A., Lagarde, N., Michos, O., Soete, G., Zuniga, A. and Zeller, R. (2006). Differential regulation of gene expression in the digit forming area of the mouse limb bud by SHH and gremlin 1/FGF-mediated epithelial-mesenchymal signaling. *Development* **133**, 3419-3428.
- Pizette, S. and Niswander, L. (2000). BMPs are required at two steps of limb chondrogenesis: formation of prechondrogenic condensations and their differentiation into chondrocytes. *Dev. Biol.* **219**, 237-249.
- Pizette, S., Abate-Shen, C. and Niswander, L. (2001). BMP controls proximodistal outgrowth, via induction of the apical ectodermal ridge, and dorsoventral patterning in the vertebrate limb. *Development* **128**, 4463-4474.
- Probst, S., Kraemer, C., Demougin, P., Sheth, R., Martin, G. R., Shiratori, H., Hamada, H., Iber, D., Zeller, R. and Zuniga, A. (2011). SHH propagates distal limb bud development by enhancing CYP26B1-mediated retinoic acid clearance via AER-FGF signaling. *Development* **138**, 1913-1923.
- Roark, E. F. and Greer, K. (1994). Transforming growth factor-beta and bone morphogenetic protein-2 act by distinct mechanisms to promote chick limb cartilage differentiation in vitro. *Dev. Dyn.* **200**, 103-116.
- Robledo, R. F., Rajan, L., Li, X. and Lufkin, T. (2002). The Dlx5 and Dlx6 homeobox genes are essential for craniofacial, axial, and appendicular skeletal development. *Genes Dev.* **16**, 1089-1101.
- Rock, R., Heinrich, A. C., Schumacher, N. and Gessler, M. (2005). Fjx1: a notch-inducible secreted ligand with specific binding sites in developing mouse embryos and adult brain. *Dev. Dyn.* **234**, 602-612.
- Sanchez-Adams, J. and Athanasiou, K. A. (2012). Dermis isolated adult stem cells for cartilage tissue engineering. *Biomaterials* **33**, 109-119.
- Sanford, L. P., Ormsby, I., Gittenberger-de Groot, A. C., Sariola, H., Friedman, R., Boivin, G. P., Cardell, E. L. and Doetschman, T. (1997). TGFbeta2 knockout mice have multiple developmental defects that are non-overlapping with other TGFbeta knockout phenotypes. *Development* **124**, 2659-2670.
- Scherz, P. J., Harfe, B. D., McMahon, A. P. and Tabin, C. J. (2004). The limb bud Shh-Fgf feedback loop is terminated by expansion of former ZPA cells. *Science* **305**, 396-399.
- Schweitzer, R., Chung, J. H., Murtaugh, L. C., Brent, A. E., Rosen, V., Olson, E. N., Lassar, A. and Tabin, C. J. (2001). Analysis of the tendon cell fate using Scleraxis, a specific marker for tendons and ligaments. *Development* **128**, 3855-3866.
- Scotti, C., Tonarelli, B., Papadimitropoulos, A., Scherberich, A., Schaeren, S., Schauerte, A., Lopez-Rios, J., Zeller, R., Barbero, A. and Martin, I. (2010). Recapitulation of endochondral bone formation using human adult mesenchymal stem cells as a paradigm for developmental engineering. *Proc. Natl. Acad. Sci. USA* **107**, 7251-7256.
- Scotti, M. and Kmita, M. (2012). Recruitment of 5' Hoxa genes in the allantois is essential for proper extra-embryonic function in placental mammals. *Development* **139**, 731-739.
- Selever, J., Liu, W., Lu, M. F., Behringer, R. R. and Martin, J. F. (2004). Bmp4 in limb bud mesoderm regulates digit pattern by controlling AER development. *Dev. Biol.* **276**, 268-279.
- Seo, H. S. and Serra, R. (2007). Deletion of Tgfb2 in Prx1-cre expressing mesenchyme results in defects in development of the long bones and joints. *Dev. Biol.* **310**, 304-316.
- Sharpe, J., Ahlgren, U., Perry, P., Hill, B., Ross, A., Hecksher-Sørensen, J., Baldock, R. and Davidson, D. (2002). Optical projection tomography as a tool for 3D microscopy and gene expression studies. *Science* **296**, 541-545.
- Suzuki, T., Hasso, S. M. and Fallon, J. F. (2008). Unique SMAD1/5/8 activity at the phalanx-forming region determines digit identity. *Proc. Natl. Acad. Sci. USA* **105**, 4185-4190.
- ten Berge, D., Brugmann, S. A., Helms, J. A. and Nusse, R. (2008). Wnt and FGF signals interact to coordinate growth with cell fate specification during limb development. *Development* **135**, 3247-3257.
- Verheyden, J. M. and Sun, X. (2008). An Fgf/Gremlin inhibitory feedback loop triggers termination of limb bud outgrowth. *Nature* **454**, 638-641.
- Witte, F., Chan, D., Economides, A. N., Mundlos, S. and Stricker, S. (2010). Receptor tyrosine kinase-like orphan receptor 2 (ROR2) and Indian hedgehog regulate digit outgrowth mediated by the phalanx-forming region. *Proc. Natl. Acad. Sci. USA* **107**, 14211-14216.
- Woltering, J. M. and Duboule, D. (2010). The origin of digits: expression patterns versus regulatory mechanisms. *Dev. Cell* **18**, 526-532.
- Wong, Y. L., Behringer, R. R. and Kwan, K. M. (2012). Smad1/5/8 signaling in limb ectoderm functions redundantly and is required for interdigital programmed cell death. *Dev. Biol.* **363**, 247-257.
- Wu, X., Shi, W. and Cao, X. (2007). Multiplicity of BMP signaling in skeletal development. *Ann. N. Y. Acad. Sci.* **1116**, 29-49.
- Yang, X., Li, C., Herrera, P. L. and Deng, C. X. (2002). Generation of Smad4/Dpc4 conditional knockout mice. *Genesis* **32**, 80-81.
- Yashiro, K., Zhao, X., Uehara, M., Yamashita, K., Nishijima, M., Nishino, J., Saijoh, Y., Sakai, Y. and Hamada, H. (2004). Regulation of retinoic acid distribution is required for proximodistal patterning and outgrowth of the developing mouse limb. *Dev. Cell* **6**, 411-422.
- Yoon, B. S., Ovchinnikov, D. A., Yoshii, I., Mishina, Y., Behringer, R. R. and Lyons, K. M. (2005). Bmpr1a and Bmpr1b have overlapping functions and are essential for chondrogenesis in vivo. *Proc. Natl. Acad. Sci. USA* **102**, 5062-5067.
- Yu, P. B., Hong, C. C., Sachidanandan, C., Babitt, J. L., Deng, D. Y., Hoyng, S. A., Lin, H. Y., Bloch, K. D. and Peterson, R. T. (2008). Dorsomorphin inhibits BMP signals required for embryogenesis and iron metabolism. *Nat. Chem. Biol.* **4**, 33-41.
- Zakany, J. and Duboule, D. (2007). The role of Hox genes during vertebrate limb development. *Curr. Opin. Genet. Dev.* **17**, 359-366.
- Zakin, L. and De Robertis, E. M. (2010). Extracellular regulation of BMP signaling. *Curr. Biol.* **20**, R89-R92.
- Zeller, R., López-Ríos, J. and Zuniga, A. (2009). Vertebrate limb bud development: moving towards integrative analysis of organogenesis. *Nat. Rev. Genet.* **10**, 845-858.
- Zhu, J., Nakamura, E., Nguyen, M. T., Bao, X., Akiyama, H. and Mackem, S. (2008). Uncoupling Sonic hedgehog control of pattern and expansion of the developing limb bud. *Dev. Cell* **14**, 624-632.
- Zúñiga, A., Haramis, A. P., McMahon, A. P. and Zeller, R. (1999). Signal relay by BMP antagonism controls the SHH/FGF4 feedback loop in vertebrate limb buds. *Nature* **401**, 598-602.

6.1.2. Paper 2: “Conserved *cis*-regulatory regions in a large genomic landscape control SHH and BMP-regulated *Gremlin1* expression in mouse limb buds”

In this publication, the three conserved HMCO elements located in the *Grem1 cis*-regulatory landscape were tested for their capacity to regulate the expression of *Grem1* during limb bud development. The analysis focuses on the 9kb region that includes HMCO1, termed *Grem1 Regulatory Sequence 1 (GRS1)*. The *GRS1* region was used to generate stable transgenic mouse lines with *LacZ* reporter. My contribution to this project includes the detailed genomic sequence alignment for the HMCOs element in additional species (Figure 1 and Figure S1). I also carried out the analysis of *GRS1-βglob-LacZ* transgene reporter expression in seven transgenic founders (data not shown), and the subsequent analysis of *GRS1-βglob-LacZ* reporter expression in stable *GRS1^{tg10/+}* and *GRS1^{tg2/+}* embryos in wild-type and various mutant backgrounds (Figures 4-6 and Figures S2-S4). Finally, I prepared all figures and genomic schemes of the manuscript.

RESEARCH ARTICLE

Open Access

Conserved *cis*-regulatory regions in a large genomic landscape control SHH and BMP-regulated *Gremlin1* expression in mouse limb buds

Aimée Zuniga^{1*}, Frédéric Laurent¹, Javier Lopez-Rios¹, Christian Klasen^{2,3}, Nicolas Matt^{1,4} and Rolf Zeller^{1*}

Abstract

Background: Mouse limb bud is a prime model to study the regulatory interactions that control vertebrate organogenesis. Major aspects of limb bud development are controlled by feedback loops that define a self-regulatory signalling system. The SHH/GREM1/AER-FGF feedback loop forms the core of this signalling system that operates between the posterior mesenchymal organiser and the ectodermal signalling centre. The BMP antagonist Gremlin1 (GREM1) is a critical node in this system, whose dynamic expression is controlled by BMP, SHH, and FGF signalling and key to normal progression of limb bud development. Previous analysis identified a distant *cis*-regulatory landscape within the neighbouring *Formin1* (*Fmn1*) locus that is required for *Grem1* expression, reminiscent of the genomic landscapes controlling *HoxD* and *Shh* expression in limb buds.

Results: Three highly conserved regions (HMCO1-3) were identified within the previously defined critical genomic region and tested for their ability to regulate *Grem1* expression in mouse limb buds. Using a combination of BAC and conventional transgenic approaches, a 9 kb region located ~70 kb downstream of the *Grem1* transcription unit was identified. This region, termed *Grem1* Regulatory Sequence 1 (*GRS1*), is able to recapitulate major aspects of *Grem1* expression, as it drives expression of a *LacZ* reporter into the posterior and, to a lesser extent, in the distal-anterior mesenchyme. Crossing the *GRS1* transgene into embryos with alterations in the SHH and BMP pathways established that *GRS1* depends on SHH and is modulated by BMP signalling, i.e. integrates inputs from these pathways. Chromatin immunoprecipitation revealed interaction of endogenous GLI3 proteins with the core *cis*-regulatory elements in the *GRS1* region. As GLI3 is a mediator of SHH signal transduction, these results indicated that SHH directly controls *Grem1* expression through the *GRS1* region. Finally, all *cis*-regulatory regions within the *Grem1* genomic landscape locate to the DNase I hypersensitive sites identified in this genomic region by the ENCODE consortium.

Conclusions: This study establishes that distant *cis*-regulatory regions scattered through a larger genomic landscape control the highly dynamic expression of *Grem1*, which is key to normal progression of mouse limb bud development.

Background

During embryonic development, the spatio-temporal expression of transcriptional regulators and morphogenetic signals is tightly controlled. In fact, different types of congenital malformations are caused by mutations affecting specific *cis*-regulatory and non-coding genomic regions that alter the expression of genes or gene clusters in

specific tissues (reviewed in ref. [1-3]). Genome-wide functional mapping revealed many of the large genomic landscapes that control the expression of developmental regulator genes in a global and tissue-specific manner [4]. This study and others reveal that the *cis*-regulatory regions controlling gene expression in a particular tissue are often located several hundred kilobases (kb) or even megabases (Mb) up- or downstream of the transcriptional start sites in other loci, and may control the expression of several genes [5-7]. Recently, it has been shown how multiple *cis*-regulatory regions interact to control the

* Correspondence: aimee.zuniga@unibas.ch; rolf.zeller@unibas.ch

¹Developmental Genetics, Department of Biomedicine, University of Basel, Mattenstrasse 28, CH-4058, Basel, Switzerland

Full list of author information is available at the end of the article

expression of the *5'HoxD* gene complex in the presumptive digit territory. The transcriptionally active part of the *5'HoxD* gene cluster forms a so-called regulatory archipelago in which dispersed *cis*-regulatory elements cooperate to control gene expression in the distal limb bud by interacting with proximal promoters over large distances [8]. In fact, regulatory landscapes with distant and dispersed *cis*-regulatory regions seem to be a recurring theme in the dynamic spatio-temporal regulation of genes that are essential for limb bud development (reviewed in ref. [2,9,10], see also below).

Vertebrate limb bud development is controlled by interactions between two main signalling centres, the apical ectodermal ridge (AER) and the zone of polarizing activity (ZPA) located in the posterior limb mesenchyme. These two signalling centres interact as part of a self-regulatory feedback signalling system involving several signalling pathways [11]. In particular, ZPA cells produce the Sonic Hedgehog (SHH) signal, which together with GREMLIN1-mediated antagonism of Bone Morphogenetic Proteins (BMPs) in the posterior-distal limb bud mesenchyme propagates Fibroblast Growth Factor (FGF) signalling in the AER [11-14]. This SHH/GREMLIN1/AER-FGF feedback-signalling loop promotes distal progression of limb bud outgrowth and formation of the autopod which gives rise to carpals and digit rays (reviewed in ref. [15]). SHH expression in the posterior limb bud mesenchyme is controlled by a *cis*-regulatory region located about 800 kb upstream of the transcriptional start site. Deletion of this ZPA regulatory region (ZRS) results in loss of distal limb structures [16], while point mutations within the ZRS result in anterior ectopic *Shh* expression and duplications of the thumb and/or anterior digits in different species [17,18]. In cells actively transcribing *Shh*, the ZRS loops out of its chromosomal territory to the *Shh* transcription unit, which reveals how distant *cis*-regulatory elements control gene expression [19]. Recently, several transcriptional regulators have been identified that control *Shh* expression by directly interacting with the distant ZRS region. These include HOX proteins, the bHLH transcription factor HAND2, and ETS transcription factors, providing a glimpse of the complex transcriptional regulation of *Shh* in the posterior limb bud mesenchyme [20-22].

SHH signalling is transduced by the GLI family of transcriptional regulators and inhibits the constitutive processing of the full-length GLI3 activator to its repressor form GLI3R (see e.g. ref. [23]). Of the three GLI transcription factors expressed during limb bud development, only *Gli3* is essential on its own (see e.g. ref. [24]). The inactivation of *Gli3* alters morphogenetic feedback signalling and results in formation of additional anterior digits [23,25-27]. In particular, GLI3 restrains the proliferation of mesenchymal progenitors in the anterior limb bud mesenchyme and promotes initiation of digit ray

chondrogenesis by directly repressing *Grem1* expression during handplate formation [26].

We have previously shown that the expression of *Grem1* in the limb bud mesenchyme is controlled by a large genomic landscape downstream of its transcription unit [7]. In fact, several of the classical *limb deformity* mutations that disrupt distal limb bud development and formation of metanephric kidneys in the mouse are caused by deletions affecting this *cis*-regulatory landscape rather than directly altering the *Grem1* gene products [7,13,28]. Molecular and genetic analysis in the mouse identified a 70 kb genomic region located downstream of the *Grem1* transcription unit within the neighbouring *Formin1* (*Fmn1*) gene that is required for *Grem1* expression in the limb bud mesenchyme [7,29]. Detailed analysis of this *Grem1* genomic landscape revealed similarities with the global control region (GCR) that controls the expression of *5'HoxD* genes in the limb bud mesenchyme [6], but did not reveal the structural nature and transacting factors and/or signalling pathways controlling these *cis*-regulatory regions.

To gain further insights into the *Grem1* landscape, the potential *cis*-regulatory activities of the three highest evolutionarily conserved genomic regions within the 70 kb *Grem1* critical region were analysed. In addition to its expression in the posterior mesenchyme, emphasis was also given to the coordinated distal-anterior expansion of *Grem1* expression, which is key to orderly progression of limb bud development [14,30]. Combining BAC with conventional transgenic approaches, we identified a 9 kb genomic region that is able to recapitulate major but not all aspects of the dynamic spatio-temporal *Grem1* expression in the limb bud mesenchyme. This 9 kb region was termed *Grem1 Regulatory Sequence 1* (*GRS1*), and contains a core sequence that is essential to express a *LacZ* transgene under control of a β -globin minimal promoter in a *Grem1*-like pattern. The *GRS1* region drives gene expression into the posterior and subsequently distal-anterior mesenchyme, i.e. reproduces aspects of the distal-anterior expansion of *Grem1* expression during progression of limb bud development. By crossing *GRS1* transgenic mice into different mutant contexts, we establish that the *GRS1* region is controlled by inputs from both the SHH and BMP signalling pathways in limb buds. In addition, chromatin immunoprecipitation (ChIP) shows that GLI3 interacts with the conserved HMCO1 sequences in the *GRS1* region. The functionally relevant *cis*-regulatory regions identified by the present and two previous studies [31,32] map to the endogenous DNase I hypersensitive sites within the *Grem1* genomic landscape recently identified by the ENCODE consortium [33,34]. This indicates that the *Grem1 cis*-regulatory landscape is composed of at least five active *cis*-regulatory

regions that control the spatio-temporal expression of *Grem1* in mouse embryos and limb buds.

Results and Discussion

Identification of conserved limb bud regulatory regions within the *Grem1* genomic landscape

Using functional genetics in the mouse, we previously identified a ~70 kb region located downstream of *Grem1* that is required for its expression in the limb bud mesenchyme (Figure 1A, [7]). This limb bud *cis*-regulatory region is located between coding exons 19 and 23 of the neighbouring *Fmn1* gene. The Evolutionary Conserved Regions (ECR) genome browser (<http://ecrbrowser.dcode.org/>) was used for multiple sequence alignments to compare the mouse genome with different mammalian and the chicken genomes. This analysis revealed several blocks of highly conserved sequences among mammalian species, but only three of them were also highly conserved in the chicken and termed HMCO1, 2 and 3 (Human-Mouse-Chicken-Opossum conserved sequences 1 to 3, Figure 1A). The most conserved parts of these three HMCO core regions are ~80% identical (for details see Additional file 1 and Additional file 2). Of these three regions only HMCO1 is also present in the orthologous genomic region in frogs (Figure 1A), which express *Grem1* during limb bud development [35]. Despite the fact that *Grem1* is expressed during fin bud development [36], no HMCO homologies are present in the zebrafish genome (Figure 1A). ClustalW2 alignments (<http://www.ebi.ac.uk/Tools/msa/clustalw2/>) of the *Fmn1-Grem1* regions from different species revealed the absence of HMCO homologies in other ray-finned fish species such as fugu and medaka (Figure 1B). In contrast, all three HMCO regions are present in the genome of coelacanth, a lobe-finned fish closely related to tetrapods (Figure 1B and Additional file 1) [37]. As the *Grem1* and *Fmn1* loci are linked in all species analysed (Figure 1B), the distance between the orthologous *Fmn1* coding exon 22 (located adjacent to HMCO1) and *Grem1* coding exon 2 was determined. During evolution, this distance increased as it is smallest in the genomes of ray finned fishes and at least ~10-fold larger in tetrapods and coelacanth (Figure 1B). In addition, the distance between *Fmn1* exon 19 (close to HMCO3) and exon 22 correlates well with the presence or absence of the three HMCO regions (Figure 1B and data not shown). In ray-finned fishes and frogs (lacking all or specifically HMCO2, 3, respectively), the distance is ~3-7 kb, while in mammals and coelacanth it ranges from ~50-70 kb. Thus, the increase of intronic and intergenic regions in the *Fmn1-Grem1* landscape correlates well with appearance of the three HMCO regions during vertebrate evolution.

To determine the requirement of each of these three HMCO regions for *Grem1* expression in mouse limb

buds, we used a BAC-based strategy in combination with analysis of transgenic founder embryos (Figure 2A-D and Additional file 3). A 250 kb mouse genomic BAC encoding the critical region and the *Grem1* transcription unit was used to fuse the *LacZ* gene in frame with the *Grem1* ORF [7]. We assessed the expression of the *LacZ* reporter transgene by analysing the spatio-temporal distribution of β -galactosidase activity (Figure 2A-D). Expression of the *Grem1-LacZ* fusion protein in the forelimb bud mesenchyme was detected in a posterior-distal domain (Figure 2A), mimicking the early endogenous *Grem1* expression rather accurately. Therefore, the *Grem1-LacZ* BAC construct was used to engineer deletions of the three HMCO regions and determine their requirement for *Grem1-LacZ* expression in the posterior mesenchyme. To control for reproducible generation of expressing BAC transgenic founder embryos, the *Grem1-LacZ* BAC (Figure 2A) was injected in parallel to the BACs with engineered deletions (Figure 2B-D). While the control *Grem1-LacZ* BAC was always robustly expressed in the posterior mesenchyme (Figure 2A), deletion of the 520 bp HMCO1 core region resulted in complete loss of *LacZ* expression from limb buds (Figure 2B, n = 5/7 embryos with *LacZ* expression, for details see Additional file 3). In contrast, deletion of the 1279 bp HMCO2 core region only caused partial loss of *LacZ* expression from the posterior limb bud mesenchyme (Figure 2C; Additional file 3). *LacZ* remained expressed normally in the majority of founder embryos carrying a 924 bp deletion of the HMCO3 region (Figure 2D, n = 3/5 embryos with *LacZ* expression, for details see Additional file 3). Taken together, this BAC transgenic analysis establishes HMCO1 as most critical for *Grem1* expression in the posterior-distal limb bud mesenchyme. As the HMCO1 core region is highly conserved in tetrapods and lobe-finned fish but not ray-finned fish (Figure 1B), it likely represents a *cis*-regulatory region important to tetrapod evolution. The other two HMCO regions might contribute to robust expression of *Grem1-LacZ* in the posterior mesenchyme, as in particular the deletion of HMCO2 results in significantly reduced *LacZ* expression (Figure 2C).

In an attempt to gain further insight into the enhancer potential and possible interactions of HMCO2/3 with HMCO1, conventional transgenic approaches using a minimal human β -globin promoter (β glob-*LacZ*) were employed. However, neither individual HMCO regions (data not shown) nor in a combination of all three was able to drive robust expression of the β glob-*LacZ* transgene in the posterior limb bud mesenchyme (Figure 3A, compare to Figure 2A). Expression of the β glob-*LacZ* transgene under control of all three HMCO core regions resulted in scattered *LacZ* positive cells in the anterior-distal mesenchyme of forelimb buds (left panel,

(See figure on previous page.)

Figure 1 Identification of three highly conserved non-coding regions in tetrapods and a lobe-finned fish. (A) Sequence alignment of the genomic region critical for *Grem1* expression in mouse limb buds [7] using the ECR browser with the mouse genome release 9 (mm9) as reference genome. The critical genomic region on mouse chromosome 2 is shown in centromeric (CEN) to telomeric (TEL) orientation and is located downstream of the *Grem1* coding exons. As the critical genomic region is part of the *Fmn1* locus, the interspersed *Fmn1* coding exons are indicated as open boxes in the scheme. Three blocks of highly conserved non-coding sequences were identified (HMCO1-3) and are indicated in blue. Conserved coding regions are indicated in black and non-coding regions conserved $\geq 74\%$ over ≥ 100 bp are coloured salmon. The peak detected in the region of HMCO1 in the zebrafish genome corresponds to *Fmn1* exon 22. Regions consisting of repetitive sequences are shown in green (see Additional file 2). (B) Conserved linkage between the *Grem1* and *Fmn1* loci in vertebrates. Increased intergenic distances correlate with the presence of HMCO regions in tetrapods and coelacanth in contrast to ray-finned fishes. The phylogenetic tree analysis was done with the UCSC multiple alignment functions to align the 3' part of the *Fmn1* locus and the *Grem1* locus from different species. Open boxes represent the orthologous *Fmn1* coding exons 19 and 22, black box represents *Grem1* coding exon 2. The intergenic distances between *Fmn1* orthologous exon 22 and *Grem1* coding exon 2 are indicated to the right of the scheme. ENSEMBL genomes used for alignment: mouse: *M. musculus* (mm10); human: *H. sapiens* (hg19); chimpanzee: *P. troglodytes* (panTro3); dog: *C. familiaris* (canFam2); bovine: *B. taurus* (bosTau6); opossum: *M. domestica* (monDom5); chicken: *G. gallus* (galGal3); lizard: *A. carolinensis* (anoCar2); frog: *X. tropicalis* (xenTro2); coelacanth: *L. chalumnae* (LatCha1); fugu: *T. rubripes* (fr3); medaka: *O. latipes* (oryLat2); zebrafish: *D. rerio* (danRer7).

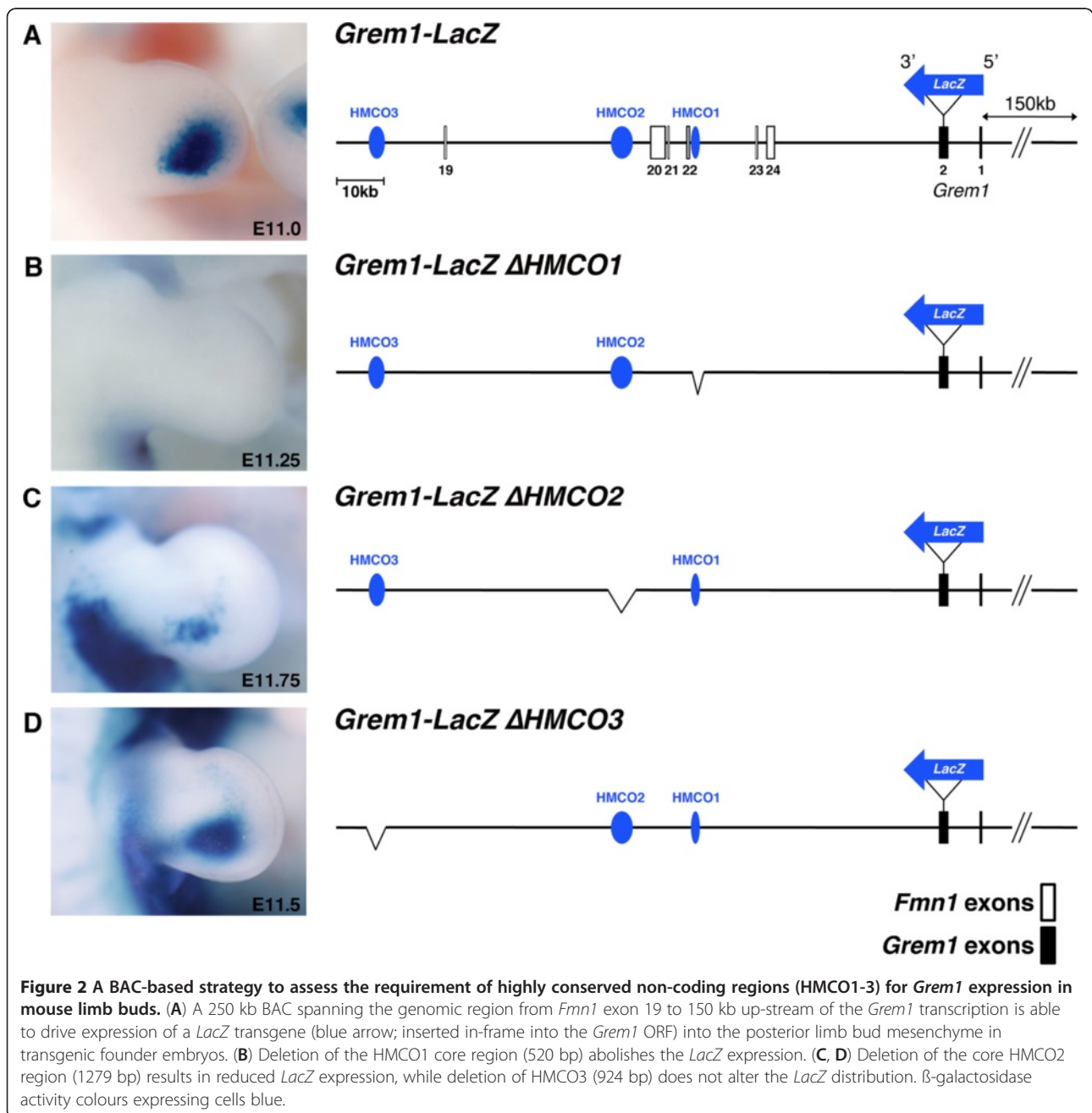
Figure 3A, $n = 3/3$). In contrast, the transgene was strongly expressed in the posterior embryo including hindlimb buds (right panel, Figure 3A). These results show that a transgene consisting of an array of the HMCO core regions is unable to drive *LacZ* expression into the posterior forelimb bud mesenchyme. This indicates that additional elements of the *Grem1* genomic landscape are required for *Grem1* expression in limb buds.

Next, we assessed to which extent a larger genomic fragment containing HMCO1 and flanking regions could drive β glob-*LacZ* expression into the posterior limb bud mesenchyme (Figure 3B). Analysis of transgenic founder embryos revealed that this transgenic construct drives robust β glob-*LacZ* expression in the posterior limb bud mesenchyme (Figure 3B, see also Figure 4), strikingly similar to the domain of the parental *Grem1-LacZ* BAC construct (Figure 2A). Taken together, these results indicate that this *cis*-regulatory region enhances *Grem1* expression in the posterior limb bud mesenchyme, which prompted us to term this 9 kb region *Grem1 Regulatory Sequence 1* (*GRS1*, Figure 4A). *GRS1* encompasses the HMCO1 region next to *Fmn1* coding exon 22 and a further downstream region that is highly conserved in mammals. This region, like HMCO1 overlaps with a previously identified GLI binding region (GBR, [32]). In addition, two potential GLI binding sites were identified by *in silico* analysis (Figure 4A).

Spatio-temporal activity of the *GRS1* region during mouse limb bud development

To analyze comparatively the activity of the *GRS1* region with respect to the spatio-temporal regulation of *Grem1* expression, transgenic mouse strains expressing the *GRS1- β glob-LacZ* reporter construct were established (Figure 4). Seven transgenic founders were obtained. In three independent strains, *LacZ* was expressed in the posterior fore- and hindlimb bud mesenchyme in a pattern comparable to the transgenic founder embryos

(Figure 3B and data not shown). Two of these three transgenic strains were analyzed in detail and used to study the spatio-temporal *LacZ* distribution (Figure 4B, C and Additional file 4). Initial analysis revealed that β -galactosidase activity of the *LacZ* transgene was detected earlier in one strain and is significantly higher than in the other strain (Figure 4B, compare to Figure 4C). As levels did not change during subsequent generations (data not shown), this is likely due to differences in transgene copy number and/or integration site. Therefore, the copy number of both strains was determined by real-time qPCR analysis (Additional file 4). This analysis revealed that ten copies of the *GRS1- β glob-LacZ* transgene were integrated into the genome of the strain expressing higher *LacZ* levels (*GRS1^{tg10}*), while only two copies were detected in the *GRS1^{tg2}* strain (Additional file 4). In *GRS1^{tg10/+}* embryos, β -galactosidase activity is first detected at \sim E10.25 in the posterior forelimb bud mesenchyme and continuously increases until \sim E11.75 (Figure 4B). From \sim E11.0 onwards, scattered positive cells were detected in the anterior mesenchyme, and this anterior expression increased during distal limb bud outgrowth to form a crescent in the distal-anterior autopod (right panels, Figure 4B). By E11.75, β -galactosidase activity was rather variable, such that the anterior crescent separated from the posterior domain in some forelimb buds. In *GRS1^{tg2/+}* embryos, the spatio-temporal pattern is similar, but expression levels are significantly reduced due to the lower transgene copy number, resulting in detection of β -galactosidase activity from only \sim E10.5 onwards (Figure 4C, arrowhead). In both strains, *GRS1* drove expression of the β glob-*LacZ* reporter specifically in the limb bud mesenchyme, despite some low β -galactosidase activity detected in the developing eyes of *GRS1^{tg10/+}* transgenic embryos (Additional file 4). This analysis reveals the robust nature of the *GRS1* region, which functions in positive regulation of *Grem1* expression in the limb bud mesenchyme. The posterior domain



of β-galactosidase activity at E10.5 (Figure 4B) is comparable to the *Grem1* transcript distribution in wild-type limb buds at earlier stages (E9.5-E10.25, Figure 4D). This temporal delay is likely due to postponed transcriptional activation and/or up-regulation of the *GRS1* transgene as the establishment of a posterior *LacZ* expression domain is also only apparent at E10.5 in *GRS1*^{tg10/+} transgenic limb buds (Additional file 5). Therefore, additional *cis*-regulatory regions likely control the temporally correct early onset of *Grem1* expression. Similar delays in the onset of *LacZ* reporter gene expression have been previously observed by

analyzing the ZRS *cis*-regulatory region that controls *Shh* expression in mouse limb buds [38]. During distal progression of limb bud development, endogenous *Grem1* expression expands distal-anterior within the developing handplate and begins to fade by E11.75 (Figure 4D), due to termination of the SHH/GREM1/AER-FGF feedback loop and GLI3-mediated repression in the anterior limb bud mesenchyme [11,26,39,40]. In contrast, β-galactosidase activity remains high in the posterior limb bud mesenchyme of *GRS1* transgenic embryos and the distal-anterior expansion of its expression is significantly delayed and only

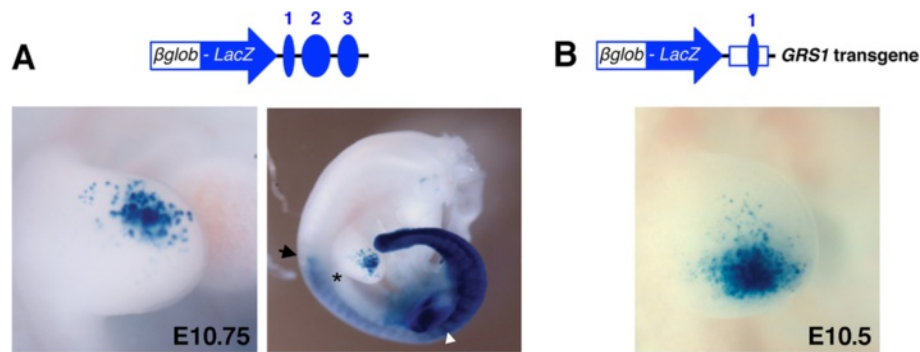


Figure 3 A 9 kb *GRS1* transgene encompassing HMCO1 drives β glob-LacZ expression into the posterior limb bud mesenchyme. (A) A transgene encoding the three HMCO core regions downstream of the β glob-LacZ minimal promoter and reporter results in aberrant β -galactosidase activity in the anterior-distal limb bud mesenchyme. An asterisk marks the posterior border of the forelimb bud. A black arrow marks the anterior border of LacZ expression in the trunk. A white arrowhead points to the hindlimb bud. (B) The *GRS1*- β glob-LacZ transgene is expressed in the posterior limb bud mesenchyme of transgenic founder embryos. The 9 kb *GRS1* region was inserted downstream of the β glob-LacZ reporter to keep the same arrangement as in the endogenous *Grem1* locus (Figure 2A).

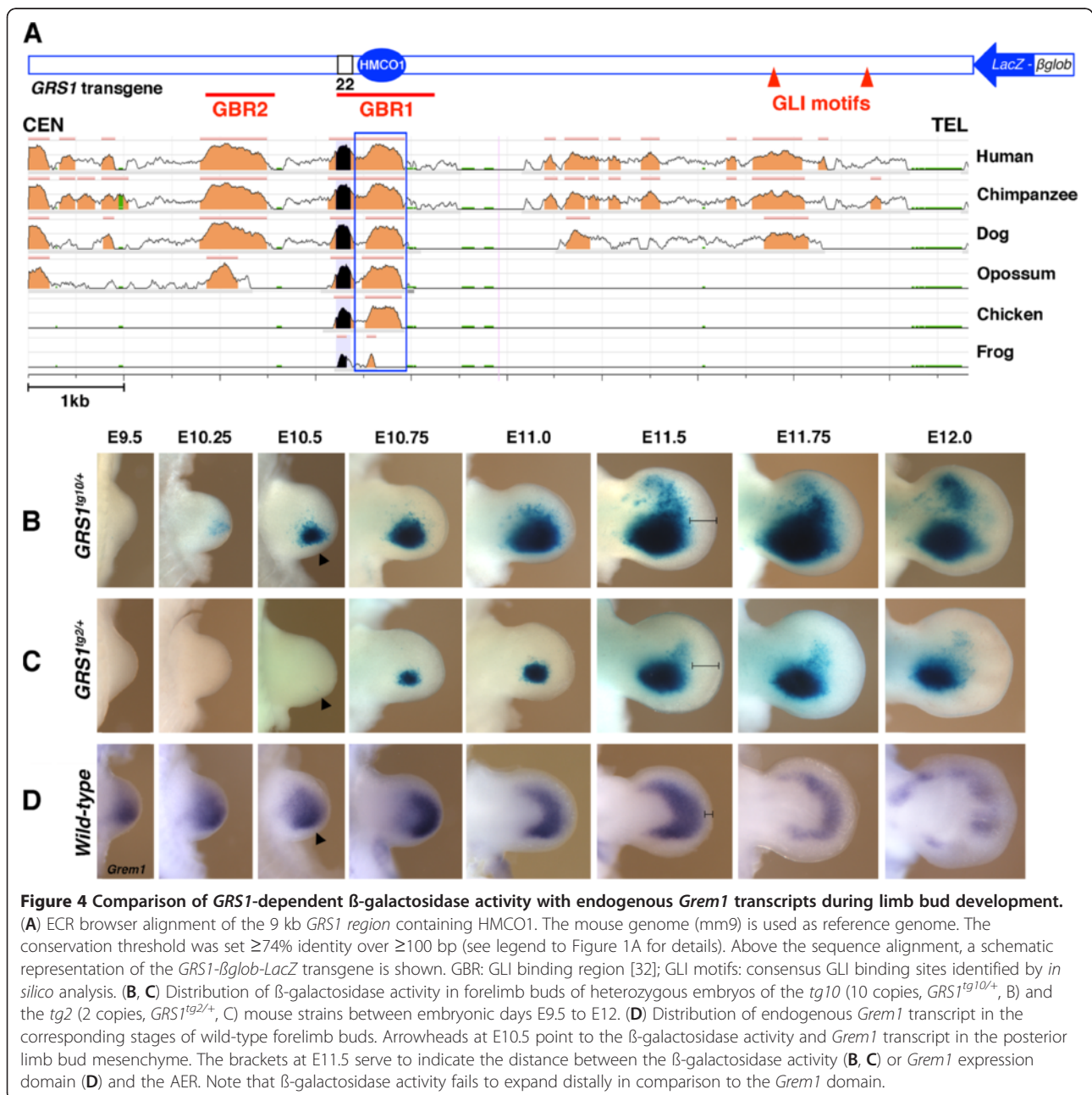
occurs as transcription of the endogenous *Grem1* locus is starting to terminate (E11.5 onwards Figure 4B, C, compare to Figure 4D).

Grem1 expression is restricted to dorsal and ventral limb bud mesenchyme and excluded from the chondrogenic core mesenchyme (Figure 5A), which is relevant to BMP-mediated induction of chondrogenesis (ref. [26,41] and Benazet et al., submitted). Furthermore, the LIM-homeodomain transcription factors *Lhx2* and *Lhx9* have been implicated in regulating *Grem1* expression predominantly in the ventral limb bud mesenchyme in response to SHH signalling [42]. Therefore, the extent to which the dorso-ventral transcript distribution is maintained by the *GRS1* transgene was assessed (Figure 5B). Indeed, the expression of both the high (Figure 5B) and low copy transgenes (Additional file 6) remained excluded from the core mesenchyme throughout limb bud outgrowth and patterning. Similar to *Grem1* transcripts, β -galactosidase activity is higher dorsally than ventrally (Figure 5B, compare to Figure 5A). By E11.75, β -galactosidase activity expands anteriorly in both the dorsal and ventral mesenchyme (E11.75, Figure 5B), reminiscent of the crescent of *Grem1* transcript (Figure 5A and see before), which indicates that the *GRS1* contains *cis*-regulatory regions controlled by *Lhx* transcription factors [42]. Taken together, the results shown in Figures 4 and 5 establish that the 9 kb *GRS1* *cis*-regulatory region is able to recapitulate major aspects of *Grem1* expression in the limb bud mesenchyme. In particular, the *GRS1* also recapitulates aspects of the distal-anterior expansion of *Grem1* expression in limb buds (Figure 4, 5), which was not observed in previous attempts to identify *cis*-regulatory regions that control *Grem1* expression in limb buds [7,32]. The fact that the *GRS1* transgene recapitulates some aspects of this distal-anterior expansion is important, as *Grem1* transcription

normally expands anteriorly in register with posterior AER-FGFs and allows propagation of SHH/GREM1/AER-FGF signalling [14,30]. However, the delay in activation and lack of termination of the *GRS1* transgene (Figure 4) indicates that other regulatory inputs from the *Grem1* genomic landscape are required to regulate its dynamic expression in mouse limb buds.

The *GRS1* *cis*-regulatory region integrates inputs from the SHH and BMP signalling pathways

During limb bud initiation, mesenchymal BMP4 signal transduction is likely required to activate *Grem1* expression in the posterior mesenchyme, while SHH is primarily required for up-regulation and distal-anterior expansion during progression of limb bud development [11,14,43]. Furthermore, GLI3 in the anterior mesenchyme and AER-FGF signal transduction are required to restrict and eventually terminate *Grem1* expression (starting ~E11.5-11.75) [26,40]. Therefore, *GRS1*^{tg10/+} embryos lacking key components of both the SHH and BMP signalling pathway in their limb buds were generated to gain insight into the possible direct impact of these main signalling pathways on the *GRS1* element (Figure 6). Analysis of *Shh*^{Δ/Δ} *GRS1*^{tg10/+} embryos revealed the complete absence of β -galactosidase activity in *Shh*-deficient forelimb buds (Figure 6A). This contrasts with the endogenous *Grem1* expression, which is activated but not maintained in *Shh*-deficient limb buds [11,14]. These results show that activation of the *GRS1* region depends on SHH signalling, which indicated that it could also participate in ectopic *Grem1* activation due to anterior ectopic SHH signalling in mouse [14] and chicken limb buds [12]. Furthermore, GLI3 proteins interact with specific *cis*-regulatory regions in the *Grem1* genomic landscape [32] and genetic analysis has shown that *Gli3* is essential for the spatio-temporally controlled



restriction and subsequent termination of *Grem1* expression in the distal anterior mesenchyme [25,26,44]. In *Gli3*-deficient *GRS1* transgenic (*Gli3*^{Xt/Xt}*GRS1*^{tg10/+}) forelimb buds, β -galactosidase activity in the posterior limb buds is comparable to *GRS1*^{tg10/+} limb buds, while expression in the anterior mesenchyme is significantly increased by E11.75 (Figure 6B, compare to right-most panels, Figure 4B). This late up-regulation of anterior β -galactosidase activity indicates that *GRS1* is required for GLI3-mediated termination of *Grem1* expression in the anterior limb bud mesenchyme, which is essential for the spatio-temporally correct initiation of mesenchymal

condensations and chondrogenic differentiation of anterior digits [26].

BMPs control *Grem1* activation in the posterior limb bud mesenchyme and directly modulate its expression as part of the self-regulatory SHH/GREM1/AER-FGF feedback signalling system. Therefore, a conditional *Smad4* loss-of-function allele [45] in combination with the *Prx1*-Cre recombinase strain [46] was used to inactivate *Smad4* (*Smad4* ^{Δ/Δ^M}) and thereby canonical BMP signal transduction in the limb bud mesenchyme. In *Smad4* ^{Δ/Δ^M} mutant limb buds, endogenous *Grem1* expression is down-regulated but not lost, while *Shh* expression remains

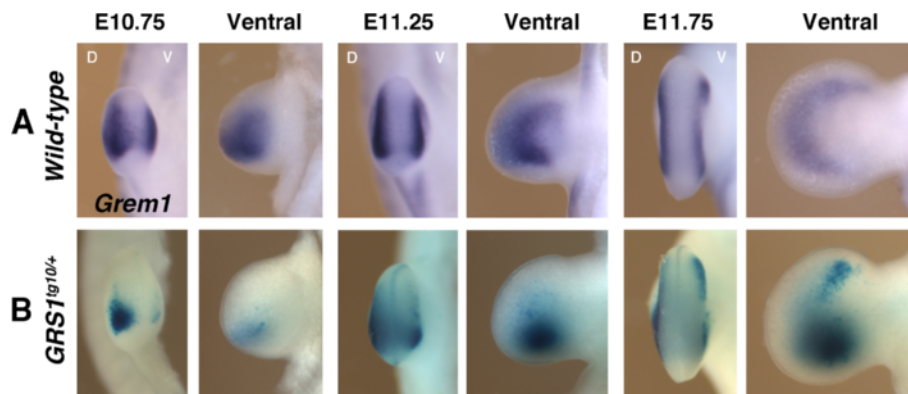


Figure 5 Dorsal and ventral restriction of *GRS1*-mediated β -galactosidase activity. (A) *Grem1* transcript remains restricted to the dorsal and ventral forelimb bud mesenchyme in wild-type embryos throughout limb bud development. (B) *GRS1*-mediated expression of *Bglob-LacZ* is able to correctly restrict β -galactosidase activity along the dorso-ventral limb bud axis. D: dorsal; V: ventral.

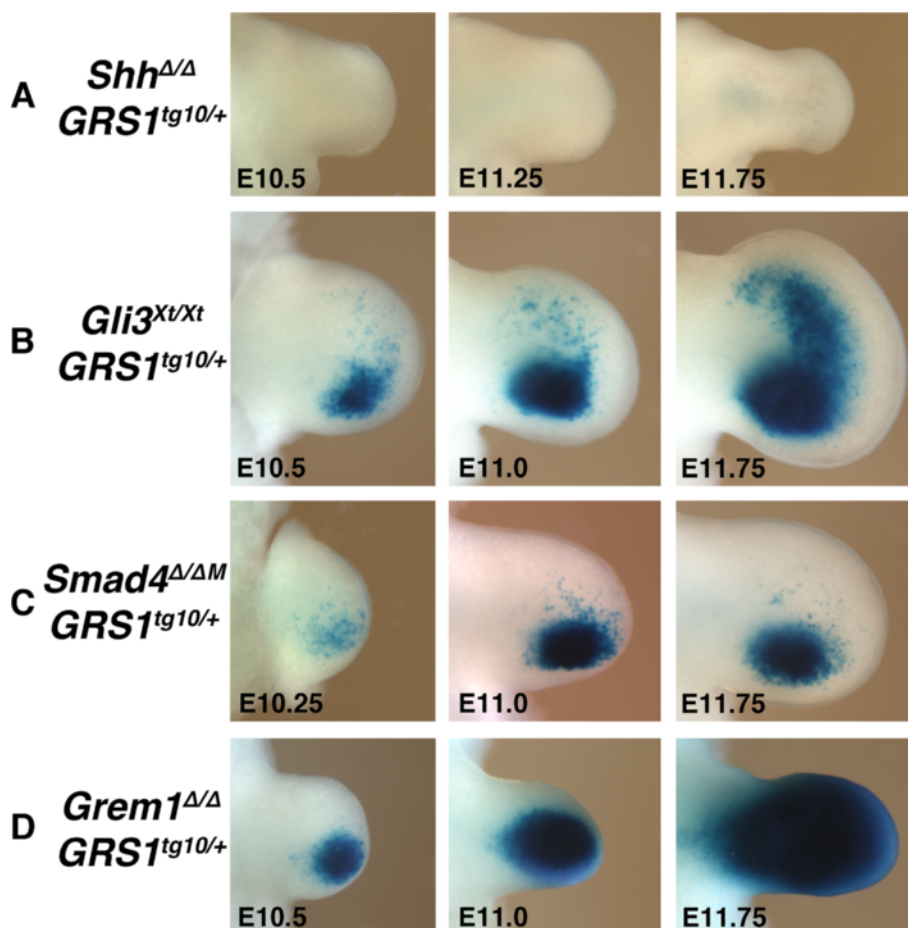


Figure 6 The *GRS1* transgene is controlled by both SHH and BMP activity. (A) *GRS1*-dependent β -galactosidase activity is completely lost from *Shh*-deficient limb buds (*Shh* $^{\Delta/\Delta}$ *GRS1* $^{tg10/+}$). (B) In contrast, inactivation of *Gli3* results in anterior up-regulation of β -galactosidase activity at E11.75 (*Gli3* $^{Xt/Xt}$ *GRS1* $^{tg10/+}$). (C) β -galactosidase activity fails to expand anteriorly in *Smad4*-deficient limb buds (*Smad4* $^{\Delta/\Delta M}$ *GRS1* $^{tg10/+}$). (D) β -galactosidase activity is up-regulated in *Grem1*-deficient limb buds from E11.0 onward (*Grem1* $^{\Delta/\Delta}$ *GRS1* $^{tg10/+}$).

(Benazet et al., submitted). In *Smad4*^{Δ/ΔM}*GRS1*^{tg10/+} forelimb buds, β-galactosidase activity appears normal in the posterior mesenchyme, while distal-anterior expansion fails to occur (Figure 6C, compare to Figure 4B). This indicates that *GRS1* activity is modulated by SMAD4-mediated signal transduction during the progression of limb bud development. These results indicate that also the distal-anterior expansion of *Grem1* expression depends on BMP activity and agree with the observation that genetic lowering of *Bmp4* results in a global reduction of *Grem1* expression in the limb bud mesenchyme [11].

Finally, in *Grem1*-deficient embryos, BMP activity is increased due to reduced BMP antagonism, which results in up-regulation of non-functional *Grem1* transcript [13]. As BMP signal transduction modulates *GRS1* activity during advanced limb bud development (Figure 6C), we also determined the potential influence of *Grem1* deficiency on *GRS1* activity. In *Grem1*^{Δ/Δ}*GRS1*^{tg10/+} E10.5 limb buds β-galactosidase activity is initially similar to *GRS1*^{tg10/+} limb buds (Figure 6D, compare to Figure 4B). Subsequently, β-galactosidase activity is increased and by E11.75 the entire *Grem1*^{Δ/Δ}*GRS1*^{tg10/+} limb bud is positive (Figure 6D). These alterations of β-galactosidase activity in *Smad4*^{Δ/ΔM} and *Grem1*^{Δ/Δ} forelimb buds reveal that *GRS1* activity is extensively modulated by changes in BMP activity, in particular also the anterior expansion of its expression. Taken together, this genetic analysis (Figure 6) shows that *GRS1* activity critically depends on SHH and is modulated extensively by BMP signal transduction. This analysis identifies the *GRS1*, located ~70 kb downstream of the *Grem1* transcription unit as a *cis*-regulatory region that integrates inputs by both SHH and BMP signal transduction. However, as previous analysis provided good evidence that *Grem1* is activated by mesenchymal BMP signalling upstream of establishing the SHH/FGF feedback loop [11], these studies point to the existence of additional unknown BMP response regions that activate *Grem1* expression in the posterior limb bud mesenchyme.

Endogenous GLI3 proteins are part of the chromatin complexes interacting with specific parts of the *GRS1* region in mouse limb buds

The observed loss of *GRS1* activity in *Shh*-deficient limb buds (Figure 6A) indicated that the *GRS1* region could be regulated directly by GLI proteins. Indeed, two GLI binding regions without consensus GLI binding motif (GBR1 and GBR2, [32]) were previously mapped to the 9 kb *GRS1* region using transgene-mediated expression of an epitope-tagged GLI3 transgene in combination with chromatin immunoprecipitation (ChIP). To study the potential interaction of endogenous GLI3 proteins with the *GRS1* region in its normal genomic context in

wild-type limb buds, ChIP analyses using antibodies that detect both the GLI3 activator and repressor protein isoforms were performed [26,47]. GLI3 ChIP using extracts of wild-type and *Gli3*-deficient limb buds at E11.5 revealed significant enrichment of one specific region within *GRS1* by real-time qPCR analysis (Figure 7A). A significant ~4-fold enrichment of an amplicon located within HMCO1 was observed by comparing wild-type to *Gli3*-deficient limb buds (amplicon “d”; $p = 0.008$) and to a less conserved region (amplicon “e”; located outside HMCO1 close to a putative GLI binding site; Figure 7A). In contrast, no significant enrichments of the other amplicons located in *GRS1* were detected (Figure 7A). As the amplicons located in HMCO2 (Figure 7B) and HMCO3 (Figure 7C) were also not significantly enriched, the GLI3-containing chromatin complexes appear to interact rather specifically with a region within the highly conserved HMCO1 in wild-type limb buds. These results not only corroborates the identity of previously identified GBR1 [32], but indicate that this region mediates the effects of SHH signal transduction on *GRS1* activity in the posterior limb bud mesenchyme.

Spatio-temporal *Grem1* expression is regulated by the interaction of multiple *cis*-regulatory regions far downstream of the transcription unit

Previous genetic analysis showed that *Grem1* transcription in limb buds is initiated by BMP signalling and up-regulated under the influence of SHH and AER-FGF signaling as limb bud development progresses [11]. Finally, *Grem1* expression is terminated concomitantly with the initiation of digit formation by high levels of FGF signal transduction and GLI3-mediated repression in the anterior mouse limb bud mesenchyme [26,40]. This dynamic spatio-temporal regulation of *Grem1* expression indicates that the activity of different *cis*-regulatory elements may change over time. The spatio-temporal activity of the *GRS1* transgene (Figure 4B) indicates that it is primarily regulated by the SHH/GREM1/AER-FGF feedback signaling system as limb bud development progresses. In particular, its activity is first apparent when the SHH/GREM1/AER-FGF feedback is already established, and the expected termination does not occur, as β-galactosidase activity remains in the posterior mesenchyme after the endogenous *Grem1* transcripts have been down-regulated (Figure 4B, D). These results indicate that FGF-mediated termination of *Grem1* expression and the underlying self-regulatory feedback signalling system [40] does not occur by FGF signal transduction impacting the *GRS1* region. In addition, neither the 70 kb critical region of the *Grem1* landscape (*Grem1-LacZ*, Figure 2A) nor transgenes derived from this region (Figures. 2, 3, 4 and ref. [32]) are able to accurately recapitulate the entire spatio-temporal distribution of *Grem1* transcript in the

limb bud mesenchyme. Therefore, either the interactions among these elements or additional as yet unknown *cis*-regulatory regions located outside the critical region must also participate in the regulation of *Grem1* expression. Indeed, there is circumstantial evidence for the latter, as deletion of the GC-rich *Fmn1* coding exon 9 (located ~200 kb downstream of the *Grem1* transcription unit) results in non-complementation with a *Grem1* null allele, causing a hypomorphic *Grem1* limb skeletal phenotype, and significantly reduced *Grem1* expression (ref. [29] and A.Z. and R.Z., unpublished data).

Mapping of DNase I hypersensitive (HS) sites is used to identify active regulatory regions in chromatin (reviewed in ref. [48]). Recently, the ENCODE consortium has done genome-wide mapping of HS sites in several mouse tissues including limb buds (ENCODE Group, University of Washington) [33,34]. Interestingly, this analysis revealed three HS sites within the GBRs of the *GRS1* and HMCO2, while no HS sites mapping to HMCO3 were detected in limb buds at E11.5 (Figure 8). The five HS sites mapped by the ENCODE consortium in the *Grem1* genomic landscape overlap with the *cis*-regulatory elements required for *Grem1* expression in

mouse limb buds (Figure 8). The HS site mapping to HMCO1 overlaps well with the amplicon enriched by GLI3-ChIP analysis (Figure 7A). In fact, all HS sites in the *Grem1* genomic landscape overlap either with the GBR regions interacting with GLI3 [26,32] or CTCF binding sites [31]. Analysis of *Ctcf*-deficient limb buds revealed its requirement for up-regulation and distal-anterior expansion of *Grem1* expression [31]. Interestingly, the HS site overlapping with GBR4 [32] is not conserved between mammals and birds (Figure 8 and data not shown). While the early GBR4 activity is comparable to *GRS1* in the posterior mesenchyme (Figure 4B), it does not support distal-anterior expansion of the expression during subsequent development [32]. Thus, the interaction of the GBR4 and *GRS1 cis*-regulatory regions could provide *Grem1* expression with the necessary robustness and evolutionary plasticity, as has been postulated for the transcriptional regulation of *HoxD* genes by multiple interacting regulatory regions during limb bud development [8]. Taken together, these studies establish that the five HS sites in the *Grem1* genomic landscape are functionally relevant for *Grem1* expression in mouse limb buds, but not all of them are evolutionary highly

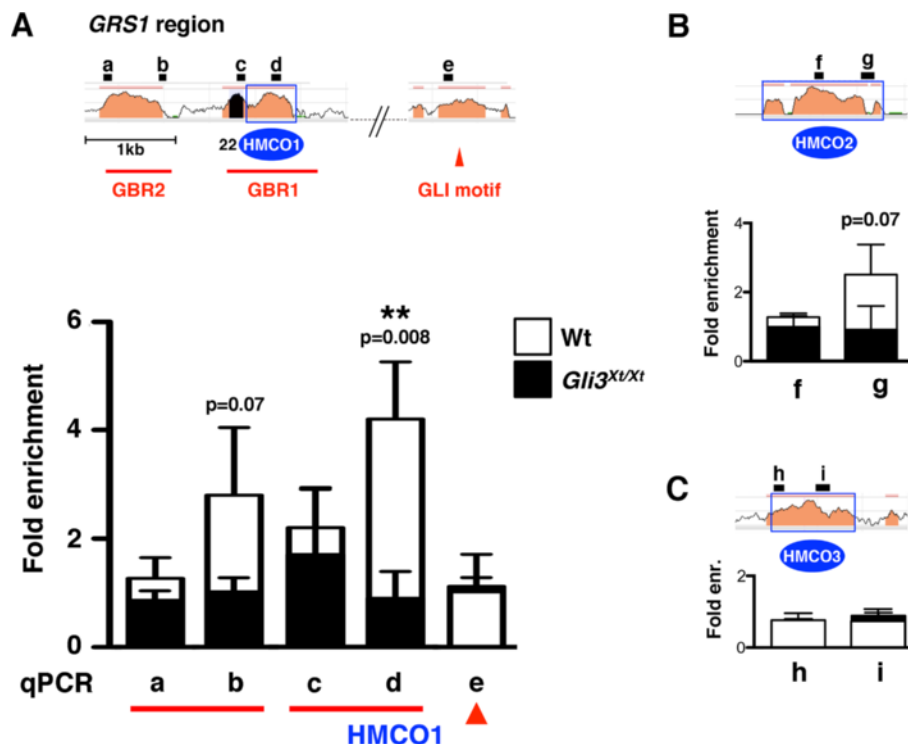
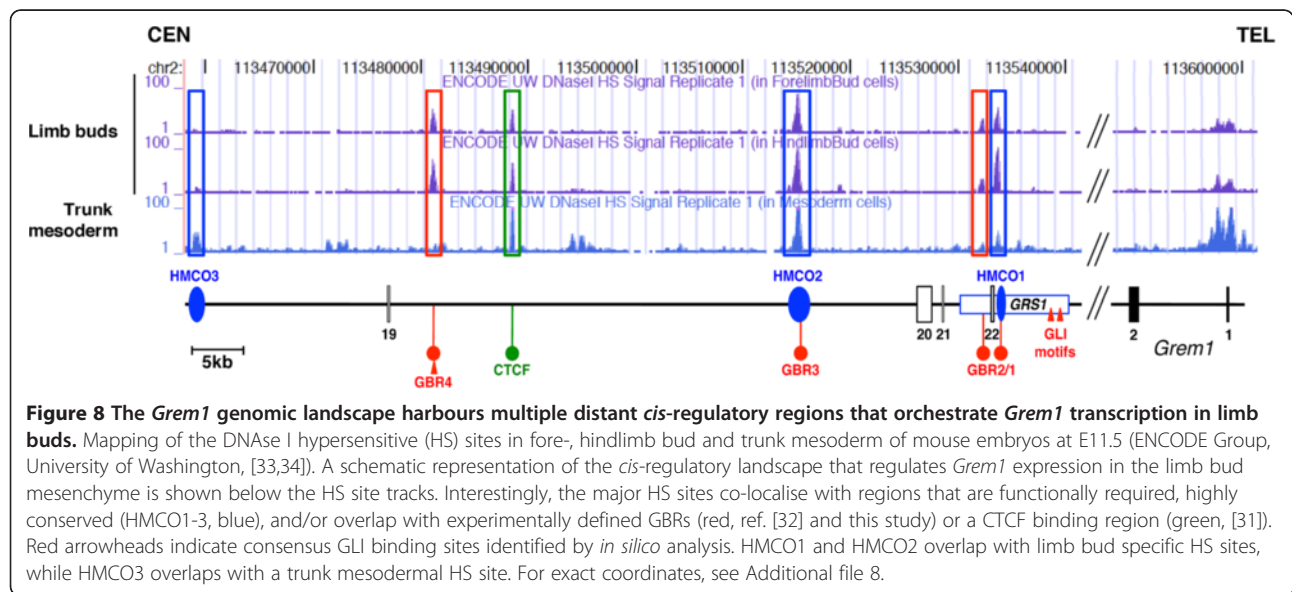


Figure 7 Endogenous GLI3 complexes bind to specific HMCO and GBR regions in the *Grem1* genomic landscape. (A) Several amplicons were designed to detect the conserved and functionally relevant regions within the *GRS1* region. The exact genomic locations of all amplicons are listed in Additional file 7. The potential interaction of endogenous GLI3 proteins with these critical amplicons was analysed by ChIP-qPCR analysis of wild-type (open bars) and *Gli3^{Xt/Xt}* (black) limb buds at E11.5. Two stars indicate significant enrichment of amplicon "d" in the HMCO1 region (p=0.008). (B) GLI3 ChIP-qPCR analysis of the HMCO2 region. Amplicons "f" and "g" are located inside HMCO2 and the previously identified GBR3 [32]. (C) GLI3 ChIP-qPCR analysis of HMCO3. All values are shown as mean \pm SD.



conserved. Indeed, experimental and comparative evolutionary evidence indicates that alterations in the spatio-temporal expression of *Grem1*, and thereby the activity of the SHH/GREM1/AER-FGF feedback loop, likely contributes significantly to variations in digit numbers and morphologies (reviewed in ref. [49]).

Conclusions

In this study, we identify *GRS1* as a distant *cis*-regulatory region that encompasses the highly conserved HMCO1 region and show that it controls important aspects of *Grem1* expression in the posterior and distal-anterior limb bud mesenchyme. *GRS1* activity depends critically on SHH signalling and endogenous GLI3 protein complexes interact with specific regions within HMCO1 in wild-type limb buds. In addition, the anterior expansion of *GRS1* activity is also regulated by BMP signal transduction. These results together with previous studies reveal the large genomic architecture composed of several distant *cis*-regulatory regions that control the highly dynamic *Grem1* expression in response to signalling inputs from the BMP, SHH and FGF pathways. It is likely that the interactions among these dispersed *cis*-regulatory regions provide the dynamic *Grem1* expression in limb buds with the necessary robustness, but at the same time allow for evolutionary plasticity of its expression [8].

Methods

Ethics Statement

All the experiments were conducted in strict accordance with Swiss law following the 3R principles and the conduct defined by the Basel Declaration. All studies involving mice were classified as grade zero by the Animal

Welfare and Ethics Commission of both cantons of Basel and Argovia, which implies minimal suffering.

Mouse strains

The *Shh* loss-of-function allele [50], the *Gli3 extra-toes-J* allele [51], the *Grem1* null allele [13] and the *GRS1*^{tg/+} alleles (this study) were maintained in an NMRI background, while the *Smad4* conditional allele (*Smad4*^{fllox}, [45]) and the *Prx1-Cre* transgene [46] were maintained in a C57BL/6 J background.

BAC modifications

BAC constructs were engineered using ET cloning as previously described [7]. The deletions ΔHMCO1, ΔHMCO2 and ΔHMCO3 were induced in the *Grem1-LacZ* BAC clone using a *Kanamycin* resistance selection cassette. All primer sequences are available upon request. See Additional file 8 for the genomic coordinates of HMCO1-3.

βglob-LacZ transgene constructs

An expression cassette was constructed in pKS-Bluescript using *LacZeocin* reporter under control of the minimal human β-globin promoter sequences [52]. Various combinations of HMCO sequences were inserted downstream into this cassette. The HMCO1, -2 and -3 core sequences were amplified by PCR directly from mouse genomic DNA (primers available on request). The 9 kb *GRS1* region was initially subcloned as a 9.6 kb *Bgl2* fragment from BAC RP23-113 H17 (chr2: 113,611,499-113,847,299 (mm10). BacPac Resources, Children's Hospital, Oakland, USA). All constructs were linearized with *Ksp1* before microinjection.

Generation of transgenic founder embryos and transgenic strains

BAC and β glob-*LacZ* transgenic constructs were injected into the pronucleus of fertilized mouse eggs. Several founder embryos for each construct were scored for β -galactosidase activity (Additional file 3). For the *GRS1*- β glob-*LacZ* transgene, seven independent transgenic mouse strains were established by crossing founders into the NMRI background. Transgene copy numbers were determined by real time qPCR [53] using the Bio-Rad CFX96 Real-Time PCR System in combination with the iQ SYBR Green Supermix (Bio-Rad). For each mouse, 20 ng of genomic DNA were analysed in triplicate. The primers to amplify the *DBH* genomic region were used for normalization and non-transgenic littermate DNA was used as control. The normalized control levels were set to 2 as the primers also amplified both alleles of the endogenous HMCO1 regions. The $2^{-\Delta\Delta C_t}$ formula was used to calculate and normalize transgene copy numbers. In addition to three different F1 males, three embryos from the F2 and three embryos from the F3 generation were analysed for the two transgenic strains shown to ascertain stable transmission of the transgenes. Primers sequences are available on request.

Detection of β -galactosidase activity

Embryos were isolated in ice-cold PBS and staged according to somites numbers, then fixed in 1% formaldehyde, 0.2% glutaraldehyde, 0.02% NP40, 0.01% sodium deoxycholate in 1x PBS for 20–30 minutes at 4°C. Subsequently, embryos were washed three times in 1x PBS for 5 minutes at room temperature and incubated overnight at 37°C and in the dark in 1 mg/mL X-Gal, 0.25 mM K3Fe(CN6), 0.25 mM K4Fe(CN6), 0.01% NP-40, 0.4 mM MgCl2 and 1% sodium deoxycholate to detect β -galactosidase activity, which colours cells blue. To stop the reaction, embryos were washed three times in 1x PBS for 5 minutes each at room temperature.

Chromatin Immunoprecipitation (ChIP)

Forelimbs and hindlimbs of 10 wild-type or *Gli3*^{Xt/Xt} embryos at E11.5 were dissected and processed for ChIP as described [26] using a polyclonal anti-GLI3 antibody (#2676, Genentech, [47]). To compute the level of enrichment of a given region, the Ct values of both input and ChIP samples were compared with those of a negative control amplicon located in the mouse β -actin locus [21]. All results (mean \pm SD) were obtained by analysing three completely independent experiments per genotype. The significance of all differences was assessed using the two-tailed, non-parametric Mann–Whitney test. The coordinates of the relevant amplification are shown in Additional file 7.

All genomic sequence alignments of the *Fmn1-Grem1* locus region were performed using the ECR browser [54] and the ClustalW2 program [55].

Additional files

Additional file 1: Figure S1. Conservation of the HMCO core regions. ClustalW2 multiple sequence alignment of the HMCO1, HMCO2 and HMCO3 core regions of mouse (mm10), human (hg19), chimpanzee (panTro3), dog (canFam2), bovine (bosTau6), opossum (monDom5), chicken (galGal3), lizard (anoCar2), frog (xenTro2), and coelacanth (LatCha1) genomes. The corresponding genomic coordinates are indicated. HMCO1: 73 of 149 nucleotides were conserved in all species; HMCO2: 182/298 conserved nucleotides, HMCO3: 45/137 conserved nucleotides.

Additional file 2: Table S1. Genomic coordinates for the sequence comparisons shown in Figure 1A.

Additional file 3: Table S2. Analysis of transgenic founder embryo.

Additional file 4: Figure S2. Limb bud mesenchymal expression of *GRS1*- β glob-*LacZ* transgene in two independent transgenic mouse strains. (A) Expression of the *GRS1*- β glob-*LacZ* transgene is restricted to limb buds, with expression initiating earlier in forelimb than hindlimb buds. Note the differences in β -galactosidase activity in *GRS1*^{Tg10/+} (left panel) and *GRS1*^{Tg2/+} (right panel) transgenic mouse embryos. (B) Using real-time qPCR, the transgene copy numbers in both the *GRS1*^{Tg10/+} and *GRS1*^{Tg2/+} mouse strains were determined in comparison to wild-type mice (carrying 2 copies of the endogenous *GRS1* regions). This analysis revealed that the *GRS1*^{Tg10/+} strain carries 10 copies and *GRS1*^{Tg2/+} 2 copies of the transgene, respectively.

Additional file 5: Figure S3. Comparison of the *LacZ* mRNA and β -galactosidase reporter activity in early limb buds of *GRS1*^{Tg10/+} embryos. Distribution of β -galactosidase activity (A) and *LacZ* transcripts (B) in forelimb buds of *GRS1*^{Tg10/+} embryos at E10.0 and E10.5. Arrowheads point to the posterior expression domains.

Additional file 6: Figure S4. Dorsal-ventral distribution of β -galactosidase activity in forelimb buds expressing the *GRS1*^{Tg2/+} transgene. The *GRS1*^{Tg2/+} transgene respects the dorsal and ventral restriction of the mesenchymal expression domains. Note that overall expression is significantly lower than in *GRS1*^{Tg10/+} limb buds (compare to Figure 5B). D: dorsal, V: ventral.

Additional file 7: Table S3. qPCR amplicons for GLI3 ChIP analysis.

Additional file 8: Table S4. Genomic coordinates of identified *Grem1* regulatory regions.

Authors' contributions

AZ conceived most of the experiments and wrote the manuscript together with RZ. AZ also carried out most of the genetic and transgenic analysis together with FL. FL also prepared the figures for the manuscript. FL, JLR and NM performed the *in silico* analysis. JLR carried out the ChIP analysis to detect the endogenous GLI3 protein complexes. NM contributed in the initial phase of this project (generation of transgenic constructs and initial analysis of founder embryos). CK generated the transgenic founders for all constructs. RZ conceived part of the study and wrote the manuscript together with AZ. All authors read and approved the final manuscript.

Acknowledgements

The authors are grateful to A. Offinger and her staff for excellent animal care. L. d'Amato and Christina Torres are thanked for technical assistance. S. Scales (Genentech) provided the GLI3 antibodies. We thank group members for critical input on the manuscript. The ENCODE Group at University of Washington (J. Stamatoyannopoulos and coworkers) are acknowledged for the genome-wide DNase I hypersensitive site mapping data made available freely through the ENCODE Data Coordination Center at UCSC (release date on March 29, 2012). NM received a EU Marie Curie postdoctoral fellowship. This research is supported by grants of the Swiss National Science Foundation (grants no. 31003A_130803 to RZ and 310000_122558 to AZ), a

EU reintegration grant (PERG-GA-2009-246576 to JLR) and the University of Basel. The authors declare no conflict of interest.

Author details

¹Developmental Genetics, Department of Biomedicine, University of Basel, Mattenstrasse 28, CH-4058, Basel, Switzerland. ²Transgenic Service, EMBL, Meyerhofstrasse 1, 69012, Heidelberg, Germany. ³Present address: Max-Delbrueck-Centrum Berlin, Robert Roessle-Strasse 10, 13215, Berlin, Germany. ⁴Present address: Université de Strasbourg, Institut de Biologie Cellulaire et Moléculaire, UPR 9022 CNRS, 15 rue René Descartes, 67084, Strasbourg, France.

Received: 28 March 2012 Accepted: 12 July 2012

Published: 13 August 2012

References

- Gordon CT, Tan TY, Benko S, Fitzpatrick D, Lyonnet S, et al: Long-range regulation at the SOX9 locus in development and disease. *Journal of medical genetics* 2009, **46**:649–656.
- Vandermeer JE, Ahituv N: cis-regulatory mutations are a genetic cause of human limb malformations. *Dev Dyn* 2011, **240**:920–930.
- Zuniga A, Probst S, Zeller R: The molecular basis of human congenital limb malformations. *Wiley Interdisciplinary Reviews: Developmental Biology*; 2012.
- Ruf S, Symmons O, Uslu W, Dolle D, Hot C, et al: Large-scale analysis of the regulatory architecture of the mouse genome with a transposon-associated sensor. *Nat Genet* 2011, **43**:379–386.
- Lettice LA, Horikoshi T, Heaney SJ, Van Baren MJ, Van Der Linde HC, et al: Disruption of a long-range cis-acting regulator for Shh causes preaxial polydactyly. *Proc Natl Acad Sci U S A* 2002, **99**:7548–7553.
- Spitz F, Gonzalez F, Duboule D: A global control region defines a chromosomal regulatory landscape containing the HoxD cluster. *Cell* 2003, **113**:405–417.
- Zuniga A, Michos O, Spitz F, Haramis AP, Panman L, et al: Mouse limb deformity mutations disrupt a global control region within the large regulatory landscape required for Gremlin expression. *Genes Dev* 2004, **18**:1553–1564.
- Montavon T, Soshnikova N, Mascrez B, Joye E, Thevenet L, et al: A regulatory archipelago controls Hox genes transcription in digits. *Cell* 2011, **147**:1132–1145.
- Spitz F: Control of vertebrate Hox clusters by remote and global cis-acting regulatory sequences. *Adv Exp Med Biol* 2010, **689**:63–78.
- Zeller R, Zuniga A: Shh and Gremlin1 chromosomal landscapes in development and disease. *Curr Opin Genet Dev* 2007, **17**:428–434.
- Benazet JD, Bischofberger M, Tiecke E, Goncalves A, Martin JF, et al: A self-regulatory system of interlinked signaling feedback loops controls mouse limb patterning. *Science* 2009, **323**:1050–1053.
- Capdevila J, Tsukui T, Rodriguez Esteban C, Zappavigna V, Izpisua Belmonte JC: Control of vertebrate limb outgrowth by the proximal factor Meis2 and distal antagonism of BMPs by Gremlin. *Mol Cell* 1999, **4**:839–849.
- Michos O, Panman L, Vintersten K, Beier K, Zeller R, et al: Gremlin-mediated BMP antagonism induces the epithelial-mesenchymal feedback signaling controlling metanephric kidney and limb organogenesis. *Development* 2004, **131**:3401–3410.
- Zuniga A, Haramis AP, McMahon AP, Zeller R: Signal relay by BMP antagonism controls the SHH/FGF4 feedback loop in vertebrate limb buds. *Nature* 1999, **401**:598–602.
- Zeller R, Lopez-Rios J, Zuniga A: Vertebrate limb bud development: moving towards integrative analysis of organogenesis. *Nat Rev Genet* 2009, **10**:845–858.
- Sagai T, Hosoya M, Mizushima Y, Tamura M, Shiroishi T: Elimination of a long-range cis-regulatory module causes complete loss of limb-specific Shh expression and truncation of the mouse limb. *Development* 2005, **132**:797–803.
- Lettice LA, Hill AE, Devenney PS, Hill RE: Point mutations in a distant sonic hedgehog cis-regulator generate a variable regulatory output responsible for preaxial polydactyly. *Hum Mol Genet* 2008, **17**:978–985.
- Maas SA, Suzuki T, Fallon JF: Identification of spontaneous mutations within the long-range limb-specific Sonic hedgehog enhancer (ZRS) that alter Sonic hedgehog expression in the chicken limb mutants oligozeugodactyly and silkie breed. *Dev Dyn* 2011, **240**:1212–1222.
- Amano T, Sagai T, Tanabe H, Mizushima Y, Nakazawa H, et al: Chromosomal dynamics at the Shh locus: limb bud-specific differential regulation of competence and active transcription. *Dev Cell* 2009, **16**:47–57.
- Capellini TD, Di Giacomo G, Salsi V, Brendolan A, Ferretti E, et al: Pbx1/Pbx2 requirement for distal limb patterning is mediated by the hierarchical control of Hox gene spatial distribution and Shh expression. *Development* 2006, **133**:2263–2273.
- Galli A, Robay D, Osterwalder M, Bao X, Benazet JD, et al: Distinct roles of Hand2 in initiating polarity and posterior Shh expression during the onset of mouse limb bud development. *PLoS Genet* 2010, **6**:e1000901.
- Lettice LA, Williamson I, Wiltshire JH, Peluso S, Devenney PS, et al: Opposing Functions of the ETS Factor Family Define Shh Spatial Expression in Limb Buds and Underlie Polydactyly. *Dev Cell* 2012, **22**:459–467.
- Wang B, Fallon JF, Beachy PA: Hedgehog-Regulated Processing of Gli3 Produces an Anterior/Posterior Repressor gradient in the Developing Vertebrate Limb. *Cell* 2000, **100**:423–434.
- Mo R, Freer AM, Zinyk DL, Crackower MA, Michaud J, et al: Specific and redundant functions of Gli2 and Gli3 zinc finger genes in skeletal patterning and development. *Development* 1997, **124**:113–123.
- Litingtung Y, Dahn RD, Li Y, Fallon JF, Chiang C: Shh and Gli3 are dispensable for limb skeleton formation but regulate digit number and identity. *Nature* 2002, **418**:979–983.
- Lopez-Rios J, Speziale D, Robay D, Scotti M, Osterwalder M, et al: GLI3 Constrains Digit Number by Controlling Both Progenitor Proliferation and BMP-Dependent Exit to Chondrogenesis. *Developmental Cell* 2012, **22**:837–848.
- te Welscher P, Zuniga A, Kuijper S, Drenth T, Goedemans HJ, et al: Progression of Vertebrate Limb Development through SHH-Mediated Counteraction of GLI3. *Science* 2002, **298**:827–830.
- Khokha MK, Hsu D, Brunet LJ, Dionne MS, Harland RM: Gremlin is the BMP antagonist required for maintenance of Shh and Fgf signals during limb patterning. *Nat Genet* 2003, **34**:303–307.
- Zhou F, Leder P, Zuniga A, Dettenhofer M: Formin1 disruption confers oligodactylism and alters Bmp signaling. *Hum Mol Genet* 2009, **18**:2472–2482.
- Panman L, Galli A, Lagarde N, Michos O, Soete G, et al: Differential regulation of gene expression in the digit forming area of the mouse limb bud by SHH and gremlin 1/FGF-mediated epithelial-mesenchymal signalling. *Development* 2006, **133**:3419–3428.
- Soshnikova N, Montavon T, Leleu M, Galjart N, Duboule D: Functional analysis of CTCF during mammalian limb development. *Dev Cell* 2010, **19**:819–830.
- Vokes SA, Ji H, Wong WH, McMahon AP: A genome-scale analysis of the cis-regulatory circuitry underlying sonic hedgehog-mediated patterning of the mammalian limb. *Genes Dev* 2008, **22**:2651–2663.
- Birney E, Stamatoyannopoulos JA, Dutta A, Guigo R, Gingeras TR, et al: Identification and analysis of functional elements in 1% of the human genome by the ENCODE pilot project. *Nature* 2007, **447**:799–816.
- Myers RM, Stamatoyannopoulos J, Snyder M, Dunham I, Hardison RC, et al: A user's guide to the encyclopedia of DNA elements (ENCODE). *PLoS biology* 2011, **9**:e1001046.
- Pearl EJ, Barker D, Day RC, Beck CW: Identification of genes associated with regenerative success of *Xenopus laevis* hindlimbs. *BMC Dev Biol* 2008, **8**:66.
- Nicoli S, Gilardelli CN, Pozzoli O, Presta M, Cotelli F: Regulated expression pattern of gremlin during zebrafish development. *Gene expression patterns: GEP* 2005, **5**:539–544.
- Boisvert CA, Mark-Kurik E, Ahlberg PE: The pectoral fin of Panderichthys and the origin of digits. *Nature* 2008, **456**:636–638.
- Lettice LA, Heaney SJ, Purdie LA, Li L, de Beer P, et al: A long-range Shh enhancer regulates expression in the developing limb and fin and is associated with preaxial polydactyly. *Hum Mol Genet* 2003, **12**:1725–1735.
- Scherz PJ, Harfe BD, McMahon AP, Tabin CJ: The limb bud Shh-Fgf feedback loop is terminated by expansion of former ZPA cells. *Science* 2004, **305**:396–399.
- Verheyden JM, Sun X: An Fgf/Gremlin inhibitory feedback loop triggers termination of limb bud outgrowth. *Nature* 2008, **454**:638–641.
- Bandyopadhyay A, Tsuji K, Cox K, Harfe BD, Rosen V, et al: Genetic Analysis of the Roles of BMP2, BMP4, and BMP7 in Limb Patterning and Skeletogenesis. *PLoS Genet* 2006, **2**:e216.

42. Tzchori I, Day TF, Carolan PJ, Zhao Y, Wassif CA, *et al*: LIM homeobox transcription factors integrate signaling events that control three-dimensional limb patterning and growth. *Development* 2009, **136**:1375–1385.
43. Nissim S, Hasso SM, Fallon JF, Tabin CJ: Regulation of Gremlin expression in the posterior limb bud. *Dev Biol* 2006, **299**:12–21.
44. te Welscher P, Fernandez-Teran M, Ros MA, Zeller R: Mutual genetic antagonism involving GLI3 and dHAND prepatterns the vertebrate limb bud mesenchyme prior to SHH signaling. *Genes Dev* 2002, **16**:421–426.
45. Yang X, Li C, Herrera PL, Deng CX: Generation of Smad4/Dpc4 conditional knockout mice. *Genesis* 2002, **32**:80–81.
46. Logan M, Martin JF, Nagy A, Lobe C, Olson EN, *et al*: Expression of Cre recombinase in the developing mouse limb bud driven by a Prxl enhancer. *Genesis* 2002, **33**:77–80.
47. Wen X, Lai CK, Evangelista M, Hongo JA, de Sauvage FJ, *et al*: Kinetics of hedgehog-dependent full-length Gli3 accumulation in primary cilia and subsequent degradation. *Molecular and cellular biology* 2010, **30**:1910–1922.
48. Ong CT, Corces VG: Enhancer function: new insights into the regulation of tissue-specific gene expression. *Nature reviews Genetics* 2011, **12**:283–293.
49. Zeller R: The temporal dynamics of vertebrate limb development, teratogenesis and evolution. *Curr Opin Genet Dev* 2010, **20**:384–390.
50. St-Jacques B, Dassule HR, Karavanova I, Botchkarev VA, Li J, *et al*: Sonic hedgehog signaling is essential for hair development. *Curr Biol* 1998, **8**:1058–1068.
51. Maynard TM, Jain MD, Balmer CW, LaMantia AS: High-resolution mapping of the Gli3 mutation extra-toes reveals a 51.5-kb deletion. *Mamm Genome* 2002, **13**:58–61.
52. Morgan BA, Conlon FL, Manzanares M, Millar JB, Kanuga N, *et al*: Transposon tools for recombinant DNA manipulation: characterization of transcriptional regulators from yeast, *Xenopus*, and mouse. *Proc Natl Acad Sci U S A* 1996, **93**:2801–2806.
53. Tesson L, Heslan JM, Menoret S, Anegon I: Rapid and accurate determination of zygosity in transgenic animals by real-time quantitative PCR. *Transgenic research* 2002, **11**:43–48.
54. Ovcharenko I, Nobrega MA, Loots GG, Stubbs L: ECR Browser: a tool for visualizing and accessing data from comparisons of multiple vertebrate genomes. *Nucleic acids research* 2004, **32**:W280–W286.
55. Larkin MA, Blackshields G, Brown NP, Chenna R, McGettigan PA, McWilliam H, Valentin F, Wallace IM, Wilm A, Lopez R, Thompson JD, Gibson TJ, Higgins DG: ClustalW and ClustalX version 2. *Bioinformatics* 2007, **23**:2947–2948.

doi:10.1186/1471-213X-12-23

Cite this article as: Zuniga *et al*: Conserved *cis*-regulatory regions in a large genomic landscape control SHH and BMP-regulated *Gremlin1* expression in mouse limb buds. *BMC Developmental Biology* 2012 **12**:23.

Submit your next manuscript to BioMed Central and take full advantage of:

- Convenient online submission
- Thorough peer review
- No space constraints or color figure charges
- Immediate publication on acceptance
- Inclusion in PubMed, CAS, Scopus and Google Scholar
- Research which is freely available for redistribution

Submit your manuscript at
www.biomedcentral.com/submit



Fig. S1

HMCO1 conserved core

Mouse	-----TGAGCCCTTA---TGGGCAAGATACATTCACATGATCTGATAAAGCTCCA-T	2:113693360
Human	-----TGCTGTCCACA----CAGGCAGATATGCTCACATGATCTGATAA-GTTACA-C	15:33090823
Chimpanzee	-----TGCTGTCCACA----CAGGCAGATATGCTCACATGATCTGATAA-GTTACA-C	15:29568630
Dog	GGAGGTGTGCTATCCACA----CTAGCAGATA-GCTCCCGTGGTCTGCTAA-GTTACA-T	30:5150165
Bovine	-----TGCTGTCCACA----CAGGCAGATACTCTCAGCTGATCTGATAA-GTTACA-C	10:29933362
Opossum	-----TGCTGCCCCCACTCAAGCAGATAAACACACATGATCTGATAA-GTTACA-C	1:188935233
Chicken	-----TGCTGTCCCA----CAAAAAGATAAACACATATAATCTGATAA-ATTACA-C	5:32849615
Lizard	-----TGCTGTCCCTG-----CAAAAAGATAAACACGCTATAATCTGATAA-ATTACA-C	1:32921655
Frog	-----AAGATAAACACGCCAGATCTGATAA-GTTACACT	GL172673.1:3687453
Coelacanth	-----TGCTGTCTCT---CAAAA-GATAAATACATAATCTGATAA-GTTACA-C	JH126706.1:163591

**** * **** ** * **

Mouse	TCTCTTAGCCCTTCCAATTACTAGCTAGTAAA-TGAAAGGCGAGTTGTGCTAATTTGCA	2:113693419
Human	TTTCTTAACCCCTTCCAATTACTAGCTAGTAAA-TGAAAGGAGGGTTGTGCTAATTTGCA	15:33090750
Chimpanzee	TTTCTTAACCCCTTCCAATTACTAGCTAGTAAA-TGAAAGGAGGGTTGTGCTAATTTGCA	15:29568557
Dog	GTTCTTACCCTTCCAATTACTAGCTAGTAAA-TGAAAGGGGAGCAGCGCTAATTTGCA	30:5150224
Bovine	TTTCTTAACCCCTTCCAATTACTAGCTAGTAAA-TGAAAGGGGAGCTGTGCTAATTTGCA	10:29933421
Opossum	TTTCTTAACCCCTTCCAATTACTAGCTAGTAAA-TGAAAGGGGAGCAGTGTGCTAATTTGCA	1:188935293
Chicken	TTTTGTAACCCCTTCCAATTACTAGCTAGTAAA-TGAAAGGGGAGCTGTGCTAATTTGTA	5:32849675
Lizard	TTTCTTAACCCCTTCCAATTACTAGCTAGTAAA-TGAAAGGGGAGCTGTGCTAATTTGTA	1:32921606
Frog	TTTCTTACCCTTCCAATTACTAGCTAGTAAA-TGAAAGGAGACCTCAGCTAATTTGGA	GL172673.1:3687391
Coelacanth	TTTCTTAACCCCTTCCAATTACTAGCTAGTAAA-TGAAAGGGGAGCTGTGCTAATTTGTA	JH126706.1:163651

* * * * * ***** ** ***** ***** * ***** *

Mouse	ACAGATTGCTTCTC-TGTGTATTTTTCACATCGGCCCAAGCTAAATGAGGCAGCCTTGCTG	2:113693478
Human	ACAGATTGCTTCTC-TGTGTATTTTTCATGTTGGCCAGGCTAAATGAGGCAGCCTTGCTG	15:33090707
Chimpanzee	ACAGATTGCTTCTC-TGTGTATTTTTCATGTTGGCCAGGCTAAATGAGGCAGCCTTGCTG	15:29568501
Dog	ACAGATTGCTTCTC-TGTGTATTTTTCATGTTGGCCAGGCTAAATGAGGCAGCCTTAGTG	30:5150283
Bovine	ACAGATTGCTTCTC-TGTGTATTTTTCATGTTGGCCCAAGCTAAATGAGGCAGCCTTGCTG	10:29933480
Opossum	ACAGATTGCTTCTC-TGGGCATTTCTCATGTTGGCCAGGCTAAATGAGGTGGTATTGCTG	1:188935352
Chicken	ACAGATTGCTTCTC-TGTGCATTTTTCATGTTGAAC TAGCCTAAATGAGGCAGATTTGCTG	5:32849734
Lizard	ACAGATTGCTTCTC-TTTCATTTTTCATGTTAGCAGTGCCTAAATGAGGCAAGATTGCTG	1:32921536
Frog	CCAGATTTTTT-----TTTCTCTTGG-----TGCTGAG-----TTAC--	GL172673.1:3687349
Coelacanth	ACAGATTGCTTCTCCTGTGCATTTTCATGTTGAAC TAGCCCAATGAGGTGATATTACTG	JH126706.1:163711

***** ** *

HMCO3 conserved core

Mouse	A-----CTCTAAACTATTTCTGATCTTCATC-TTTATTTT-CAGACAA	2:113618954
Human	A-----CTCTAAACTGTTTCTGATATCAAC-TCTATTTT-CAAACAC	15:33165537
Chimpanzee	A-----CTCTAAACTGTTTCTGATCTTCAC-TCATTTT-CAAACAC	15:29643510
Dog	AAGA-----AATAGCTCTAAACTATTTCTGAATTTTAGC-TTCATTTT-CAGACAT	30:5079021
Bovine	-----AGC-TTTATTTT-CAGACAC	10:29837054
Opossum	-----TTT-CAGAAAG	1:188837695
Chicken	-----	
Lizard	A-----CACTGAACTATTTCTAGTGTT--ACATTTATTTT-AAAAATG	1:32940147
Coelacanth	AAAAGCAGTGTGAAATTTCCAGGTTGTACTTGGTCTTTCTCATTTGCTTTACAGTATG	JH126706.1:97666

Mouse	ATCCTGAGAAACCTGACTCCCAGCGAATGACAATGTGGCCCTCTTTATG-TGAAGCCT	2:113619013
Human	ATCCTAAGAAATCCTACTCCCACAAATGACAATGCAGCCTCTTTATA-TGAAACCT	15:33165478
Chimpanzee	ATCCTAAGAAATCCTACTCCCACAAATGACAATGCAGCCTCTTTATA-TGAAACCT	15:29643451
Dog	ATTCGAGAAAGTCCCAACTCTTAGTGAAGTGCAGCAGCCTCTTTATA-TGAAGCCT	30:5079080
Bovine	ATCCTAAGAAATCCTGACTCCCAGCAATGACAATACAGCCTCTTTATA-TGAAACCT	10:29837113
Opossum	GTCTTCAGAAATATGGCTTCCAACCTGATGACAGTGCAGTCTTATTTTACAAAAGTCT	1:188837754
Chicken	-----AATCCAGTCT-----GATTGACACTGAAATGCTCTTTACA-TGAAAGTT	5:32819795
Lizard	ACATTTAAAAATACCAACTCCCTACCTGGCAGACATGTCAGTACTACTTGCA-TGAAGGTT	1:32940088
Coelacanth	GTCC--ATAAAGACCAATTCCTGCTTGTAGATACCATAGGCCCTTTAATG-TGGTGACT	JH126706.1:97723

* *

Mouse	TGTTTATAGGCCCAATTCCTCCGACAGATTTACAAGTCTGTGGAGTTTAAAAGGACG	2:113619073
Human	TGTTTATAGGCCCAATTCCTCCGACAGATTTACAAGTCTGTGGAGTTTAAAAGGACG	15:33165418
Chimpanzee	TGTTTATAGGCCCAATTCCTCCGACAGATTTACAAGTCTGTGGAGTTTAAAAGGACG	15:29643391
Dog	TGTTTATAGGCCCAATTCCTCCGACAGATTTACAAGTCTGTGGAGTTTAAAAGGACG	30:5079140
Bovine	TGTTTATAGGCTACAATTCCTCCGACAGATTTACAAGTCTGTGGAGTTTAAAAGATG	10:29837173
Opossum	TGTTTATAAACCTCAATTCCTCCGACAGATTTACAAGTCTGTGGAGTTTAA--GACG	1:188837812
Chicken	TGTTTATAGGCCAGTGATTTCTTTGACAGATTTACAAGTGCCTGTGGAGTTTAAAAGATG	5:32819855
Lizard	TGTTTATACATAATGATTTCTTAGCAGATTTACAAGTGCCTGTGGAGTTTAAAAGATG	1:32940028
Coelacanth	TAACCATAGGTGATGACGCCAATGACAGGTTTACAAGTGCCTGTTTAAAAGATG	JH126706.1:97783

* ** *

Mouse	ATTGCTTAACAAGCATTAAGTGAG-----	2:113619097
Human	ATTGCTTAACAAGCATTAAGTGAG-----	15:33165394
Chimpanzee	ATTGCTTAACAAGCATTAAGTGAG-----	15:29643367
Dog	ATTGCTTAACAAGCATTAAGTGAG-----	30:5079164
Bovine	ATTGCTTAACAAGCATTAAGTGAG-----	10:29837197
Opossum	GTTGCCTAATAGGCATTAAGTGAG-----	1:188837836
Chicken	ATTGCCAATAGGCATTAAGTGAG-----	5:32819879
Lizard	ATTGCCAACAAGGCATTAAGGAG-----	1:32940004
Coelacanth	CTTAGCCAATAGATATCTAGTGAATTTGTGTGTAATAAATGAACTAATAAATACAGCTG	JH126706.1:97843

** ** * * * *

Table S1**Genomic coordinates for the sequence comparisons shown in Fig. 1A**

<i>Region</i>	<i>Species</i>	<i>% ID (threshold 74%)</i>	<i>Length (100bp threshold)</i>	<i>Coordinates</i>
HMCO1	Zebrafish	-	-	-
HMCO1	Xenopus	74.7%	100	xenTro2 scaffold_37:3687354-3687453
HMCO1	Chicken	80.2%	381	galGal3 chr5:32849567-32849947
HMCO1	Opossum	81.3%	430	monDom5 chr1:188935147-188935576
HMCO1	Dog	80.5%	387	canFam2 chr30:5150126-5150512
HMCO1	Chimpanzee	81.5%	508	panTro3 chr15:29568244-29568751
HMCO1	Human	81.5%	508	hg19 chr15:33090437-33090944
HMCO2	Zebrafish	-	-	-
HMCO2	Xenopus	-	-	-
HMCO2	Chicken	80.4%	377	galGal3 chr5:32836351-32836727
HMCO2	Opossum	80.1%	380	monDom5 chr1:188909506-188909885
HMCO2	Dog	84.2%	494	canFam2 chr30:5129238-5129731
HMCO2	Chimpanzee	84.6%	818	panTro3 chr15:29588916-29589733
HMCO2	Human	84.5%	818	hg19 chr15:33111145-33111962
HMCO3	Zebrafish	-	-	-
HMCO3	Xenopus	-	-	-
HMCO3	Chicken	74%	272	galGal3 chr5:32819753-32820024
HMCO3	Opossum	77%	331	monDom5 chr1:188837685-188838015
HMCO3	Dog	78.3%	842	canFam2 chr30:5078806-5079647
HMCO3	Chimpanzee	80.7%	940	panTro3 chr15:29642824-29643763
HMCO3	Human	80.1%	937	hg19 chr15:33164854-33165790

Table S2

Analysis of transgenic founder embryo

Transgene	Embryos *	Forelimb bud expression	Figure
<i>Grem1-LacZ</i>	3	3 posterior	Fig.1B
<i>Grem1-LacZ ΔHMCO1</i>	7	1 strong 1 very weak 5 no expression	Fig.1C
<i>Grem1-LacZ ΔHMCO2</i>	3	2 weak posterior 1 no expression	Fig.1D
<i>Grem1-LacZ ΔHMCO3</i>	5	3 posterior 2 no expression	Fig.1E
<i>HMCO123-βglob-LacZ</i>	3	3 anterior	Fig.2A
<i>GRS1-βglob-LacZ</i>	2	2 posterior	Fig.2B

* Founder embryos with β-galactosidase activity anywhere in limb buds and/or trunk

Fig.S2

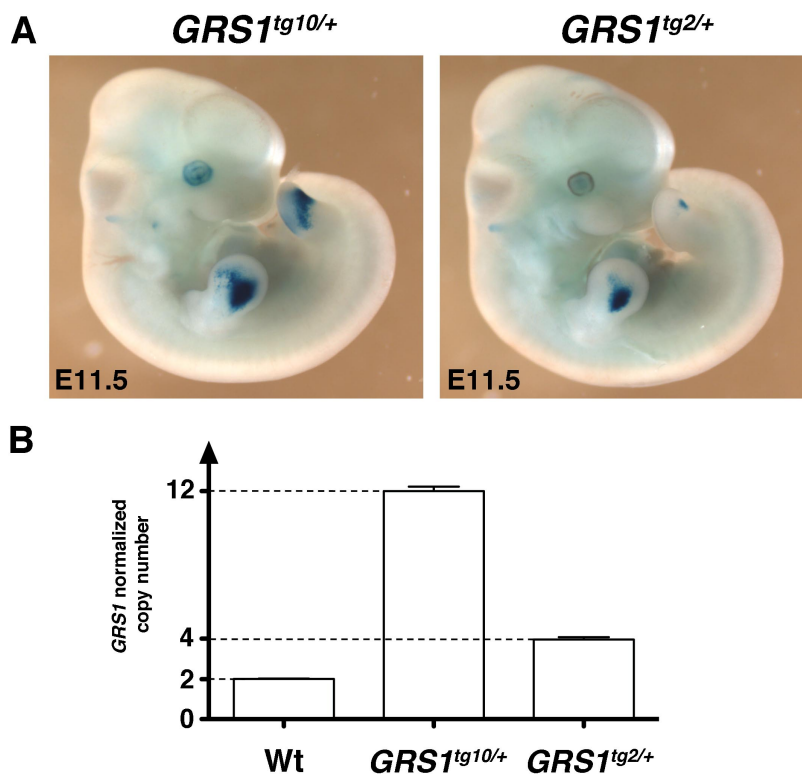


Fig.S3

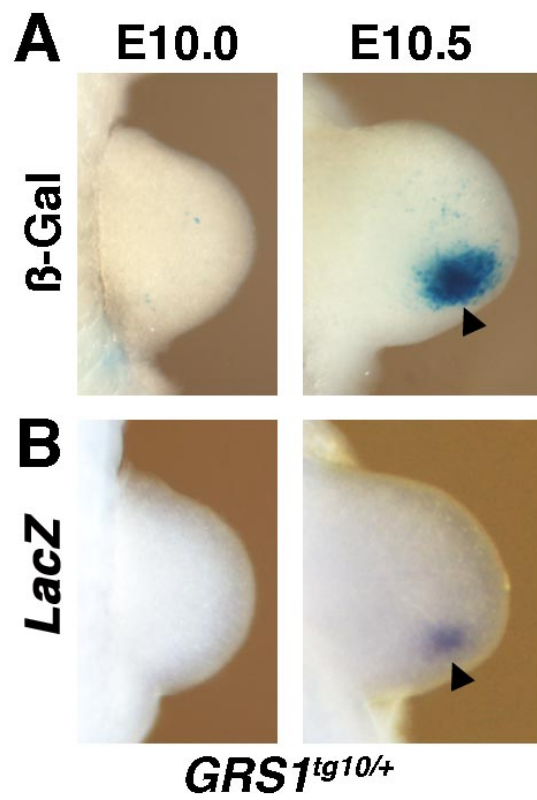


Fig.S4

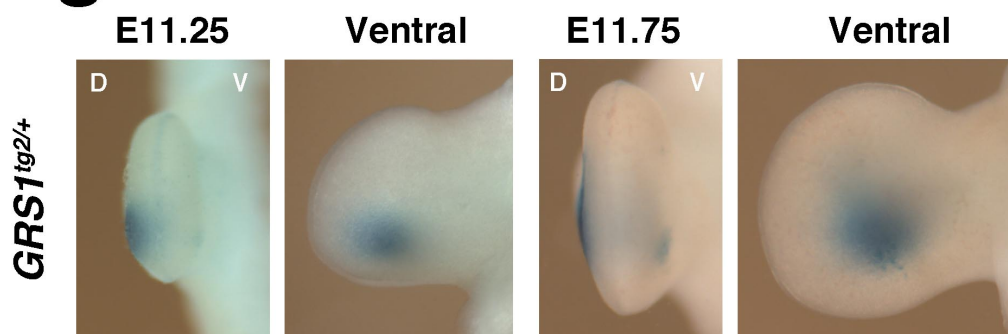


Table S3**qPCR amplicons for GLI3 ChIP analysis**

<i>GLI3 ChIP amplicon</i>	<i>Coordinates (mm10)</i>
a	chr2:113691635-113691714
b	chr2:113692244-113692320
c	chr2:113693100-113693179
d	chr2:113693471-113693578
e	chr2:113697427-113697518
f	chr2:113674650-113674732
g	chr2:113675141-113675273
h	chr2:113618703-113618814
i	chr2:113619171-113619319

Table S4**Genomic coordinates of identified *Grem1* regulatory regions**

<i>Annotation</i>	<i>Length</i>	<i>Coordinates (mm10)</i>
HMCO1	520 bp	chr2:113693204-113693723
HMCO2	1279 bp	chr2:113674096-113675374
HMCO3	924 bp	chr2:113618678-113619601
<i>GRS1-βglob-LacZ</i> transgene	9'831 bp	chr2:113689791-113699621
GBR1 (HMCO1, ChIP amplicons c-d) [32]	439 bp	chr2:113693005-113693989
GBR2 (ChIP amplicons a-b) [32]	700 bp	chr2:113691653-113692352
GBR3 (HMCO2, ChIP amplicons f-g) [32]	985 bp	chr2:113674455-113675313
GBR4 (with GLI binding motif) [32]	439 bp	chr2:113640843-113641281
CTCF binding region [31]	468 bp	chr2:113648107-113648574

6.1.3. The *Grem1* cis-regulatory landscape integrates several signaling inputs from multiple CRMs

In this study, we showed that a 9kb region located in the *cis*-regulatory landscape of *Grem1* regulates aspects of the posterior activation and distal anterior expansion of *Grem1* expression during progression of limb bud outgrowth. This *Gremlin1* Regulatory Sequence 1 (*GRS1*) is activated by the Sonic hedgehog (SHH) pathway and interacts with GLI3 containing protein complexes. Furthermore, *GRS1* expansion towards the distal anterior part of the limb bud is dependent on BMP signaling, as seen by conditionally inactivating the BMP signal transducer SMAD4 in limb bud mesenchyme. Several other studies identified additional CRMs located outside of *GRS1* that contribute to *Grem1* expression and interact with GLI3 or CTCF chromatin complexes (Vokes et al., 2008; Soshnikova et al., 2010). Together, these data reveal that the large *cis*-regulatory landscape of *Grem1* is an archipelago composed of multiple CRMs that integrate signaling inputs from various pathways to regulate the robust and dynamic expression of *Grem1* in limb buds.

As limb bud outgrowth advances, several factors eventually contribute to the termination of *Grem1* expression and feedback signaling: 1) increasing high levels of FGF signaling from the AER repress *Grem1* in the distal mesenchyme (Verheyden and Sun, 2008); 2) GLI3 represses *Grem1* in the anterior limb bud mesenchyme, which enables the rise of BMP activity and BMP-dependent initiation of chondrogenesis (Lopez-Rios et al., 2012); 3) the induction of TBX2 by BMP signaling represses *Grem1* by direct interaction of this transcription factor with the GBR4 element in Shh descendant cells in the posterior limb bud (Farin et al., 2013); and 4) Shh descendant cells become unable to express *Grem1* in the posterior limb bud (Scherz et al., 2004). Our study shows that *GRS1* activity is not terminated with the same kinetics as endogenous *Grem1* expression. In particular, a strong *LacZ* expression domain remains in the posterior mesenchyme. This domain becomes spatially separated from the distal anterior domain at E12.0. This suggests that the CRM(s) that mediates FGF dependent repression of *Grem1* are not part of *GRS1*. In contrast, the anterior expansion and upregulation of *GRS1-LacZ* domain in *Gli3*-

deficient limb buds show that *GRS1* encodes CRMs involved in GLI3R-mediated repression of *Grem1* expression.

The GBR4 CRM interacts both with the GLI3 and TBX2 transcriptional regulators and is able to direct *LacZ* expression in the posterior but not anterior mesenchyme (Lopez-Rios et al., 2012; Farin et al., 2013; Vokes et al., 2008). This region, located ~50kb upstream of *GRS1*, was called GLI Responsive Element 1 (GRE1) in a recent study (Li et al., 2014). GRE1 is activated by SHH and bound by GLI3A chromatin complexes in the posterior limb bud, and its activity is not affected by inhibiting FGF signaling. In addition to its enhancer activity in the posterior limb bud, GRE1 participates in GLI3R-mediated silencing of *Grem1* in the anterior mesenchyme (Li et al., 2014). GRE1 and *GRS1* are both directly regulated by SHH/GLI3 and may thus be functionally redundant and/or are likely required cooperatively for regulating the dynamic expression of *Grem1* in the limb bud mesenchyme.

The activation of *Grem1* expression in the posterior limb bud mesenchyme requires BMP signaling and the HOX transcriptional regulators upstream of SHH signaling. SHH signaling is subsequently required to upregulate and distal-anteriorly expand *Grem1* expression (Zuniga et al., 1999; Panman et al., 2006; Nissim et al., 2006; Benazet et al., 2009; Sheth et al., 2013). Interestingly, the expression of the *GRS1* reporter requires SHH signaling and β -galactosidase activity is first detected only after initiation of *Grem1* endogenous expression in the limb bud mesenchyme. Thus, the BMP Responsive Elements (BRE) and HOX CRMs are not encoded by the *GRS1* and remain to be identified.

In *Smad4* ^{$\Delta\Delta M$} limb buds, the initial expression of *Grem1* in the posterior mesenchyme is reduced, fails to expand anteriorly, and is lost in *Shh* ^{$\Delta\Delta$} ; *Smad4* ^{$\Delta\Delta M$} forelimb buds (Benazet et al., 2012). Thus, *Grem1* initiation depends on positive regulation by both SHH and SMAD4-mediated BMP signal transduction. Moreover, the absence of anterior expansion of *GRS1* expression domain in *Smad4* ^{$\Delta\Delta M$} limb buds suggests that *GRS1* contains BREs controlling SMAD4-dependant expansion of *Grem1* expression after its initial activation (this study and (Benazet et al., 2012). The distal anterior expansion of *Grem1* expression is also regulated by CTCF and HOX transcriptional regulators (Soshnikova et al., 2010; Sheth et al., 2013).

To summarize the integration of these various signaling inputs by multiple CRMs located in *Grem1* cis-regulatory landscape, we propose the following kinetics for the regulation of *Grem1* expression: 1) An early expression domain is initiated in the posterior limb bud mesenchyme by BMP signaling and HOX transcriptional regulators through CRMs that need to be identified. This posterior domain is maintained by SHH/GLI3A inputs acting on the GLI-binding regions in *GRS1* and GRE1 CRMs. 2) The dynamic expansion of *Grem1* expression in the distal anterior mesenchyme depends on BMP/SMAD4 signal transduction impacting on *GRS1* and on CRMs regulated by CTCF and HOX complexes. This distal-anterior domain is likely silenced by GLI3R impacting on GRE1 CRM. 3) The termination of the posterior domain may in part be mediated by TBX2 interacting with GRE1. 4) In contrast, termination of the distal-anterior domain likely depends on GLI3R-mediated repression via the *GRS1* and GRE1 CRMs and unknown FGF-responsive elements. DNase HS sites mark all the known *Grem1* CRMs. Each of them likely encodes binding sites for the different *trans*-acting factors that fulfill different activities depending on the specific spatial and temporal developmental context.

GLI3 direct interactions with relevant regions in *GRS1* and GRE1 have been well characterized (this study and (Li et al., 2014)). The next major challenge is to understand how *Grem1* cis-regulatory landscape integrates BMP signaling inputs. We are attempting this by identifying the CRMs that interact with SMAD4-containing chromatin complexes.

6.1.4. Identification of SMAD4 target CRMs during limb bud development: the need for a new tool

In addition to the role of SMAD4 in the regulation of *GRS1* activity (Zuniga et al., 2012), we showed that *Smad4* is crucial for the initiation of digits primordia and chondrogenesis (Benazet et al., 2012). Furthermore, limb bud ectodermal *Smad4* is required for AER initiation and for AER-FGF mediated termination of epithelial-mesenchymal signaling (Benazet and Zeller, 2013). Despite the inactivation of *Smad4* in limb buds affects the expression of a large number of downstream genes, there is no evidence that these genes are direct SMAD4 transcriptional targets.

We thus decided to initiate a genome-wide analysis of the SMAD4 chromatin complexes in limb buds using ChIP-Seq to: 1) identify SMAD4 interacting CRMs in *Grem1* regulatory landscape and 2) to get further insights into the direct BMP targets that are involved in chondrogenic differentiation.

Several SMAD4 ChIP-Seq studies using cell lines in combination with different types of antibodies have been published (Koinuma et al., 2009; Qin et al., 2009; Fei et al., 2010; Kennedy et al., 2011; Morikawa et al., 2011). Therefore, we tested supposedly ChIP-grade anti-SMAD4 antibodies on a known BRE located in the promoter of the gene *Id1* using wild-type embryonic limb buds, but no SMAD4 chromatin complexes were detected (data not shown). Therefore, we decided to introduce a 3xFLAG epitope tag in the endogenous SMAD4 protein as we have successfully done for HAND2 (see Chapter 6.2).

6.1.5. Generation of *Smad4*^{3xFLAG} mice by homologous recombination

Targeting and testing ES cells for SMAD4^{3xFLAG} expression

Two previous attempts were made to produce a mouse line expressing a SMAD4^{3xFLAG} protein using cassette exchange approaches. However, the resulting *Smad4*^{3xF-dRMCE} and *Smad4*^{3xF-R26} alleles were expressed at levels too low for genome-wide ChIP-Seq analysis (see Appendix 12.1). Therefore, we decided to introduce the 3xFLAG epitope tag in the endogenous SMAD4 protein using conventional homologous recombination. A targeting vector consisting of two homology arms flanking the 3'-end of *Smad4* coding sequence, in which the 3xFLAG was inserted in frame between the exon 12 and the 3'UTR, was constructed (Fig.11A). A floxed Neomycin selection cassette was inserted downstream of *Smad4* locus in the 3' homology arm. This targeting vector was linearized and electroporated in R1 embryonic stem (ES) cells to generate the *Smad4*^{3xF-HR} allele (Fig.11A, thereafter referred as *S4*^{3xF-HR}). 662 ES cells clones were picked (together with A.Zuniga) and 424 of them screened for correct recombination by Southern Blot using a probe located outside of the 5' homology arm (Fig.11A and Fig.11B, top panel).

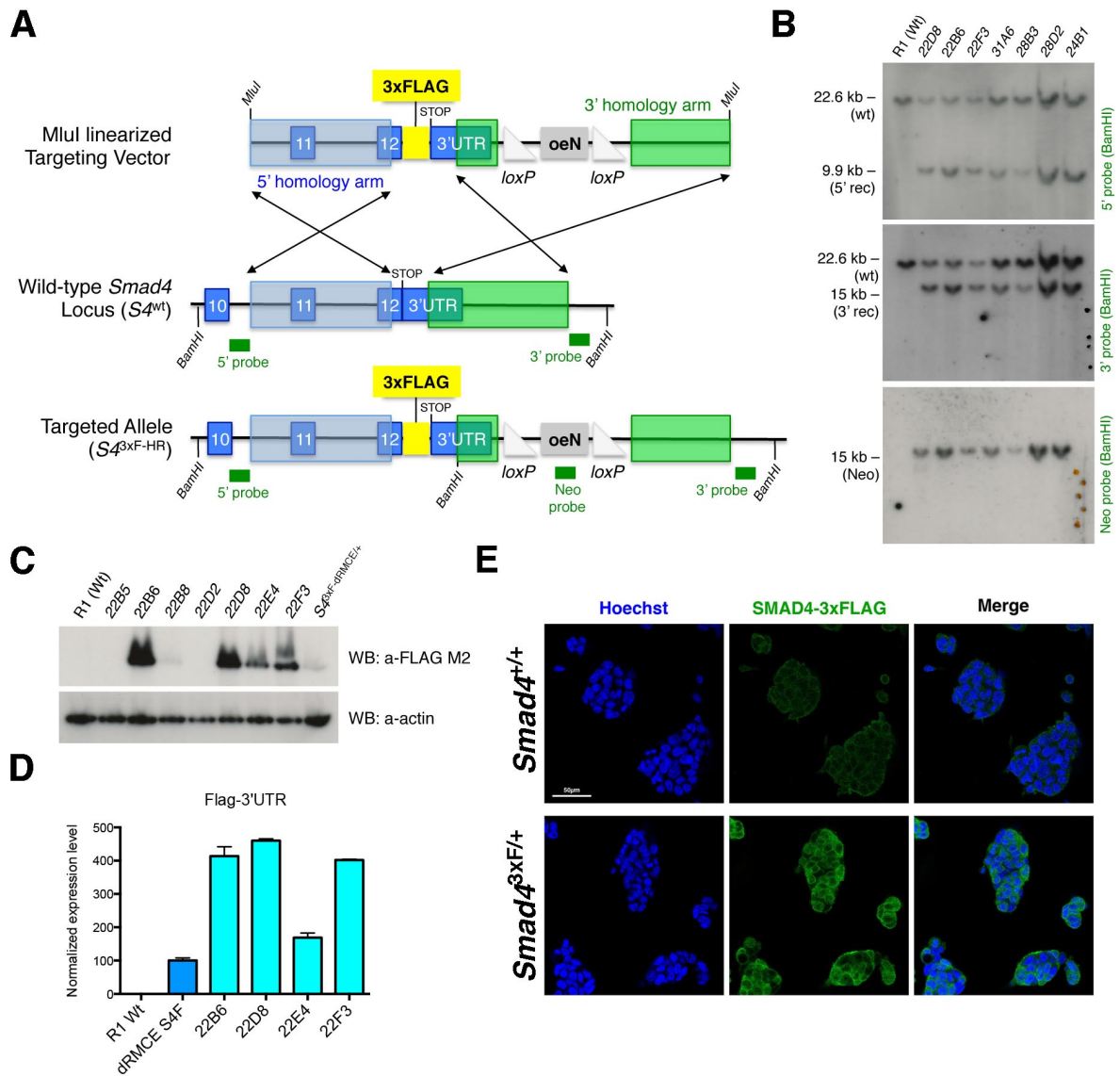


Figure 11. Expression of the *Smad4*^{3xFLAG-HR} allele in mouse ES cells

(A) Homologous recombination strategy. Top scheme: linearized targeting vector containing two homology arms flanking the 3'-end of *Smad4* coding sequence. A 3xFLAG epitope tag was fused in frame between coding exon 12 and the 3'UTR. A floxed Neo cassette is inserted downstream of *Smad4* locus in the 3' homology arm. Homologous recombination generates the *Smad4*^{3xFLAG-HR} allele (bottom scheme). The restriction sites used for Southern Blot analysis are indicated in italic, and the Southern Blot probes are shown as green boxes. (B) Southern Blot analysis of seven ES cells clones. Wild-type R1 ES cells were used as control. Left panel: Genomic DNA digested with BamHI and blotted with the 5' probe shown in (A). The sizes of the expected wild-type and 5'-recombined bands are indicated on the left. Middle panel: 3' probe blot following BamHI digestion. Right panel: blot probed for the Neo cassette following BamHI digestion. (C) Western Blot detection of the SMAD4^{3xFLAG} protein in extracts of several different *S4*^{3xFLAG-HR/+} ES cells clones. Wild-type R1 ES cells and the negative clone 22B5 were used as controls, while *S4*^{3xFLAG-dRMCE/+} ES cells were used as a control for a low SMAD4^{3xFLAG} expression (see Appendix 12.1). Clones 22B6 and 22D8 express the highest levels of SMAD4 (~63kDa). ACTIN (42kDa) was used as a loading control and is present in similar amounts in all samples. (D) qPCR on *Smad4* cDNA from wild-type, *S4*^{3xFLAG-dRMCE/+} and several clones of the *S4*^{3xFLAG-HR/+} ES cells. Intermediate expression in clone 22E4 indicates that this is a mixed clone. (E) Immunofluorescence detection of the SMAD4^{3xFLAG} protein in undifferentiated wild-type or *S4*^{3xFLAG-HR/+} ES cells. Green: SMAD4^{3xFLAG} protein. Blue: nuclei stained by Hoechst. Scale bar: 50 μ m

Positively recombined ES cell clones were further screened for correct 3' recombination (Fig.11A and Fig.11B, middle panel). Finally, single insertion of the Neomycin cassette was assessed to exclude ES cell clones with random integration of the targeting construct (Fig.11A and Fig.11B, bottom panel). In total, 29 of the 424 ES cell clones carried the $S4^{3xF-HR}$ allele (6.8%, similar to the expected 3-6% of correct targeting on *Smad4* locus (Chu et al., 2004; Takaku et al., 1998)). In addition, Western Blot analysis detected the intact SMAD4^{3xFLAG} protein in ES cells (Fig.11C). Western Blot analysis also allowed identifying mixed ES cell clones expressing the tagged protein at lower levels (Fig.11C, compare ES cell clones 22B6, 22D8 to 22E4. Clone 22B5 is a negative control). Finally, the levels of the SMAD4^{3xFLAG} protein in the different ES cell clones carrying the $S4^{3xF-HR}$ allele was much higher compared to those in ES cells carrying the damaged $S4^{3xF-dRMCE}$ allele (Fig.11C and Appendix 12.1). These results and the mixed nature of some ES cell clones, such as 22E4, were confirmed by qPCR analysis (Fig.11D). Immunocytochemistry showed that the 3xFLAG epitope tag allows detection of endogenous SMAD4 proteins both in the cytoplasm and nuclei of ES cell clones (Fig.11E). Three of the tested clones were karyotyped and did not show any obvious chromosomal abnormalities (data not shown).

Smad4^{3xFLAG} allele: a new tool for future ChIP-Seq studies

Eight of the positive $S4^{+/3xF-HR}$ ES cell clones were injected in C57BL/6 blastocysts at the Transgenic Mouse Core Facility (TMCF, Basel, see Fig.12A). Chimeric males were obtained from three independent clones and mated to *CMV-Cre* females (C57BL/6 background) to delete the floxed Neo selection cassette. Four chimeras transmitted the $S4^{3xF-HR}$ allele to 67-100% of their offspring (Fig.12B). Germline transmission was assessed by coat color (Fig.12A) and confirmed by PCR genotyping. *CMV-Cre*-mediated deletion of the floxed Neo selection cassette resulted in the $S4^{3xF-HR\Delta Neo}$ allele (Fig.12C). Specific primers were used to discriminate between the $S4^{wt}$, $S4^{3xF-HR}$ and $S4^{3xF-HR\Delta Neo}$ alleles (Fig.12C, arrows, and Fig.12D). Mice homozygous for the $S4^{3xF-HR\Delta Neo}$ allele are viable and obtained in the expected Mendelian ratio from two independent ES cell clones (data not shown).

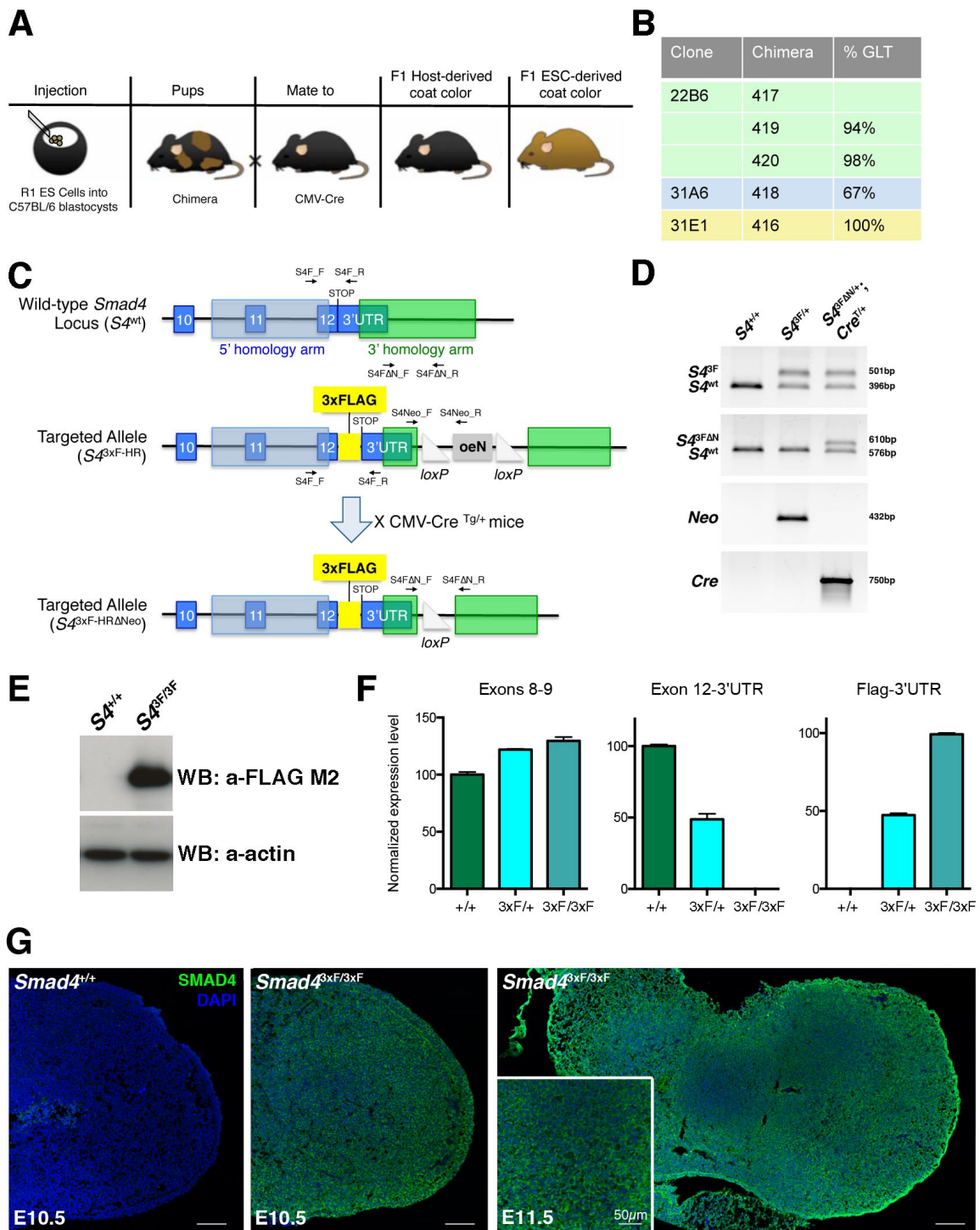


Figure 12. Establishment of $Smad4^{3xF/3xF}$ mouse strain

(A) Schematic representation of the generation of chimeras and F1 offspring from $S4^{3xF-HR/+}$ ES cells (adapted from (Pettitt et al., 2009)). (B) Table summarizing the percentage of germline transmission observed for each of the chimeras derived from $S4^{3xF-HR/+}$ ES cells clones (22B6, 31A6 and 31E1). (C) Schematic representation of the $S4^{wt}$ (top), $S4^{3xF-HR}$ (middle) and $S4^{3xF-HR\Delta Neo}$ (bottom) alleles. The $S4^{3xF-HR\Delta Neo}$ allele is obtained by *CMV-Cre* mediated recombination of the *loxP* sites in the $S4^{3xF-HR}$ allele. Arrows indicate primers used for the genotyping of these alleles. (D) PCR genotyping of all three considered alleles. The sizes of the expected bands are indicated on the right. (E) Detection of the $SMAD4^{3xF}$ protein in limb buds of $S4^{3xF/3xF}$ embryos (E11.75). Protein extracts from wild-type limb buds were used as control. (F) RT-qPCR analysis of E11.75 limb buds from $S4^{+/+}$, $S4^{3xF/+}$ and

$S4^{3x^F/3x^F}$ embryos. Normalized *Smad4* transcript level using the junction between exon 8-9 (left panel), exon 12-3'UTR junction (middle panel) and FLAG-3'UTR (right panel) for amplification. (G) The anti-FLAG M2 antibody was used to detect SMAD4^{3xFLAG} proteins in frozen sections of limb buds. From left to right: wild-type forelimb (E10.5), $S4^{3x^F/3x^F}$ forelimb (E10.5) and $S4^{3x^F/3x^F}$ forelimb (E11.5). Scale bar: 100 μ m (50 μ m in high magnification).

The *Smad4*^{3xFLAG} strain was established by breeding the *Smad4*^{3x^F-HR Δ Neo} allele from the ES cell clone 31A6 into a NMRI background (to obtain the most embryos possible for future analysis). The SMAD4^{3xFLAG} protein is detected with high sensitivity and specificity in limb bud tissues from *Smad4*^{3x^F/+} (not shown) and *Smad4*^{3x^F/3x^F} embryos (E11.75, Fig.12E). The levels of *Smad4* transcripts in *Smad4*^{3x^F/+} and *Smad4*^{3x^F/3x^F} limb buds were similar to wild-type controls (E11.75, Fig.12F, left panel). In heterozygous embryos, the $S4^{wt}$ allele was expressed as expected at ~50% in comparison to *Smad4*^{+/+} embryos (Fig.12F, middle panel). Conversely, in heterozygous embryos the $S4^{3x^F}$ allele was expressed at ~50% in comparison to *Smad4*^{3x^F/3x^F} embryos (Fig.12F, right panel). Altogether, these data establish that the *Smad4*^{3x^F-HR Δ Neo} allele is expressed like the wild-type allele, which makes this allele a promising tool to study SMAD4 chromatin complexes and protein interactions *in vivo*. Finally, we performed immunohistochemistry on frozen limb bud sections to assess SMAD4 *in vivo* localization (together with J.Leclercq). As seen by whole-mount antibody staining (Benazet et al., 2012), SMAD4 is evenly distributed throughout limb bud mesenchyme at E10.5 and E11.5 (Fig.12G). In most of the limb bud cells, SMAD4 proteins are detected both in the cytoplasm and nuclei (Fig.12G, high magnification).

We will now use the *Smad4*^{3x^F-HR Δ Neo} allele to determine the genome-wide range of SMAD4 target sequences using ChIP-Seq analysis. To this aim, we have collected limb buds from around 600x E10.75-E11.0 embryos (37-42 somites). The chromatin of these limb buds was crosslinked and snap frozen and is now being processed for ChIP-Seq analysis. The range of SMAD4 interacting sequences will provide us interesting insights into the transcriptional networks regulated by SMAD4 during mouse limb bud development. In addition, identifying the CRMs that interact with SMAD4 chromatin complexes in the *Grem1* *cis*-regulatory landscape will be of particular interest to understand how this complex landscape integrates various signaling inputs.

6.2. From *trans*-acting factor to *cis*-regulatory modules:

identification of the direct transcriptional targets of HAND2 during heart morphogenesis

6.2.1. The *Hand2*^{3xFLAG} allele is a new genetic tool to study HAND2 distribution during heart development

By taking advantage of the straightforward and high efficient strategy to target mouse ES cells using Dual Recombinase-Mediated Cassette Exchange (dRMCE, (Osterwalder et al., 2010a), a mouse line with a 3xFLAG epitope-tag inserted into the endogenous *Hand2* locus was generated by M.Osterwalder. The generation and characterization of this *Hand2*^{3xFLAG} allele is described in (Osterwalder et al., in press). Briefly, the 3xFLAG epitope tag was fused in frame the N-terminal part of the *Hand2* coding sequence and used to replace the corresponding region in conditional *Hand2* R1 ES cells by dRMCE (Galli et al., 2010) (Fig.13A). The insertion of this epitope tag does not affect the expression and the function of the *Hand2* gene products, and the tagged HAND2 proteins are readily detected in all *Hand2* expressing tissues (heart, limb buds and branchial arches) with high specificity and sensitivity, both by Western Blot and by immunohistochemistry (Osterwalder et al., in press). Homozygous *Hand2*^{3xF/3xF} develop normally and do not exhibit any phenotype or sign of embryonic lethality as observed in *Hand2*-deficient embryos (Srivastava et al., 1997). The *Hand2*^{3xFLAG} allele is thus a new fantastic tool to study the endogenous spatio-temporal distribution of HAND2 proteins and identify its downstream functional interactions during heart, limb buds and branchial arch morphogenesis.

During the onset of heart development, *Hand2* transcripts are mainly expressed in the myocardium of second heart field (SHF) derived structures such as the outflow tract (OFT) and right ventricle (RV), the endocardium of various cardiac compartments, the proepicardial organ (PEO) and derived epicardium, and structures derived from cardiac neural crest cells (cNCC) (Srivastava, 1995; Biben and Harvey, 1997; Srivastava et al., 1997; Barnes et al., 2011). In contrast to these studies, relying on whole-mount or section *in situ*-hybridization, we used

immunohistochemistry to detect the $HAND2^{3xFLAG}$ proteins with the M2 anti-FLAG antibody (Sigma). This allowed us to determine the $HAND2$ proteins distribution with higher single-cell resolution than using conventional *in-situ* hybridization techniques and allowed us to co-localize $HAND2$ with other proteins (see below).

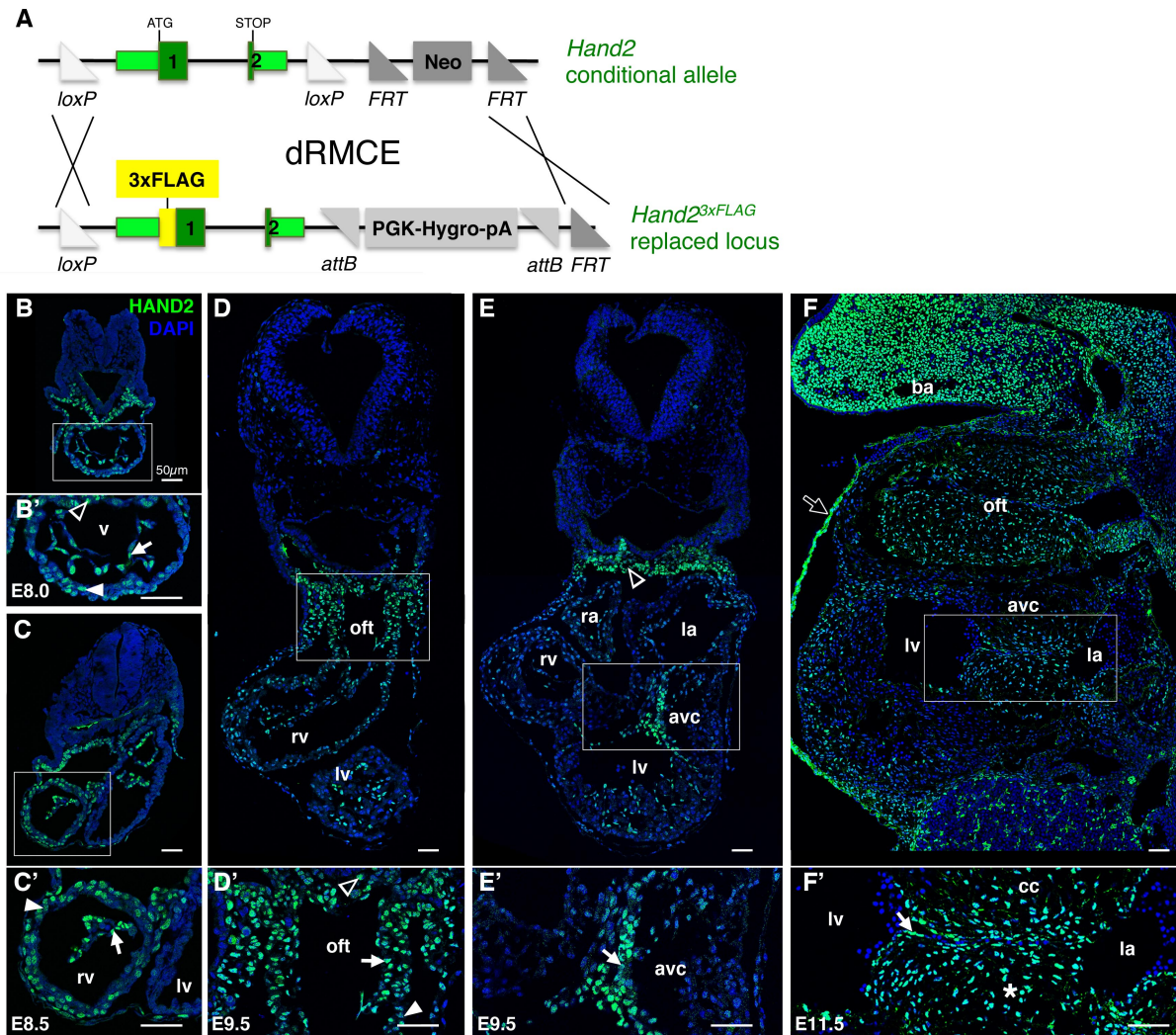


Figure 13. The $Hand2^{3xFLAG}$ allele is expressed throughout cardiac development

(A) Schematic illustration of the $Hand2^{3xFLAG}$ allele (Osterwalder et al., in press). The 3xFLAG epitope tag (yellow box) is fused in frame downstream of the endogenous $Hand2$ ATG translation start site. (B-F) Distribution of the endogenous $HAND2^{3xFLAG}$ protein during heart development at (B) E8.0, (C) E8.5, (D-E) E9.5 and (F) E11.5. Enlargement of the boxed areas are shown in (B'-F'). (B-E) Transverse paraffin sections and (F) sagittal frozen section from the left side of the embryo. The section in (D) is localized more cranially than the section in (E). Scale bars: $50\mu\text{m}$. Open arrowhead: splanchnic pharyngeal mesoderm, white arrowhead: myocardium, white arrow: endocardium, white asterisk: mesenchymal cells of the cardiac cushions, open arrow: epicardium. avc: atrioventricular canal, ba: branchial arches, cc: cardiac cushions, la: left atrium, lv: left ventricle, oft: outflow tract, ra: right atrium, rv: right ventricle, v: common ventricular chamber.

We initially wanted to establish HAND2 proteins distribution during key stages of early cardiac development. At E8.0, HAND2^{3xFLAG} proteins are detected in the entire primary heart tube in both the myocardial and endocardial layers and in the adjacent splanchnic pharyngeal mesoderm (Fig.13B-B'). During cardiac looping (E8.5), HAND2^{3xFLAG} remains in the endocardium of the two developing ventricles. In contrast, HAND2^{3xFLAG} proteins remain in the myocardium of the right ventricle while they are absent from the myocardium of the left ventricle (LV)(Fig.13C-C'). At E9.5, HAND2^{3xFLAG} proteins are detected in the myocardium and endocardium in a region extending from the outflow tract to the right ventricle, (Fig.13D-D') and in the endocardial cells of the atrioventricular canal (AVC, Fig.13E-E'). At E11.5, HAND2^{3xFLAG} proteins are present not only in the endocardium but also in the cells of the cardiac cushions (CC), formed by endothelial-mesenchymal transition (EndMT) in both OFT and AVC (Fig.13F-F'). HAND2^{3xFLAG} proteins are also detected in the epicardium at this stage. HAND2^{3xFLAG} proteins are nuclear, which agrees with their function as a transcription factor. In summary, our analysis of the cardiac HAND2^{3xFLAG} distribution confirms and refines its previously described expression pattern to single cell resolution during early heart development.

6.2.2. ChIP-Seq analysis using pooled *Hand2* expressing tissues identifies the genome-wide HAND2 target regions in association with tissue-specific gene functions

Over the past two decades, numerous studies have been published aiming to decipher the functions of HAND2 during cardiogenesis, and genes downregulated during altered heart development in *Hand2*-deficient embryos had been identified. These putative HAND2 target genes include *Gata4*, *Irx4*, *Nppa*, *Plxna2* and *Cx40* (Srivastava et al., 1997; Bruneau et al., 2000; Thattaliyath et al., 2002; Morikawa and Cserjesi, 2008; McFadden et al., 2005). However, none of these genes has been confirmed as direct endogenous target of HAND2, and the gene regulatory networks controlled by HAND2 during normal embryonic development remained unknown (Vincentz et al., 2011). Therefore, we used the *Hand2*^{3xFLAG} allele to identify the direct transcriptional targets of HAND2 during embryonic development.

For this purpose, M.Osterwalder and colleagues performed a chromatin immunoprecipitation in combination with deep sequencing (ChIP-Seq) using the *Hand2*^{3xFLAG} allele and the M2 anti-FLAG antibody. This analysis was performed using pooled *Hand2* expressing embryonic tissues (heart, limb buds and branchial arches, see Fig.14A) from a pool of approximately 150 *Hand2*^{3xFLAG/+} and *Hand2*^{3xFLAG/3xFLAG} embryos at E10.5. *Hand2* is expressed at high levels in all these tissues, with the expression in cardiac tissues being very similar as observed at E11.5 (Fig.13F-F' and data not shown). Expressing tissues were pooled to generate the significant amounts of chromatin immunoprecipitates required to assemble the genomic library for deep-sequencing. In addition, this allows the identification of both tissue-specific and shared candidate HAND2 targets genes.

The HAND2^{3xFLAG} ChIP sample and the input control sample were sequenced using an Illumina Genome Analyzer in the Laboratory of Quantitative Genomics (D-BSSE, ETHZ, Basel). The resulting sequence tags were mapped to the reference mouse genome (NCBI37/mm9) and enrichment of ChIP versus input for each sequence tag were computed by R.Ivanek using MACS-based peak calling analysis (Model-based Analysis of ChIP-Seq data), see (Zhang et al., 2008b). The HAND2^{3xFLAG} ChIP-Seq peaks were visualized using the UCSC browser (Karolchik et al., 2014). A wild-type control ChIP sample was also processed and sequenced in parallel to the HAND2^{3xFLAG} sample to identify non-specific antibody-related false hits. Such false hits were excluded from further analysis, which reveals a major advantage of using epitope-tagged transcription factors for ChIP-Seq experiments. Analysis of the input was a critical control to confirm that the signal enrichment of the sequence tags in the HAND2^{3xFLAG} ChIP is representative of real transcription factor binding and not due to an experimental or computational bias (Rozowsky et al., 2009). To restrain the HAND2^{3xFLAG} ChIP-Seq dataset to the statistically relevant enriched genomic regions, only the 2000 highest enriched peaks according to MACS analysis (Top 2000, Fig.14B, left panel, green) were considered for further analysis using GREAT (Genomic Regions Enrichment Annotations Tool), (McLean et al., 2010). Most of the target regions mapped between 10-100kb from known transcriptional start sites (TSS), and encoded *bona-fide* E-box consensus CRTCTGKHTT sequences that were identified using the Homer software (Heinz et al., 2010).

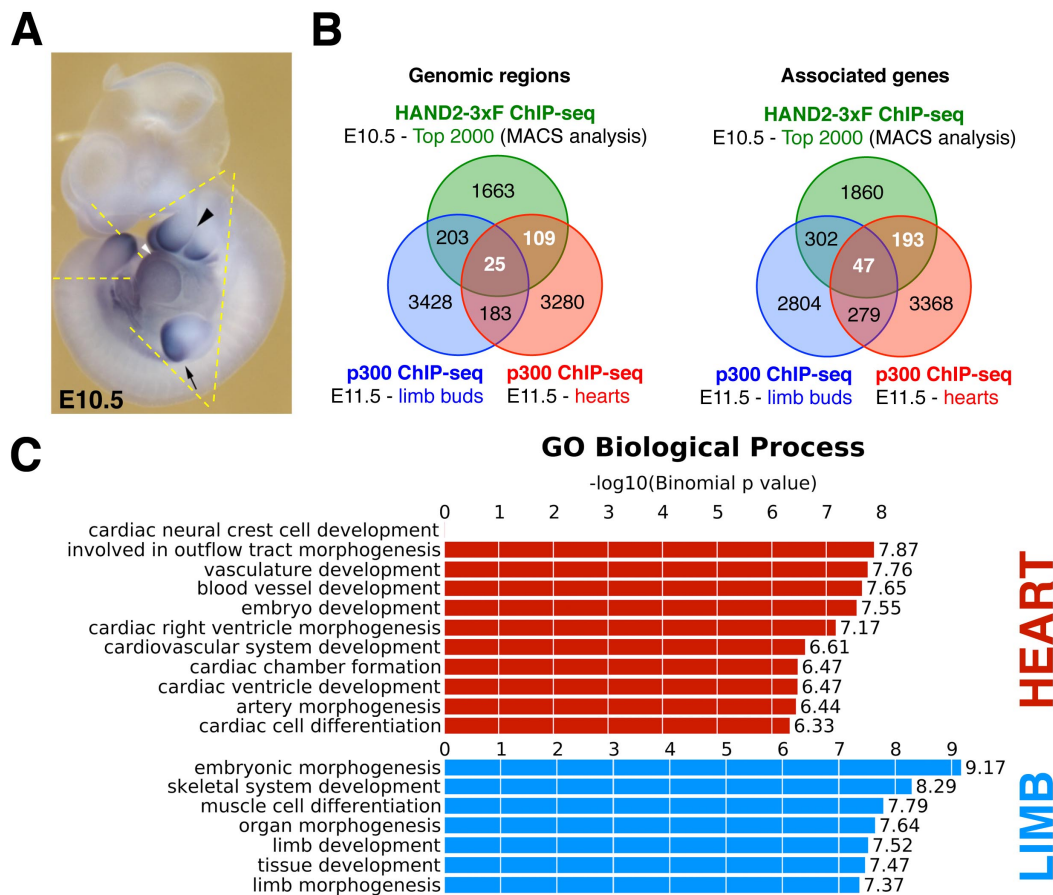


Figure 14. ChIP-Seq using HAND2^{3xFLAG} embryos reveals HAND2 candidate target genes in developing heart and limb buds

(A) *Hand2*^{3xFLAG} embryos were used for ChIP-Seq analysis from pooled dissected *Hand2* expressing tissues at E10.5 (white arrowhead: heart. Black arrow: forelimb bud. Black arrowhead: branchial arches). For details see (Osterwalder et al., in press). (B) The top 2000 enriched genomic regions (green, left diagram) and their 2402 associated genes (green, right diagram) were intersected with regions bound by the transcriptional co-activator p300 in developing hearts (E11.5, red) and limb buds (E11.5, blue). (C) Gene Ontology analysis shows that genes associated with regions bound by both HAND2 and p300 are involved in cardiac (red, 240 genes) or limb bud (blue, 349 genes) development, respectively.

This consensus sequence matches the CATCTG HAND2 binding site identified previously (Dai and Cserjesi, 2002). These whole-genome data are described in (Osterwalder et al., in press). The 2402 genes associated to the Top 2000 enriched genomic regions represent HAND2 candidate target genes in developing hearts, limb buds and branchial arches. To identify potential cardiac targets of HAND2, we intersected the Top 2000 peaks with regions interacting with the transcriptional co-activator p300 in developing hearts (Blow et al., 2010) (Fig.14B, red), and limb buds (Visel et al., 2009a) (Fig.14B, blue) using the UCSC browser. p300 is a critical histone acetyltransferase that is part of the majority of enhancer-associated protein

complexes (Eckner et al., 1994; Yao et al., 1998; Visel et al., 2009a). Tissue-specific p300 ChIP-Seq datasets (Blow et al., 2010; Visel et al., 2009a) thus provide an additional validation of the range of HAND2 target sequences that act as potential *cis*-regulatory modules (CRMs) in heart and/or limb bud tissues development. GREAT analysis further identified the genes in proximity to the Top 2000 regions bound by both HAND2 and p300. The weak overlap suggests that most of the regions interacting with HAND2 are not associated with active genes, in agreement with the function of HAND2 as a transcriptional repressor (Fig.14B). The biological relevance of these genes was determined by Gene Ontology (GO) analysis (Ashburner et al., 2000) (Fig.14C). In each tissue, HAND2 interacting regions were associated with genes involved in development (e.g. GO “embryo development” or “embryonic morphogenesis”) and in DNA binding (e.g. GO “regulation of DNA binding”, not shown), relevant for HAND2 function as a transcription factor. Moreover, tissue-specific HAND2 p300 bound regions were associated with either cardiac (Fig.14C, red) or limb bud development GO terms, respectively (Fig.14C, blue). Notably, cardiogenesis related GO terms were representative of heart compartments with known *Hand2* functions (e.g. GO “cardiac neural crest cell development involved in outflow tract morphogenesis” and GO “cardiac right ventricle morphogenesis”). In addition to *Hand2* itself, several genes relevant to heart development were identified among the 240 genes associated with regions interacting with both HAND2 and p300. Table 1 summarizes the main functions of some of these genes.

Table 1. Genes involved in cardiac development associated with a genomic region interacting with HAND2 and p300

Gene	Function	Putative HAND2 target	References
<i>Hes1</i>	OFT development	-	(Rochais et al., 2009a)
<i>Sox4</i>	Ventricular septation and OFT formation	-	(Schilham et al., 1996)
<i>Tgfβ2</i>	Inducing role in the EndMT process resulting in cardiac cushion formation, and cardiac valves remodeling	-	(Ma et al., 2005; Rivera-Feliciano and Tabin, 2006; Shirai et al., 2009; Azhar et al., 2011)
<i>Tbx2</i>	Involved at several steps of cardiogenesis (Chambers differentiation, AVC patterning, formation of cardiac cushions, cardiac valves, and conduction system)	-	(Hariri et al., 2012; Greulich et al., 2011; Hoogaars et al., 2007a; Stennard et al., 2005; Plageman and Yutzey, 2005)
<i>Tbx3</i>			
<i>Tbx20</i>			
<i>Plxna2</i>	Cardiac neural crest cells migration	Yes	(Brown et al., 2001; Morikawa and Cserjesi, 2008)
<i>Cx40</i> (<i>Gja5</i>)	Heart-specific gap-junction coding gene	Yes	(Delorme et al., 1995; Kirchhoff et al., 2000; McFadden et al., 2005)

In contrast, the *cis*-regulatory landscapes of the putative HAND2 targets *Gata4* and *Nppa* contain no associated ChIP-Seq peak. We used a Hi-C dataset representing the range of potential distant chromatin-chromatin interactions (Dixon et al., 2012), but could not detect any distant HAND2^{3xFLAG} ChIP-Seq peak associated with *Gata4* or *Nppa*, suggesting that these two genes are indirect targets of HAND2 (data not shown).

Crossing the HAND2^{3xFLAG} ChIP-Seq data with the p300 tissue-specific genome-wide targets datasets thus identified tissue-specific targets and likely biological functions for *Hand2*. Therefore, this Gene Ontology analysis validates pooling embryonic tissues for ChIP-Seq analysis. In addition, it narrows the range of potential HAND2 targets genes involved in each of the relevant developing tissues. A complete and functional analysis of the HAND2 target genes during limb bud development was performed by Osterwalder and colleagues (Osterwalder et al., in press), while I focused on the analysis of potential HAND2 target genes during heart development.

6.2.3. HAND2 controls the expression of genes involved in early second heart field morphogenesis

The transcriptional regulators *Tbx2* and *Tbx3* function during early development of second heart field (SHF) derived structures (Harrelson et al., 2004; Mesbah et al., 2008; Mesbah et al., 2012). Both genes were identified by ChIP-Seq analysis as associated with genomic regions interacting with HAND2^{3xFLAG} chromatin complexes (Table 1, see chapter 6.2.10 for the analysis of their *cis*-regulatory landscapes). SHF progenitors reside initially in the splanchnic pharyngeal mesoderm in the dorsal wall of the pericardial cavity, before progressively migrating to the primary heart tube to contribute to the myocardium of the OFT and RV (Kelly, 2012). These cardiac structures and the pharyngeal mesoderm express high levels of HAND2 (Fig.13B-D), and are hypoplastic in *Hand2-deficient* embryos (Srivastava et al., 1997). We therefore wanted to gain insights into HAND2 functions in the transcriptional networks governing SHF morphogenesis by looking at the early expression of key cardiac genes. The early marker of the SHF *Isl1* remains expressed normally in the pharyngeal mesoderm of *Hand2-deficient* embryos (E8.25, Fig.15A-B), indicating that the SHF forms normally.

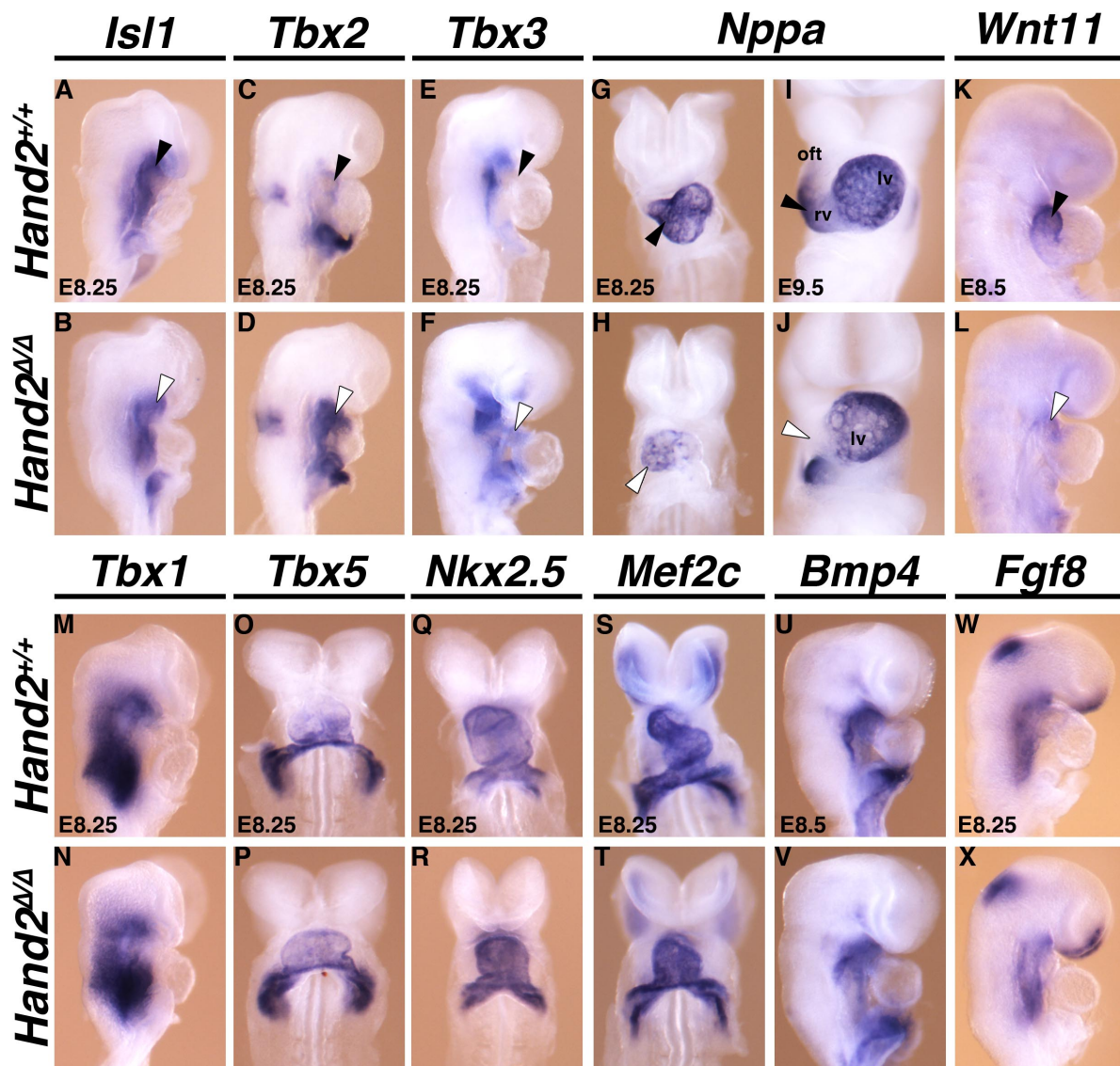


Figure 15. Expression of early cardiac development markers in wild-type and *Hand2*-deficient embryos

Effects of *Hand2* inactivation on the expression of cardiac genes at E8.25-E8.5. (A-B) *Isl1* expression is not altered (right side view). (C-D) *Tbx2* expression is ectopically expressed in pharyngeal mesoderm (arrowheads, compare with *Isl1* expression domain in (A)). (E-F) *Tbx3* expression is expanded towards the OFT (arrowheads). (G-J) *Nppa* expression is reduced at E8.25 (G-H, front view) and lost in the RV at E9.5 (I-J, arrowheads). (K-L) *Wnt11* expression is reduced in the OFT (arrowheads). (M-X) The expression of *Tbx1* (M-N), *Tbx5* (O-P), *Nkx2.5* (Q-R), *Mef2c* (S-T), *Bmp4* (U-V), and *Fgf8* (X-Y) are not altered in *Hand2*-deficient embryos.

Interestingly, *Tbx2* and *Tbx3* are expressed ectopically in the *Isl1* positive cells of the pharyngeal mesoderm (compare Fig.15C with Fig.15A and Fig.15D with Fig.15B), and expands to the OFT (compare Fig.15D,F with Fig.15C,E). In contrast, the expression of *Nppa*, which is repressed by TBX2 and TBX3 and required for cardiac

chambers differentiation (Habets et al., 2002; Hoogaars et al., 2004; Houweling et al., 2005) is reduced in *Hand2*-deficient embryos (E8.25, Fig.15G-J), and totally absent from the hypoplastic RV (E9.5, Fig.15I-J, arrowheads (Morikawa and Cserjesi, 2008; Thattaliyath et al., 2002). These data indicate that the ectopic expression of *Tbx2/Tbx3* in myocardial progenitors of the anterior SHF in *Hand2*-deficient embryos (Fig.15D,F) accounts for the loss of *Nppa* expression in the right ventricle, while the right ventricle hypoplasia might be an indirect consequence of these alterations. *Wnt11* is also essential for the differentiation of SHF cells in the OFT and RV (Cohen et al., 2012; Zhou et al., 2007; Pandur et al., 2002), and its expression is strongly reduced in the OFT of *Hand2*-deficient embryos (Fig.15K-L). A region located 58kb upstream of *Wnt11* is among the highly enriched candidate CRMs associated to HAND2^{3xFLAG} chromatin complexes, but this remains to be verified and functionally analyzed further (data not shown).

In contrast, the expression of several other important cardiac genes involved in the balance between proliferation and differentiation of the SHF progenitors was not affected by the loss of *Hand2* (*Tbx1*, *Tbx5*, *Nkx2.5*, *Mef2c*, *Bmp4*, *Fgf8*: Fig.15M-X). In conclusion, *Hand2* controls distinct aspects of the formation of SHF derived structures through a specific set of cardiac regulators (*Tbx2*, *Tbx3*, *Wnt11*).

6.2.4. HAND2 controls the expression of genes associated with known cardiac-specific enhancers

The VISTA enhancer browser is a database consisting of conserved enhancer elements that were tested for *LacZ* reporter expression (Visel et al., 2007; Attanasio et al., 2013). It can therefore be used to identify overlaps between known cardiac enhancers and the putative CRMs identified by HAND2^{3xFLAG} ChIP-Seq analysis. Indeed, this analysis identified *Furin* and *Myocardin* (*Myocd*) as potential direct HAND2 target genes. These two genes have been previously established as essential for cardiac development and their landscapes encode VISTA enhancers that are expressed in the heart and interact with HAND2 and p300 protein complexes.

Furin encodes a proprotein convertase that activate signals from the TGF β family such as BMP4, TGF β 1 and BMP10 by proteolytic cleavage (Cui et al., 1998; Cui et

al., 2001; Dubois et al., 2001; Susan-Resiga et al., 2011). In the developing heart, both the endocardial and myocardial layers express *Furin* (Roebroek et al., 1998). Embryos deficient in *Furin* suffer from cardia bifida, which may still result in formation of a short single heart tube that fails to undergo looping, and eventually die around E10.5 (Roebroek et al., 1998; Constam and Robertson, 2000). Endothelial-specific inactivation of *Furin* results in ventricular septation defects and cardiac valve thickening, which is paralleled by reduced BMP4 activation processing (Kim et al., 2012).

MYOCD is a transcriptional co-activator of serum response factor (SRF) that modulates the expression of tissue-specific SRF-target genes by functioning as a switch between smooth and cardiac skeletal muscle differentiation (Wang et al., 2001; Li et al., 2003; Wang et al., 2003; Long et al., 2007; Hoofnagle et al., 2011). *Myocd* expression is restricted to these two types of muscles cells, and its inactivation induces embryonic lethality by E10.5 due to defective smooth muscle vasculature (Li et al., 2003). In adult mice, *Myocd* function is critical for cardiomyocytes survival (Huang et al., 2009).

We used the UCSC browser to visualize the HAND2^{3xFLAG} ChIP-Seq peaks together with the cardiac p300 ChIP-Seq peaks and the conservation of these regions in placental mammals (Fig.16A,E). All other panels representing ChIP-Seq data are organized in accordance with Fig.16A,E. The *Furin cis*-regulatory landscape encodes a -43kb region, highly enriched for HAND2 and p300 binding (green bar in Fig.16A). This region overlaps (blue bar in Fig.16A) the VISTA enhancer mm169 that is expressed in the heart (Fig.16B) and abdominal region (data not shown, see VISTA browser). The direct interaction of HAND2 complexes with this enhancer was confirmed by ChIP-qPCR using embryonic hearts (E10.5, Fig.16C. See chapter 9.4.6 for fold enrichments calculations). This analysis established the significant 200-fold enrichment of HAND2 interactions with *Furin* -43kb enhancer in comparison to an unrelated other region chosen for its absence of enrichment by ChIP-Seq analysis (-50kb, Fig.16A and Fig.16C). To determine if *Furin* is indeed a direct transcriptional target of HAND2, we compared its expression in wild-type and *Hand2*-deficient embryos (E9.0-E9.25, Fig.16D). *Furin* expression is altered in *Hand2* mutant hearts, in particular in the endocardium (Fig.16D, right panels, arrows).

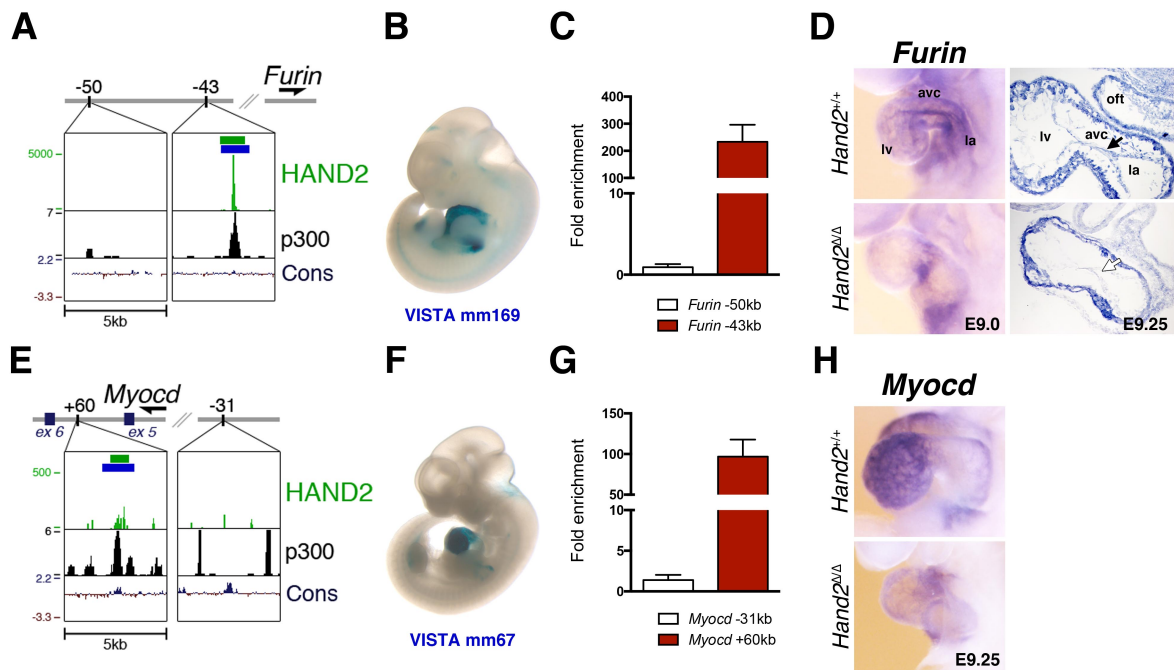


Figure 16. *Furin* and *Myocd* are direct targets of HAND2 in the developing heart

UCSC browser windows representing the *Furin* (A) and *Myocd* (E) cis-regulatory landscapes. Distances to TSS are indicated in kb. HAND2^{3xFLAG} ChIP-Seq peaks are shown in green and p300 ChIP-Seq peaks in hearts (E11.5) are shown in black, above the placental mammal conservation (Cons) plot (PhyloP, UCSC Genome Browser). Green bars indicate HAND2^{3xFLAG} peaks in the top 2000 enriched regions. (B,F) *LacZ* reporter expression of the VISTA browser enhancers represented by blue bars in (A) and (E). (C,G) ChIP-qPCR establishing binding of HAND2^{3xFLAG} chromatin complexes at *Furin* (C) and *Myocd* (G) associated cardiac enhancers in E10.5 hearts. No enrichment was seen in control regions. Mean \pm SD (n=3) is shown. (D,H) Expression of *Furin* (D) and *Myocd* (H) in wild-type and *Hand2* ^{$\Delta\Delta$} embryonic hearts (E9.0-9.5) using whole mount RNA *in-situ* hybridization. *In-situ* hybridization on paraffin sections shows the specific loss of *Furin* from the endocardium (indicated by arrows).

Similarly, HAND2 containing chromatin complexes are enriched at an intronic region located +60kb upstream of the *Myocd* TSS (Fig.16E, green bar), which overlaps with the heart-specific VISTA enhancer mm67 (blue bar in Fig.16E, expression in Fig.16F). Direct interaction of HAND2 with this CRM was confirmed by ChIP-qPCR (Fig.16G). In agreement, *Myocd* expression is altered in *Hand2*-deficient embryos (Fig.16H). Together, these results indicate that *Hand2* is required for *Furin* and *Myocd* expression, and that these genes are likely direct HAND2 targets whose expression is regulated by cardiac enhancers.

6.2.5. *Hand2*-deficient mouse embryos lack the delaminated endocardial cells in the atrioventricular canal

In response to myocardial signals, endocardial cells in the AVC undergo an endothelial-mesenchymal transition (EndMT) around E9.5. These cells delaminate and migrate into the cardiac jelly, where they proliferate and form the cardiac cushions that will ultimately give rise to the cardiac valves (Armstrong and Bischoff, 2004; von Gise and Pu, 2012; Kovacic et al., 2012; Lim and Thiery, 2012; Lin et al., 2012). As HAND2 is expressed by both the endocardium of the AVC and the mesenchymal cells of the cardiac cushions (Fig.13E-F), we investigated if HAND2 regulates endocardial genes that control EndMT mechanism and formation of the cardiac cushions.

Using sagittal sections, I first studied the morphological alterations of the AVC in *Hand2*-deficient embryos. Compared to wild-type hearts in which AVC endocardial cells delaminate normally (E9.5, Fig.17A, asterisk in top panel), a total absence of delaminated cells was apparent in *Hand2*-deficient embryos (E9.5, Fig.17A, bottom panel). Furthermore, the superior and inferior layers of the endocardium were not in contact, leaving an opening in the AVC lumen (Fig.17A). To confirm that the absence of delaminated cells was not due to increased endocardial cell death, wild-type and *Hand2*-deficient hearts were analyzed by TUNEL (E9.5, Fig.17B). No increase in apoptotic cell number was observed in *Hand2*-deficient hearts, which thus excludes cell death as likely cause of delamination failure. In addition, the expression of the transcription factor NFATC1 (Nuclear Factor of Activated T cells) was analyzed as it is expressed specifically in endothelial cells of the endocardium and not required for EndMT. Its functions in maintaining the endocardial lineage are crucial for valve remodeling at later stages (Ranger et al., 1998; de la Pompa et al., 1998; Wu et al., 2011; Chang et al., 2004). NFATC1 is coexpressed with HAND2 in the endocardium and remains expressed normally in *Hand2*-deficient embryos (Fig.17C). This analysis indicate that the endocardium of *Hand2*-deficient embryos is normally patterned with respect to the fates of cardiac valve progenitors. The absence of delaminated cells is thus not due to an endocardial defect but likely a consequence of defective EndMT and/or migration of the cardiac cushion progenitors.

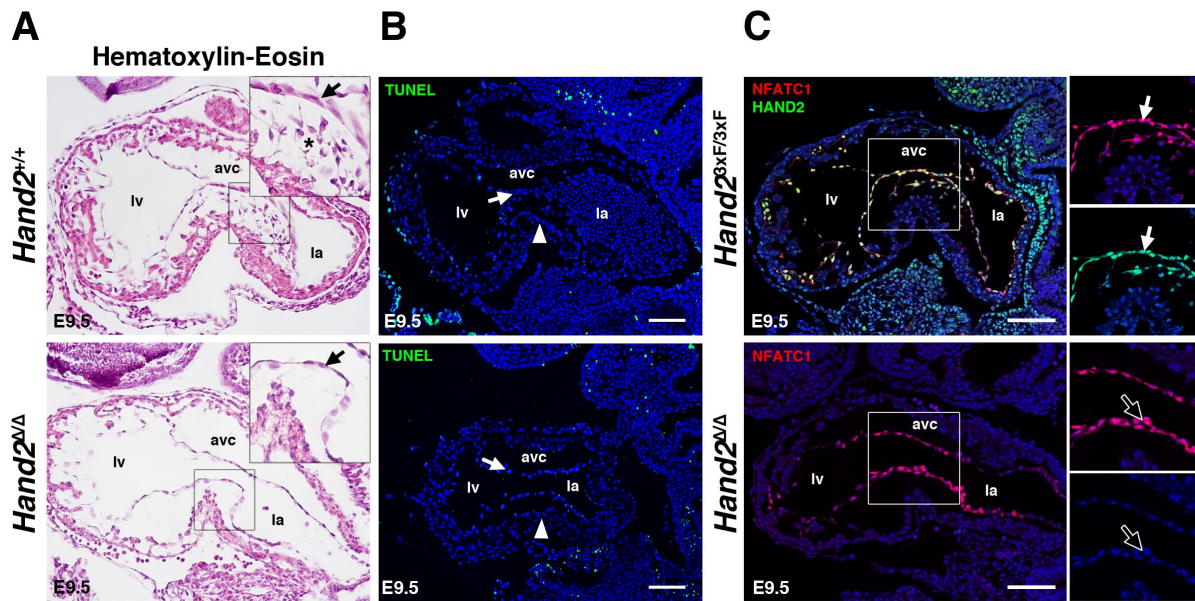


Figure 17. Absence of delaminated endocardial cells in the atrioventricular canal (AVC) of *Hand2*-deficient embryos

(A) Hematoxylin-eosin staining of sagittal heart sections in *Hand2*-deficient embryo (lower panel) compared to wild-type embryos (top panel) (E9.5). Black arrow: endocardium, black asterisk: mesenchymal cells of the cardiac cushions, lv: left ventricle, avc: atrioventricular canal, la: left atrium. (B) TUNEL assay using sagittal heart sections of *Hand2*-deficient embryos (lower panel) and wild-type controls (top panel) (E9.5). Apoptotic cells are shown in green, nuclei are counterstained with Hoechst (blue). White arrow: endocardium, white arrowhead: myocardium. (C) The endocardial marker NFATC1 co-localizes with HAND2 in the AVC (white arrow, top panel) and remains expressed in *Hand2*-deficient embryos (open arrow, lower panel). Scale bar: 100 μ m.

6.2.6. HAND2 directly regulates *Has2*-mediated extracellular matrix deposition in the cardiac jelly

To gain further insight into the defective delamination of AVC endocardial cells, the glycosaminoglycans in the extracellular matrix (ECM) were stained by alcian blue. Glycosaminoglycans are required for the migration of cardiac cushion progenitors into the cardiac jelly. Indeed, the ECM in the cardiac jelly of the AVC appears reduced in *Hand2*-deficient hearts in comparison to wild-type controls (Fig.18A). This suggests that the endocardial cells are unable to migrate properly, which would explain the lack of cardiac cushion progenitors in the absence of *Hand2* (Fig.17A).

The enzyme *Hyaluronan Synthase 2* (*Has2*) produces one major component of the ECM, the hyaluronic acid (HA). *Has2* is downregulated by *Hand2*-deficient embryos, which, together with its requirement for cardiac jelly and cardiac cushion formation, points to it being a potential direct HAND2 target (Tsuchihashi et al., 2011;

Camenisch et al., 2000). Indeed, our ChIP-Seq analysis revealed two HAND2 binding regions within the proximal promoter of *Has2* located 2.4kb downstream and 0.9kb upstream of the TSS, respectively (Fig.18B). ChIP-qPCR analysis of E10.5 HAND2^{3xFLAG} hearts established that HAND2 complexes interact with the +2.4kb region but neither to the -0.9kb nor to a control region (Fig.18C). In agreement, the expression of *Has2* is altered in the AVC of *Hand2*-deficient hearts (Fig.18D).

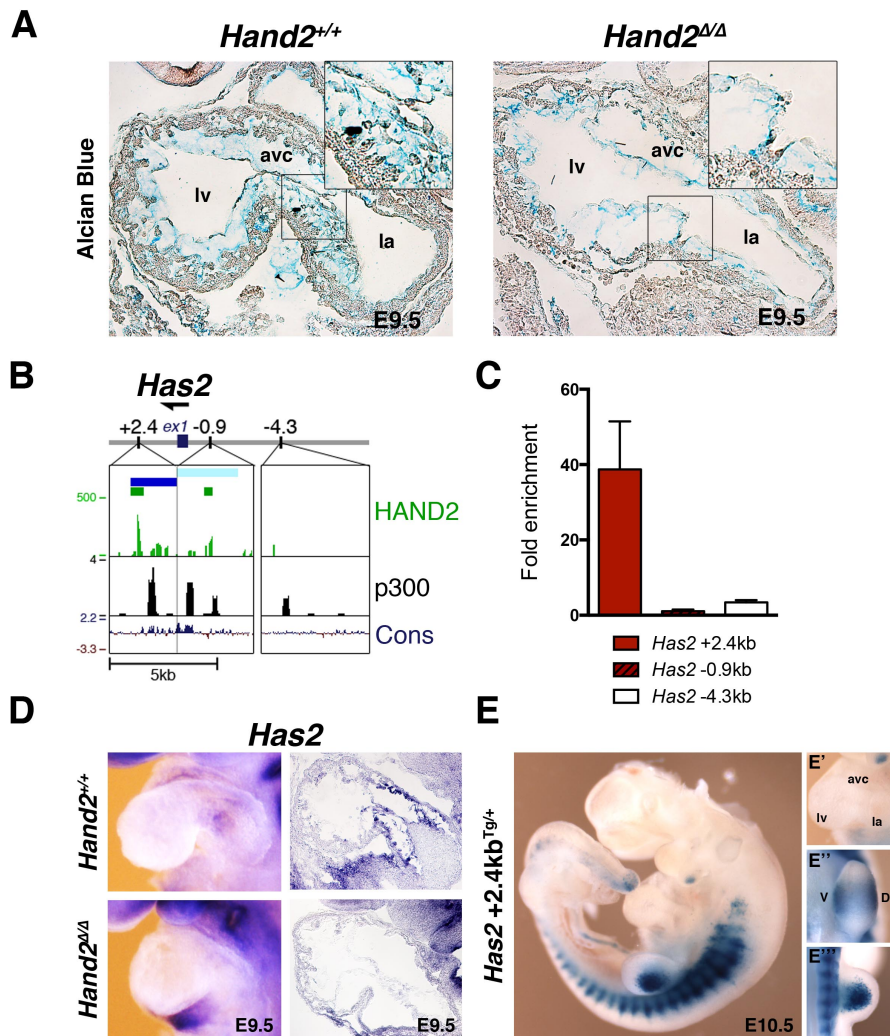


Figure 18.
The production of extracellular matrix in AVC cardiac jelly is regulated by HAND2, possibly by direct regulation of *Has2* expression

(A) Alcian Blue staining of sagittal heart sections in *Hand2*-deficient embryos (right panel) and wild-type controls (left panel) (E9.5). (B) UCSC browser windows representing the *Has2* proximal promoter region. Green bars indicate HAND2^{3xFLAG} peaks in the top 2000 enriched regions. The light blue bar at -0.9kb represents the location of a published enhancer that is active in limb buds (Liu et al., 2013). (C) ChIP-qPCR

establishing direct interaction of HAND2^{3xFLAG} chromatin complexes with the *Has2* proximal promoter in E10.5 hearts (E10.5). The -4.3kb region is used as negative control. Mean \pm SD (n=3) is shown. (D) Expression of *Has2* in wild-type and *Hand2* ^{Δ/Δ} embryonic heart by whole mount (left panels) and section (right panels) *in-situ* hybridization (E9.5). (E) Transgenic embryo (E10.5, n=1) showing *LacZ* expression under control of the +2.4kb CRM in the *Has2* intronic region indicated by a dark blue bar in panel (B). The transgene is not expressed in the heart (E') but in the dorsal and ventral forelimb bud mesenchyme (E'') and in the dorsal hindlimb bud mesenchyme (E''').

These results support the proposal that *Has2* is as a direct target of HAND2 in the developing heart. To assess the potential transcription enhancing activity of the +2.4kb region, we used a *LacZ* reporter assay in transgenic mouse embryos. Preliminary analysis shows that the region encompassing the *Has2* +2.4kb HAND2 peak (Fig.18B, dark blue bar) drives reporter expression in the somites, second branchial arch and in the limb buds of a transgenic embryo at E10.5 (n=1, Fig.18E). However, no *LacZ* reporter expression was detected in the heart (Fig.18E'). In limb buds, the *LacZ* expression is restricted to the dorsal and ventral forelimb sub-ectodermal mesenchyme (Fig.18E'') and to the dorsal hindlimb (Fig.18E'''). Preliminary ChIP-qPCR analysis confirms that HAND2 complexes bind to this +2.4kb region in developing limb buds (E10.5, data not shown). The lack of reporter expression in the heart may be an effect of the transgene insertion site and needs to be investigated by the generation of additional independent transgenic founders embryos (currently ongoing). This is important as our other findings support a role of HAND2 in regulating *Has2* during the formation of the cardiac cushions.

6.2.7. *Twist1* but not *Sox9* is a direct transcriptional target of HAND2 during cardiac cushion formation

Twist1 and *Sox9* are required for the proliferation and differentiation of the mesenchymal cells of the cardiac cushions (Shelton and Yutzey, 2008; Akiyama et al., 2004) and regions interacting with HAND2 complexes were detected in the regulatory landscapes of both genes. We therefore investigated if alterations in these two putative HAND2 targets could contribute to the disruption of cardiac cushion morphogenesis in *Hand2*-deficient embryos. HAND2 complexes interact with several regions within *Twist1* cis-regulatory landscape; the most enriched being located at +10kb and at +130kb from *Twist1* TSS (Fig.19A). ChIP-qPCR analysis confirmed that both regions are enriched in HAND2 containing chromatin complexes in developing hearts (E10.5, Fig.19B). Furthermore, preliminary ChIP-qPCR results indicate that the binding region at +130kb is not enriched in limb buds, suggesting that it could be a heart-specific CRM bound by HAND2 complexes (data not shown). Therefore, the corresponding genomic region encoding this peak is currently being used to generate *LacZ* reporter transgenic embryos (dark blue bar in Fig.19A).

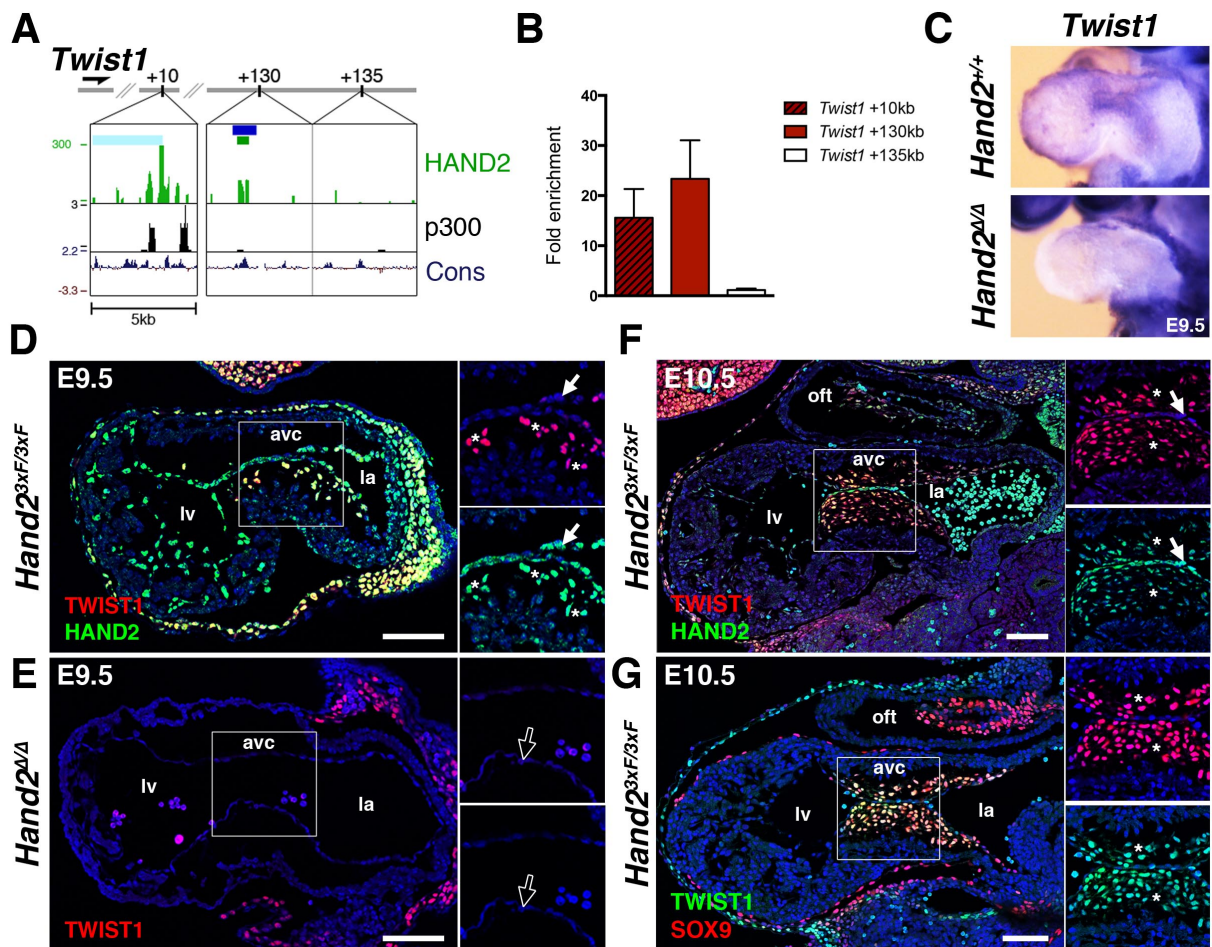


Figure 19. HAND2 directly control *Twist1* expression in the cells of the cardiac cushions
 (A) UCSC browser windows representing the *Hand2*^{3xFLAG} ChIP-Seq peaks within *Twist1* cis-regulatory landscape. The green bar at +130kb from *Twist1* TSS indicates top2000 enriched region. The dark blue bar at +130kb represents the genomic region used to generate transgenic reporter embryos. The light blue bar at +10kb represents the location of the VISTA enhancer hs1880 not active at E11.5. (B) ChIP-qPCR establishing direct interaction of *Hand2*^{3xFLAG} chromatin complexes with the *Twist1* +10kb and +130kb regions in hearts (E10.5), but not with the control region located at +135kb. Mean \pm SD (n=3) is shown. (C) Expression of *Twist1* in wild-type and *Hand2*^{Δ/Δ} embryonic heart at E9.5. (D,F) TWIST1 is co-expressed with HAND2 in the mesenchymal cells of the cardiac cushions (white asterisks) but not endocardial cells (white arrow) at E9.5 (D) and E10.5 (F). (E) TWIST1 is not expressed by the AVC of *Hand2*-deficient embryos (open arrow: endocardium). (G) TWIST1 is also co-expressed with SOX9 in the mesenchymal cells of the cardiac cushions (white asterisks) at E10.5. Scale bar: 100 μ m

In contrast, the human orthologous region encompassing the putative HAND2 CRM at +10kb does not drive *LacZ* reporter expression in transgenic reporter embryos (E11.5, VISTA element hs1880, light blue bar in Fig.19A). *Twist1* expression is totally lost from the AVC of *Hand2*-deficient hearts (E9.5, Fig.19C), in agreement with *Twist1* being a direct transcriptional target of HAND2. Indeed, the TWIST1 protein is

co-expressed with HAND2 in the progenitors that have delaminated after the initial EndMT (Fig.19D, white asterisks). In *Hand2*-deficient hearts, no cells expressing TWIST1 are detected in the AVC as expected from the absence of delaminated cells (Fig.19E). By E10.5, TWIST1 is co-expressed in all cardiac cushion progenitors with HAND2 (Fig.19F) and SOX9 (Fig.19G). In summary, this analysis shows that *Twist1* expression depends on HAND2 during cardiac cushion formation. The CRM identified 130kb upstream of *Twist1* TSS is likely involved in mediating direct transcriptional regulation of *Twist1* expression by HAND2 after delamination.

The expression of *Sox9* is downregulated in the AVC of *Twist1*-deficient embryos (Vrljicak et al., 2012). The co-expression of HAND2, TWIST1 and SOX9 by cardiac cushion progenitor cells suggests that *Sox9* may also be a direct target of HAND2 in these cells, but no region interacting with HAND2 in *Sox9* genomic landscape in developing hearts could be confirmed to date (ChIP-Seq and ChIP-qPCR, data not shown). In wild-type embryos, SOX9 expression initiates on the atrial side of the AVC in cells that have undergone EndMT. In these cardiac cushion progenitors, SOX9 is coexpressed with HAND2 (E9.5, Fig.20A, white asterisks).

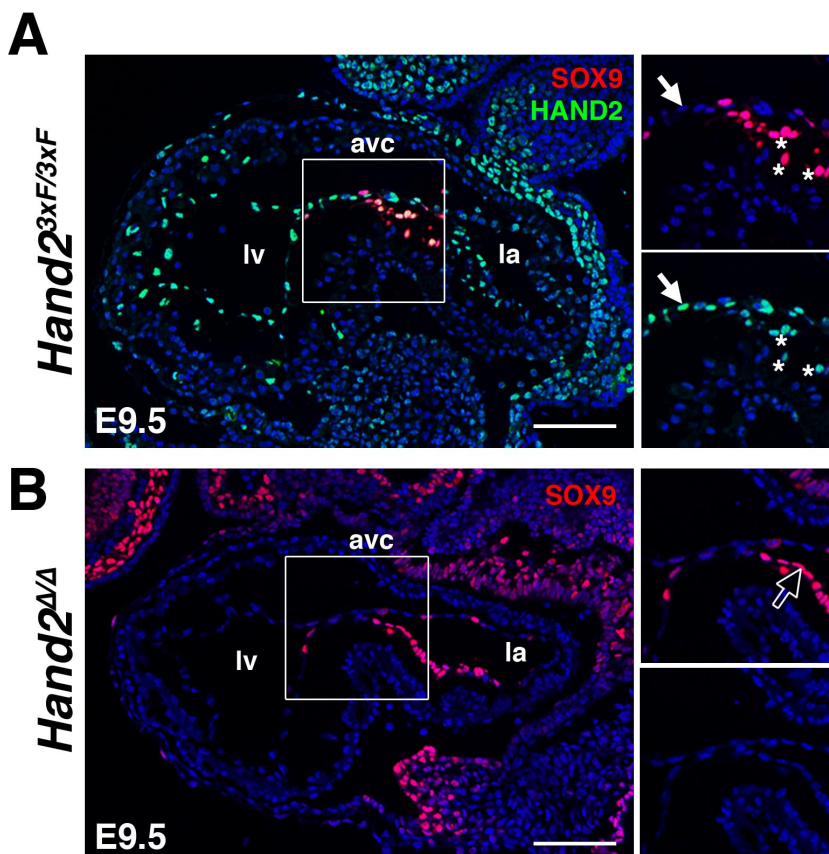


Figure 20. *Sox9*-mediated cardiac jelly invasion is not regulated by HAND2

(A) SOX9 is co-expressed with HAND2 in the mesenchymal cells of the cardiac cushions (white asterisks) but not endocardial cells (white arrow) at E9.5. (B) In *Hand2*-deficient embryos, SOX9 remains expressed in endocardial cells (open arrow). Scale bar: 100 μ m

The remainder of the AVC endocardium expresses only HAND2 (Fig.20A, white arrow). Interestingly, in *Hand2*-deficient hearts SOX9 is expressed in endocardial cells located on the atrial side of the AVC (Fig.20B, open arrow), at the atrial-ventricular position where the first delaminated SOX9-positive cells normally would appear. As these cells express SOX9 but fail to delaminate, it suggests that the initial EndMT, prior to *Sox9*-dependant cardiac jelly invasion, might be impaired in *Hand2*-deficient hearts.

6.2.8. *Snai1*-dependent initiation of endothelial-mesenchymal transition in the atrioventricular canal is regulated by HAND2

We have shown that *Hand2*-deficient embryos lack delaminated cardiac cushion progenitors, and have obtained evidence that this phenotype could be caused by 1) deficient *Has2*-mediated control of ECM production impairing cellular migration; and by 2) a defect in *Twist1*-mediated regulation of the proliferation of post-EndMT delaminated cardiac cushion progenitors. We therefore wondered whether the initial EndMT was also affected by the *Hand2* deficiency, and investigated the expression of the EMT inducing transcription factor SNAI1 and its downstream effectors.

Consistent with the hypothesis of a likely underlying EndMT defect in *Hand2* mutant hearts, *Snai1* expression was totally lost from mutant AVC by E9.5 (Fig.21A). Furthermore, several HAND2 interacting regions were identified within *Snai1* genomic landscape (Fig.21B). ChIP-qPCR analysis confirmed the existence of HAND2 binding regions located 45kb, 58kb and 59kb downstream of *Snai1* TSS in developing hearts (E10.5, Fig.21C). The genomic region encompassing the peaks at +58/59kb (blue bar in Fig.21B) was used to generate *LacZ* reporter transgenic mouse embryos (n= 5, Fig.21D). This CRM is active in the branchial arches, craniofacial structures (Fig.21D'), forelimbs, and epicardium (Fig.21D''). The extent of cardiac expression will require histological analysis. The pattern of *LacZ* reporter expression in these embryonic structures is similar to the *Snai1* endogenous expression at an equivalent developmental stage (E10.5, (Sefton et al., 1998)).

To gain further insight into the potential disruption of the EndMT in *Hand2*-deficient hearts, VE-Cad and VIM distribution were studied. Both these genes are established *Snai1* targets during cardiac cushion formation (Timmerman et al., 2004; Cano et al., 2000; Batlle et al., 2000).

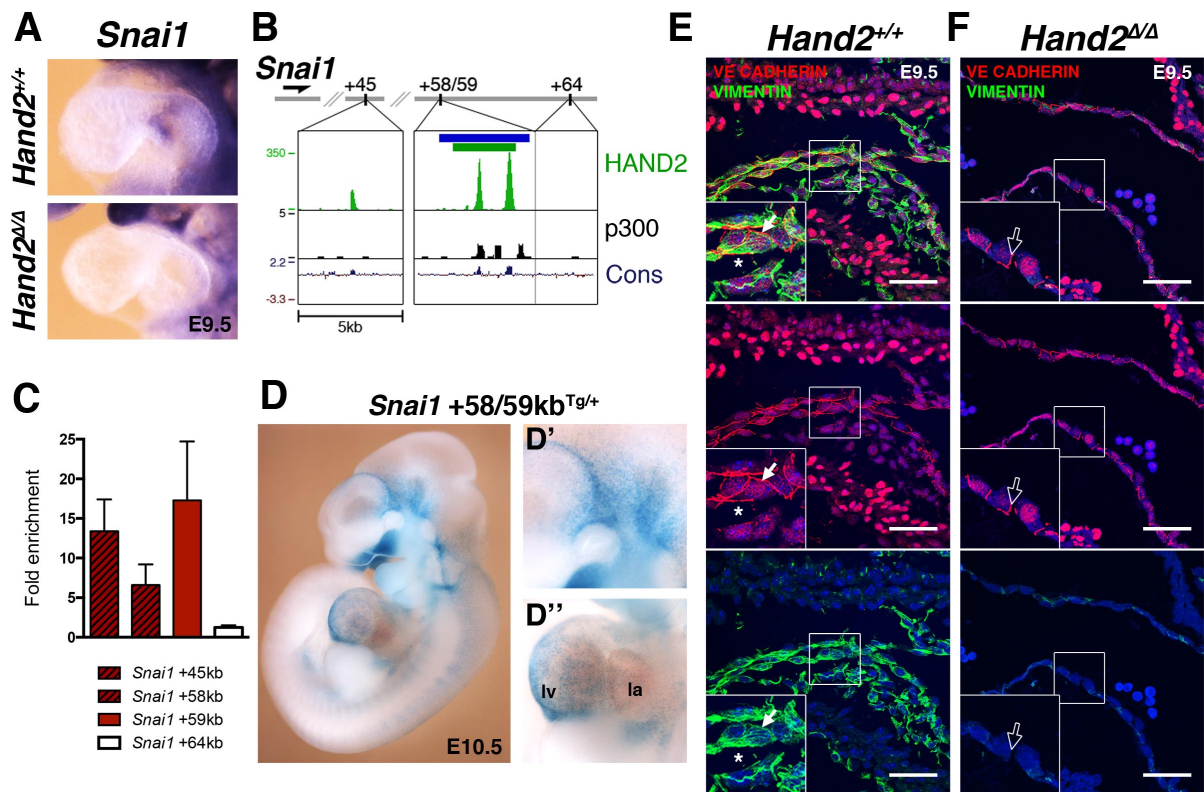


Figure 21. *Snai1* expression and the downstream endothelial-mesenchymal transition are altered in the AVC of *Hand2*-deficient embryos

(A) Expression of *Snai1* in wild-type and *Hand2*^{Δ/Δ} embryonic heart at E9.5. (B) UCSC browser windows representing the regions enriched in *HAND2*^{3xFLAG} chromatin complexes in *Snai1* cis-regulatory landscape. The green bar at +58-59kb from *Snai1* TSS indicates top2000 enriched region. The dark blue bar represents the genomic region used to generate transgenic reporter embryos. (C) ChIP-qPCR establishing direct interaction of *HAND2*^{3xFLAG} chromatin complexes with the *Snai1* +45kb, +58kb and +59kb regions in hearts (E10.5). The +64kb region is used as negative control. Mean ±SD (n=3) is shown. (D) Transgenic embryo (E10.5, n=5) showing *LacZ* expression under control of the CRM located +58/59kb from the *Snai1* TSS. The transgene is active mainly in craniofacial structures (D') and in the epicardium (D''). (E) In the wild-type AVC, VE-Cad is expressed at intercellular junctions in the endocardium (red, white arrow) but not delaminated cardiac cushion cells (white asterisk). VIM is expressed by both endocardial and cardiac cushion cells. (F) The endocardium of *Hand2*-deficient embryos expresses VE-Cad but not VIM (red, open arrow) but not VIM. Scale bar: 50μm

In wild-type embryos, VE-Cadherin marks the intercellular junctions between the cells of the endocardium (Fig.21E, white arrow) while it is no longer expressed by the delaminated progenitors (Fig.21E, white asterisk). In contrast, VIM is expressed by both endocardial (Fig.21E, white arrow) and delaminated progenitors (Fig.21E, white asterisk). Remarkably, VE-Cad remains expressed by the endocardium of *Hand2*-

deficient hearts (Fig.21F, open arrow), while VIM is lost from these cells (Fig.21F, white arrow). Endocardial cells of the AVC in *Hand2*-deficient embryos lack *Snai1* expression and characteristic EndMT changes that normally allow them to initiate delamination and migration. Both SNAI1-mediated disassembly of VE-Cad positive junctions between endocardial cells and the activation of the motile cellular phenotype in VIM positive cells are disrupted in the absence of HAND2. Together, these findings indicate that HAND2 regulates EndMT by directly controlling *Snai1* expression.

6.2.9. The *Hand2* loss-of-function affects the EndMT upstream signaling but not the patterning of the myocardium

The EndMT of the AVC endocardial progenitors is initiated by BMP2 signaling from the surrounding myocardium and additionally involves myocardial TGF β 2 and endocardial GATA4 and Notch1 (Ma et al., 2005; Rivera-Feliciano et al., 2006; Timmerman et al., 2004; Luna-Zurita et al., 2010). As HAND2 appears to directly regulate the expression of key genes involved in EndMT, we investigated if the upstream myocardial signaling events are also altered by loss of *Hand2* functions.

In the myocardium of E9.5 *Hand2*-deficient embryos, *Bmp2* is expressed in a smaller subdomain of the AVC than in wild-type (Fig.22A) and the expression of its downstream effector *Msx1* is lost from the endocardium (Fig.22B). In addition, in *Hand2*-deficient embryos *Gata4* expression is also lost from the endocardium (Fig.22C) and *Tgf β 2* expression from the myocardium (Fig.22D). In contrast, *Notch1* expression is not affected by the loss of *Hand2* (Fig.22E). These alterations raise the possibility that in addition to a direct role in EndMT, *Hand2* also functions in regulating these signaling cascades in the endocardium, possibly downstream of Notch1 and BMP2 and upstream of *Gata4*. The reduced *Bmp2* expression in the AVC myocardium (Fig.22A) could be a consequence of a patterning defect in the AVC, which would impact on myocardium-endocardium signaling. For this reason, we also analyzed the expression of *Tbx2* and *Tbx3* that are required downstream of *Bmp2* for the patterning of the AVC by inhibiting chamber differentiation through *Nppa* repression (Ma et al., 2005; Christoffels et al., 2004).

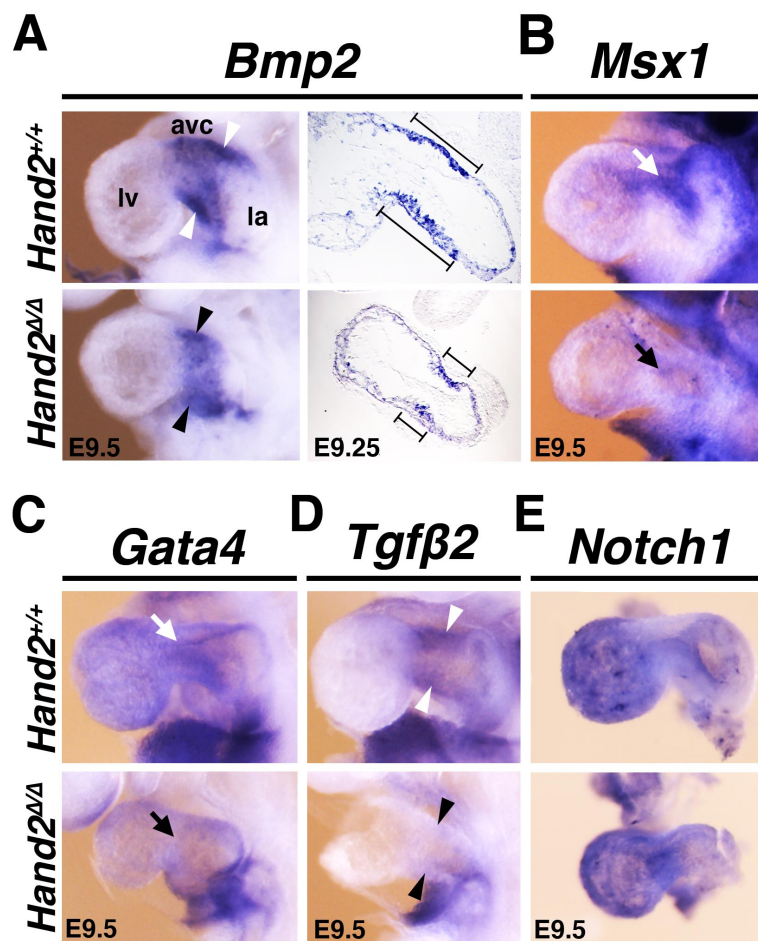


Figure 22. Expression of EndMT-inducing signals in wild-type and *Hand2*-deficient embryos

(A) The *Bmp2* expression domain in the AVC myocardium of *Hand2*-deficient embryos is reduced in comparison to wild-type embryos (E9.5, arrowheads). (B,C) The expression of *Msx1* (B) and *Gata4* (C) are lost from the endocardium of the AVC in *Hand2*-deficient embryos (E9.5, arrows). (D) *Tgfβ2* expression is lost from the myocardium of the AVC in *Hand2*-deficient embryos (E9.5, arrowheads). (E) *Notch1* expression is not significantly altered in *Hand2*-deficient hearts.

In *Hand2*-deficient embryos, the expression of TBX2 and TBX3 is not altered in the myocardium of the AVC (Fig.23A-10D) and remains complementary to *Nppa* expression in the left ventricle and atrium (Fig.23E). Finally, the delineation of LV-AVC boundary by *Hey2* is also not altered by the inactivation of *Hand2* (Fig.23F), which shows that the AVC myocardium is correctly patterned in spite of the more restricted *Bmp2* expression domain. Therefore, the defects in the EndMT in *Hand2*-deficient embryos cannot be a consequence of altered myocardial signaling. The loss of *Tgfβ2* and *Msx1* expression (Fig.22B,D) is rather caused by an intermediate role of HAND2 between the *Notch1/Bmp2/Tgfβ2* endocardium-myocardium feedback loops and the direct regulation of the *Snai1* dependent EndMT.

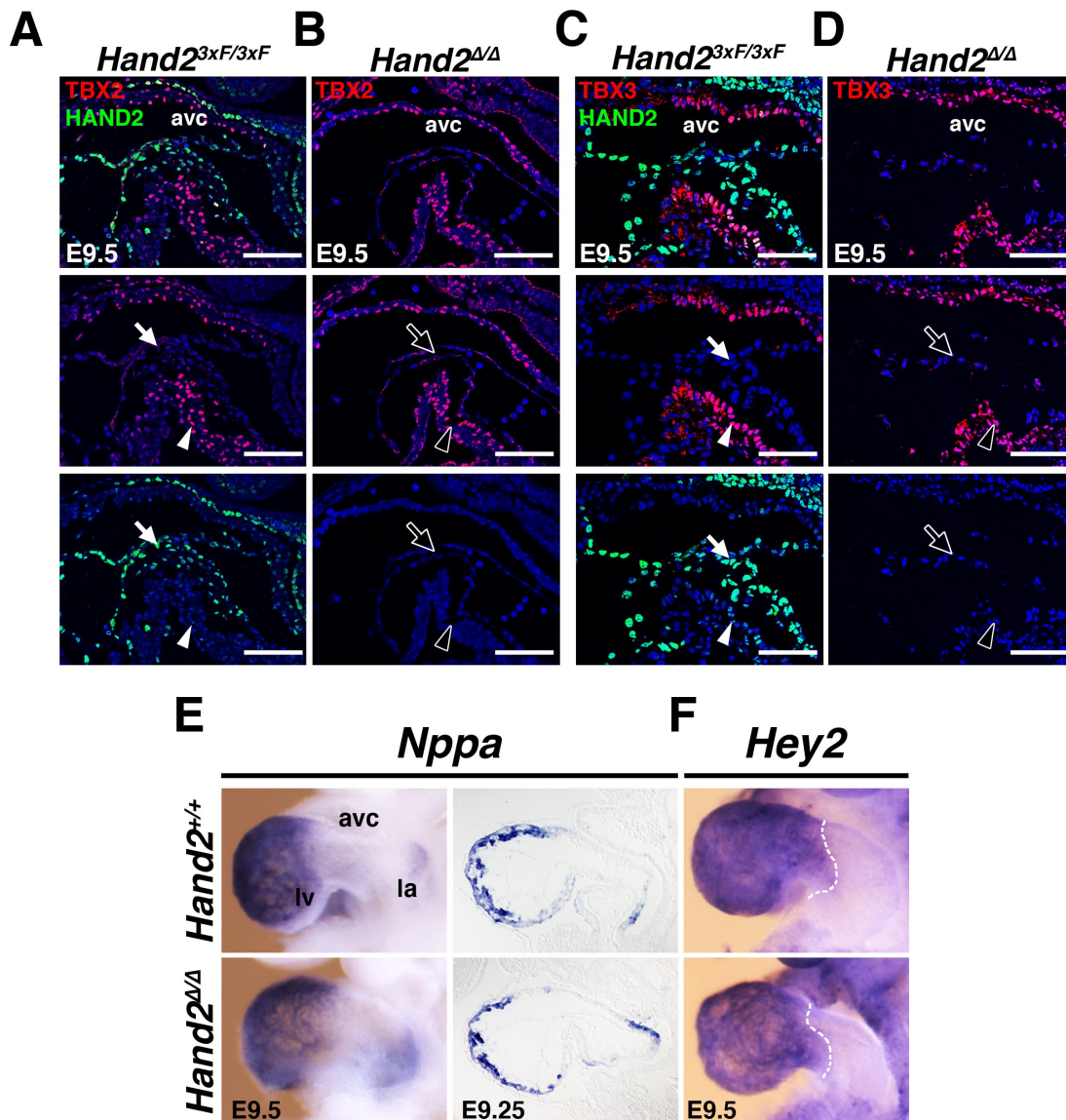


Figure 23. The myocardium of the AVC is normally patterned in *Hand2*-deficient embryos

(A-D) In wild-type embryos (E9.5), TBX2 (A) and TBX3 (C) are expressed in the myocardium of the AVC (white arrows) whereas HAND2 is expressed in the endocardium (white arrowheads). In *Hand2*-deficient embryos, both TBX2 (B) and TBX3 (D) remain expressed by the myocardium (open arrowheads). Scale bar: 50 μ m (E) *Nppa* expression is identical in the LV and LA myocardium of wild-type and *Hand2*-deficient embryos. (F) The LV-AVC boundary is marked by the limit of *Hey2* expression domain and remains in *Hand2*-deficient embryos.

6.2.10. *Tbx2* and *Tbx3* are direct targets of HAND2 during cardiac development

We showed that *Hand2* deficiency alters *Tbx2* and *Tbx3* expression in SHF progenitors (E8.25, Fig.15C-F), but not their expression in the myocardium of the AVC (E9.5, Fig.23A-D). Several regions within both *Tbx3* and *Tbx2* cis-regulatory landscapes were identified by the HAND2^{3xFLAG} ChIP-Seq analysis (Fig.24A and Fig.25C).

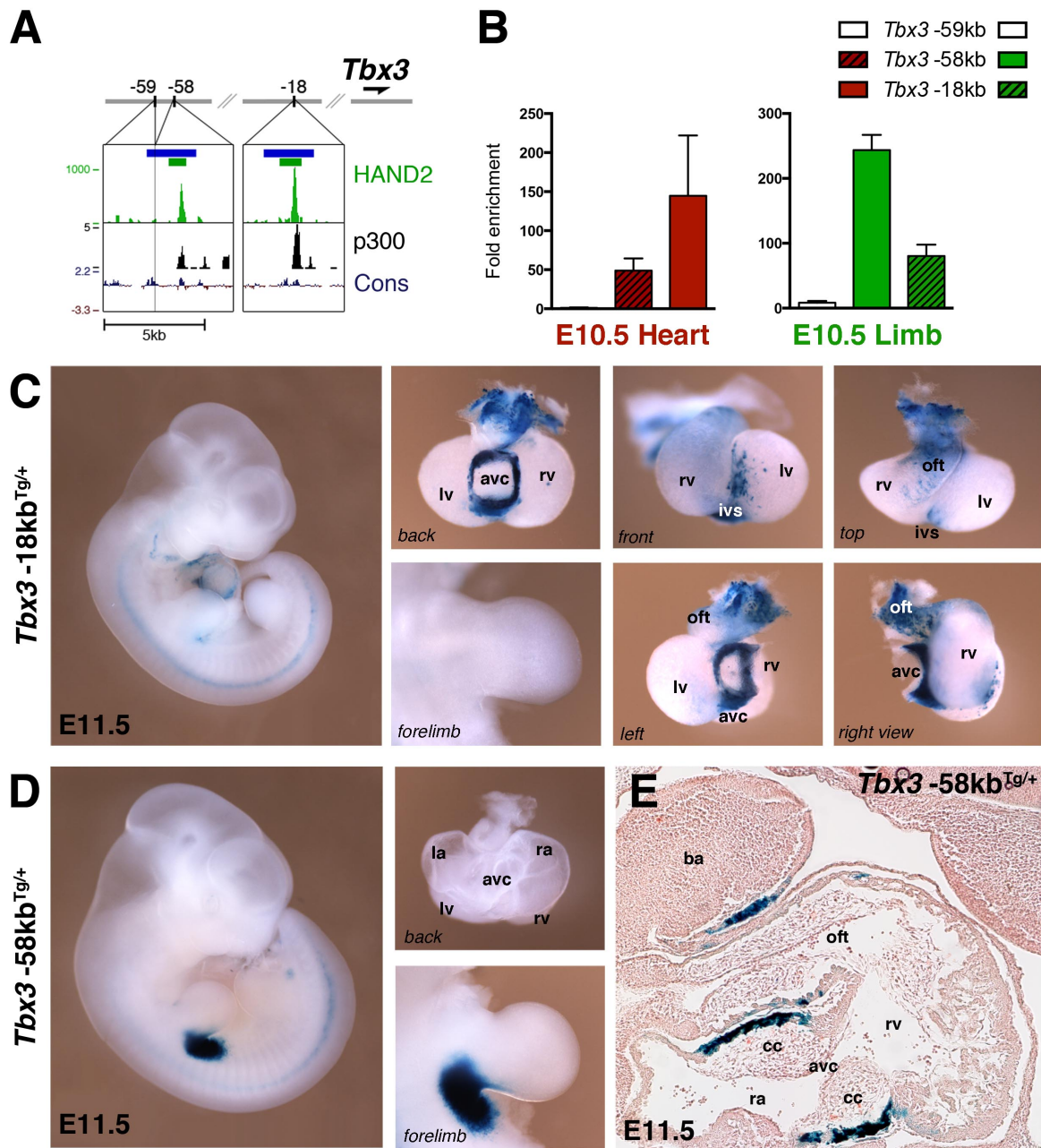


Figure 24. The *Tbx3* -18kb element is bound by HAND2 chromatin complexes in developing hearts and displays cardiac-specific enhancer activity

(A) UCSC browser windows representing HAND2^{3xFLAG} ChIP-Seq peaks in the *Tbx3* cis-regulatory landscape. The green bars at -58kb and -18kb from *Tbx3* TSS indicate top2000 enriched regions. The dark blue bar represents the genomic regions used to generate transgenic reporter embryos which expression are shown in (C) and (D). (B) ChIP-qPCR from embryonic hearts (E10.5, red, left panel) and limb buds (E10.5, green, right panel) establish that HAND2 chromatin complex interact preferentially with the *Tbx3* -18kb CRM in developing hearts and with the -58kb CRM in limb buds. (C) The *Tbx3* -18kb CRM shows heart-specific enhancer activity in *LacZ*-reporter transgenic embryos. The transgene is expressed in the AVC, OFT and interventricular septum (IVS). (D) In contrast, the -58kb CRM drives reporter expression in limb buds and flank mesoderm but not in the developing heart. (E) The *Tbx3* -18kb CRM is active in the cells of the prospective atrioventricular node.

Tissue-specific ChIP-qPCR established that the region located -18kb upstream of the *Tbx3* TSS was enriched mostly in HAND2 chromatin complexes isolated from developing hearts (E10.5, Fig.24B, left panel), while the -58kb region was enriched mostly in developing limb buds and flank tissues (E10.5, Fig.24B, right panel). To further determine if these candidate CRMs function as transcriptional enhancers, transgenic mouse embryos using a *LacZ* reporter construct were produced by M.Shoukry in the laboratory of A.Visel (Berkeley, USA). This analysis reveals that the -18kb CRM enhances expression in the AVC, OFT and interventricular septum (Fig.24C). In contrast, the activity of the -58kb CRM is restricted to the posterior-proximal forelimb bud and flank mesenchyme (Fig.24D). The CRM-*LacZ* reporter expression patterns are consistent with the ChIP-qPCR binding profiles (Fig.24B), which reveal tissue-specific functional relevance of the HAND2 interaction with these two *Tbx3* CRMs. The CRM located at -18kb is expressed in the atrioventricular node (AVN) in the cells that express *Tbx3* in the myocardium adjacent to the cardiac cushions (Fig.24E, (Christoffels et al., 2010)). Prior to formation of the AVN, no *LacZ* expression driven by this CRM was observed (data not shown). Interestingly, this CRM is located within the 160kb genomic landscape (spanning from -83kb to +77kb) previously identified as regulating *Tbx3* expression in both AVN and limb buds (Horsthuis et al., 2009). Our ChIP-Seq analysis not only identified a discrete AVN-specific CRM within *Tbx3* cis-regulatory landscape, but also established this CRM as interacting directly with HAND2 chromatin complexes during the regulation of *Tbx3*-mediated development of the cardiac conduction system.

Next, we determined the TBX3 and HAND2 protein distribution at E11.5, when *Tbx3* -18kb CRM drives reporter expression in the AVN (Fig.24E), but no evidence of cells co-expressing both transcription factors was obtained. While TBX3 is confined to the myocardium (Fig.25A, white arrowheads), HAND2 is expressed in the endocardium (Fig.25A, white arrows) and mesenchymal cells of the cardiac cushions (Fig.25A, white asterisks). One possible explanation is that the *Tbx3* -18kb CRM is repressed in HAND2 expressing cells and is active in the myocardium of the AVN due to the lack of HAND2 chromatin complexes. The enrichment of HAND2 complexes at this CRM in limb buds (Fig.24B, right panel), in combination with lack of *LacZ* reporter

expression (Fig.24C) is in agreement with the proposal that the HAND2 chromatin complexes repress this CRM.

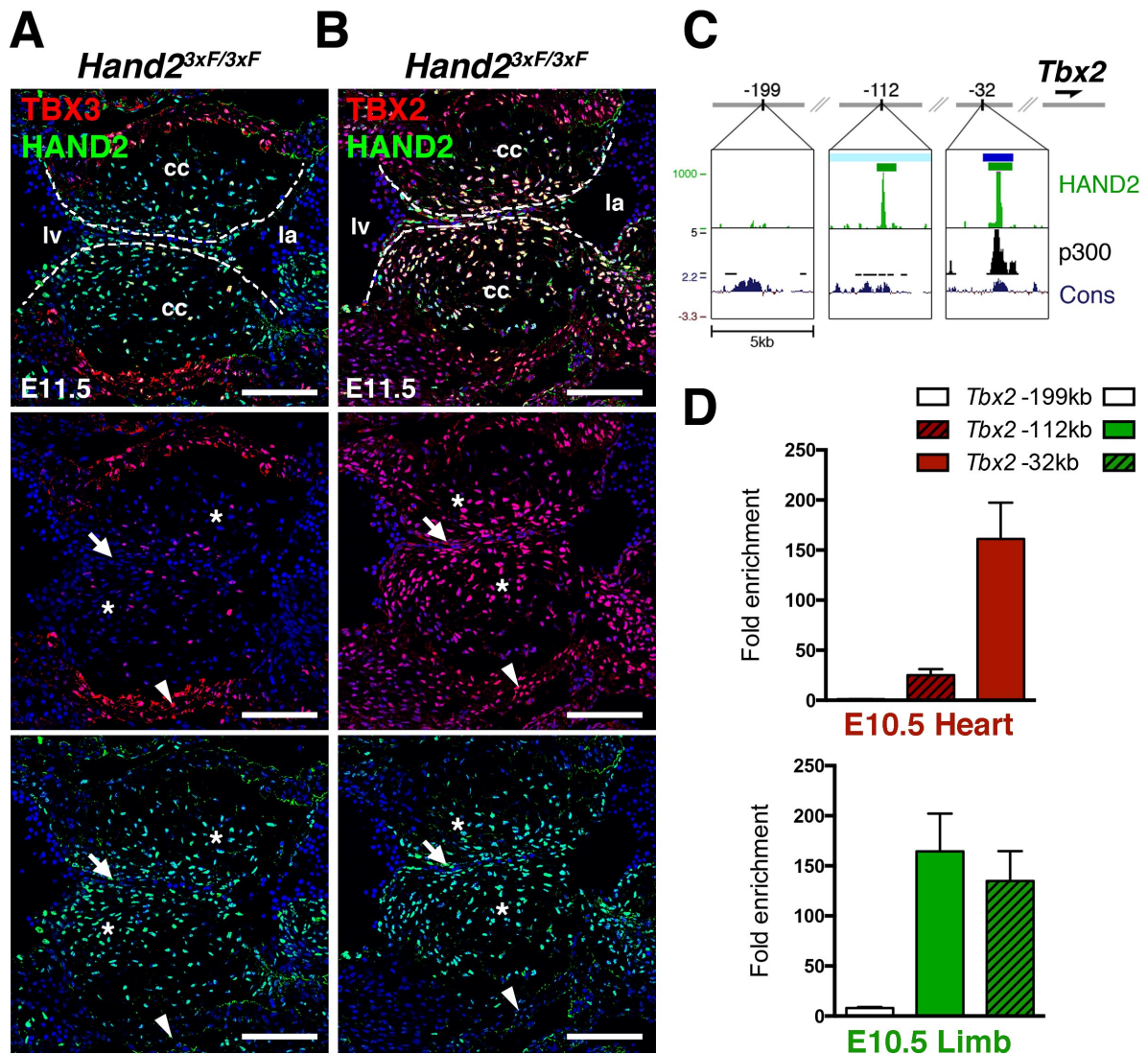


Figure 25. HAND2 directly interacts with a CRM located in *Tbx2* cis-regulatory landscape in developing hearts

(A) Expression of TBX3 (red) and HAND2 (green) in the AVC at E11.5. TBX3 is expressed by myocardial cells (white arrowheads) and HAND2 in endocardial cells (white arrows) and mesenchymal cells of the cardiac cushions (white asterisks). (B) Expression of TBX2 (red) and HAND2 (green) in the AVC at E11.5. TBX2 is expressed in myocardial cells (white arrowheads) and co-expressed with HAND2 in mesenchymal cells of the cardiac cushions (white asterisks). Scale bar: 100 μ m. (C) UCSC browser windows representing HAND2^{3xFLAG} ChIP-Seq peaks in the *Tbx2* cis-regulatory landscape. The green bars at -112kb and -32kb from *Tbx2* TSS indicate top2000 enriched regions. The light blue bar at -112kb indicates a limb bud enhancer (Infante et al., 2013). The dark blue bar at -32kb indicates the genomic region used to generate transgenic reporter embryos. (D) ChIP-qPCR from E10.5 embryonic hearts (red, top panel) and limb buds (green, bottom panel) establishes that HAND2 chromatin complexes interacts preferentially with the *Tbx2* -32kb CRM in the heart and with the -112kb CRM in limb bud.

In contrast to TBX3, TBX2 is coexpressed with HAND2 in the cardiac cushion cells at E11.5 (Fig.25B, white asterisks). Of the two candidates CRMs interacting with HAND2 within *Tbx2* regulatory landscape, the CRM located 112kb upstream of *Tbx2* (Fig.25C, light blue bar) has previously been shown to act as a transcriptional enhancer active in the posterior limb bud mesenchyme (Infante et al., 2013). Accordingly, the enrichment of HAND2 chromatin complexes encompassing this CRM was higher in developing limb buds than hearts (Fig.25D). In contrast, the -32kb candidate CRM is enriched both in developing hearts and limb buds (Fig.25D). Transgenic embryos using this region are currently being generated (dark blue bar in Fig.25C, results not yet available). Given the colocalization of TBX2 and HAND2 in mesenchymal cells of the cardiac cushions (E11.5, Fig.25B), we expect this -32kb CRM to drive *LacZ* expression in developing cushions. If the enrichment of this CRM in HAND2 chromatin complexes isolated from limb buds is functionally relevant (Fig.25D, lower panel), *LacZ* expression should also be detected in limb buds.

Another member of the T-box gene family important for cardiac development is *Tbx20*. While myocardial *Tbx20* regulates *Bmp2* expression in the AVC, endocardial *Tbx20* is not required for EndMT (Cai et al., 2011; Cai et al., 2013). A prominent HAND2 ChIP-Seq peak was identified 200kb upstream of the *Tbx20* TSS (Fig.26A, green bar). This region is the orthologous of a human VISTA enhancer element (hs463, Fig.26A, dark blue bar) that drives *LacZ* reporter expression in the heart of transgenic embryos (Fig.26B). However, no changes in *Tbx20* expression were detected in the developing hearts of *Hand2*-deficient embryos (Fig.26C). This agrees with previous observations indicating that *Tbx20* acts upstream of *Hand2* (Singh et al., 2005; Takeuchi et al., 2005). Nevertheless, the high enrichment of HAND2 chromatin complexes at the CRM located -200kb from *Tbx20* points to a possible involvement of HAND2 at late stages on *Tbx20*-mediated maturation of the cardiac cushions (Cai et al., 2013).

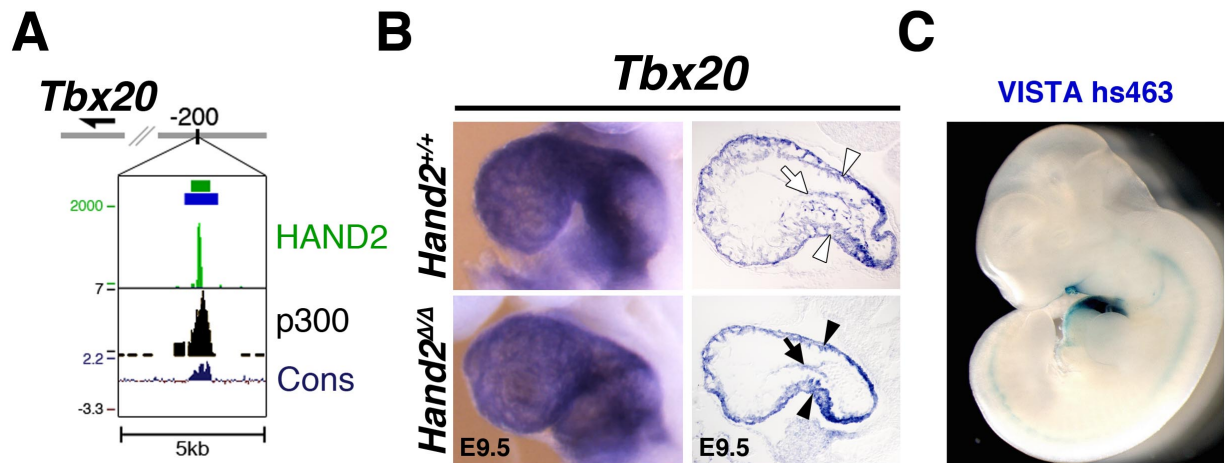


Figure 26. HAND2 directly interacts with a cardiac CRM located in *Tbx20* cis-regulatory landscape

(A) UCSC browser window showing a region from the *HAND2*^{3xFLAG} ChIP-Seq top 2000 enriched region located 200kb upstream of *Tbx20* TSS (green bar). The dark blue bar represents the location of the VISTA enhancer hs463. (B) *Tbx20* expression in the endocardium (arrows) and myocardium (arrowheads) of wild-type and *Hand2*-deficient embryos. (C) *LacZ* reporter activity driven by the VISTA enhancer hs463.

7. Discussion

7.1. Identification of HAND2 target gene networks that function during heart morphogenesis

The development of the four-chambered mammalian heart depends on complex spatial and temporal coordination of signaling pathways and transcription factors directing the proliferation and commitment of myocardial and endocardial progenitors into multiple cell types (Lescroart and Meilhac, 2012; Vincent and Buckingham, 2010). The wide range of life-threatening congenital heart diseases resulting from perturbations during cardiogenesis reflects the complexity and importance of the tightly regulated mechanisms governing heart development (Bruneau, 2008). It is thus crucial for both diagnosis and potential regenerative therapies to understand how hierarchical gene regulatory networks interact to orchestrate the morphogenesis of cardiac structures (Srivastava and Olson, 2000; Olson, 2006; Srivastava, 2006; Rana et al., 2013; Xin et al., 2013; Wamstad et al., 2014). Transcription factors active in the second heart field have been well studied, but knowledge on the gene networks regulated by HAND2 and its direct targets is limited (Rochais et al., 2009b; Dyer and Kirby, 2009; Kelly, 2012; Vincentz et al., 2011). Mutations of *HAND2* have been linked to human congenital heart diseases, which makes the identification of the gene networks controlled by HAND2 of particular interest (Shen et al., 2010; Strehle et al., 2012).

7.1.1. Genome-wide identification of cardiac CRMs

Several studies have determined the genomic target range of transcriptional co-activators and the distribution of different chromatin modifications marks in the heart (May et al., 2012; Blow et al., 2010; Shen et al., 2012). In contrast, so far few ChIP-Seq datasets from cardiac transcription factors (TFs) are available. Many of them are cell type or lineage specific and have been generated using commercial ChIP-grade antibodies in adult tissues. For example, TBX3, which is expressed by the conduction system, has been overexpressed in the adult myocardium to study its target range (van den Boogaard et al., 2012). This approach identified common transcriptional targets of TBX3, NKX2.5 and GATA4, but overexpression likely does not reflect the physiological TF-chromatin complexes and is potentially prone to the identification of

false positive interactions. Expression of several biotinylated cardiac TFs in cultured HL1 cardiomyocytes also led to the identification of cardiac *cis*-regulatory modules (CRMs), but targets in cultured cells may differ from those *in vivo* (He et al., 2011; Massie and Mills, 2008). In another study, TBX20 binding regions in adult hearts were identified using a BAC transgenic mouse line expressing a *Tbx20* allele tagged by eGFP, but a transgenic approach may again not reveal all endogenous targets (Shen et al., 2011). Altogether, the limitations of these studies show the importance of using endogenous levels of expression of TFs for ChIP-Seq approaches to accurately profile the DNA binding of transcriptional regulators. For this purpose, epitope tagging of TFs for high-throughput genome-wide approaches has become a powerful tool (Zhang et al., 2008a; Kidder et al., 2011; Landt et al., 2012). In particular, mouse alleles that express endogenously epitope-tagged TFs have been successfully used for ChIP-Seq analysis in various embryonic tissues (Attanasio et al., 2014). We have also chosen to insert a 3xFLAG epitope into the HAND2 protein to identify the CRMs interacting with HAND2 in a physiological manner during mouse embryogenesis. As the ChIP-Seq analysis used in this study was done using pooled *Hand2*-expressing embryonic tissues, we plan to perform a cardiac-specific ChIP-Seq analysis to identify additional heart-specific targets of HAND2.

7.1.2. HAND2 and its target CRMs in the heart: direct and indirect DNA-binding interactions

The genome-wide range of HAND2-containing chromatin complexes does not imply that all candidate CRMs are directly bound by HAND2. For instance, embryos homozygous for a mutant form of HAND2 deficient for DNA-binding exhibit right ventricle (RV) hypoplasia and lethality two to three days later than *Hand2* null embryos (Liu et al., 2009). This suggests that the control of gene expression during second heart field (SHF) patterning may be regulated independently of the direct interaction of HAND2 with DNA, while the subsequent growth of the ventricle requires direct binding of HAND2 to its target CRMs (Liu et al., 2009). These mutant embryos also display disorganized and enlarged cardiac cushions by E11.5, which points to a role of *Hand2* in the formation of these structures. The DNA binding mutation of *Hand2* does not affect the expression of the HAND2 genetic targets *Gata4* and *Nppa*, suggesting that

these genes are regulated by HAND2 in a DNA-binding independent manner (Srivastava et al., 1997; Thattaliyath et al., 2002; Liu et al., 2009). In agreement, our results suggest that *Gata4* and *Nppa* are indirect targets of HAND2 as the ChIP-Seq analysis and Hi-C data did not detect any HAND2 candidate CRMs in their *cis*-regulatory landscapes (Dixon et al., 2012).

In addition, heterodimerization of HAND2 with other transcriptional regulators as part of chromatin complexes adds another level of complexity to the attempt to identify direct HAND2 target CRMs (Vincentz et al., 2011). Indeed, several studies have shown that HAND2 interacts with the *Nppa* promoter as part of a complex with MEF2C, GATA4 and/or NKX2.5, and that at least some of these interactions do not require E-box motifs (Zang et al., 2004; Dai et al., 2002; Thattaliyath et al., 2002). It is tempting to speculate that the CRMs that are directly interacting with HAND2 should encode the consensus E-box sequence CANNTG (Dai and Cserjesi, 2002). In contrast, this sequence could be absent from CRMs to which HAND2 binds indirectly. Indeed, 47% of the peaks identified in the HAND2^{3xFLAG} ChIP-Seq analysis were enriched in motifs containing a variant of the E-box sequence (Osterwalder et al., in press), showing that in about half of the candidate CRMs HAND2 might not directly bind to DNA. The identification of potential HAND2-interacting proteins within transcriptional complexes could be achieved by searching known transcription factor binding sites motifs in the identified CRMs, or by Mass Spectrometry that takes advantage of the 3xFLAG tag that we have introduced in HAND2.

7.1.3. HAND2 target genes in the progenitors of the second heart field

Our analysis mainly focuses on HAND2 transcriptional targets at E9.5, which is the developmental stage at which *Hand2*-deficient embryos are still alive that is closest to the stages used for ChIP-Seq analysis. The early embryonic lethality could likely be circumvented by conditionally inactivating *Hand2* e.g. in the endothelial compartment using the *Tie2-Cre* or *Nfatc1-Cre* alleles to study its functions in the endocardium in more details (Kisanuki et al., 2001; Wu et al., 2012).

Our data show that both the myocardium and endocardium of the AVC in *Hand2*-deficient embryos are not affected by apoptosis at E9.5. However, the apoptosis is increased already at E8.5 in the bulbus cordis that connects the OFT to the RV and by

E9.5 also in the pharyngeal mesoderm and OFT (data not shown and (Yamagishi et al., 2001; Tsuchihashi et al., 2011)). These two studies concluded that *Hand2* is required for the survival of SHF cells. In particular, the RV hypoplasia is caused by the defective contribution of SHF progenitors to the heart (Yamagishi et al., 2001; Tsuchihashi et al., 2011). Therefore, we analyzed several markers of the SHF at the stage where these cells start to invade the heart tube (E8.25-E8.5). In *Hand2*-deficient embryos, we observed ectopic expression of *Tbx2* and *Tbx3* in the anterior SHF progenitors in the pharyngeal mesoderm (the *Tbx2* and *Tbx3* cis-regulatory landscapes are discussed below). In another study, early induction of a *Tbx2* transgene at E7.5 severely alters cardiac development and results in hypoplasia of the heart tube. This alteration is caused by impaired deployment of the SHF progenitors, reduced myocardial proliferation, and repression of the chamber differentiation markers *Nppa* and *Cx40* (Dupays et al., 2009). As TBX2 directly repress *Nppa* expression (Habets et al., 2002), and as *Nppa* expression is lost from the hypoplastic RV in *Hand2*-deficient embryos, we can establish a signaling cascade with direct (*Tbx2*) and indirect (*Nppa*) effects of *Hand2* on the development of the RV.

The expression of *Nkx2.5* in the pharyngeal mesoderm is necessary for the development of the SHF (Zhang et al., 2014). The ChIP-Seq analysis also identified a CRM highly enriched in HAND2 chromatin complexes in the *Nkx2.5* proximal promoter (data not shown). This CRM drives *LacZ* reporter expression in *Hand2*-expressing structures such as the OFT and RV (Tanaka et al., 1999). As *Nkx2.5* expression is not affected in *Hand2*-deficient embryos, this suggests a very robust regulation of its expression through additional cardiac CRMs or compensation by other TFs and reflects the central role of *Nkx2.5* for cardiac development.

7.1.4. *Furin* and *Myocd* are direct transcriptional targets of HAND2

We identified *Furin* as a new direct target of HAND2 in the endocardium of the AVC. Indeed, the inactivation of *Furin* in endothelial cells results in malformation of the mitral and tricuspid valves, which are derived from the AVC cardiac cushions and do not form in *Hand2*-deficient embryos (see below) (Kim et al., 2012; Lin et al., 2012). FURIN is involved in processing of BMP10, and in *Bmp10*-deficient embryos, the formation of the

cardiac cushions and trabeculations is impaired and the ventricular wall remains hypoplastic (Susan-Resiga et al., 2011; Chen et al., 2004). *Bmp10* participates in ventricular chamber formation by activating the expression of *Tbx20* (Zhang et al., 2011). In agreement, the inactivation of *Tbx20* disrupts trabeculation and cardiac cushion formation (Stennard et al., 2005). Both the acellular AVC cardiac cushions and hypotrabeulation phenotype are reminiscent of the ones observed in *Hand2*-deficient embryos. In addition, *Hand2* expression in the whole ventricular myocardium in transgenic mice promotes the formation of trabeculations and the expression of *Bmp10* (Togi et al., 2006). Finally, *Bmp10* is transactivated by the MYOCD/SRF complex, which induces cardiomyocytes proliferation and chamber maturation (Huang et al., 2012). This is interesting in light of our observation that *Myocd* is a direct target of HAND2. Together, these results suggest that the trabeculation and cardiac cushion defects in *Hand2*-deficient embryos may be partially mediated by impairing downstream BMP10 signaling via *Furin* or/and *Myocd*. This will be analyzed further by assessing *Bmp10* expression in *Hand2* constitutive and/or conditional mutant embryos.

7.1.5. A causal link between atrioventricular canal defects and embryonic lethality in *Hand2*-deficient embryos?

The AVC of *Hand2*-deficient embryos displays two major defects compared to wild-types. First, the cells delaminating from the endocardium to form the cardiac cushions are absent (see below). Second, there is an opening between the superior and inferior layers of the endocardium that leaves the AVC lumen open, in contrast to wild-type hearts. Such defects in AVC closure have only been described for *Endoglin*-deficient embryos (Bourdeau et al., 1999). *Endoglin* is expressed by the endocardium and by the endothelium compartment of blood vessels. Its inactivation results in defective EndMT, acellular cardiac cushions and embryonic lethality by E10.5. (Bourdeau et al., 1999). In addition, the inactivation of *Bmp2*, *Has2*, *Cspg2* or *Tbx20* also alter the formation of the cardiac cushions and leads to embryonic lethality prior to E10.5-E11.5, similarly to the *Hand2* inactivation (Rivera-Feliciano and Tabin, 2006; Camenisch et al., 2000; Yamamura et al., 1997; Mjaatvedt et al., 1998; Cai et al., 2011). All these mutants also display a failure in the AVC lumen closure, despite this phenotype is not described in these studies. In zebrafish, the two sides of the AVC are brought together by the

contractions of the myocardium (Scherz et al., 2008). Thus, myocardial contraction failure is a possible explanation to the defective closure of the AVC. In physiological conditions, the electrical impulse driving peristaltic cardiac contractions in early embryos at the heart tube stage is generated in the venous pole. Conduction is rapid in atria and ventricles, while in the AVC and OFT the conduction is slow resulting in a contraction delay in these compartments (de Jong et al., 1992; Moorman and Christoffels, 2003; Christoffels and Moorman, 2009). The primordia of the future components of the adult conduction system start to develop at ~E9.5, which is around the onset of embryonic lethality in *Hand2*-deficient mouse embryos (Christoffels and Moorman, 2009; Christoffels et al., 2010; Srivastava et al., 1997). Unidirectional blood flow without regurgitation is also established at this stage and requires coordinated cardiac contractions and formation of the AVC cardiac cushions (Nishii and Shibata, 2006). Thus, irregular contractions and absence of cardiac cushions results in retrograde blood flow into the atria, which reduces cardiac output and leads to death (Scherz et al., 2008). In *Hand2*-deficient mouse embryos, cardiac contractions are observed at E9.5 but appear slightly less coordinated in comparison to wild-type controls. This observation would require recording and careful analysis to firmly establish this phenotype (Nishii and Shibata, 2006). Together, these results are in agreement with the proposal that defective AVC closure in *Hand2* and other mutants may be causally linked to impaired blood pumping and thus to their early embryonic lethality.

In conclusion, the cardiac failure and lethality of *Hand2*-deficient embryos is likely multifactorial, including atresia of the aortic arches arteries, massive cell death of SHF progenitors in the branchial arches, hypotrabeulation that reduce the myocardial surface and impairs oxygenation, and absence of cardiac cushions and possibly impaired cardiac contractions ((Srivastava et al., 1997; Aiyer et al., 2005) and this study). This plethora of defects illustrates the complexity of heart morphogenesis and of the regulatory networks controlled by HAND2 in this process.

7.2. Gene networks controlling endothelial-mesenchymal transition in the atrioventricular canal are directly regulated by HAND2

Previous studies have postulated a role for *Hand2* in cardiac cushion formation but no direct involvement or mechanism was established (Camenisch et al., 2000; Liu et al., 2009; Holler et al., 2010; Vincentz et al., 2011; VanDusen and Firulli, 2012). The HAND2^{3xFLAG} ChIP-Seq analysis identified CRMs in the *cis*-regulatory landscapes of several genes with a role in the EndMT and differentiation of the AVC cardiac cushions. Our in-depth analysis of these interactions uncovered a gene network controlled by HAND2 that functions in the initiation of EndMT and cardiac cushion formation. The block in EndMT initiation has not been analyzed in previous studies and is morphologically strikingly similar to the consequences of inactivating other genes functioning in this process (e.g. *Cspg2*, which encodes the extracellular matrix protein Versican (Yamamura et al., 1997; Mjaatvedt et al., 1998)).

7.2.1. *Hand2* participates in extracellular matrix deposition within the cardiac jelly

The deposition of extracellular matrix (ECM) in the cardiac jelly of the AVC is required for the migration of the mesenchymal cells of the cardiac cushions (Bernanke and Markwald, 1979). Versican and hyaluronic acid (HA) are both ECM components of the cardiac jelly. Inactivation of the HA producing enzyme *Has2* also disrupts cardiac cushion formation and results in phenotypes similar to those observed in *Hand2*-deficient embryos (Camenisch et al., 2000). Our study establishes that *Has2* expression in the AVC depends on *Hand2*, and that *Has2* is a direct target of HAND2-containing chromatin complexes (Fig.27A). However, at this stage it is not clear how HAND2 complexes regulate *Has2* expression in the developing heart. The CRM we identified in the first intron of *Has2* drives reporter expression in the limb buds, suggesting that the previously described limb enhancer of *Has2* located in its proximal promoter is part of a larger CRM (Liu et al., 2013).

We showed that the ECM in the cardiac jelly is reduced in *Hand2*-deficient mouse embryos, and several studies support an involvement of *Hand2* in the composition and modeling of ECM components. Conditional deletion of *Hand2* within the PEO and epicardium results in disorganization of Fibronectin (Fn1) fibrils in the epicardial ECM

(Barnes et al., 2011). In *Hand2*-deficient zebrafish embryos, the Fibronectin network is also disorganized (Le et al., 2005). Detailed analysis suggests that *Hand2* negatively regulate *Fn1* expression, which allows cardiomyocyte movements required for fusion of the cardiac tube (Garavito-Aguilar et al., 2010). This is likely an indirect effect as *Fn1* transcripts are not altered in *Hand2*-deficient mouse embryos (Barnes et al., 2011), and no evident HAND2-enrichments are detected around the *Fn1* locus by ChIP-Seq analysis. In addition, *Hand2* regulates the expression of matrix metalloproteinases (MMP), which in turn degrade laminin and enable the migration of lateral plate mesodermal cells and leftward gut looping in zebrafish (Yin et al., 2010). In the mouse, MMPs belonging to the ADAMTS family function in the formation of the cardiac jelly in the AVC by cleaving Versican in the cells that undergo EndMT (Kern et al., 2006). Haploinsufficiency for *Adamts9* causes valves malformations (Kern et al., 2010), and interestingly, several members of the ADAMTS family contain one to several regions enriched in the HAND2^{3xFLAG} ChIP-Seq analysis. However, these HAND2 associated regions have not yet been analyzed to establish if HAND2 acts indeed upstream of ADAMTS metalloproteinases in mouse embryos.

Together, these data indicate that *Hand2* participates in regulating the ECM composition in vertebrate embryos. In particular, HAND2 may directly participate in remodeling the ECM components of the AVC cardiac jelly, which in turn contribute to the migration of the mesenchymal cells of the cardiac cushions. In addition, it would be interesting to determine if the functions of *Hand2* in controlling ECM components/regulators are also relevant in other embryonic and adult tissues or in pathological situations such as cancer (Lu et al., 2012).

7.2.2. HAND2 directly regulates *Twist1* and *Snai1* expression during formation of the AVC cardiac cushions

In addition to the ECM formation, the secondary EMT of epicardial cells is also affected by the inactivation of *Hand2* (Barnes et al., 2011). Therefore, we decided to investigate other potential direct targets of HAND2 that are required for the EndMT in the AVC. In particular, *Twist1*, *Sox9* and *Snai1* function at crucial steps of the AVC cardiac cushion morphogenesis (Vrljicak et al., 2012; Akiyama et al., 2004; Timmerman et al., 2004). Our ChIP-Seq analysis identified potential CRMs in all of their *cis*-regulatory

landscapes. Indeed, the expression of both *Twist1* and *Snai1* is lost from the AVC in *Hand2*-deficient embryos, while *Sox9* expression remains normal. In agreement, ChIP-qPCR from embryonic hearts confirmed that HAND2 chromatin complexes interact with CRMs within the *Twist1* and *Snai1* but not *Sox9* cis-regulatory landscapes, which allowed us to conclude that *Twist1* and *Snai1* are direct transcriptional targets of HAND2 (Fig.27A).

TWIST1 is expressed in the AVC upon delamination of endocardial cells, most likely as a consequence of its regulation by HAND2. Previous studies have shown that *Twist1* regulates the expression of genes involved in the proliferation of AVC cardiac cushion cells but is, on its own, not required for their formation (Chakraborty et al., 2010; Vrljicak et al., 2012; Vincentz et al., 2008). However, the migration of the cNCC that populate the OFT cardiac cushions is impaired or delayed in *Twist1*-deficient embryos. These cNCC form nodules that express *Hand2* inside the mesenchyme of the cardiac cushions (Vincentz et al., 2008). Interestingly, *Hand2* is required for the migration of the cNCC in the OFT (Holler et al., 2010). As our study establishes direct transcriptional control of *Twist1* by HAND2, this regulation could also be operational in migratory cNCC. In fact, previous analysis already suggested that the absence of EndMT and cardiac cushion phenotype in *Twist1*-deficient embryos could be due to functional redundancy with *Hand2* (Vincentz et al., 2008). TWIST1 forms heterodimers with HAND2 and other bHLH TFs, and these interactions are regulated by phosphorylation that dictate the DNA binding specificity of the transcriptional complexes (Firulli et al., 2005; Firulli et al., 2007). The *Hand2*^{3xFLAG} allele could be a suitable tool to assess this protein-protein interaction by co-immunoprecipitation of the transcriptional complexes from developing hearts followed by Mass Spectrometry. Finally, we have initiated transgenic reporter analysis to determine the activity of the *Twist1* +130kb candidate CRM. We expect this element to be active in the cardiac cushions of the AVC, but if *LacZ* reporter expression is also detected in the cushions of the OFT, this would support the proposal that *Twist1* expression in the cNCC is regulated by HAND2.

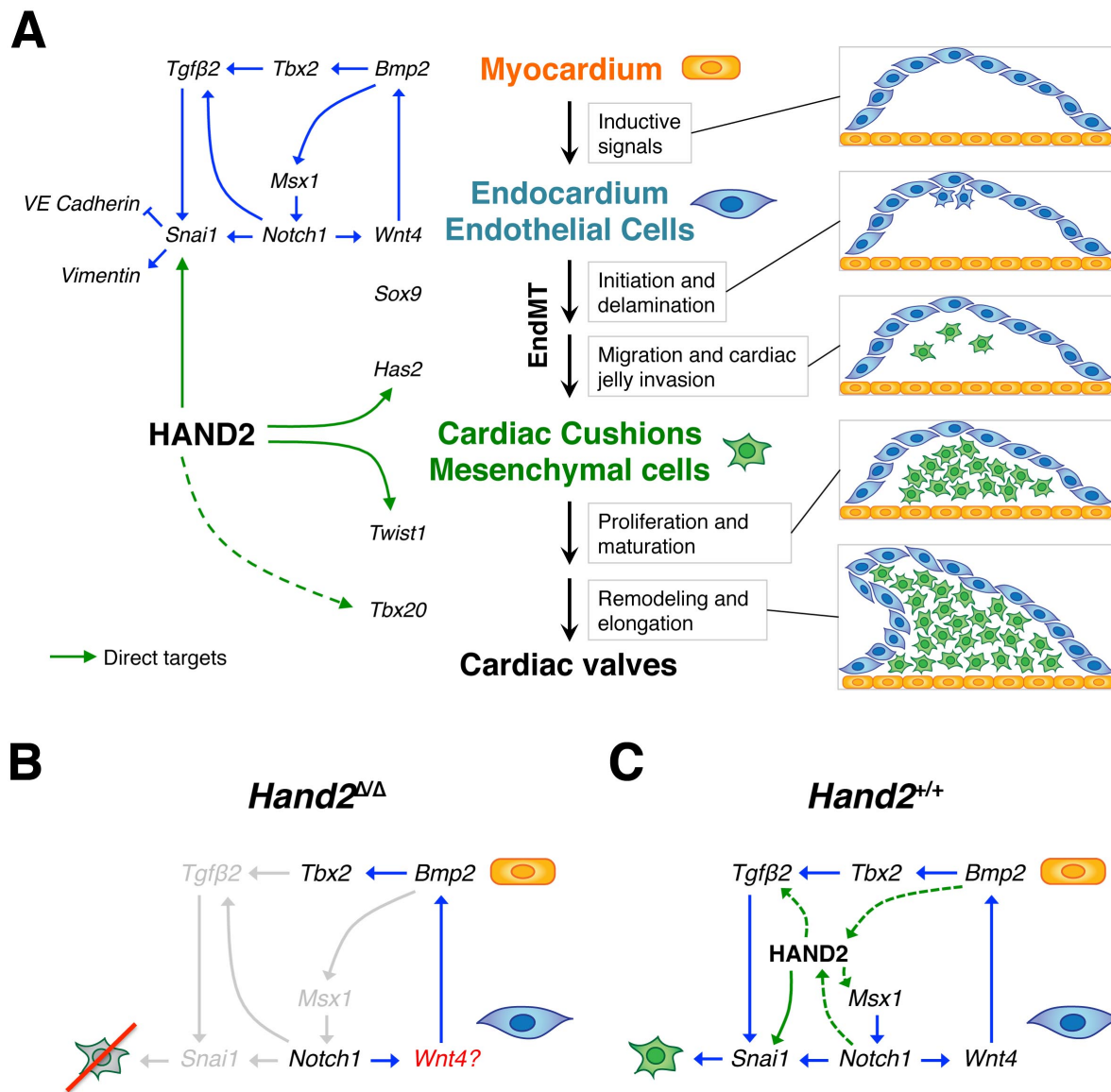


Figure 27. A model of the regulatory network controlled by *Hand2* during endothelial-mesenchymal transition and cardiac cushion formation in the atrioventricular canal

(A) Model of HAND2 functions during cardiac cushion formation. *Snai1*, *Has2* and *Twist1* are newly identified direct targets of HAND2 during initiation of EndMT, migration of delaminated cells and/or cardiac cushion proliferation. (B) Schematic representation of the gene whose expression is altered in *Hand2*-deficient embryos (grey), and (C) proposed model of HAND2 as an intermediate relay in the signaling interactions between *Notch1*, *Bmp2* and *Tgfβ2*. Dashed green arrows indicate interactions that remain to be tested or confirmed.

Genetic targets of TWIST1 in the cardiac cushions of the AVC include *Bmp2* and *Sox9*, whose expression is reduced in the AVC of *Twist1*-deficient embryos (Vrljicak et al., 2012). As *Sox9* expression is initiated in endocardial cells of *Hand2*-deficient embryos, it suggests that TWIST1 upregulates *Sox9* expression in cells after delamination for

proper cardiac cushion remodeling but is not necessary for *Sox9* activation (Lincoln et al., 2007).

SNAI1 is a prototypic transcription factor involved in many different physiological and pathological EMT processes by controlling genes that induce changes in cell shape, adhesion and motility (Barrallo-Gimeno and Nieto, 2005; Thiery et al., 2009). In particular, SNAI1-mediated downregulation of *E-Cadherin* genes is a key event in the initiation of EMT (Batlle et al., 2000; Cano et al., 2000). The formation of the cardiac cushions is no exception, as SNAI1-mediated downregulation of the vascular E-Cadherin (VE-Cadherin) is necessary for progression of the endocardial EMT (Timmerman et al., 2004; Vestweber, 2008). In parallel, SNAI1 upregulates *Vimentin* expression to increase the motility of the delaminating cells (Cano et al., 2000; Ivaska, 2011; Mendez et al., 2010). In addition to the total absence of *Snai1* in the AVC, VIM expression is not activated and VE-Cad junctions are maintained in the endocardium of *Hand2*-deficient embryos. These results indicate that *Hand2* is required for *Snai1* activation and initiation of the EndMT. Indeed, HAND2 chromatin complexes interact with two candidate CRMs in the *Snai1* cis-regulatory landscape. As *Snai1* acts cooperatively with *Snai2* to induce the EndMT (Niessen et al., 2008), we also looked into a potential direct regulation of *Snai2* by HAND2 but no experimental evidence in favor of such direct regulation were obtained (data not shown).

Despite *Snai1* is expressed in the premigratory and migratory neural crest cells, it is not required for their initial delamination (Sefton et al., 1998; Murray and Gridley, 2006). The *Snai1* CRM we identified by ChIP-Seq analysis drives *LacZ* reporter expression in migratory neural crest cells, craniofacial structures, and in the epicardium. Indeed, *Snai1* is important both for the development of craniofacial structures and for the EMT of epicardial cells (Cordero et al., 2011; Murray et al., 2007; Tao et al., 2013). Interestingly, *Hand2* is also expressed in craniofacial neural crest derivatives and regulates the formation of the palate, mandible and tongue (Charité et al., 2001; Yanagisawa et al., 2003; Funato et al., 2009; Barron et al., 2011; Xiong et al., 2009). *Hand2* is also involved in the EMT of epicardial cells and their differentiation into coronary vasculature (Barnes et al., 2011). We have thus identified a CRM active in

several embryonic tissues where both *Snai1* and *Hand2* are expressed, suggesting that *Snai1* might be a universal target of HAND2. The precise role of this *Snai1* CRM during cardiac cushion formation and in other biological contexts remains to be investigated.

To gain further insight into the roles of HAND2 in the EndMT, we will use AVC explant culture, which has been successfully used to determine the role of different TFs in EndMT and cardiac cushion formation (Runyan and Markwald, 1983; Camenisch et al., 2000; Akiyama et al., 2004; Timmerman et al., 2004; Luna-Zurita et al., 2010; Moskowitz et al., 2011). This assay allows dissection of the molecular mechanisms and interactions that control the formation of cardiac cushions by analyzing the migratory and invasive capacities of the endocardial cells. Initially, we will compare wild-type versus *Hand2*^{ΔΔ} AVC explants in culture. In addition, *Hand2* could be specifically inactivated in explants using *Adeno-Cre* viral particles in combination with the *Hand2* conditional allele, and we could also attempt rescue experiments by re-expressing *Hand2* using viral vectors as well. Adding hyaluronic acid to *Hand2*-deficient cultured explants could provide insights into the extent to which *Hand2*-mediated ECM defects contribute to the failure to form the cardiac cushions in these mutants.

7.2.3. HAND2 is an intermediate factor in the myocardial/endocardial signaling events that induce the EndMT

To determine the possible involvement of myocardial signals in the disruption of *Snai1*-mediated EndMT in *Hand2*-deficient embryos, we looked at the expression of *Bmp2*, *Tgfβ2*, *Notch1* and other key genes involved in the myocardial-endocardial crosstalk that patterns the AVC and initiates the EndMT. Our results indicate that the AVC myocardium is correctly patterned in the absence of HAND2, and that *Hand2* acts downstream of the relevant signals and upstream of activating *Snai1*. Furthermore, this gene expression analysis allowed us to make some assumptions regarding the exact position and role of HAND2 in the signaling network that control the EndMT in the AVC.

The loss of the BMP2 target *Msx1* in the endocardium shows that the absence of *Hand2* alters BMP2 downstream signaling (Fig.27B). Endothelial deletion of the BMP signal transducer *Smad4* results in defective EndMT and in acellular cardiac cushions,

as in *Hand2*-deficient embryos (Moskowitz et al., 2011). Furthermore, *Smad4* genetically interacts with *Gata4* in the endocardium, and both proteins can heterodimerize and cooperatively activate the expression of target genes in the AVC endocardium (Moskowitz et al., 2011). The new *Smad4*^{3xFLAG} allele that I generated could thus be used to study the impaired signaling activity of BMP2 in the endocardium of *Hand2*-deficient embryos (Fig.27C). We are currently generating the compound *Hand2*^{Δ/+};*Smad4*^{3xFLAG-HR/+} mice to assess this hypothesis.

In the endocardium, Notch1 signaling represses *Bmp2* expression through *Hey1* and *Hey2*, which in turns prevents endocardial cells to acquire a cardiomyocyte cell fate (Luna-Zurita et al., 2010). In *Hand2*-deficient embryos, *Notch1* and *Hey2* are expressed normally and there is no ectopic activation of *Bmp2* in the endocardium. This indicates that *Hand2* is not part of the Notch1-HEY1/2-BMP2 endocardial signaling module.

The myocardial expression of *Tgfβ2* depends on both Notch1 signaling through a postulated retrograde endocardial to myocardial signal (Timmerman et al., 2004), and on BMP2 signaling through *Tbx2* (Ma et al., 2005; Shirai et al., 2009). In addition, Notch1 promotes paracrine endocardial to myocardial Wnt4 signaling that in turns regulates *Bmp2* expression (Wang et al., 2013). In *Hand2*-deficient embryos, the expression of *Tgfβ2* but not of *Notch1*, *Bmp2* and *Tbx2* is lost (Fig.27B). This suggests that *Tgfβ2* is regulated indirectly by *Hand2* downstream of Notch1. In this model, *Hand2* would occupy an intermediate signaling role between Notch1 and the other postulated endocardial signal that regulates *Tgfβ2* expression, rather than in the Notch1-Wnt4-BMP2-TBX2 signaling module (Fig.27C).

Finally, *Snai1* expression in the endocardium and subsequent EndMT depends on the synergic action of Notch1, TGFβ2 and BMP2 signaling (Timmerman et al., 2004; Niessen et al., 2008; Luna-Zurita et al., 2010; Garside et al., 2013). Our data established that HAND2 is also directly required for the activation of *Snai1* expression. To determine whether HAND2 acts in parallel or as an intermediate transcriptional relay in these signaling interactions will require further analysis of embryos deficient for some of the other key genes discussed here (Fig.27C).

7.2.4. A role for *Hand2* in cardiac valves maturation and remodeling?

The cardiac valves are derived from the cardiac cushions. The ChIP-Seq analysis identified numerous potential CRMs associated with genes that function in cardiac valve remodeling. However, the lethality of *Hand2*-deficient embryos prior to the stage of valve remodeling precludes the analysis of *Hand2* functions during cardiac cushion maturation. Nevertheless, we established that HAND2 chromatin complexes bind a cardiac enhancer of *Tbx20*, which controls proliferation of the valve endothelial cells during valve elongation (Fig.27A) (Cai et al., 2013). Other likely direct targets of HAND2 with ChIP-Seq peaks in their *cis*-regulatory landscapes include *Col1a1*, which is important for valves structure and maintenance, and *Scleraxis*, required for differentiation and ECM organization during valve remodeling (Peacock et al., 2008; Levay et al., 2008). The conditional removal of *Hand2* from the mesenchymal cells of the cardiac cushions from E10.5 does not affect cardiac valves maturation (VanDusen et al., 2014). Therefore, the requirement of *Hand2* for EndMT initiation is a critical step, whereas *Hand2* appear to be dispensable during cardiac cushion remodeling, maybe due to a compensatory mechanism mediated by *Twist1* (see above).

7.3. The paralogous *Tbx2* and *Tbx3* genomic landscapes encode heart and limb bud specific CRMs bound by HAND2 chromatin complexes

The HAND2^{3xFLAG} ChIP-Seq analysis identified several candidate CRMs in the *cis*-regulatory landscapes of the T-box genes *Tbx2* and *Tbx3*. Using these candidate CRMs in *LacZ* reporter assays, we identified one heart and one limb bud specific CRM within the *Tbx3* ~160kb *cis*-regulatory landscape. In addition to the heart and limb buds, this large landscape is able to activate reporter expression in the eye, snout and mammary glands (Horsthuis et al., 2009). As *Hand2* is not expressed in these other structures where the two identified CRMs are also not active, it appears that *Tbx3* expression is regulated by an archipelago containing several other tissue-specific CRMs. Indeed, a recent study used chromatin architecture profiling from embryonic hearts and established that the *Tbx3* promoter physically contacts the HAND2-interacting cardiac CRM and an additional pan-cardiac enhancer (van Weerd et al.,

2014). Both CRMs synergize to activate *Tbx3* expression in the atrioventricular conduction system. In addition, the cardiac-specific CRM that we identified by HAND2^{3xFLAG} ChIP-Seq analysis requires the synergic action of GATA4 and SMADs to be active (van Weerd et al., 2014). This CRM is able to drive *LacZ* reporter expression in the myocardium of the AVC, where the atrioventricular node will form. As HAND2 is not expressed in these cells, it is possible that this CRM is repressed by HAND2 chromatin complexes. In addition, the ectopic expression of *Tbx3* at early stages in *Hand2*-deficient embryos argues in favor of a general repressive effect of HAND2 on this gene during cardiac development. The additional HAND2-independent CRM(s) accounting for robust expression of *Tbx3* could explain why genetic inactivation of *Hand2* does not result in ectopic activation of *Tbx3* expression at the onset of cardiac conduction system formation, but only at earlier stages.

The *Tbx3/Tbx5* and *Tbx2/Tbx4* landscapes are likely similar, as they evolved by two rounds of gene duplication from a single ancestral gene (Fig.28A) and (Agulnik et al., 1996). Indeed, we also detected two CRMs interacting with HAND2 chromatin complexes in the *Tbx2* landscape. The activity of one of them is currently being analyzed, while the other drives *LacZ* reporter expression in the posterior limb bud mesenchyme (Infante et al., 2013). An additional HAND2^{3xFLAG} ChIP-Seq peak located closer to *Tbx4* was reported to be a *Tbx4* hindlimb enhancer (Menke et al., 2008). When we compare the HAND2 ChIP-Seq profiles for the *Tbx2/Tbx4* and *Tbx3/Tbx5* cis-regulatory landscapes, we observe a similar distribution that argues in favor of similar cardiac and limb bud CRM activities in both landscapes (Fig.28B). However, the functions of *Tbx5* and *Tbx4* have diverged as they are specifically functioning in forelimb and hindlimb induction, respectively. The amphioxus ancestral *Tbx4/5* gene lacks the CRM required for limb initiation but is able to initiate limb formation in mouse transgenic embryos under control of a limb mesenchymal promoter. This indicates that changes in the CRMs rather than gene functions underlie the specialization of *Tbx4* and *Tbx5* during limb evolution (Minguillon et al., 2009). It would be interesting to study the evolutionary and functional relationship of the cardiac CRMs of *Tbx2* and *Tbx3*, as gene duplications can also result in the acquisition of new structures and functions in the developing heart (Olson, 2006). The orthologous human and chicken sequences of

the CRM of *Tbx3* that interacts with HAND2 complexes in the heart display similar reporter activity as their murine counterpart in the AVC. This indicates evolutionary conserved functions of this CRM during *Tbx3*-mediated formation of the conduction system (van Weerd et al., 2014).

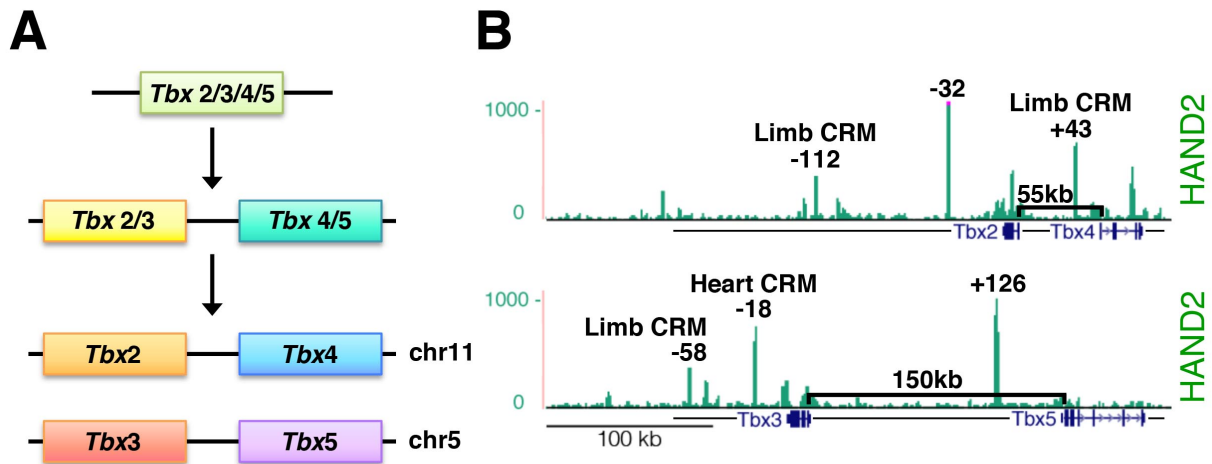


Figure 28. Regulation of T-box genes *cis*-regulatory landscapes by HAND2

(A) Evolution of *Tbx 2/3/4/5* subfamily by gene duplications and unequal crossovers. Adapted from (Agulnik et al., 1996). (B) UCSC browser window showing the linkage of *Tbx2/4* and *Tbx3/5* genes and the HAND2 interacting regions identified by ChIP-Seq analysis in these two genomic landscapes. Distances to ChIP-Seq peaks are indicated relative to *Tbx2* (upper panel) and *Tbx3* (lower panel) TSS.

During cardiac development, *Tbx2* and *Tbx3* are both upregulated in the SHF progenitors of *Hand2*-deficient embryos, while they are downregulated in limb buds (Osterwalder et al., in press). In contrast, the expression of *Tbx4* and *Tbx5* is not changed in any of the tissues. This shows that HAND2-mediated regulation of *Tbx2* and *Tbx3* is common between the two clusters, whereas this is not the case for *Tbx4* and *Tbx5*. Indeed, the chromatin architecture profile of the *Tbx3/Tbx5* landscape clearly establishes that these two genes are regulated independently (van Weerd et al., 2014). In summary, the *cis*-regulatory mechanisms controlling *Tbx2* and *Tbx3* expression are shared between cardiac and limb tissues. These mechanisms involve the action of the common *trans*-acting factor HAND2 on tissue-specific CRMs embedded in *cis*-regulatory landscapes of likely similar architecture due to a common evolutionary origin.

8. Conclusions and Outlook

The two major aims of this thesis were (1) to generate a new genetic tool to identify the transcriptional networks controlled by SMAD4 during mouse limb bud development, and (2) to analyze the transcriptional networks controlled by HAND2 during mouse cardiac development. Both projects involved the use of endogenously tagged versions of these two transcription factors.

The mouse line expressing the *Smad4*^{3xFLAG} allele that I generated and characterized is now ready to be used for ChIP-Seq analysis. This new allele will allow us identifying the direct targets of SMAD4 chromatin complexes in developing limb buds and in other tissues such as the embryonic heart. In particular, the dynamics of BMP signaling activity during the different phases of limb bud development and the consequential transcriptional response of its target genes can now be monitored *in vivo* by assessing the temporal occupancy of SMAD4-containing chromatin complexes. This will provide us more insights into the downstream molecular circuitry that controls initiation of limb bud outgrowth, patterning, and chondrogenic differentiation. Moreover, the question of how BMP signaling regulates the expression of *Grem1* can now be investigated at the transcriptional level by the identification of the *Grem1* CRMs that interact with SMAD4 complexes. The ChIP-Seq data that this new mouse line will allow us to generate will also be intersected with ChIP-Seq data from additional transcription factors (e.g. GLI3), in order to understand how *cis*-regulatory landscapes integrate several signaling inputs and how it affects their transcriptional output.

The analysis of the HAND2^{3xFLAG} ChIP-Seq data allowed me to uncover new direct transcriptional targets of HAND2 in the developing heart, such as *Furin*, *Tbx2* and *Tbx3*. In addition, I identified a defect during the endothelial-mesenchymal transition in the atrioventricular canal of *Hand2*-deficient embryos and could establish that HAND2 is a key regulator of cardiac cushion formation by directly controlling the expression of *Snai1*. The functional analysis of the HAND2 target CRMs that I identified in the *cis*-regulatory landscapes of *Snai1*, *Twist1* and *Has2* is still ongoing

and could help us to determine if HAND2 controls EMT in additional developmental/pathological processes. Furthermore, the future use of AVC explant cultures will allow us to study the role of HAND2 during EndMT and cardiac cushion formation at the cellular level, and the conditional deletion of *Hand2* in the endothelium using *Tie2-Cre* will also enable us to analyze further this EndMT phenotype. Finally, a cardiac-specific ChIP-Seq analysis will be an important complement to this study in order to identify additional CRMs that interact with HAND2 specifically during heart development.

The data presented in my thesis constitute **the first identification of the HAND2 direct transcriptional targets during cardiogenesis**. The use of an endogenously epitope-tagged form of HAND2 illustrates the power of such genetic tools to understand the functions of transcription factors during embryonic development.

9. Materials and Methods

9.1. Genetic engineering of plasmids

9.1.1. General cloning procedures

DNA fragments used to construct plasmid vectors were either recovered from restriction enzyme digested vectors or BACs; or produced by PCR using the Expand High Fidelity^{PLUS} PCR System (Roche) with specific primers to introduce the desired restriction enzyme recognition sites at both ends. Following digestion of plasmids/BACs and inserts with compatible restriction enzymes (from Roche or NEB), fragments of interest were recovered from agarose gels and purified using QIAquick Gel Extraction Kit (Qiagen). De-phosphorylation was performed with the rAPid alkaline phosphatase kit (Roche). Ligation of compatible plasmids and inserts was done for 15min-1hr at room temperature (RT) using T4 Ligase (NEB). Then the ligated mixture was dialysed using MFTM nitrocellulose membrane filters (Millipore). Electrocompetent bacteria (XL1-Blue, XL10-Gold or DH5a) were electroporated with ligated vectors in Gene Pulser 0.2cm cuvettes using the Biorad MicroPulserTM. Afterwards, bacteria were plated on LB Agar plates containing the appropriate antibiotic selection. Plasmid DNA was purified by alkaline lysis using the Plasmid Midi Kit (Qiagen) or the NucleoBond® Xtra Midi kit (Machery Nagel) from bacteria grown in liquid cultures. Correct ligation and orientation of the insert was assessed by restriction digest or PCR. Alternatively, colony lifts onto nylon membrane were used and positive clones identified using a DIG-dUTP labeled probe. All construct inserts were sequenced (Microsynth).

To generate linkers, 100nM of each oligonucleotide were mixed in 1x annealing buffer (0.1M NaCl, 10mM Tris-HCl pH 7.4) in 50 μ l and transferred to a water bath at 85-95°C on a floating rack for annealing. Annealed linkers were cooled gradually to RT in H₂O for 3-4hrs. For ligation, serial dilutions of 1 μ l annealed linkers (1:100, 1:1000 or 1:5000) in 0.5x annealing buffer were used. Plasmids were not de-phosphorylated for ligation of linkers, as oligonucleotides do not harbor a 5' phosphate.

9.1.2. Construction of pBSK *Smad4*^{3xFLAG} targeting vector for Homologous Recombination

The targeting vector was designed to introduce a sequence encoding the 3xFLAG epitope tag in frame into the 3' end of *Smad4* coding sequence. Additional modifications included a STOP codon after the 3xFLAG, which was followed by the endogenous *Smad4* 3'UTR and a SV40 polyadenylation site. A *Neomycin* selection cassette flanked by *loxP* sites was also inserted 366bp downstream of *Smad4* locus as part of the 3' homology arm. Firstly, 5' and 3' homology arms were recovered from pBACe3.6 encoding the bMQ420b13 clone, which covers the *Smad4* coding sequence. The 5' arm was subcloned into pBluescript II KS (pBSK, Stratagene) as an *Apal-Apal* 4277bp fragment encoding a part of *Smad4* locus covering the intron 10/11, exon 11, intron 11/12 and exon 12. The 3' arm was inserted into the plasmid pcDNA3 (Invitrogen) as a *BgIII-BgIII* 6045bp fragment, which encodes a part of the 3'UTR and the downstream intergenic region. The fragment containing the 3' end of exon 12, the 3xFLAG-STOP and the 5' part of the 3'UTR was obtained from a previously assembled pXCH-*Smad4*^{3xFLAG} vector (data not shown) as a 295bp *Apal-BgIII* fragment. The floxed *Neo* cassette was recovered from the pLoxpNeo-2 vector (Michos et al., 2004) as a 2026bp *EcoRI-XhoI* fragment that was blunted. To generate the targeting vector, these DNA fragments were assembled in pBSK using a linker containing the following restriction sites: *Asp718-MluI-Apal-BgIII-BamHI-BclI-MluI-SacI*. The *Asp718* and *SacI* restriction sites in pBSK were destroyed by insertion of the linker. The *BamHI* site was used for screening purposes. The sequence of this linker is displayed in the Primers Tables in the chapter 9.7.2. DNA fragments were assembled sequentially as follows: first the *Apal-FLAG-BgIII* fragment, then the *BgIII-3'arm-BgIII* fragment from pCDNA3 (inserted in the compatible *BclI* site on the linker), then the *Apal-5'arm-Apal* insert from pBSK, and finally the blunt *Neo* cassette in reverse orientation into a *BmgBI* site located in the 3'arm. For electroporation, the targeting fragment was released from its pBSK backbone as a 12'344bp *MluI-MluI* fragment (see Fig.29 for a detailed scheme).

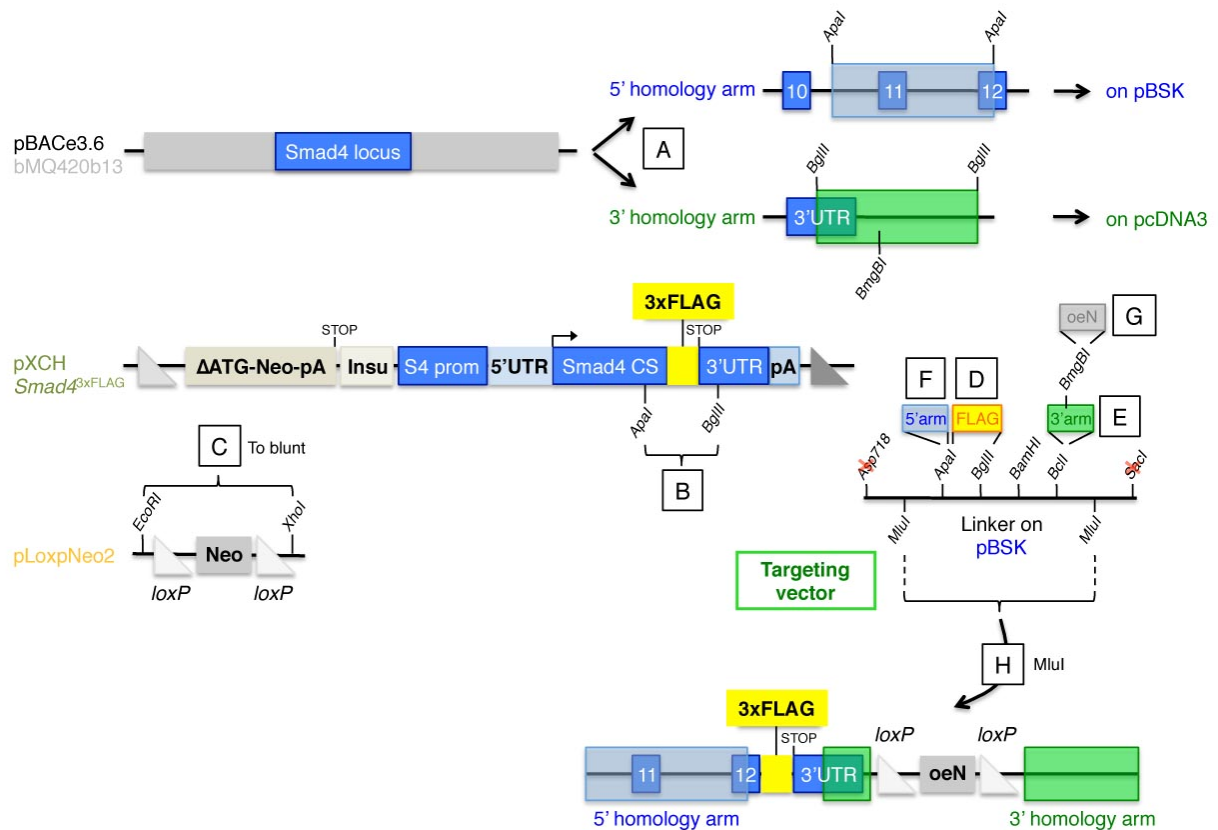


Figure 29. Generation of the pBSK-*Smad4*^{3xFLAG} targeting vector for homologous recombination

(A) 5' and 3' homology arms were recovered from pBACe3.6 clone bMQ420b13. (B) A fragment containing the 3' end of exon 12, the 3xFLAG-STOP and the 5' part of the 3'UTR was obtained from a previously assembled pXCH-*Smad4*^{3xFLAG} vector. (C) The floxed *Neomycin* cassette was recovered from the pLoxpNeo2 vector and blunted. The targeting vector was assembled in pBSK template vector using a linker containing the following restriction sites: Asp718-*MluI*-*ApaI*-*BglIII*-*BamHI*-*BclI*-*MluI*-*SacI*. Fragments were cloned in the following order: (D) 3xFLAG containing fragment, (E) 3' arm, (F) 5' arm and (G) *Neo* cassette in reverse orientation. (H) For electroporation, the targeting fragment was released from pBSK as a *MluI*-*MluI* fragment. See main text for details.

9.2. Cell culture

9.2.1. Embryonic Fibroblasts (EMFIs) culture

EMFIs were used as feeder cells for embryonic stem cells and grown at 37°C in 5% CO₂. EMFI medium consists of DMEM containing 4.5g/l Glucose (Gibco 41966-029), 10% FCS (Gibco 10270-106), 100U Penicillin, 0.1mg/ml Streptomycin (Pen Strep, Gibco 15140-122) and 2mM L-Glutamine (Gibco 25030-024). A frozen vial of EMFIs was thawed at 37°C in a water bath and diluted in a 15ml Falcon tube containing 10ml of EMFI medium. After centrifugation at 1200rpm for 5min, the medium was removed by aspiration and the EMFIs resuspended in 3ml prewarmed medium. Cells

were distributed equally to five 10cm culture dishes (BD Falcon). Medium was changed every two days. When EMFIs became confluent, they were split using 0.05% Trypsin EDTA (Gibco 25300-054) onto another plate (for a maximum of two passages) or treated with Mitomycin C (Sigma M-0503) to stop cell division. For trypsinization, EMFIs were rinsed with 4ml prewarmed trypsin and incubated in 3ml trypsin for 5min at 37°C. Single cells were collected in 7ml EMFI medium and spun for 5min at 1200 rpm. Cell pellets were resuspended in a small volume, diluted and seeded at 1:4-1:6 in 10cm dishes. Mitomycin C at 1mg/ml in DPBS (Gibco 14190-094) (stored at 4°C in the dark for \leq two weeks) was diluted to 10 μ g/ml in EMFI medium for treatment of cells. EMFIs plates were incubated at 37°C with 5% CO₂ for 2h, washed 3x with PBS and transferred back to the incubator in fresh EMFI medium. Growth-arrested EMFIs were kept in culture for maximally one week and their medium was changed every two days.

9.2.2. Embryonic Stem (ES) cell culture

ES cells were grown at 37°C with 7.5% CO₂ on a layer of growth arrested EMFIs. ESC medium consists of Knockout DMEM (Gibco 10829-018) supplemented with 15% Hyclone FBS (Thermo Scientific), 100U-0.1mg/ml Pen Strep, 2mM L-Glutamine, 1mM β -mercaptoethanol (Gibco 31350-010), 1x Non-essential Amino Acids (Gibco 11140-035), 1mM Sodium Pyruvate (Gibco 11360-039) and 10³ units/ml ESGRO LIF (Millipore ESG1106). The medium was changed every day, and the ES cells split every two days using 0.05% Trypsin EDTA. After a brief wash in 4ml trypsin, cells were incubated in 3ml trypsin for 15min at 37°C. A single-cell suspension was obtained by gentle pipetting, and ES cells were separated from EMFIs by incubating the cells at 37°C for 15min. While EMFIs adhere to the surface of the dish, the floating ES cells were carefully recovered and transferred to a 15ml Falcon tube. After 5min centrifugation at 1200rpm, the ES cell pellet was resuspended in ES cells medium and split to 1:3-1:10 on growth arrested EMFIs. Alternatively, ES cells were grown on gelatin instead of EMFIs. A solution of 0.1% gelatin in H₂O (Sigma G-2500) was used to coat culture dishes for 10min at RT. The gelatin solution was removed and the gelatin-coated dishes dried for 10min at RT before use. For freezing, trypsinized ES cell pellets were resuspended in ice-cold filtered freezing medium

(50% ES cells medium 40% FCS, 10% DMSO (Sigma D-8418)). 5-6 precooled Cryovials (NUNC) were filled with 1.5ml of ES cells recovered from a 10cm culture dish. Cryovials were transferred to -80°C in a Styrofoam box and transferred to liquid N₂ the next day.

9.2.3. ES cells electroporation and selection

R1 ES cells (129 background) were thawed 6 days before electroporation and split twice, on day 2 and day 4. On day 6, the ES cells were trypsinized, pooled in 50ml Falcon tubes and centrifuged for 5min at 1200rpm. Then ES cells were resuspended in 3ml medium and counted using a Neubauer chamber. After re-centrifugation, the cells were resuspended in DPBS (Gibco 14190-094) at a final concentration of 1.875×10^7 cells/ml. For electroporation, 35µg of linearized targeting vector (pBSK-*Smad4*^{3xFLAG}) were added to Gene Pulser cuvettes (Biorad 165-2088) and then 0.8ml ES cells suspension was added (1.5×10^7 cells). Water was used as a control instead of DNA in some ES cell samples. Electroporation was done using Biorad Gene Pulser II set at 0.24kV and 475µF capacitance. Cuvettes were immediately transferred on ice and incubated for 20min after electroporation. The contents of the cuvettes were then pooled and transferred to a 50ml Falcon tubes containing prewarmed ES cell medium, and the cuvettes rinsed with ES cell medium to recover all cells. Medium was added to a total volume of 20ml, and the ES cell suspension was gently mixed before plating at 1:5 or 1:10 dilutions on gelatin-coated dishes containing ES cell medium. Non-electroporated ES cells were diluted and plated at similar dilutions as control. Medium was changed after 24h, and antibiotic selection started after 48h. For this, 190µg/ml of G-418 Geneticin (Gibco 10131-019) were used in ES cell medium with medium change everyday during 11-13 days. One dish for each condition/dilution (+DNA, -DNA, no electroporation) was maintained in culture medium without G-418 as selection control. In these dishes, the ES cells grew normally. In the dishes of ES cells under selection that were electroporated without DNA, no ES cell clones were observed. Following selection, ES cell clones were picked and transferred on growth arrested EMFIs in 48 well plates. The ES cell selection medium was changed everyday. Clones were passaged after two days. After two additional days, the clones were trypsinized and half of the cells transferred

to a fresh 48 well plate coated with gelatin, while the other half were plated on growth arrested EMFIs. Upon reaching confluency, the cells grown on gelatin were used to extract DNA for screening, while the plates with cells grown on EMFIs were frozen in freezing medium after two additional days and stored at -80°C . Screening of the correctly targeted clones was done by Southern Blotting (see below). Then, the plates containing positive clones were carefully thawed at 37°C and the medium was changed several times to remove all traces of DMSO. The recovery and growth of each clone was then individually monitored and the medium changed every day for 3-4 days until growing colonies became visible. Clones were passaged to larger wells and finally to 10cm dishes to freeze several vials per expanded ES cell clone.

9.2.4. ES cell clones screening by Southern Blot

Extraction of DNA from confluent ES cells grown on gelatin-coated 48 multiwell plates was achieved as follows: each well was gently washed 3 times with $750\mu\text{l}$ PBS without disturbing the monolayer of cells, and $250\mu\text{l}$ lysis buffer (100mM Tris-HCl pH 8.5, 5mM EDTA pH 8.0, 0.2% SDS, 200mM NaCl, $100\mu\text{g}$ Proteinase K) were then added in each well. The plates were incubated overnight at 55°C in a moist chamber. The next day, $500\mu\text{l}$ of absolute EtOH were added dropwise to the sides of the wells. The plates were incubated overnight at RT, which resulted in appearance of white strands of DNA. The plates were then carefully inverted to remove the EtOH and each well gently washed 3 times with $750\mu\text{l}$ of 70% EtOH. Finally, plates were dried overnight upside-down and then stored at RT. For Southern Blot screening, such precipitated DNAs were digested overnight in a volume of $100\mu\text{l}$ with 30 units of the appropriate restriction enzyme. The next day the reaction was spiked with 10 units and digested for additional 7hrs. Half of the content of the well was then loaded on a 0.7% agarose gel containing 5% EtBr and ran in 1xTBE at 60V for $\sim 24\text{h}$ until appropriate separation was achieved. The agarose gel was then depurinated in 0.25M HCl for 10min; rinsed in H_2O ; washed 2 times 15min in denaturation solution (0.5M NaOH, 1.5M NaCl); rinsed in H_2O ; washed 2 times 15min in neutralization solution (0.5M Tris-HCl pH 7.5, 1.5M NaCl); rinsed in H_2O and finally equilibrated for at least 15min in 20xSSC (3M NaCl, 150mM sodium citrate, pH 7.0). The separated DNA fragments were then transferred onto a positively charged nylon membrane

(Roche) by capillary transfer. The membrane was pre-soaked in H₂O and equilibrated in 2xSSC, and the transfer was done overnight in 20xSSC. Following the transfer, the membrane was soaked in 2xSSC for 5min and dried for 1h at RT on a sheet of Whatman 3MM paper (Sigma). The membrane was subsequently baked for 2hrs at 80°C in a sheet of 3MM paper, and stored at RT. Prehybridization of the membrane was done using a rolling bottle system with side DNA facing inside at 42°C for ≥1hr in prewarmed prehybridization solution (5xSSC, 50% deionized formamide, 0.1% N-lauroylsarcosine, 0.02% SDS, 2% blocking solution). The blocking solution was prepared as 10% (w/v) Blocking Reagent (Roche) in 1x maleic acid buffer (0.1M C₄H₄O₄ 0.15M NaCl, pH 7.5) at 60°C. The prehybridization solution was replaced by prewarmed hybridization solution containing 4μl of DIG-dUTP labeled probes generated using the PCR DIG probe synthesis kit (Roche). Probes detected correct recombination of both the 5' and 3' homology arms. The presence of a single insertion was assessed by detection of the Neomycin cassette (see Fig.11A for the location of the probes). Clones were first screened using the 5' probe, and positive clones further screened with the 3' and Neo probes. The sequences of the primers used to generate these probes are shown in the chapter 9.7.2. Hybridization was done overnight at 42°C in rolling bottles. The next day, the membrane was washed twice for 15min with 2xSSC, 0.1% SDS at RT and twice for 15min with 0.2xSSC, 0.1% SDS at 68°C in rolling bottles. The membrane was then rinsed in maleic acid wash buffer (0.1M C₄H₄O₄ 0.15M NaCl, 0.3% Tween-20, pH 7.5) and blocked with 1% blocking solution in maleic acid buffer for 30min-3hrs. Subsequently, the membrane was incubated in 1% blocking solution in maleic acid buffer containing 1:20'000 anti-digoxigenin-AP antibody (Roche) for 30min at RT. The membrane was then transferred to a plastic tray and washed 3 times for 15min in maleic acid wash buffer, and equilibrated in detection buffer (0.1M Tris-HCl, 0.1M NaCl, pH 9.5) for 2min at RT. The specifically hybridized bands were detected as follows: the membrane was placed on an overhead foil and covered with detection buffer that contained 4μl/ml of CDP Star (Roche) for 5min at RT. The membrane was then exposed for 10min to Kodak BioMax MR films or Amersham Hyperfilm™ ECL (GE Healthcare) and developed using the Fujifilm FPM-100A Desktop Processor. To allow re-hybridization to another probe, the membrane was washed extensively with H₂O in

a plastic tray, transferred back to a rolling bottle and washed 2x for 15min with 0.2M NaOH, 0.1% SDS at 37°C. After rinsing in 2xSSC, the membrane was stored at 4°C in 2xSSC prior re-incubation in pre-hybridization solution.

9.3. Mice husbandry and experiments with embryos

9.3.1. Ethic statement

All experiments conducted with mice were performed with strict respect of the Swiss law, 3R principles and Basel Declaration. They were classified as grade 0, implying minimal suffering.

9.3.2. Mouse strains

The following mouse strains were used for these studies: *GRS1* transgene (Zuniga et al., 2012), *Grem1* null (Michos et al., 2004), *Shh* loss-of-function (St-Jacques et al., 1998), *Gli3* extra-toes-J (Maynard et al., 2002) and *Hand2*^{3xF} (Osterwalder et al., in press) alleles were maintained in an NMRI background; the *Smad4* conditional allele (Yang et al., 2002), *Prx1-Cre* transgene (Logan et al., 2002), *CMV-Cre* transgene (Schwenk et al., 1995) and *Dre* transgene (Anastassiadis et al., 2009) were maintained in a C57BL/6 background; and the *Smad4*^{3xF} and *Hand2* null alleles (Galli et al., 2010) in a mixed background. All mice and embryos were genotyped by PCR for relevant alleles using primers listed in the chapter 9.7.2.

9.3.3. Generation of *LacZ* reporter transgenic embryos

Candidate CRM regions were either amplified by PCR from mouse genomic DNA (*Has2* +2.4kb and *Twist1* +130kb CRMs) or recovered as restriction fragment from a BAC (*Snai1* +58/59kb CRM, BAC clone RP23-193B17) and cloned into a β globin promoter-*LacZ* reporter-SV40 polyA vector. Transgenic embryos were generated by pronuclear injection at the Transgenic Mouse Core Facility (TMCF), Basel (*Has2* CRM) or by Cyagen for the *Twist1* and *Snai1* CRMs. Founder embryos were stained for *LacZ* activity as described below. The transgenic embryos for the candidate CRMs of *Tbx2* and *Tbx3* were generated by M.Shoukry and A.Visel (Genomics Division, Lawrence Berkeley National Laboratory) as described by (Osterwalder et

al., in press). See chapter 9.7.2 for the genomic coordinates of the candidate CRM regions and for the primers used for their amplification by PCR.

9.3.4. Whole-mount *LacZ* staining of mouse embryos

Embryos were isolated in ice-cold PBS and staged by counting their somites numbers, before fixation in 1% formaldehyde, 0.2% glutaraldehyde, 0.02% NP-40, 0.01% sodium deoxycholate in PBS for 20-30min at 4°C. After washing the embryos 3 times in PBS for 5min at RT, they were incubated overnight at 37°C in the dark in 1mg/mL X-Gal in dimethyl formamide, 0.25mM K₃Fe(CN)₆, 0.25mM K₄Fe(CN)₆, 0.01% NP-40, 0.4mM MgCl₂, 1% sodium deoxycholate in PBS. β-galactosidase activity results in expressing cells being colored in blue. The reaction was stopped by washing the embryos 3 times in PBS for 5min at RT.

9.3.5. Whole-mount *in situ* hybridization (WISH)

Embryos isolated in ice-cold PBS were transferred in 2ml Eppendorf tubes and fixed overnight in 4% paraformaldehyde (PFA) in PBS at 4°C. The next day they were washed 2 times in PBS-0.1%Tween-20 (PBT) and subsequently dehydrated in a gradient series of 25%, 50%, 75% MetOH/PBT and finally 2 times 100% MetOH. Such dehydrated embryos were stored at -20°C in MetOH. For the first day of the WISH, embryos were rehydrated in a reverse series of 75%, 50%, 25% MetOH/PBT followed by 2 washes in PBT (5min each). Embryos were then bleached in 6% hydrogen peroxide (H₂O₂)/PBT for 15min at RT and washed 3 times in PBT (5min at RT). This was followed by treatment with 10μg/ml proteinase K in PBT for 5min (E8.5) to 15min (E10.5), depending on the embryonic stage. It is important to not move the embryos during this step. Freshly prepared 2mg/ml glycine in PBT was used to inactivate the proteinase K (5min at RT). Then the embryos were washed twice in PBT for 5min at RT. Embryos were refixed in fresh 0.2% glutaraldehyde, 0.1% Tween-20 in 4%PFA (in PBS) for 20min at RT and washed twice in PBT. Then they were equilibrated in 2ml prewarmed prehybridization buffer (50% deionized formamide, 5xSSC pH 4.5, 2% BCI blocking powder, 0.1% Tween-20, 0.5% CHAPS (Sigma), 50μg/ml yeast RNA (Sigma R8759), 5mM EDTA, 50μg/ml heparin (Sigma H5515)) at 70°C for 1hr or longer. The prehybridization buffer was then replaced by

1ml of fresh prewarmed hybridization buffer containing 10 μ l/ml of digoxigenin-labelled RNA riboprobe (see below) and incubated overnight at 70°C.

On the second day, the probe-containing hybridization buffer was replaced by prewarmed prehybridization buffer, followed by a series of 75%, 50%, 25% prehybridization buffer in 2xSSC (0.3M NaCl, 0.03M sodium citrate pH 4.5). All these washing steps were performed for 5min at 70°C. Subsequently, the embryos were washed twice in 2xSSC, 0.1%CHAPS for 30min at 70°C. To remove unbound DNA probes, embryos were treated with 20 μ g/ml RNase A in 2xSSC,0.1% CHAPS for 45min at 37°C. Embryos were then washed twice with 100mM maleic acid disodium, 150mM NaCl pH 7.5 for 10min at RT and twice for 30min at 70°C. Three washes in freshly prepared TBST (140mM NaCl, 2.7mM KCl, 25mM Tris-HCl pH 7.5, 1% Tween 20) of 5min each at RT were then done. This was followed by blocking in 10% lamb serum/TBST for at least 1hr at RT. This blocking solution was replaced with a solution containing anti-digoxigenin-AP Fab fragments (Roche) conjugated to alkaline phosphatase. These Fab fragments were diluted 1:5000 in 1% lamb serum in TBST. Embryos were incubated overnight at 4°C with gentle rocking.

On the third day, embryos were washed 3 times in TBST for 5min at RT and 5 times in TBST for 1hr-1.5hrs at RT. This was followed by an overnight wash in TBST at 4°C. All washes were performed on a rocking platform. On the fourth day, the embryos were washed 3 times in freshly prepared NTMT (100mM NaCl, 100mM Tris-HCl pH 9.5), 50mM MgCl₂, 1% Tween-20) for 10min at RT and transferred into 1ml BM purple AP substrate (Roche) at RT. Development of the WISH was performed in the dark and monitored every hour until reaching appropriate probe-specific signal intensity. The development was stopped by washing 5 times in PBT (10min) and twice in PBS (5min). Finally, embryos were post-fixed in 4% PFA in PBS and stored at 4°C. WISH pictures were taken using a Leica MZ FLIII stereomicroscope and the Leica Application Suite V3 software.

9.3.6. Preparation of digoxigenin-labelled RNA riboprobe

To prepare riboprobes for *in-situ* hybridization, the plasmid containing the cloned cDNA of interest were linearized and transcribed using the appropriate T3, T7 or SP6 RNA polymerase in combination with the DIG RNA labeling kit (Roche). The resulting

dig-UTP riboprobes were purified by two steps of ethanol precipitation (including linearized polyacrylamide in the first one), resuspended in TE (10mM Tris HCl pH 7.4, 1mM EDTA pH 8.0) and stored at -20°C. Before use, the riboprobes were heated for 5min at 85°C and equilibrated at 70°C in pre-hybridization buffer. Probes in hybridization buffer were stored at -20°C and re-used several times.

9.4. Molecular Biology

9.4.1. Immunocytochemistry

Cultured cells were carefully washed 2 times with prewarmed PBS (Gibco, 37°C) and fixed 30min in 4% PFA in PBS at RT with gentle rocking. After 3 times washes in PBS for 5min each at RT, fixed cells were permeabilized with 0.3% Triton X-100 in PBT and blocked in 10% goat serum, 0.3% Triton X-100, 0.3% BSA (Sigma) in PBT for 1h at RT. Primary antibody incubation was performed overnight at 4°C in 1% goat serum, 0.3% Triton X-100, 0.3% BSA in PBS containing the relevant primary antibody at the appropriate dilution (see Antibodies Tables in chapter 9.7.1). The following day, after three 5min washes in PBT, the cells were incubated with secondary antibodies (see chapter 9.7.1) diluted in 1% goat serum in PBS for 1hr at RT in the dark. Cells were washed 3 times in PBT (5min) and incubated with 1µg/ml Hoechst-33258 (Calbiochem) in PBS for 5min to stain nuclei. After three 5min washes in PBT, the cells were stored in PBS at 4°C in a moist chamber. High-resolution fluorescent images were acquired using the Leica SP5 confocal microscope.

9.4.2. Protein detection by Western Blot (WB)

Proteins were extracted either from cultured cells or from embryonic tissues dissected in ice-cold PBS. Cultured cells were carefully washed with prewarmed PBS (Gibco, 37°C), detached and pelleted by centrifugation (3min, 1000 rpm). The cells were then resuspended in PBS and pelleted again by centrifugation (5min, 5000 rpm). After discarding the supernatant, cell pellets were snap-frozen in liquid N₂ and stored at -80°C before further processing. For embryonic tissues dissected and collected in cold PBS in Eppendorf tubes, snap-freezing in liquid N₂ and -80°C storage was performed after removing as much cold PBS as possible from the

dissected tissues. Cellular lysis of frozen cells or tissues was performed by gently resuspending the frozen sample in an appropriate volume of ice-cold complete RIPA buffer (50mM Tris-HCl pH 7.5, 1% NP-40, 0.25% Na-deoxycholate, 150mM NaCl, 1mM EDTA, 0.4mM Pefabloc, 1x Complete Mini protease inhibitor cocktail (Roche), 1mM activated Na_3VO_4 , 1mM NaF) followed by a 30min incubation on ice. Lysed cells were then centrifuged 15min at 13'000 rpm (4°C) to remove cellular debris, and the supernatant was transferred to a new ice cold Eppendorf tube. The protein concentration was determined using the BiCinchoninic acid Assay (BC Assay, Pierce) and specific amounts of BSA as standard controls. Protein extracts were then aliquoted and stored at -80°C.

For SDS-PAGE, protein extracts were transferred on ice and mixed with 5x protein gel sample buffer (GSB: 0.5M Tris-HCl pH 6.8, 2% SDS, 20% glycerol, 0.0025% bromophenol blue, with freshly added 5% β -mercapoethanol) to a final concentration of 20% GSB. Protein extracts were denatured for 5min at 98°C and cooled down on ice for 3min before being loaded on a 10% SDS polyacrylamide gel. Proteins were separated by electrophoresis in running buffer (25mM Tris base, 192mM Glycine, 0.1% (w/v) SDS) for 30min at 80V and 2-3hrs at 100-120V. Following SDS-PAGE, the SDS acrylamide gel was equilibrated in transfer buffer (25mM Tris base, 192mM Glycine, 20% (v/v) MeOH) for 15min. The proteins were then transferred from the gel to a PVDV (polyvinylidene fluoride) Immobilon-P transfer membrane (Millipore). Prior to transfer, the membrane was activated for 1min in MeOH and equilibrated in transfer buffer for 15min. Wet transfer was then conducted at 4°C at 100V for 2hrs. Following transfer, the membrane was rinsed in TBST (0.01M Tris-HCl pH 8, 0.05% Tween-20, 0.15M NaCl) and then blocked in 5% (w/v) milk powder in TBST for 1h at RT. The membrane was then incubated with primary antibody diluted in 5% milk powder in TBST (see chapter 9.7.1 for dilutions) overnight at 4°C. The following day, the membrane was rinsed in TBST and washed 3 times for 15min in TBST. Then it was incubated with the appropriate HRP conjugated secondary antibody (see chapter 9.7.1) diluted in 5% milk powder in TBST for 1hr at RT. After three 15min washes in TBST, ElectroChemiluminescence (ECL) detection of the antibody-labeled proteins was performed for 5min at RT using a 1:1 mixture of the SuperSignal™ West Pico Chemiluminescent Substrate kit (Thermo Scientific) and the Visualizer™ Western

Blot Detection Kit (Millipore). The membrane was then exposed to Kodak BioMax MR film or Amersham Hyperfilm™ ECL (GE Healthcare) and developed in the Fujifilm FPM-100A Desktop Processor. To detect another protein, the membrane was stripped in Restore™ Western Blot Stripping Buffer (Thermo Scientific) for 5min at RT and extensively washed in TBST. After 30min of blocking, the membrane was incubated with primary antibody for 1hr at RT (for anti-actin antibody) or overnight at 4°C. Subsequent steps were performed as described above.

9.4.3. Immunoprecipitation (IP)

Protein extracts from cultured cells or from dissected embryonic tissues were prepared as described above. For each IP reaction, 150µg of total protein extract were used together with 15µl (45µg) of Dynabeads® Protein G (Life Technologies) and 1µg of anti-FLAG M2 antibody (Sigma) in a total volume of 150µl. First, for each IP reaction 150µg of total protein extract (in complete RIPA buffer with 3x Complete Mini protease inhibitor cocktail, see above) were transferred to 0.2ml PCR microtubes (Thermo Scientific) and topped up to 150µl with modified RIPA buffer. 1µg of anti-FLAG M2 antibody was added and the mixture was incubated for 3hrs at 4°C on a rotating wheel. During this incubation time, appropriate amounts of Dynabeads were transferred to a 1.5ml Eppendorf tube containing 1ml of cold RIPA buffer (without proteases and phosphatases inhibitors: 50mM Tris-HCl pH 7.5, 1% NP-40, 0.25% Na-deoxycholate, 150mM NaCl, 1mM EDTA). Dynabeads were washed 3 times with 1ml cold RIPA buffer using a magnetic rack, then resuspended in an appropriate volume of cold RIPA buffer and equally divided into new Eppendorf tubes according to the number of samples and kept on ice. After the 3hrs of incubation, the mixture was used to resuspend the Dynabeads, transferred back in the microtubes and incubated overnight at 4°C on a rotating wheel. The following day, the Dynabeads solution was transferred back to a 1.5ml Eppendorf tube and put on a magnetic rack. The supernatant (=unbound protein fraction) was transferred to a new Eppendorf tube, and the beads were washed 5 times with 0.8ml of ice-cold complete RIPA buffer. Dynabeads were resuspended in 100µl of ice-cold complete RIPA buffer, transferred to a new tube to avoid co-elution of proteins bound to the tube, and finally resuspended in 20µl cold complete RIPA buffer. To elute the

immunoprecipitated proteins from the Dynabeads, 8 μ l of GSB containing 5% β -mercapoethanol (see above) were added to each sample. Samples were heated at 98°C for 5min and incubated 3min on ice. The magnetic rack was then used to separate the Dynabeads from the denatured immunoprecipitated protein complexes. The eluted proteins were transferred into a new tube and stored at -20°C if not directly loaded on a SDS-PAGE gel. In addition to the IPP samples, input control (20 μ g of total protein extract) and unbound protein fraction control (20 μ l of the 1 μ l/ μ g total protein extract recovered following the immunoprecipitation) were also analyzed on SDS-PAGE gels. Immunoblotting using primary biotinylated anti-FLAG M2 antibody and Streptavidin-HRP secondary antibody was performed as described above for regular Western-Blotting.

9.4.4. Chromatin Immunoprecipitation (ChIP)

This ChIP protocol for embryonic tissues is adapted from (Visel et al., 2009a) for tissue collection and crosslinked chromatin preparation, and on (Kim et al., 2007) and (Vokes et al., 2008) for subsequent steps, and has been modified and optimized by Marco Osterwalder and Javier Lopez-Rios. Embryos were collected in ice-cold PBS, and dissected tissues (forelimbs/hindlimbs or hearts) from somites-matched embryos of the same genotype were pooled and collected in ice-cold PBS into 2ml Eppendorf tubes. Dissected tissues were washed 2 times with ice-cold DPBS containing Ca²⁺ and Mg²⁺ (Gibco) and transferred to a 2ml glass douncer (Tissue Grind Tube Size 2ml, Kimble-Chase) on ice. Tissue disaggregation was achieved by applying 25 strokes with pestle A (Tissue Grind Pestle LC 2ml, Kimble-Chase) followed by 25 strokes with pestle B (Tissue Grind Pestle SC 2ml, Kimble-Chase). The solution containing nuclei was transferred back to a 2ml Eppendorf tube, and the douncer was rinsed with 0.3ml cold DPBS w/Ca²⁺Mg²⁺ that was also added to the sample. After centrifugation at 3000 rpm for 3min (4°C), the supernatant was discarded and nuclei were resuspended in 1.5ml RT DPBS w/Ca²⁺Mg²⁺ containing 150 μ l 11x crosslinking buffer (0.1M NaCl, 1mM EDTA, 0.5mM EGTA, 50mM HEPES pH 8.0; add 11% formaldehyde just before use). The mixture was incubated for 5min at RT with gentle horizontal shaking. To stop crosslinking, 75 μ l of 2.5M Glycine were added, followed by another incubation of 5min at RT with horizontal shaking. The samples were then

centrifuged at 3000 rpm for 3min (4°C), supernatants removed, and pellets resuspended in 1.5ml ice-cold DPBS w/Ca²⁺Mg²⁺. After re-centrifugation at 3000 rpm for 3min (4°C), the supernatants were discarded and the nuclear pellets snap-frozen in liquid N₂ and stored at -80°C. In order to use sufficient material for the ChIP, crosslinked nuclear pellets from different embryo collections can be pooled in one single sample. Generally, 3 samples containing crosslinked nuclei from similar amounts of dissected embryos were processed for ChIP in parallel in one experiment.

Before performing the ChIP, antibodies coupled to magnetic beads were prepared. For one ChIP sample, 20µl of Dynabeads® Protein G were used and transferred to a 2ml Eppendorf tube containing 1ml freshly prepared ice-cold BSA (5mg/ml in DPBS w/Ca²⁺Mg²⁺). Beads were washed 6 times with 1ml cold BSA/PBS using a magnetic rack, resuspended in a volume corresponding to 2.5x the original volume of beads (50µl per sample) and transferred to a 2ml screw cap microtube (Starstedt). 2µg of anti-FLAG M2 antibody were used for each ChIP sample and incubated overnight on a rotating wheel at 4°C.

The following day, the Dynabeads-antibodies complexes were transferred back to a 2ml Eppendorf tube and washed 6 times with 1ml cold BSA/PBS before being resuspended in the original volume of suspended beads (20µl per sample) and kept on ice. In the meantime, snap-frozen crosslinked nuclear pellets were thawed on ice and resuspended in 6ml cold Lysis buffer (50mM Hepes pH 7.5, 140mM NaCl, 1mM EDTA pH 8.0, 10% Glycerol, 0.5% NP-40, 0.25% Triton X-100, 1x Complete Mini protease inhibitor cocktail (Roche)). If necessary, several crosslinked nuclear pellets were pooled and resuspended in 6ml of ice-cold Lysis buffer (see comment above). Lysates were incubated for 10min at 4°C with gentle rocking, followed by 10min centrifugation at 2500 rpm (4°C). Supernatants were discarded and the pellets resuspended in 2ml of RT Protein Extraction Buffer (0.2M NaCl, 1mM EDTA pH 8.0, 0.5mM EGTA pH 8.0, 10mM Tris-HCl pH 8.0, 1x Complete Mini protease inhibitor cocktail) to which 3ml of Protein Extraction Buffer were added. The samples were incubated for 10min at RT on a rocking platform and the nuclei were pelleted by centrifuging 10min at 2500 rpm at 4°C. After discarding the supernatant, the nuclei were resuspended in 1ml ice-cold Chromatin Extraction Buffer (1mM EDTA pH 8.0,

0.5mM EGTA pH 8.0, 10mM Tris-HCl pH 8.0, 0.1% Na-Deoxycholate, 0.5% N-lauroylsarcosine, 3x Complete Mini protease inhibitor cocktail). Samples were then transferred to Covaris TC 12x12 tubes and sonicated to shear the crosslinked chromatin using the S220 Covaris Ultra-sonicator. Each sample was sonicated for 15min using the 5% duty cycle, 140 watts Peak Incident Power and 200 Cycles per Burst. The sheared chromatin was then transferred back to 1.5ml Eppendorf tubes, and insoluble debris were pelleted by centrifuging for 10min at 13'000 rpm (4°C). The supernatants were moved to new 2ml screw cap microtubes, and the volume was topped up to 1.060ml with Chromatin Extraction Buffer. At this stage, 2x 30 μ l aliquots were taken and separated to new Eppendorf tubes: one for input control and the other to assess the quality of the sonicated chromatin on an agarose gel. Both aliquots were kept overnight at 4°C to be treated identical to the ChIP sample. Then, 300 μ l of ChIP cocktail Mix (130 μ l Triton X-100 10%, 3 μ l Na-Deoxycholate 10%, 26 μ l Complete protease inhibitor solution (from a 50x tablet dissolved in 1ml mQ H₂O), 131 μ l TE buffer (100mM Tris HCl pH 7.4, 10mM EDTA pH 8.0) and 10 μ l mQ H₂O) were added to each 1ml ChIP sample to adjust to RIPA buffer conditions (see below). For each ChIP sample, 20 μ l of the freshly washed Dynabead-antibody complexes were added and incubated overnight on a rotating wheel (4°C).

The next day, the dynabeads were transferred to 1.5ml Eppendorf tubes containing 1ml of freshly prepared cold RIPA buffer (50mM Hepes pH 8.0, 1mM EDTA pH 8.0, 1% NP-40, 0.7% Na-Deoxycholate, 0.5M LiCl, 1x Complete Mini protease inhibitor cocktail), and subsequently washed 6 times with 1ml cold RIPA buffer on a magnetic rack. The beads were rinsed once with 1ml TE-plus (100mM Tris HCl pH 8.0, 10mM EDTA pH 8.0, 50mM NaCl, 1x Complete Mini protease inhibitor cocktail) and centrifuged for 3min at 1000 rpm (4°C). All residual liquid was removed from the beads using the magnetic rack, and the beads were resuspended in 100 μ l freshly prepared Elution Buffer (1mM EDTA, 1% SDS, 10mM Tris-HCl pH 8.0). Elution of the crosslinked protein-DNA complexes from the Dynabead-antibody complexes was performed at 65°C for 15min on a heat block shaking at 1300 rpm. Beads were then centrifuged for 1min at 13'000 rpm and retained in the tube using a magnetic rack, while 100 μ l of supernatant containing the protein-DNA complexes were transferred to a PCR microtube. In parallel, the 30 μ l input aliquot and the 30 μ l chromatin aliquot

(kept on ice) were also transferred to PCR microtubes containing 120 μ l of Elution Buffer. Reverse crosslinking was performed for all three samples by incubating them overnight at 65°C (\geq 12hrs).

The next day, samples were transferred back to 1.5ml Eppendorf tubes and treated with RNase A (from bovine pancreas, Sigma) in TE (100mM Tris HCl pH 8.0, 10mM EDTA pH 8.0) at a final concentration of 0.2 μ g/ μ l. After 1hr incubation at 37°C, Proteinase K was added to a final concentration of 0.2 μ g/ μ l and proteins were digested for 2hrs at 55°C. Finally, DNA was purified from all three samples using the QIAquick Gel Extraction Kit (Qiagen). Elution was achieved in two steps using 30 μ l Buffer EB each, and the eluted ChIP and input samples were aliquoted and stored at -20°C before use for qPCR. To assess the quality of the sonication, half of the purified chromatin control samples were loaded on an agarose gel to estimate the range of DNA fragments sizes (between 150bp to ~1.5kb with an maximal intensity at ~300bp, data not shown).

9.4.5. Extraction of RNA and cDNA synthesis

RNA was extracted either from cultured ES cells or from embryonic tissues dissected in cold PBS. For cultured ES cells, trypsin was used to detach the cells. These cells were then preplated as described in chapter 9.2.2 to separate them from EMFIs. ES cells were recovered in a 15ml Falcon tube, centrifuged for 5min at 1200 rpm and resuspended in 1.5ml ES cell medium. After re-centrifugation (3min at 5000 rpm), the medium was discarded and the cell pellet covered with 100 μ l RNeasy Lysis Buffer (Qiagen) and left overnight at 4°C before storage at -20°C.

For embryonic samples, the dissected tissues were transferred in ice-cold PBS in 1.5ml Eppendorf tubes. After PBS removal, samples were covered with 100 μ l of RNeasy Lysis Buffer and left overnight at 4°C before storage at -20°C. Total RNA was extracted using the RNeasy Micro Kit (Qiagen). The RNA concentration was assessed using a Nanodrop 2000 C (Thermo Scientific), and RNA samples were stored at -20°C.

To synthesize cDNA, 10pg-5 μ g RNA were mixed with the following reagents: 1 μ l oligo (dT)₁₂₋₁₈ (500ng); 1 μ l dNTP mix (10mM each of dATP, dGTP, dCTP and dTTP at neutral pH); sterile water to a total volume of 13 μ l. The reaction mixture was heated

at 65°C for 5min and incubated on ice for at least 1min. After brief centrifugation, the following reagents were added: 4µl 5x First Strand Buffer, 1µl 0.1M DTT, 1µl RNaseOUT™ 40U/µl, 1µl Superscript™ III RT 200U/µl (all from Invitrogen). The mixture was incubated 1hr at 50°C, and cDNA synthesis was terminated by heating for 15min at 70°C. cDNAs were stored at -20°C before amplification by PCR (to generate templates for *in situ* hybridization probes or for cloning purposes) or by qPCR (to quantify target genes expression).

9.4.6. Real-time quantitative PCR (RT-qPCR)

Real-time quantitative PCR was done using the Bio-Rad CFX96 Real-Time PCR System in combination with the iQ SYBR Green Supermix (Bio-Rad). qPCR was used to determine transgene copy numbers from genomic DNA (Tesson et al., 2002), to quantify gene expression from embryonic tissues or cultured cells cDNA, or to compute levels of enrichment of genomic regions following ChIP. Each qPCR reaction was done in a 20µl reaction containing 0.3µM of each primer diluted in EB buffer (10mM Tris-HCl pH 8.5), 50% of SYBR green, and DNA template diluted in MiliQ H₂O. All primers sequences are shown in chapter 9.7.2.

- For the *GRS1* transgene copy number determination, 20ng of genomic DNA was used as template. Triplicates were analyzed, using primers amplifying the *Dopamine Beta-Hydroxylase (DBH)* genomic region as normalizers. Transgene relative quantification cycle (Cq) values were normalized to *DBH* Cq values. Results are reported as mean ± standard deviation (SD) of normalized fold expression levels ($2^{-\Delta\Delta Cq}$) of transgenic individuals (n= 9 or more), relative to non-transgenic control littermates (n=3) encoding the two endogenous copies of the *GRS1* region.
- For gene expression quantification, 0.05µl of cDNA were used as template and analyzed in triplicate. Primers detecting the ribosomal protein L19 (*RPL19*) transcripts were used as internal normalizer. Relative Cq values of target transcripts were normalized to the Cq values of *RPL19*, and normalized fold expression levels ($2^{-\Delta\Delta Cq}$) are shown as mean ± SD relative to the mean value (set at 100%) of a control sample.

- For computation of enrichment levels of a region of interest (ROI) following ChIP, 1 μ l of immunoprecipitated genomic DNA or input DNA were used as template and analyzed in duplicate. Primers recognizing an unlinked amplicon in the *β -actin* locus (Galli et al., 2010) were used as normalizing control region (NCR). Fold-change enrichments between input samples and ChIP samples were calculated as follows:

$$(CqROI \text{ ChIP}) - (CqROI \text{ input}) = \Delta CqROI$$

$$(CqNCR \text{ ChIP}) - (CqNCR \text{ input}) = \Delta CqNCR$$

$$\text{Fold enrichment} = 2^{-(\Delta CqROI - \Delta CqNCR)}$$

All results are displayed as mean \pm SD and are based on analyzing 3 independent samples (90-100 hearts each for HAND2^{3xFLAG} ChIP). To avoid artifact bias of fold enrichment, a Cq of 32 was defined as minimum background value threshold.

9.5. Histology

9.5.1. Paraffin embedding procedure

For paraffin embedding, embryos were dissected in ice-cold PBS and fixed overnight in 4% PFA in PBS (4°C). After three 5min washes in PBS, the embryos were dehydrated into EtOH using a graded series (25% EtOH/PBS, 50% EtOH/PBS, 75% EtOH/H₂O, 100% EtOH). Each EtOH incubation was done for 10min to 1hr depending on the size of the embryos, in ice-cold EtOH solution (4°C). Embryos were then transferred to RT and left to warm for 30min. This was followed by two incubations in EtOH for 10min each at RT. Following dehydration, embryos were cleared in Xylene for twice 25min at RT and transferred to a 50:50 (v/v) Xylene/paraffin mixture for 30min at 60°C. Then they were incubated with freshly melted paraffin 5-10 times for at least 30min each at 60°C. Then the samples were embedded in fresh paraffin wax (60°C) using a stereomicroscope for proper positioning. Paraffin blocks were then transferred to a 4°C cooling plate overnight and then stored at RT. The Microm HM 355 microtome was used to cut sections of 7 μ m (for immunohistochemistry and other histological stainings) or 14 μ m (for section *in-situ* hybridization) that were mounted on Superfrost Plus slides (Thermo Scientific) and stored at RT until use.

9.5.2. Preparation of frozen sections

For some section *in-situ* hybridization and some immunohistochemistry stainings, samples were embedded in Optimum Cutting Temperature (O.C.T) compound (Tissue-Tek) for cryoprotection as follows. Embryos were dissected in ice-cold PBS and fixed for 2hrs at 4°C in 4% PFA in PBS and washes 3 times in PBS (5min). Embryos were then transferred to 10% sucrose/PBS (w/v), 20% sucrose/PBS and 30% sucrose/PBS (1hr each) with gentle shaking at 4°C. Then the embryos were transferred into embedding molds, the 30% sucrose solution carefully removed with a plastic pipette and replaced by 50:50 (v/v) O.C.T/30% sucrose. Embryos were positioned using a stereomicroscope. Freezing was achieved by dipping and holding the bottom of the embedding mold into 2-Methylbutane cooled on dry ice in a Styrofoam box until the embedding medium was completely frozen. Samples were stored at -80°C and sectioned (10 μ m) using a Microm HM 500 OM Cryostat (-20°C). Frozen sections were mounted on Superfrost Plus slides and stored at -80°C before use.

9.5.3. Immunohistochemistry

IHC on paraffin sections

Sections of embryonic tissues were deparaffinized with twice 10min in Xylene followed by twice 10min in 100% EtOH. Sections were rehydrated in a reverse EtOH/H₂O series (70% EtOH/H₂O, 50% EtOH/H₂O, 30% EtOH/H₂O, 5' each), rinsed in H₂O and washed twice 5min in PBS. Antigen retrieval was achieved by autoclaving the sections in 10mM Sodium Citrate (pH 6.0) with 0.05% Tween-20 for 5min at 120°C. The sections were then cooled to RT (30min), washed twice in PBS (5min) and 4 times in PBT (PBS with 0.1% Tween-20, 5min). Sections were blocked in 10% goat serum in PBT for 1hr at RT and incubated overnight in a moist chamber in 1% goat serum in PBT containing primary antibody at the proper dilution (4°C) (see chapter 9.7.1). The following day, sections were washed three times 10min in PBT and incubated in 1% goat serum/PBT containing the appropriate secondary antibody for 1hr at RT (in the dark). The sections were then washed three times for 10min in PBT and twice in PBS (5min). Incubation in 1 μ g/ml Hoechst-33258/PBS (Calbiochem) for 5min counterstained nuclei. Sections were washed 5 times in PBS

(5min) and a drop of mounting medium Mowiol 4-88 (Calbiochem) was added. They were covered with a coverslip and the slides were dried overnight at RT in the dark. For immunohistochemistry and for TUNEL assays (see below), the Leica SP5 confocal microscope was used to acquire high-resolution fluorescent images. Slides were then stored at 4°C. For double staining with two mouse primary antibodies, the anti-FLAG M2 antibody was directly labeled using the APEX™ Alexa Fluor® 488 Antibody Labeling Kit (Life Technologies). Immunostaining was performed as follows: 1) overnight incubation with mouse primary antibody (anti-NFATC1 or anti-TWIST1) 2) 1hr incubation with goat anti-mouse Alexa 594 3) overnight incubation with Alexa 488-labelled anti-FLAG M2 4) 1hr incubation with rabbit anti-Alexa488 and 5) 1hr incubation with goat anti-rabbit Alexa 488.

IHC on frozen sections

Sections were washed with PBS 3 times (5min), with 0.2% Triton X-100/PBS for 20min, and again three times with PBS (5min). Sections were then blocked in 1% BSA in PBT for 1hr at RT, followed by incubation with primary antibodies (see chapter 9.7.1) in 1% BSA/PBS overnight (4°C). The second day, the sections were washed 3 times for 10min in PBS and once in PBT (5min). Incubation with the appropriate secondary antibodies diluted in 1% BSA/PBS was done for 1hr at RT in the dark. Sections were washed 3 times for 10min in PBS and once in PBT (5min), counterstained with 1µg/ml Hoechst-33258/PBS (5min), followed by final washes in PBS (≥ 5x 5min). Mowiol 4-88 was used for mounting before addition of a coverslip. Before analysis, slides were dried overnight at RT in the dark and stored at 4°C.

9.5.4. TUNEL assay

Cell death in embryonic tissues was detected on paraffin section using the *In situ* Cell Death Detection Kit (Fluorescein, Roche). Following deparaffinization, rehydration and two PBS washes (5min), sections were washed with Tris-HCl 10mM pH 7.5 (5min) and permeabilized in 20µg/ml Proteinase K in Tris-HCl 10mM pH 7.5 (20min at RT). After two PBS washes (5min), sections were incubated with the TUNEL reaction mixture for 1hr at 37°C in a moist chamber in the dark. Then, the sections were washed 3 times in PBS (5min), and the nuclei counterstained with 1µg/ml

Hoechst-33258/PBS (5min). Finally, after two more PBS washes (5min), sections were mounted in Mowiol 4-88 and stored as described.

9.5.5. Hematoxylin/Eosin staining

Sections of paraffin embedded samples were deparaffinized and rehydrated as described above, and then washed extensively in tap water for 5min. Histological staining was done by incubating the sections 3min in filtered Hematoxylin solution (Sigma) and washing in tap water for 3min. Then the sections were incubated for 1-3min in filtered 0.15% Eosin/EtOH. Sections were then incubated in 95% EtOH (5min), followed by two incubations in 100% EtOH (5min) and three incubations in Xylene (5min). For mounting, the sections were covered with a drop of Eukitt (Fluka) and a coverslip was added. Slides were stored as described. Pictures were acquired using a Zeiss Axioskop 2 Plus microscope.

9.5.6. Alcian Blue staining

To stain proteoglycans, sections of paraffin embedded samples were deparaffinized, rehydrated and washed in tap water as described above. Sections were washed for 3min in 3% acetic acid in H₂O (v/v), pH 2.5. Staining was performed for minimum 1hr in 1% Alcian Blue (Sigma) in 3% acetic acid solution (w/v), pH 2.5. After extensive washes in tap water, the sections were incubated in Fastred (Sigma) for 5min at RT to counterstain nuclei. Slides were mounted with Mowiol 4-88 and stored as describe. Protocol adapted from (Rivera-Feliciano and Tabin, 2006).

9.5.7. *In situ* hybridization on sections

For all steps prior to probe hybridization, 0.1% DEPC (v/v) solutions were used. Paraffin sections of embryos were deparaffinized twice in Xylene (5min) and twice in 100% EtOH (5min). Sections were rehydrated as follows: 75% EtOH/H₂O-DEPC, 50% EtOH/H₂O-DEPC, 25% EtOH/H₂O-DEPC, and twice in PBS-DEPC (5min each). Following rehydration, sections were fixed in 4% PFA/PBS-DEPC (10min), rinsed in PBT-DEPC and washed twice in PBT-DEPC (5min). Sections were then incubated in 1μg/ml Proteinase K in PBS-DEPC (10min) and washed twice in PBT-DEPC (5min). For *in situ* hybridization on frozen sections, the protocol was started after the

Proteinase K incubation. Post-fixation was done in 4% PFA/PBS-DEPC (5min), followed by a rinse in PBT-DEPC and two washes in PBT-DEPC (5min). Sections were blocked with 0.25% (v/v) Acetic Anhydride in 0.1M Triethanolamine (pH 8) for 15min, rinsed in PBT-DEPC and washed three times in PBT-DEPC (5min). Sections were then incubated in 65°C prewarmed pre-hybridization buffer (10mM Tris-HCl pH 7.5, 600mM NaCl, 1mM EDTA, 0.25% SDS, 10% Dextran Sulfate, 200µg/ml yeast tRNA (Gibco), 50% Formamide, 1x Denhardt's (0.02% (w/v) Ficoll 400, 0.02% (w/v) Polyvinylpyrrolidone, 0.02% BSA in H₂O-DEPC)), covered with a coverslip and incubated at 65°C for 1hr. For hybridization, sections were incubated in prewarmed hybridization buffer containing 1% (v/v) DIG-labelled RNA probe, covered with a coverslip and incubated at 65°C overnight in a moist chamber. The second day, coverslips were removed from the slides by rinsing them in 5x SSC (20x SSC: 3M NaCl, 0.3M Tri-sodium citrate dehydrate, pH 4.5) prewarmed to 65°C followed by two washes in 5x SSC (5min each) at 65°C. Sections were then incubated in 1xSSC/50% formamide at 65°C (30min) and washed in TNE (50mM Tris-HCl pH 7.5, 2.5M NaCl, 5mM EDTA) at 37°C for 10min. Next, the sections were incubated in 20µg/ml RNase A in TNE at 37°C (30min) and washed in TNE at 37°C (10min). Further washes included 2xSSC at 65°C (20min), two 0.2xSSC washes at 65°C (20min) and two MABT (200mM Maleic Acid, 300mM NaCl, pH 7.5, 0.1% Tween-20 (v/v)) at RT (5min). Sections were blocked in 20% lamb serum in MABT for 1hr at RT and incubated overnight in 2% lamb serum in MABT containing 1:2000 anti-DIG-AP (Roche) in a moist chamber (4°C). The third day, the sections were rinsed and then washed three times in MABT at RT (5min each). Then, the sections were equilibrated in NTMT (100mM NaCl, 100mM Tris-HCl pH 9.5, 50mM MgCl₂, 0.1% Tween-20) at RT for 10min, and the signal developed using BM purple AP substrate (Roche). Development of the *in-situ* hybridization was performed in the dark at RT for 1hr to 3 days depending on the probe, with regular monitoring using a stereomicroscope. The reaction was stopped by rinsing the sections with NTMT and washing them at least three times in PBS (5min each). The sections were post-fixed in 0.1% glutaraldehyde, 4% PFA/PBS for 20min, washed twice in PBS (5min) and rinsed in H₂O. Sections were mounted in Mowiol 4-88 and stored as described.

9.6. Genomics online resources

All genomic sequences for cloning purposes or sequence alignments were retrieved from ENSEMBL (Flicek et al., 2014) or UCSC browser (Karolchik et al., 2014), Alignments were performed using the ECR browser (Ovcharenko et al., 2004) or the ClustalW2 program (Larkin et al., 2007). Other useful online resources include the VISTA enhancer browser (Visel et al., 2007) and the Mouse Genome Informatics website (<http://www.informatics.jax.org>).

9.7. Tables

9.7.1. Antibodies tables

Primary Antibodies					
Antigen		Host	Distributor	Use	Dilutions
FLAG (M2)	monoclonal	mouse	Sigma, F1804	WB, IP, ICC, IHC, ChIP	1:2000, 1 μ g Ab/150 μ g prot, 1:4000, 1:1000, 2 μ g/sample
FLAG BioM2-Biotin	monoclonal	mouse	Sigma, F9291	WB	1:2000
ACTIN	polyclonal	rabbit	Sigma, A2066	WB	1:10'000
HA	polyclonal	rabbit	Sigma, H6908	WB, IP, ICC	1:2000, 1:2000, 1 μ g Ab/150 μ g prot
V5	monoclonal	mouse	Invitrogen, R960-25	WB, IP, ICC	1:10'000, 1:2000, 1 μ g Ab/150 μ g prot
SMAD4	monoclonal	rabbit	Abcam, ab-40759	WB	1:1000
GLI3	polyclonal	rabbit	Genentech, 2676	WB, ChIP	1:1000, 2 μ g/sample
TBX2	polyclonal	mouse	Milipore, 07-318	IHC	1:2000
TBX3	polyclonal	goat	Santa Cruz, sc-31656	IHC	1:300
ISL1 (Mab15)	monoclonal	mouse	DSHB, 40.2D6	IHC	1:100
SOX9	polyclonal	rabbit	Milipore, ab-5535	ICC, IHC	1:5000, 1:10'000
TWIST1	monoclonal	mouse	Santa Cruz, sc-81417	IHC	1:500
VE CADHERIN	polyclonal	rabbit	Abcam, ab-33168	IHC	1:1000
VIMENTIN	monoclonal	mouse	Sigma, V2258	IHC	1:500
NFATC1	monoclonal	mouse	Santa Cruz, sc-7294	IHC	1:500
COLLAGEN 2	monoclonal	mouse	ThermoSci, MS-235-P1	ICC	1:100

Secondary Antibodies			
Antigen	Distributor	Use	Dilutions
goat α mouse IgG, HRP conjugate	Millipore, 12-349	WB	1:20'000
goat α rabbit IgG, HRP conjugate	Millipore, 12-348	WB	1:20'000
Streptavidin-HRP	Jackson, 016-030-084	WB	1:20'000
goat α mouse IgG (H+L) Alexa Fluor®488 F(ab') ₂	Invitrogen, A-11017	iCC, IHC	1:1'000
goat α mouse IgG (H+L) Alexa Fluor®594 F(ab') ₂	Invitrogen, A-11020	IHC	1:1'000
goat α rabbit IgG (H+L) Alexa Fluor®488 F(ab') ₂	Invitrogen, A-11070	IHC	1:1'000
goat α rabbit IgG (H+L) Alexa Fluor®594	Invitrogen, A11037	ICC, IHC	1:1'000
rabbit α goat IgG (H+L) Alexa Fluor®594	Invitrogen, A-11080	IHC	1:1'000
rabbit α Alexa Fluor®488 IgG	Invitrogen, A-11094	IHC	1:1'000
Anti-Digoxigenin-AP, Fab fragments from sheep	Roche, 11 093 274 910	WISH, SB	1:5000, 1:20'000

9.7.2. Primers tables

Genotyping primers for mice and embryos				
Locus	Forward primer	Reverse primer	Size	Allele
<i>GRS1</i> transgene	5'-GCCTCTTCGCTATTACGCCAGCT-3'	5'-AATTAACCCCTCACTAAAGGG-3'	300bp	Tg
<i>Shh</i>	5'-ATGCTGGCTCGCCTGGCTGTGGAA-3'	5'-GAAGAGATCAAGGCAAGCTCTGGC-3'	500bp	Wt
	5'-GGACACCATTCTATGCAGGG-3'	5'-GAAGAGATCAAGGCAAGCTCTGGC-3'	150bp	Δ
<i>Gli3</i>	5'-GGGTGAACAGCATCAAATGGAG-3'	5'-ATAGCCATGTGGTGGTGCCCATG-3'	500bp	Wt
	5'-TACCCAGCAGGAGACTCAGATTAG-3'	5'-AAACCCGTGGCTCAGAGCAAG-3'	600bp	Xtj
<i>Smad4</i>	5'-GGGCAGCGTAGCATATAAGAC-3'	5'-CCTGACCCAAACGTCACCTTC-3'	390bp + 450bp	Wt + Floxed
	5'-AAGAGCCACAGGTCAAGCAG-3'	5'-CCTGACCCAAACGTCACCTTC-3'	500bp	Δ
<i>Cre</i>	5'-GCCTGCATTACCGGTCGATGCAACGA-3'	5'-GTGGCAGATGGCGCGGCAACACCATT-3'	750bp	Tg
<i>Grem1</i>	5'-ATGAATCGCACCGCATACACTG-3'	5'-TCCAAGTCGATGGATATGCAACG-3'	750bp	Wt
	5'-GGCACATGGCTGAATATCGACGG-3'	5'-AAGCGCCTCCCCTACCCGGTA-3'	550bp	Δ
<i>Hand2</i>	5'-TGCTCTCCAGTCTGTCTCTCT-3'	5'-CCGATCTGGACAGCTAGCAA-3'	330bp + 530bp	Wt + Floxed
	5'-AGAAGAGGACCTCGGCAATT-3'	5'-CTGTGGTCTTGTTCGCGATT-3'	496bp	Δ
	5'-TGGAGGGCCACGGAAGGCGAGATG-3'	5'-GACAGGGCCATACTGTAGTCG-3'	209bp + 284bp	Wt + 3xFlag

Smad4 Homologous Recombination targeting - cloning primers				
Linker	Sequence	Restriction sites		
Linker Up	5'-ACGCGTGGGCCCTTAATAGATCTGGATCCTGATCAACGCGTAGCT-3'	MluI, ApaI, spacer, BgIII, BamHI, BclI, MluI, XbaI		
Linker Down	3'-CATGTGCGCACCCGGGAATTATCTAGACCTAGGACTAGTTGCGCA-5'	XbaI, MluI, ApaI, spacer, BgIII, BamHI, BclI, MluI		
Smad4 Homologous Recombination targeting - Southern Blot probes primers				
Probe	Forward primer	Reverse primer	Size	
5' probe	5'-ATGGAGGACCGTTGTAGAGTTC-3'	5'-TTGCTCCACAGGAGAACTAACA-3'	580bp	
3' probe	5'-AATGAGTCTTGCTGACCTTGC-3'	5'-GCCAGGATGTTGGATGAGTT-3'	515bp	
Neo probe	5'-AATCGGGAGCGGCATACCGTAAAGC-3'	5'-GACGTTGTCACTGAAGCGGGAAGGG-3'	508bp	
Smad4 Homologous Recombination targeting - mice genotyping primers				
Locus	Forward primer	Reverse primer	Size	Allele
<i>Smad4</i> <i>3xF-HR</i>	5'-ACAGCCTCCACACTTGTGCT-3'	5'-TGTCTGCTAAGAGCAAGGCA-3'	396bp + 501bp	Wt + 3xF HR
<i>Smad4</i> <i>3xF-HR</i> <i>Neo</i>	5'-CAGCCAGTTGTACCATGCAG-3'	5'-GCCTGAAGAACGAGATCAGC-3'	432bp	Neo ^r
<i>Smad4</i> <i>3xF-HR</i> <i>ΔNeo</i>	5'-AGGACTTCCCATGGACACTG-3'	5'-AGCACTGCCTGGTCAGATGA-3'	576bp + 610bp	Wt + 3xF ΔNeo

Candidates CRMs for transgenic reporters - cloning primers				
CRM	Coordinates (mm9)	Forward / Reverse primers	Size	Restr. site
<i>Has2</i> +2.4kb Tg	chr15:56,523,368-56,525,546	5'-GAGAAAGCTTGCAAGAAAAACACGATCTCA-3'	2218 bp	HindIII
		5'-CACAAAGCTTACGTTATACAGACGCGTTTG-3'		
<i>Tbx2</i> -32kb Tg	chr11:85,612,756-85,614,268	5'-ATGGCCACCTTTTCTTCTGC-3'	1513 bp	
		5'-AAGCCTTCCTAAGCCACTGT-3'		
<i>Tbx3</i> -58kb Tg	chr5:120,060,938-120,063,445	5'-GGTCCTGGAGACTGAGACA-3'	2508 bp	
		5'-GAATAGCAGAGCACAG-3'		
<i>Tbx3</i> -18kb Tg	chr5:120,100,229-120,102,755	5'-GGGGTGAAGTGTGGAGAGA-3'	2527 bp	
		5'-TCAGCTAGAGGTCACATGCA-3'		
<i>Twist1</i> +130kb Tg	chr12:34,771,890-34,772,660	5'-GAGAAAGCTTGAATGAACGTTTTGTAACTGC-3'	753bp	HindIII
		5'-CACAAAGCTTGAGCCACTGTGTTCTGTTGG-3'		
<i>Snai1</i> +58/59kb Tg	chr2:167,419,933-167,424,557	Released from BAC RP23-193B17 as HpaI/MfeI fragment	4625 bp	
Candidates CRMs for transgenic reporters - genotyping primers				
Locus	Forward primer	Reverse primer	Size	
<i>Has2</i> +2.4kb Tg	5'-TAGGAAGGTAAGGACAGTTGTGG-3'	5'-AATGTGAGCGAGTAACAACCCG-3'	916bp	

ChIP qPCR primers				
ChIP Amplicon	Forward primer	Reverse primer	Size	Rank in Top2000
<i>Id1</i> BRE -1.1kb	5'-AGAATGCTCCAGCCCAGTTT-3'	5'-TGACGTCACCCATTCATAAAA-3'	93bp	-
<i>Id1</i> -3kb (ctrl)	5'-TTCTTCTCTGGCTGCCAGTG-3'	5'-AACTGAGCCTTGCATCATGC-3'	140bp	-
<i>Actb</i> +1.8kb ctrl region	5'-GATCTGAGACATGCAAGGAGTG-3'	5'-GGCCTTGGAGTGTGTATTGAG-3'	115bp	-
<i>Tbx3</i> -58kb	5'-TGTGGTCTGTCACTGTGCACTT-3'	5'-CCAGATTGCCATCACAGACAG-3'	131bp	216
<i>Tbx3</i> -59kb (ctrl)	5'-AACTCGGGTACTACTCGCACA-3'	5'-ACAGAAAATAAGGCTGGCCC-3'	134bp	-
<i>Tbx3</i> -18kb	5'-TCCCTCAGGAGCTCTGTCTG-3'	5'-AGGATTCCAGGGAGGTCTGT-3'	118bp	944
<i>Tbx2</i> -204kb	5'-CTCCACTGATGGCTGAAAT-3'	5'-CCCAGGATGTGAACTGTCAGT-3'	138bp	164
<i>Tbx2</i> -199kb (ctrl)	5'-CTGTGTGCTACTCCGCATCA-3'	5'-CACTTCCACTTGGGTGGTG-3'	112bp	-
<i>Tbx2</i> -112kb	5'-AGGGGAAGGAGGTTAGATGG-3'	5'-GCCTGGGAAGAAAGGCTTC-3'	90bp	595
<i>Tbx2</i> -32kb	5'-GGCTCGCACCTCTCTATTA-3'	5'-TTGATCAGCCGTCAGAACT-3'	102bp	59
<i>Furin</i> -43kb	5'-TGGCTGATGACTGCCCTTAT-3'	5'-AAAGCTGTGGAGGCAAGTGT-3'	80bp	11
<i>Furin</i> -50kb (ctrl)	5'-CTACATGAGGGTTGGGGAGA-3'	5'-TGCTCTGCTGATGGCTAAAA-3'	100bp	-
<i>Myocd</i> +60kb	5'-TGGCTATTGTCCCTCCAGAC-3'	5'-GGATGATGTCAGGGCTTCTC-3'	73bp	1588
<i>Myocd</i> -31kb (ctrl)	5'-AGCATCCCTGAGAAAAGTCA-3'	5'-AGGGGCACCTAAAGATTTCC-3'	110bp	-
<i>Twist1</i> +10kb	5'-CCTCTGGTTGACACAAAGCA-3'	5'-TGGGGACTAGGACACCAGAC-3'	124bp	-
<i>Twist1</i> +130kb	5'-ACACATTGACCTGGCTGTGA-3'	5'-AGGCAGACCTTCATTGAGGA-3'	92bp	1157
<i>Twist1</i> +135kb (ctrl)	5'-AGGCTTGTGACGACCTTGT-3'	5'-AAGTGGGCTTTAGCATGTGG-3'	85bp	-
<i>Snai1</i> +45kb	5'-ACTCTCCGGGGACAGCTAATA-3'	5'-CCCCTGCTTTGATCAGCTT-3'	120bp	-
<i>Snai1</i> +58kb	5'-GTCAGAAAGGCAGCTTGGAG-3'	5'-GCTTCTCTGTCCCCTCCTT-3'	85bp	1397
<i>Snai1</i> +59kb	5'-TCTGCTGGCCTCCAGATGT-3'	5'-TTGATAAAGCCCCTCTGTGC-3'	73bp	1397
<i>Snai1</i> +64kb (ctrl)	5'-CCACCTGTCTGCCCTTAGTC-3'	5'-GGGCCCTTTCTTGAACCTACC-3'	71bp	-
<i>Sox9</i> +232kb	5'-GAGGCTTGTCTGGCACATTA-3'	5'-TCAGTTGGGAGTCCAGCAG-3'	84bp	1204
<i>Sox9</i> +234kb (ctrl)	5'-GGAGGTCCTTTAGGAAGGA-3'	5'-CTCCATCCTGTTCCCATTA-3'	112bp	-
<i>Has2</i> -4.3kb (ctrl)	5'-TTGTTCACTTGGGCATTTCA-3'	5'-CCATGAAGAGCACTTTCTGCT-3'	126bp	-
<i>Has2</i> -0.9kb	5'-TTGCTCTTGACAGCCTTTT-3'	5'-CAGTCTTGGCGTCATTGAAA-3'	70bp	1201
<i>Has2</i> +2.4kb	5'-AGAGGGAAATCCCAGGCTAA-3'	5'-CCAGCCAGAGTCCAGAGTTT-3'	139bp	1183

qPCR primers			
Locus	Forward primer	Reverse primer	Size
<i>Smad4</i> exon 6-7 / 7-8	5'-CCATCATAACAGCACTACCACC -3'	5'-GCCAGTAATGTCCAGGATGG-3'	128bp
<i>Smad4</i> exon 8-9	5'-TTTCCAATCATCCTGCTCCTGA-3'	5'-AACGTCTCTCCTACCTGAACGTCC-3'	76bp
<i>Smad4</i> exon12-3'UTR	5'-GTGCTGGATTGAGATTCACC-3'	5'-CGTGGTGTGAGATCTCAGTCTA-3'	108bp
<i>Smad4</i> 3xFlag-3'UTR	5'-AAAGATCACGACATCGACTA-3'	5'-GTGTGAGATCCAATTGTGAG-3'	70bp
<i>Rpl19</i>	5'-ACCCTGGCCCGACGG-3'	5'-TACCCTTTCCTCTCCCTATGCC-3'	53bp
<i>GRS1</i>	5'-CGCTGAATTTACAGCATCACTT-3'	5'-AGCGGCACAGTTTGTATGTC-3'	64bp
<i>Dbh</i>	5'-AGGACATCAGCCACTCTGCT-3'	5'-AATTGTCTTGGTGGCCCTC-3'	117bp

10. Acknowledgments

First and foremost, I would like to sincerely thank Prof. Rolf Zeller who gave me the fantastic opportunity to do my PhD in his laboratory. I thank him for the great mentoring and guidance over the years; his advice and ideas were always precious and useful and helped me to improve my scientific thinking and writing.

I am deeply thankful to Javier Lopez-Rios for his invaluable supervision and teaching. It was always a pleasure to work with him and an enriching source of new knowledge, science-related or not. His constant scientific enthusiasm and excitement was one of the best motivation drivers I had during these years.

I am truly indebted to Marco Osterwalder for his great help, support and patience with my numerous questions. Without the massive amount of amazing work he did in the laboratory, a vast majority of what is in this thesis regarding ChIP-Seq experiments and analysis would not have been possible.

It was also a pleasure to collaborate with Aimée Zuniga, and I would like to thank her for everything I learnt while working together in the cell culture room and on the *GRS1* project.

I would also like to express my sincere gratitude to Prof. Verdon Taylor and Prof. Markus Affolter for being members of my thesis committee.

Many thanks go to the team of the Transgenic Mouse Core Facility of the University of Basel, especially Daniela Klewe-Nebenius and Liliane Todesco, for the generation of chimeric mice and some of the transgenic founder embryos. I would also like to thank Malak Shoukry and Axel Visel from Lawrence Berkeley National Laboratory, who generated some other transgenic embryos for us. I am also very grateful to Angelika Offinger and Emilia Stanislawka Terszowska for excellent care of our mice.

I am thankful to Isabelle Ginez for her indispensable technical help with sectioning, to Pascal Lorentz for teaching and helping me with the confocal microscope, to Susie Boudebaba who always supplied us with clean and autoclaved glassware and

solutions, and to Chris Müller for all her administrative help. And special thanks go to Debora Schmitz, who was the first one to get me interested in cardiac development.

Furthermore, I would like to warmly thank Emanuele Pignatti, Sumit Jaiswal, Erkan Ünal, Dario Speziale and Ashleigh Nugent for their valuable friendship and all the great moments we shared in the laboratory, but mostly for all the ones we spent outside. In addition, I am especially grateful to Julie Leclercq, who will successfully continue some of the projects I worked on and whom I had a lot of pleasure teaching. The nice atmosphere and constructive discussions we had in the laboratory would not have been possible without all the present and past members of the group, which I thank very much: Gretel Nusspaumer, Nathalie Riesen, Jorge Dorado, Virginie Tissières, Paola Valdivieso, Rosaria Costa, Sandro Nuciforo, Patric Schlenker, Simone Probst, Catherine Vaillant, Amandine Duchesne, Alexandre Gonçalves, Alexandra Schauerte, Jean-Denis Benazet, Adrian Hermann and Dimitri Robay.

Many thanks go to the members of the DBM PhD Club committee, especially the two other founder members Carlos Mayer and Fabrizio Botindari. It was as much fun to organize all these events together, than to participate to them. I am also thankful to my friends Valérie Murset, César Metzger, Vincent Croset and Joanes Grandjean, who also survived their PhD after we graduated from the University of Lausanne, and with whom it was always a pleasure to discuss and share good times.

Last but not least, my deepest and warmest gratitude goes to my parents, to my sister and to Jérémy for their incredible support and patience during these years.

11. Bibliography

- Aanhaanen, W., Boukens, B., Sizarov, A., Wakker, V., de Gier-de Vries, C., van Ginneken, A., Moorman, A., Coronel, R. and Christoffels, V. (2011) 'Defective Tbx2-dependent patterning of the atrioventricular canal myocardium causes accessory pathway formation in mice', *J Clin Invest* 121(2): 534-544.
- Aanhaanen, W. T., Brons, J. F., Dominguez, J. N., Rana, M. S., Norden, J., Airik, R., Wakker, V., de Gier-de Vries, C., Brown, N. A., Kispert, A. et al. (2009) 'The Tbx2+ primary myocardium of the atrioventricular canal forms the atrioventricular node and the base of the left ventricle', *Circ Res* 104(11): 1267-74.
- Agulnik, S. I., Garvey, N., Hancock, S., Ruvinsky, I., Chapman, D. L., Agulnik, I., Bollag, R., Papaioannou, V. and Silver, L. M. (1996) 'Evolution of mouse T-box genes by tandem duplication and cluster dispersion', *Genetics* 144(1): 249-54.
- Ai, D., Fu, X., Wang, J., Lu, M. F., Chen, L., Baldini, A., Klein, W. H. and Martin, J. F. (2007) 'Canonical Wnt signaling functions in second heart field to promote right ventricular growth', *Proc Natl Acad Sci U S A* 104(22): 9319-24.
- Aiyer, A. R., Honarpour, N., Herz, J. and Srivastava, D. (2005) 'Loss of Apaf-1 leads to partial rescue of the HAND2-null phenotype', *Dev Biol* 278(1): 155-62.
- Akiyama, H., Chaboissier, M. C., Behringer, R. R., Rowitch, D. H., Schedl, A., Epstein, J. A. and de Crombrughe, B. (2004) 'Essential role of Sox9 in the pathway that controls formation of cardiac valves and septa', *Proc Natl Acad Sci U S A* 101(17): 6502-7.
- Anastassiadis, K., Fu, J., Patsch, C., Hu, S., Weidlich, S., Duerschke, K., Buchholz, F., Edenhofer, F. and Stewart, A. F. (2009) 'Dre recombinase, like Cre, is a highly efficient site-specific recombinase in E. coli, mammalian cells and mice', *Dis Model Mech* 2(9-10): 508-15.
- Angelo, S., Lohr, J., Lee, K., Ticho, B., Breitbart, R., Hill, S., Yost, H. and Srivastava, D. (2000) 'Conservation of sequence and expression of Xenopus and zebrafish dHAND during cardiac, branchial arch and lateral mesoderm development', *Mech Dev* 95(1-2): 231-7.
- Armstrong, E. J. and Bischoff, J. (2004) 'Heart valve development: endothelial cell signaling and differentiation', *Circ Res* 95(5): 459-70.
- Ashburner, M., Ball, C. A., Blake, J. A., Botstein, D., Butler, H., Cherry, J. M., Davis, A. P., Dolinski, K., Dwight, S. S., Eppig, J. T. et al. (2000) 'Gene ontology: tool for the unification of biology. The Gene Ontology Consortium', *Nat Genet* 25(1): 25-9.
- Attanasio, C., Nord, A. S., Zhu, Y., Blow, M. J., Li, Z., Liberton, D. K., Morrison, H., Plajzer-Frick, I., Holt, A., Hosseini, R. et al. (2013) 'Fine tuning of craniofacial morphology by distant-acting enhancers', *Science (New York, N.Y.)* 342(6157): 1241006.
- Attanasio, C., Nord, A. S., Zhu, Y., Blow, M. J., Biddie, S. C., Mendenhall, E. M., Dixon, J., Wright, C., Hosseini, R., Akiyama, J. A. et al. (2014) 'Tissue-specific SMARCA4 binding at active and repressed regulatory elements during embryogenesis', *Genome research* 24(6): 920-9.
- Azhar, M., Brown, K., Gard, C., Chen, H., Rajan, S., Elliott, D. A., Stevens, M. V., Camenisch, T. D., Conway, S. J. and Doetschman, T. (2011) 'Transforming growth factor Beta2 is required for valve remodeling during heart development', *Dev Dyn* 240(9): 2127-41.

- Bakker, M. L., Boukens, B. J., Mommersteeg, M. T., Brons, J. F., Wakker, V., Moorman, A. F. and Christoffels, V. M. (2008) 'Transcription factor Tbx3 is required for the specification of the atrioventricular conduction system', *Circ Res* 102(11): 1340-9.
- Barnes, R. M. and Firulli, A. B. (2009) 'A twist of insight - the role of Twist-family bHLH factors in development', *Int J Dev Biol* 53(7): 909-24.
- Barnes, R. M., Firulli, B. A., VanDusen, N. J., Morikawa, Y., Conway, S. J., Cserjesi, P., Vincentz, J. W. and Firulli, A. B. (2011) 'Hand2 loss-of-function in Hand1-expressing cells reveals distinct roles in epicardial and coronary vessel development', *Circ Res* 108(8): 940-9.
- Barolo, S. (2012) 'Shadow enhancers: frequently asked questions about distributed cis-regulatory information and enhancer redundancy', *Bioessays* 34(2): 135-41.
- Barrallo-Gimeno, A. and Nieto, M. A. (2005) 'The Snail genes as inducers of cell movement and survival: implications in development and cancer', *Development* 132(14): 3151-61.
- Barron, F., Woods, C., Kuhn, K., Bishop, J., Howard, M. J. and Clouthier, D. E. (2011) 'Downregulation of Dlx5 and Dlx6 expression by Hand2 is essential for initiation of tongue morphogenesis', *Development* 138(11): 2249-59.
- Battle, E., Sancho, E., Francí, C., Domínguez, D., Monfar, M., Baulida, J. and García De Herreros, A. (2000) 'The transcription factor Snail is a repressor of E-cadherin gene expression in epithelial tumour cells', *Nat Cell Biol* 2(2): 84-89.
- Bell, A., West, A. and Felsenfeld, G. (1999) 'The Protein CTCF Is Required for the Enhancer Blocking Activity of Vertebrate Insulators', *Cell* 98(3): 387-96.
- Benazet, J. D., Bischofberger, M., Tiecke, E., Goncalves, A., Martin, J. F., Zuniga, A., Naef, F. and Zeller, R. (2009) 'A self-regulatory system of interlinked signaling feedback loops controls mouse limb patterning', *Science* 323(5917): 1050-3.
- Benazet, J. D., Pignatti, E., Nugent, A., Unal, E., Laurent, F. and Zeller, R. (2012) 'Smad4 is required to induce digit ray primordia and to initiate the aggregation and differentiation of chondrogenic progenitors in mouse limb buds', *Development* 139(22): 4250-60.
- Benazet, J. D. and Zeller, R. (2013) 'Dual requirement of ectodermal Smad4 during AER formation and termination of feedback signaling in mouse limb buds', *Genesis (New York, N.Y.: 2000)* 51(9): 660-666.
- Bernanke, D. H. and Markwald, R. R. (1979) 'Effects of hyaluronic acid on cardiac cushion tissue cells in collagen matrix cultures', *Tex Rep Biol Med* 39: 271-85.
- Bertrand, N., Roux, M., Ryckebusch, L., Niederreither, K., Dolle, P., Moon, A., Capecchi, M. and Zaffran, S. (2011) 'Hox genes define distinct progenitor sub-domains within the second heart field', *Dev Biol* 353(2): 266-74.
- Berul, C. I., Aronovitz, M. J., Wang, P. J. and Mendelsohn, M. E. (1996) 'In vivo cardiac electrophysiology studies in the mouse', *Circulation* 94(10): 2641-8.
- Biben, C. and Harvey, R. P. (1997) 'Homeodomain factor Nkx2-5 controls left/right asymmetric expression of bHLH gene eHand during murine heart development', *Genes & development* 11(11): 1357-1369.
- Blow, M. J., McCulley, D. J., Li, Z., Zhang, T., Akiyama, J. A., Holt, A., Plajzer-Frick, I., Shoukry, M., Wright, C., Chen, F. et al. (2010) 'ChIP-Seq identification of weakly conserved heart enhancers', *Nat Genet* 42(9): 806-10.

- Bondue, A. and Blanpain, C. (2010) 'Mesp1: a key regulator of cardiovascular lineage commitment', *Circ Res* 107(12): 1414-27.
- Bonn, S., Zinzen, R. P., Girardot, C., Gustafson, E. H., Perez-Gonzalez, A., Delhomme, N., Ghavi-Helm, Y., Wilczynski, B., Riddell, A. and Furlong, E. E. (2012) 'Tissue-specific analysis of chromatin state identifies temporal signatures of enhancer activity during embryonic development', *Nat Genet* 44(2): 148-56.
- Bourdeau, A., Dumont, D. and Letarte, M. (1999) 'A murine model of hereditary hemorrhagic telangiectasia', *J Clin Invest* 104(10): 1343-51.
- Brickner, M., Hillis, L. and Lange, R. (2000) 'Congenital heart disease in adults. First of two parts', *N Engl J Med* 342(4): 256-63.
- Brown, C., Feiner, L., Lu, M., Li, J., Ma, X., Webber, A., Jia, L., Raper, J. and Epstein, J. (2001) 'PlexinA2 and semaphorin signaling during cardiac neural crest development', *Development* 128(16): 3071-3080.
- Bruneau, B. G., Logan, M., Davis, N., Levi, T., Tabin, C. J., Seidman, J. G. and Seidman, C. E. (1999) 'Chamber-specific cardiac expression of Tbx5 and heart defects in Holt-Oram syndrome', *Dev Biol* 211(1): 100-108.
- Bruneau, B. G., Bao, Z. Z., Tanaka, M., Schott, J. J., Izumo, S., Cepko, C. L., Seidman, J. G. and Seidman, C. E. (2000) 'Cardiac expression of the ventricle-specific homeobox gene *Ir4* is modulated by *Nkx2-5* and *dHand*', *Dev Biol* 217(2): 266-77.
- Bruneau, B. G., Nemer, G., Schmitt, J. P., Charron, F., Robitaille, L., Caron, S., Conner, D. A., Gessler, M., Nemer, M., Seidman, C. E. et al. (2001) 'A murine model of Holt-Oram syndrome defines roles of the T-box transcription factor *Tbx5* in cardiogenesis and disease', *Cell* 106(6): 709-721.
- Bruneau, B. G. (2008) 'The developmental genetics of congenital heart disease', *Nature* 451(7181): 943-8.
- Buckingham, M., Meilhac, S. and Zaffran, S. (2005) 'Building the mammalian heart from two sources of myocardial cells', *Nat Rev Genet* 6(11): 826-35.
- Bulger, M. and Groudine, M. (2011) 'Functional and mechanistic diversity of distal transcription enhancers', *Cell* 144(3): 327-39.
- Cai, C., Liang, X., Shi, Y., Chu, P., Pfaff, S., Chen, J. and Evans, S. (2003) 'Isl1 identifies a cardiac progenitor population that proliferates prior to differentiation and contributes a majority of cells to the heart', *Developmental Cell* 5(6): 877-889.
- Cai, C. L., Zhou, W., Yang, L., Bu, L., Qyang, Y., Zhang, X., Li, X., Rosenfeld, M. G., Chen, J. and Evans, S. (2005) 'T-box genes coordinate regional rates of proliferation and regional specification during cardiogenesis', *Development* 132(10): 2475-87.
- Cai, C. L., Martin, J. C., Sun, Y., Cui, L., Wang, L., Ouyang, K., Yang, L., Bu, L., Liang, X., Zhang, X. et al. (2008) 'A myocardial lineage derives from *Tbx18* epicardial cells', *Nature* 454(7200): 104-8.
- Cai, X., Nomura-Kitabayashi, A., Cai, W., Yan, J., Christoffels, V. M. and Cai, C. L. (2011) 'Myocardial *Tbx20* regulates early atrioventricular canal formation and endocardial epithelial-mesenchymal transition via *Bmp2*', *Dev Biol* 360(2): 381-90.
- Cai, X., Zhang, W., Hu, J., Zhang, L., Sultana, N., Wu, B., Cai, W., Zhou, B. and Cai, C. L. (2013) '*Tbx20* acts upstream of Wnt signaling to regulate endocardial cushion formation and valve remodeling during mouse cardiogenesis', *Development* 140(15): 3176-87.

- Calo, E. and Wysocka, J. (2013) 'Modification of enhancer chromatin: what, how, and why?', *Mol Cell* 49(5): 825-37.
- Camenisch, T., Spicer, A., Brehm-Gibson, T., Biesterfeldt, J., Augustine, M., Calabro, A. J., Kubalak, S., Klewer, S. and McDonald, J. (2000) 'Disruption of hyaluronan synthase-2 abrogates normal cardiac morphogenesis and hyaluronan-mediated transformation of epithelium to mesenchyme', *J Clin Invest* 106(3): 349-360.
- Camenisch, T. D., Schroeder, J. A., Bradley, J., Klewer, S. E. and McDonald, J. A. (2002) 'Heart-valve mesenchyme formation is dependent on hyaluronan-augmented activation of ErbB2-ErbB3 receptors', *Nat Med* 8(8): 850-5.
- Cano, A., Pérez-Moreno, M., Rodrigo, I., Locascio, A., Blanco, M., del Barrio, M., Portillo, F. and Nieto, M. (2000) 'The transcription factor Snail controls epithelial-mesenchymal transitions by repressing E-cadherin expression', *Nat Cell Biol* 2(2): 76-83.
- Capdevila, J., Tsukui, T., Rodriguez Esteban, C., Zappavigna, V. and Izpisua Belmonte, J. C. (1999) 'Control of vertebrate limb outgrowth by the proximal factor Meis2 and distal antagonism of BMPs by Gremlin', *Mol Cell* 4(5): 839-49.
- Carver, E. A., Jiang, R., Lan, Y., Oram, K. F. and Gridley, T. (2001) 'The mouse snail gene encodes a key regulator of the epithelial-mesenchymal transition', *Mol Cell Biol* 21(23): 8184-8.
- Chakraborty, S., Wirrig, E. E., Hinton, R. B., Merrill, W. H., Spicer, D. B. and Yutzey, K. E. (2010) 'Twist1 promotes heart valve cell proliferation and extracellular matrix gene expression during development in vivo and is expressed in human diseased aortic valves', *Dev Biol* 347(1): 167-79.
- Chang, C. P., Neilson, J. R., Bayle, J. H., Gestwicki, J. E., Kuo, A., Stankunas, K., Graef, I. A. and Crabtree, G. R. (2004) 'A field of myocardial-endocardial NFAT signaling underlies heart valve morphogenesis', *Cell* 118(5): 649-63.
- Charité, J., McFadden, D. G. and Olson, E. N. (2000) 'The bHLH transcription factor dHAND controls *Sonic hedgehog* expression and establishment of the zone of polarizing activity during limb development', *Development* 127: 2461-2470.
- Charité, J., McFadden, D. G., Merlo, G., Levi, G., Clouthier, D. E., Yanagisawa, M., Richardson, J. A. and Olson, E. N. (2001) 'Role of Dlx6 in regulation of an endothelin-1-dependent, dHAND branchial arch enhancer', *Genes & development* 15(22): 3039-49.
- Chen, H., Shi, S., Acosta, L., Li, W., Lu, J., Bao, S., Chen, Z., Yang, Z., Schneider, M. D., Chien, K. R. et al. (2004) 'BMP10 is essential for maintaining cardiac growth during murine cardiogenesis', *Development* 131(9): 2219-31.
- Chen, Y. H., Ishii, M., Sucov, H. M. and Maxson, R. E., Jr. (2008) 'Msx1 and Msx2 are required for endothelial-mesenchymal transformation of the atrioventricular cushions and patterning of the atrioventricular myocardium', *BMC Dev Biol* 8: 75.
- Christoffels, V. M., Hoogaars, W. M., Tessari, A., Clout, D. E., Moorman, A. F. and Campione, M. (2004) 'T-box transcription factor Tbx2 represses differentiation and formation of the cardiac chambers', *Dev Dyn* 229(4): 763-70.
- Christoffels, V. M. and Moorman, A. F. (2009) 'Development of the cardiac conduction system: why are some regions of the heart more arrhythmogenic than others?', *Circ Arrhythm Electrophysiol* 2(2): 195-207.
- Christoffels, V. M., Smits, G. J., Kispert, A. and Moorman, A. F. (2010) 'Development of the pacemaker tissues of the heart', *Circ Res* 106(2): 240-54.

- Chu, G. C., Dunn, N. R., Anderson, D. C., Oxburgh, L. and Robertson, E. J. (2004) 'Differential requirements for Smad4 in TGFbeta-dependent patterning of the early mouse embryo', *Development* 131(15): 3501-12.
- Cohen, E., Wang, Z., Lepore, J., Lu, M., Taketo, M., Epstein, D. and Morrisey, E. (2007) 'Wnt/beta-catenin signaling promotes expansion of Isl-1-positive cardiac progenitor cells through regulation of FGF signaling', *J Clin Invest* 117(7): 1794-804.
- Cohen, E. D., Miller, M. F., Wang, Z., Moon, R. T. and Morrisey, E. E. (2012) 'Wnt5a and Wnt11 are essential for second heart field progenitor development', *Development* 139(11): 1931-40.
- Combs, M. D. and Yutzey, K. E. (2009) 'Heart valve development: regulatory networks in development and disease', *Circ Res* 105(5): 408-21.
- Constam, D. and Robertson, E. (2000) 'Tissue-specific requirements for the proprotein convertase furin/SPC1 during embryonic turning and heart looping', *Development* 127(2): 245-254.
- Conway, S. J., Firulli, B. and Firulli, A. B. (2010) 'A bHLH code for cardiac morphogenesis', *Pediatr Cardiol* 31(3): 318-24.
- Cordero, D. R., Brugmann, S., Chu, Y., Bajpai, R., Jame, M. and Helms, J. A. (2011) 'Cranial neural crest cells on the move: their roles in craniofacial development', *Am J Med Genet A* 155A(2): 270-9.
- Cotney, J., Leng, J., Oh, S., DeMare, L. E., Reilly, S. K., Gerstein, M. B. and Noonan, J. P. (2012) 'Chromatin state signatures associated with tissue-specific gene expression and enhancer activity in the embryonic limb', *Genome research* 22(6): 1069-80.
- Crawford, G. E., Holt, I. E., Whittle, J., Webb, B. D., Tai, D., Davis, S., Margulies, E. H., Chen, Y., Bernat, J. A., Ginsburg, D. et al. (2006) 'Genome-wide mapping of DNase hypersensitive sites using massively parallel signature sequencing (MPSS)', *Genome research* 16(1): 123-31.
- Creyghton, M. P., Cheng, A. W., Welstead, G. G., Kooistra, T., Carey, B. W., Steine, E. J., Hanna, J., Lodato, M. A., Frampton, G. M., Sharp, P. A. et al. (2010) 'Histone H3K27ac separates active from poised enhancers and predicts developmental state', *Proc Natl Acad Sci U S A* 107(50): 21931-6.
- Cui, Y., Jean, F., Thomas, G. and Christian, J. (1998) 'BMP-4 is proteolytically activated by furin and/or PC6 during vertebrate embryonic development', *EMBO J* 17(16): 4735-4743.
- Cui, Y., Hackenmiller, R., Berg, L., Jean, F., Nakayama, T., Thomas, G. and Christian, J. L. (2001) 'The activity and signaling range of mature BMP-4 is regulated by sequential cleavage at two sites within the prodomain of the precursor', *Genes & development* 15(21): 2797-802.
- Dai, Y. S. and Cserjesi, P. (2002) 'The basic helix-loop-helix factor, HAND2, functions as a transcriptional activator by binding to E-boxes as a heterodimer', *J Biol Chem* 277(15): 12604-12.
- Dai, Y. S., Cserjesi, P., Markham, B. E. and Molkenstein, J. D. (2002) 'The transcription factors GATA4 and dHAND physically interact to synergistically activate cardiac gene expression through a p300-dependent mechanism', *J Biol Chem* 277(27): 24390-8.
- de Jong, F., Opthof, T., Wilde, A. A., Janse, M. J., Charles, R., Lamers, W. H. and Moorman, A. F. (1992) 'Persisting zones of slow impulse conduction in developing chicken hearts', *Circ Res* 71(2): 240-250.
- de la Pompa, J., Timmerman, L., Takimoto, H., Yoshida, H., Elia, A., Samper, E., Potter, J., Wakeham, A., Marengere, L., Langille, B. et al. (1998) 'Role of the NF-ATc transcription factor in morphogenesis of cardiac valves and septum', *Nature* 392(6672): 182-186.

- de Laat, W. and Duboule, D. (2013) 'Topology of mammalian developmental enhancers and their regulatory landscapes', *Nature* 502(7472): 499-506.
- Dekker, J., Marti-Renom, M. A. and Mirny, L. A. (2013) 'Exploring the three-dimensional organization of genomes: interpreting chromatin interaction data', *Nat Rev Genet* 14(6): 390-403.
- Delorme, B., Dahl, E., Jarry-Guichard, T., Marics, I., Briand, J., Willecke, K., Gros, D. and Théveniau-Ruissy, M. (1995) 'Developmental regulation of connexin 40 gene expression in mouse heart correlates with the differentiation of the conduction system', *Dev Dyn* 204(4): 358-371.
- Dirkx, E., Gladka, M. M., Philippen, L. E., Armand, A. S., Kinet, V., Leptidis, S., El Azzouzi, H., Salic, K., Bourajaj, M., da Silva, G. J. et al. (2013) 'Nfat and miR-25 cooperate to reactivate the transcription factor Hand2 in heart failure', *Nat Cell Biol* 15(11): 1282-93.
- Dixon, J. R., Selvaraj, S., Yue, F., Kim, A., Li, Y., Shen, Y., Hu, M., Liu, J. S. and Ren, B. (2012) 'Topological domains in mammalian genomes identified by analysis of chromatin interactions', *Nature* 485(7398): 376-80.
- Djebali, S., Davis, C. A., Merkel, A., Dobin, A., Lassmann, T., Mortazavi, A., Tanzer, A., Lagarde, J., Lin, W., Schlesinger, F. et al. (2012) 'Landscape of transcription in human cells', *Nature* 489(7414): 101-8.
- Dodou, E., Verzi, M. P., Anderson, J. P., Xu, S. M. and Black, B. L. (2004) 'Mef2c is a direct transcriptional target of ISL1 and GATA factors in the anterior heart field during mouse embryonic development', *Development* 131(16): 3931-42.
- Domínguez, J., Meilhac, S., Bland, Y., Buckingham, M. and Brown, N. (2012) 'Asymmetric fate of the posterior part of the second heart field results in unexpected left/right contributions to both poles of the heart', *Circ Res* 111(10): 1323-35.
- Dubois, C. M., Blanchette, F., Laprise, M. H., Leduc, R., Grondin, F. and Seidah, N. G. (2001) 'Evidence that furin is an authentic transforming growth factor-beta1-converting enzyme', *Am J Pathol* 158(1): 305-16.
- Dupays, L., Kotecha, S., Angst, B. and Mohun, T. J. (2009) 'Tbx2 misexpression impairs deployment of second heart field derived progenitor cells to the arterial pole of the embryonic heart', *Dev Biol* 333(1): 121-31.
- Dyer, L. A. and Kirby, M. L. (2009) 'The role of secondary heart field in cardiac development', *Dev Biol* 336(2): 137-44.
- Eckner, R., Ewen, M. E., Newsome, D., Gerdes, M., DeCaprio, J. A., Lawrence, J. B. and Livingston, D. M. (1994) 'Molecular cloning and functional analysis of the adenovirus E1A-associated 300-kD protein (p300) reveals a protein with properties of a transcriptional adaptor', *Genes & development* 8(8): 869-84.
- Farin, H. F., Ludtke, T. H., Schmidt, M. K., Placzko, S., Schuster-Gossler, K., Petry, M., Christoffels, V. M. and Kispert, A. (2013) 'Tbx2 terminates shh/fgf signaling in the developing mouse limb bud by direct repression of gremlin1', *PLoS Genet* 9(4): e1003467.
- Farnham, P. J. (2009) 'Insights from genomic profiling of transcription factors', *Nat Rev Genet* 10(9): 605-16.
- Fei, T., Xia, K., Li, Z., Zhou, B., Zhu, S., Chen, H., Zhang, J., Chen, Z., Xiao, H., Han, J. D. et al. (2010) 'Genome-wide mapping of SMAD target genes reveals the role of BMP signaling in embryonic stem cell fate determination', *Genome research* 20(1): 36-44.

- Ferdous, A., Caprioli, A., Iacovino, M., Martin, C., Morris, J., Richardson, J., Latif, S., Hammer, R., Harvey, R., Olson, E. et al. (2009) 'Nkx2-5 transactivates the Ets-related protein 71 gene and specifies an endothelial/endocardial fate in the developing embryo', *Proc Natl Acad Sci U S A* 106(3): 814-819.
- Firulli, A. B., Firulli, B. A., Wang, J., Rogers, R. H. and Conway, S. J. (2010) 'Gene replacement strategies to test the functional redundancy of basic helix-loop-helix transcription factor', *Pediatr Cardiol* 31(3): 438-48.
- Firulli, B. A., Hadzic, D. B., McDaid, J. R. and Firulli, A. B. (2000) 'The basic helix-loop-helix transcription factors dHAND and eHAND exhibit dimerization characteristics that suggest complex regulation of function', *J Biol Chem* 275(43): 33567-73.
- Firulli, B. A., Krawchuk, D., Centonze, V. E., Vargesson, N., Virshup, D. M., Conway, S. J., Cserjesi, P., Laufer, E. and Firulli, A. B. (2005) 'Altered Twist1 and Hand2 dimerization is associated with Saethre-Chotzen syndrome and limb abnormalities', *Nat Genet* 37(4): 373-81.
- Firulli, B. A., Redick, B. A., Conway, S. J. and Firulli, A. B. (2007) 'Mutations within helix I of Twist1 result in distinct limb defects and variation of DNA binding affinities', *J Biol Chem* 282(37): 27536-46.
- Flicek, P., Amode, M. R., Barrell, D., Beal, K., Billis, K., Brent, S., Carvalho-Silva, D., Clapham, P., Coates, G., Fitzgerald, S. et al. (2014) 'Ensembl 2014', *Nucleic Acids Res* 42(Database issue): D749-55.
- Francou, A., Saint-Michel, E., Mesbah, K., Theveniau-Ruissy, M., Rana, M. S., Christoffels, V. M. and Kelly, R. G. (2013) 'Second heart field cardiac progenitor cells in the early mouse embryo', *Biochim Biophys Acta* 1833(4): 795-8.
- Frank, D., Carter, K., Thomas, K., Burr, R., Bakker, M., Coetzee, W., Tristani-Firouzi, M., Bamshad, M., Christoffels, V. and Moon, A. (2012) 'Lethal arrhythmias in Tbx3-deficient mice reveal extreme dosage sensitivity of cardiac conduction system function and homeostasis', *Proc Natl Acad Sci U S A* 109(3): 154-163.
- Frankel, N., Davis, G. K., Vargas, D., Wang, S., Payre, F. and Stern, D. L. (2010) 'Phenotypic robustness conferred by apparently redundant transcriptional enhancers', *Nature* 466(7305): 490-3.
- Funato, N., Chapman, S. L., McKee, M. D., Funato, H., Morris, J. A., Shelton, J. M., Richardson, J. A. and Yanagisawa, H. (2009) 'Hand2 controls osteoblast differentiation in the branchial arch by inhibiting DNA binding of Runx2', *Development* 136(4): 615-25.
- Galli, A., Robay, D., Osterwalder, M., Bao, X., Benazet, J. D., Tariq, M., Paro, R., Mackem, S. and Zeller, R. (2010) 'Distinct roles of Hand2 in initiating polarity and posterior Shh expression during the onset of mouse limb bud development', *PLoS Genet* 6(4): e1000901.
- Galli, D., Dominguez, J. N., Zaffran, S., Munk, A., Brown, N. A. and Buckingham, M. E. (2008) 'Atrial myocardium derives from the posterior region of the second heart field, which acquires left-right identity as Pitx2c is expressed', *Development* 135(6): 1157-67.
- Galvin, K. E., Travis, E. D., Yee, D., Magnuson, T. and Vivian, J. L. (2010) 'Nodal signaling regulates the bone morphogenetic protein pluripotency pathway in mouse embryonic stem cells', *J Biol Chem* 285(26): 19747-56.
- Garavito-Aguilar, Z. V., Riley, H. E. and Yelon, D. (2010) 'Hand2 ensures an appropriate environment for cardiac fusion by limiting Fibronectin function', *Development* 137(19): 3215-20.
- Garside, V. C., Chang, A. C., Karsan, A. and Hoodless, P. A. (2013) 'Co-ordinating Notch, BMP, and TGF-beta signaling during heart valve development', *Cell Mol Life Sci* 70(16): 2899-917.

- Gaszner, M. and Felsenfeld, G. (2006) 'Insulators: exploiting transcriptional and epigenetic mechanisms', *Nat Rev Genet* 7(9): 703-13.
- Gordon, C. T. and Lyonnet, S. (2014) 'Enhancer mutations and phenotype modularity', *Nat Genet* 46(1): 3-4.
- Gottlieb, P. D., Pierce, S. A., Sims, R. J., Yamagishi, H., Weihe, E. K., Harriss, J. V., Maika, S. D., Kuziel, W. A., King, H. L., Olson, E. N. et al. (2002) 'Bop encodes a muscle-restricted protein containing MYND and SET domains and is essential for cardiac differentiation and morphogenesis', *Nat Genet* 31(1): 25-32.
- Greulich, F., Rudat, C. and Kispert, A. (2011) 'Mechanisms of T-box gene function in the developing heart', *Cardiovasc Res* 91(2): 212-22.
- Habets, P. E., Moorman, A. F., Clout, D. E., van Roon, M. A., Lingbeek, M., van Lohuizen, M., Campione, M. and Christoffels, V. M. (2002) 'Cooperative action of Tbx2 and Nkx2.5 inhibits ANF expression in the atrioventricular canal: implications for cardiac chamber formation', *Genes & development* 16(10): 1234-46.
- Hardison, R. C. and Taylor, J. (2012) 'Genomic approaches towards finding cis-regulatory modules in animals', *Nat Rev Genet* 13(7): 469-83.
- Hariri, F., Nemer, M. and Nemer, G. (2012) 'T-box factors: insights into the evolutionary emergence of the complex heart', *Ann Med* 44(7): 680-93.
- Harrelson, Z., Kelly, R. G., Goldin, S. N., Gibson-Brown, J. J., Bollag, R. J., Silver, L. M. and Papaioannou, V. E. (2004) 'Tbx2 is essential for patterning the atrioventricular canal and for morphogenesis of the outflow tract during heart development', *Development* 131(20): 5041-52.
- Harris, I. S. and Black, B. L. (2010) 'Development of the endocardium', *Pediatr Cardiol* 31(3): 391-9.
- Harvey, R. P. (2002) 'Patterning the vertebrate heart', *Nat Rev Genet* 3(7): 544-56.
- He, A., Kong, S., Ma, Q. and Pu, W. (2011) 'Co-occupancy by multiple cardiac transcription factors identifies transcriptional enhancers active in heart', *Proc Natl Acad Sci U S A* 108(14): 5632-7.
- Heintzman, N. D., Stuart, R. K., Hon, G., Fu, Y., Ching, C. W., Hawkins, R. D., Barrera, L. O., Van Calcar, S., Qu, C., Ching, K. A. et al. (2007) 'Distinct and predictive chromatin signatures of transcriptional promoters and enhancers in the human genome', *Nat Genet* 39(3): 311-8.
- Heinz, S., Benner, C., Spann, N., Bertolino, E., Lin, Y. C., Laslo, P., Cheng, J. X., Murre, C., Singh, H. and Glass, C. K. (2010) 'Simple combinations of lineage-determining transcription factors prime cis-regulatory elements required for macrophage and B cell identities', *Mol Cell* 38(4): 576-89.
- Hendershot, T. J., Liu, H., Clouthier, D. E., Shepherd, I. T., Coppola, E., Studer, M., Firulli, A. B., Pittman, D. L. and Howard, M. J. (2008) 'Conditional deletion of Hand2 reveals critical functions in neurogenesis and cell type-specific gene expression for development of neural crest-derived noradrenergic sympathetic ganglion neurons', *Dev Biol* 319(2): 179-91.
- Hinton, R. B., Jr., Lincoln, J., Deutsch, G. H., Osinska, H., Manning, P. B., Benson, D. W. and Yutzey, K. E. (2006) 'Extracellular matrix remodeling and organization in developing and diseased aortic valves', *Circ Res* 98(11): 1431-8.
- Ho, D., Zhao, X., Gao, S., Hong, C., Vatner, D. E. and Vatner, S. F. (2011) 'Heart Rate and Electrocardiography Monitoring in Mice', *Curr Protoc Mouse Biol* 1: 123-139.

- Holler, K. L., Hendershot, T. J., Troy, S. E., Vincentz, J. W., Firulli, A. B. and Howard, M. J. (2010) 'Targeted deletion of Hand2 in cardiac neural crest-derived cells influences cardiac gene expression and outflow tract development', *Dev Biol* 341(1): 291-304.
- Hoofnagle, M., Neppl, R., Berzin, E., Teg Pipes, G., Olson, E., Wamhoff, B., Somlyo, A. and Owens, G. (2011) 'Myocardin is differentially required for the development of smooth muscle cells and cardiomyocytes', *Am J Physiol Heart Circ Physiol* 300(5): 1707-1721.
- Hoogaars, W. M., Tessari, A., Moorman, A. F., de Boer, P. A., Hagoort, J., Soufan, A. T., Campione, M. and Christoffels, V. M. (2004) 'The transcriptional repressor Tbx3 delineates the developing central conduction system of the heart', *Cardiovasc Res* 62(3): 489-99.
- Hoogaars, W. M., Barnett, P., Moorman, A. F. and Christoffels, V. M. (2007a) 'T-box factors determine cardiac design', *Cell Mol Life Sci* 64(6): 646-60.
- Hoogaars, W. M., Engel, A., Brons, J. F., Verkerk, A. O., de Lange, F. J., Wong, L. Y., Bakker, M. L., Clout, D. E., Wakker, V., Barnett, P. et al. (2007b) 'Tbx3 controls the sinoatrial node gene program and imposes pacemaker function on the atria', *Genes & development* 21(9): 1098-112.
- Horsthuis, T., Buermans, H. P., Brons, J. F., Verkerk, A. O., Bakker, M. L., Wakker, V., Clout, D. E., Moorman, A. F., t Hoen, P. A. and Christoffels, V. M. (2009) 'Gene expression profiling of the forming atrioventricular node using a novel tbx3-based node-specific transgenic reporter', *Circ Res* 105(1): 61-9.
- Houweling, A. C., van Borren, M. M., Moorman, A. F. and Christoffels, V. M. (2005) 'Expression and regulation of the atrial natriuretic factor encoding gene Nppa during development and disease', *Cardiovasc Res* 67(4): 583-93.
- Huang, J., Min Lu, M., Cheng, L., Yuan, L. J., Zhu, X., Stout, A. L., Chen, M., Li, J. and Parmacek, M. S. (2009) 'Myocardin is required for cardiomyocyte survival and maintenance of heart function', *Proc Natl Acad Sci U S A* 106(44): 18734-9.
- Huang, J., Elicker, J., Bowens, N., Liu, X., Cheng, L., Cappola, T. P., Zhu, X. and Parmacek, M. S. (2012) 'Myocardin regulates BMP10 expression and is required for heart development', *J Clin Invest* 122(10): 3678-91.
- Hutson, M., Zeng, X., Kim, A., Antoon, E., Harward, S. and Kirby, M. (2010) 'Arterial pole progenitors interpret opposing FGF/BMP signals to proliferate or differentiate', *Development* 137(18): 3001-11.
- Hutson, M. R., Zhang, P., Stadt, H. A., Sato, A. K., Li, Y. X., Burch, J., Creazzo, T. L. and Kirby, M. L. (2006) 'Cardiac arterial pole alignment is sensitive to FGF8 signaling in the pharynx', *Dev Biol* 295(2): 486-97.
- Ilagan, R., Abu-Issa, R., Brown, D., Yang, Y. P., Jiao, K., Schwartz, R. J., Klingensmith, J. and Meyers, E. N. (2006) 'Fgf8 is required for anterior heart field development', *Development* 133(12): 2435-45.
- Infante, C. R., Park, S., Mihala, A. G., Kingsley, D. M. and Menke, D. B. (2013) 'Pitx1 broadly associates with limb enhancers and is enriched on hindlimb cis-regulatory elements', *Dev Biol* 374(1): 234-44.
- Ishikawa, T., Iwashima, S., Ohishi, A., Nakagawa, Y. and Ohzeki, T. (2011) 'Prevalence of congenital heart disease assessed by echocardiography in 2067 consecutive newborns', *Acta Paediatr* 100(8): e55-60.
- Ivaska, J. (2011) 'Vimentin: central hub in EMT induction?', *Small GTPases* 2(1): 51-53.

- James, D., Levine, A. J., Besser, D. and Hemmati-Brivanlou, A. (2005) 'TGFbeta/activin/nodal signaling is necessary for the maintenance of pluripotency in human embryonic stem cells', *Development* 132(6): 1273-82.
- Jensen, B., Wang, T., Christoffels, V. M. and Moorman, A. F. (2013) 'Evolution and development of the building plan of the vertebrate heart', *Biochim Biophys Acta* 1833(4): 783-94.
- Jiang, X., Rowitch, D., Soriano, P., McMahon, A. and Sucov, H. (2000) 'Fate of the mammalian cardiac neural crest', *Development* 127(8): 1607-1616.
- Karolchik, D., Barber, G. P., Casper, J., Clawson, H., Cline, M. S., Diekhans, M., Dreszer, T. R., Fujita, P. A., Guruvadoo, L., Haeussler, M. et al. (2014) 'The UCSC Genome Browser database: 2014 update', *Nucleic Acids Res* 42(Database issue): D764-70.
- Katagiri, T., Imada, M., Yanai, T., Suda, T., Takahashi, N. and Kamijo, R. (2002) 'Identification of a BMP-responsive element in Id1, the gene for inhibition of myogenesis', *Genes Cells* 7(9): 949-60.
- Kelly, R., Brown, N. and Buckingham, M. (2001) 'The arterial pole of the mouse heart forms from Fgf10-expressing cells in pharyngeal mesoderm', *Developmental Cell* 1(3): 435-440.
- Kelly, R. G. (2012) 'The second heart field', *Curr Top Dev Biol* 100: 33-65.
- Kennedy, B. A., Deatherage, D. E., Gu, F., Tang, B., Chan, M. W., Nephew, K. P., Huang, T. H. and Jin, V. X. (2011) 'ChIP-seq defined genome-wide map of TGFbeta/SMAD4 targets: implications with clinical outcome of ovarian cancer', *PLoS One* 6(7): e22606.
- Kern, C., Twal, W., Mjaatvedt, C., Fairey, S., Toole, B., Iruela-Arispe, M. and Argraves, W. (2006) 'Proteolytic Cleavage of Versican During Cardiac Cushion Morphogenesis', *Dev Dyn* 235(8): 2238-2247.
- Kern, C. B., Wessels, A., McGarity, J., Dixon, L. J., Alston, E., Argraves, W. S., Geeting, D., Nelson, C. M., Menick, D. R. and Apte, S. S. (2010) 'Reduced versican cleavage due to Adamts9 haploinsufficiency is associated with cardiac and aortic anomalies', *Matrix Biol* 29(4): 304-16.
- Khokha, M. K., Hsu, D., Brunet, L. J., Dionne, M. S. and Harland, R. M. (2003) 'Gremlin is the BMP antagonist required for maintenance of Shh and Fgf signals during limb patterning', *Nat Genet* 34(3): 303-7.
- Khoshnood, B., Lelong, N., Houyel, L., Thieulin, A. C., Jouannic, J. M., Magnier, S., Delezoide, A. L., Magny, J. F., Rambaud, C., Bonnet, D. et al. (2012) 'Prevalence, timing of diagnosis and mortality of newborns with congenital heart defects: a population-based study', *Heart* 98(22): 1667-73.
- Kidder, B. L., Hu, G. and Zhao, K. (2011) 'ChIP-Seq: technical considerations for obtaining high-quality data', *Nat Immunol* 12(10): 918-22.
- Kim, T. H., Barrera, L. O. and Ren, B. (2007) 'ChIP-chip for genome-wide analysis of protein binding in mammalian cells', *Curr Protoc Mol Biol* Chapter 21: Unit 21 13.
- Kim, W., Essalmani, R., Szumska, D., Creemers, J. W., Roebroek, A. J., D'Orleans-Juste, P., Bhattacharya, S., Seidah, N. G. and Prat, A. (2012) 'Loss of endothelial furin leads to cardiac malformation and early postnatal death', *Mol Cell Biol* 32(17): 3382-91.
- Kirchhoff, S., Kim, J. S., Hagedorff, A., Thonnissen, E., Kruger, O., Lamers, W. H. and Willecke, K. (2000) 'Abnormal Cardiac Conduction and Morphogenesis in Connexin40 and Connexin43 Double-Deficient Mice', *Circ Res* 87(5): 399-405.

- Kisanuki, Y. Y., Hammer, R. E., Miyazaki, J., Williams, S. C., Richardson, J. A. and Yanagisawa, M. (2001) 'Tie2-Cre transgenic mice: a new model for endothelial cell-lineage analysis in vivo', *Dev Biol* 230(2): 230-42.
- Kleiber, M. (1947) 'Body size and metabolic rate', *Physiol Rev* 27(4): 511-41.
- Kobayashi, T., Lyons, K. M., McMahon, A. P. and Kronenberg, H. M. (2005) 'BMP signaling stimulates cellular differentiation at multiple steps during cartilage development', *Proc Natl Acad Sci U S A* 102(50): 18023-7.
- Koinuma, D., Tsutsumi, S., Kamimura, N., Imamura, T., Aburatani, H. and Miyazono, K. (2009) 'Promoter-wide analysis of Smad4 binding sites in human epithelial cells', *Cancer Sci* 100(11): 2133-42.
- Kokubo, H., Tomita-Miyagawa, S., Hamada, Y. and Saga, Y. (2007) 'Hesr1 and Hesr2 regulate atrioventricular boundary formation in the developing heart through the repression of Tbx2', *Development* 134(4): 747-55.
- Korchynskiy, O. and ten Dijke, P. (2002) 'Identification and functional characterization of distinct critically important bone morphogenetic protein-specific response elements in the Id1 promoter', *J Biol Chem* 277(7): 4883-91.
- Kovacic, J. C., Mercader, N., Torres, M., Boehm, M. and Fuster, V. (2012) 'Epithelial-to-mesenchymal and endothelial-to-mesenchymal transition: from cardiovascular development to disease', *Circulation* 125(14): 1795-808.
- Krivega, I. and Dean, A. (2012) 'Enhancer and promoter interactions-long distance calls', *Curr Opin Genet Dev* 22(2): 79-85.
- Kuo, C. T., Morrissey, E. E., Anandappa, R., Sigrist, K., Lu, M. M., Parmacek, M. S., Soudais, C. and Leiden, J. M. (1997) 'GATA4 transcription factor is required for ventral morphogenesis and heart tube formation', *Genes & development* 11(8): 1048-1060.
- Kurosawa, H., Imamura, T., Koike, M., Sasaki, K. and Amano, Y. (2003) 'A simple method for forming embryoid body from mouse embryonic stem cells', *Journal of bioscience and bioengineering* 96(4): 409-411.
- Lakkis, M. M. and Epstein, J. A. (1998) 'Neurofibromin modulation of ras activity is required for normal endocardial-mesenchymal transformation in the developing heart', *Development* 125(22): 4359-67.
- Lambrechts, D. and Carmeliet, P. (2004) 'Sculpting heart valves with NFATc and VEGF', *Cell* 118(5): 532-4.
- Landt, S. G., Marinov, G. K., Kundaje, A., Kheradpour, P., Pauli, F., Batzoglou, S., Bernstein, B. E., Bickel, P., Brown, J. B., Cayting, P. et al. (2012) 'ChIP-seq guidelines and practices of the ENCODE and modENCODE consortia', *Genome research* 22(9): 1813-31.
- Larkin, M. A., Blackshields, G., Brown, N. P., Chenna, R., McGettigan, P. A., McWilliam, H., Valentin, F., Wallace, I. M., Wilm, A., Lopez, R. et al. (2007) 'Clustal W and Clustal X version 2.0', *Bioinformatics* 23(21): 2947-8.
- Laugwitz, K. L., Moretti, A., Caron, L., Nakano, A. and Chien, K. R. (2008) 'Islet1 cardiovascular progenitors: a single source for heart lineages?', *Development* 135(2): 193-205.
- Le, A. T., Yelon, D. and Stainier, D. Y. R. (2005) 'Hand2 Regulates Epithelial Formation during Myocardial Differentiation', *Current Biology* 15(5): 441-446.

- Lee, M. P. and Yutzey, K. E. (2011) 'Twist1 directly regulates genes that promote cell proliferation and migration in developing heart valves', *PLoS One* 6(12): e29758.
- Lenhard, B., Sandelin, A. and Carninci, P. (2012) 'Metazoan promoters: emerging characteristics and insights into transcriptional regulation', *Nat Rev Genet* 13(4): 233-45.
- Lescroart, F., Kelly, R. G., Le Garrec, J. F., Nicolas, J. F., Meilhac, S. M. and Buckingham, M. (2010) 'Clonal analysis reveals common lineage relationships between head muscles and second heart field derivatives in the mouse embryo', *Development* 137(19): 3269-79.
- Lescroart, F. and Meilhac, S. (2012) 'Cell Lineages, Growth and Repair of the Mouse Heart', *Results Probl Cell Differ* 55: 263-89.
- Lescroart, F., Mohun, T., Meilhac, S. M., Bennett, M. and Buckingham, M. (2012) 'Lineage tree for the venous pole of the heart: clonal analysis clarifies controversial genealogy based on genetic tracing', *Circ Res* 111(10): 1313-22.
- Lettice, L. A., Heaney, S. J., Purdie, L. A., Li, L., de Beer, P., Oostra, B. A., Goode, D., Elgar, G., Hill, R. E. and de Graaff, E. (2003) 'A long-range Shh enhancer regulates expression in the developing limb and fin and is associated with preaxial polydactyly', *Hum Mol Genet* 12(14): 1725-35.
- Levay, A. K., Peacock, J. D., Lu, Y., Koch, M., Hinton, R. B., Jr., Kadler, K. E. and Lincoln, J. (2008) 'Scleraxis is required for cell lineage differentiation and extracellular matrix remodeling during murine heart valve formation in vivo', *Circ Res* 103(9): 948-56.
- Levine, M. (2010) 'Transcriptional enhancers in animal development and evolution', *Curr Biol* 20(17): R754-63.
- Lewandoski, M. (2007) 'Analysis of mouse development with conditional mutagenesis', *Handb Exp Pharmacol*(178): 235-62.
- Li, Q., Lewandoski, J. P., Powell, M. B., Norrie, J. L., Cho, S. H. and Vokes, S. A. (2014) 'A Gli silencer is required for robust repression of gremlin in the vertebrate limb bud', *Development* 141(9): 1906-14.
- Li, S., Wang, D. Z., Wang, Z., Richardson, J. A. and Olson, E. N. (2003) 'The serum response factor coactivator myocardin is required for vascular smooth muscle development', *Proc Natl Acad Sci U S A* 100(16): 9366-70.
- Lien, C., Wu, C., Mercer, B., Webb, R., Richardson, J. and Olson, E. (1999) 'Control of early cardiac-specific transcription of Nkx2-5 by a GATA-dependent enhancer', *Development* 126(1): 75-84.
- Lim, J. and Thiery, J. P. (2012) 'Epithelial-mesenchymal transitions: insights from development', *Development* 139(19): 3471-86.
- Lin, C. J., Lin, C. Y., Chen, C. H., Zhou, B. and Chang, C. P. (2012) 'Partitioning the heart: mechanisms of cardiac septation and valve development', *Development* 139(18): 3277-99.
- Lin, Q. (1997) 'Control of Mouse Cardiac Morphogenesis and Myogenesis by Transcription Factor MEF2C', *Science* 276(5317): 1404-1407.
- Lincoln, J., Kist, R., Scherer, G. and Yutzey, K. E. (2007) 'Sox9 is required for precursor cell expansion and extracellular matrix organization during mouse heart valve development', *Dev Biol* 305(1): 120-32.
- Liu, J., Li, Q., Kuehn, M. R., Litingtung, Y., Vokes, S. A. and Chiang, C. (2013) 'Sonic hedgehog signaling directly targets Hyaluronic Acid Synthase 2, an essential regulator of phalangeal joint patterning', *Dev Biol* 375(2): 160-71.

- Liu, N., Barbosa, A. C., Chapman, S. L., Bezprozvannaya, S., Qi, X., Richardson, J. A., Yanagisawa, H. and Olson, E. N. (2009) 'DNA binding-dependent and -independent functions of the Hand2 transcription factor during mouse embryogenesis', *Development* 136(6): 933-42.
- Logan, M., Martin, J. F., Nagy, A., Lobe, C., Olson, E. N. and Tabin, C. J. (2002) 'Expression of Cre recombinase in the developing mouse limb bud driven by a Prxl enhancer', *Genesis* 33(2): 77-80.
- Long, X., Creemers, E. E., Wang, D. Z., Olson, E. N. and Miano, J. M. (2007) 'Myocardin is a bifunctional switch for smooth versus skeletal muscle differentiation', *Proc Natl Acad Sci U S A* 104(42): 16570-5.
- Loots, G. G. and Ovcharenko, I. (2004) 'rVISTA 2.0: evolutionary analysis of transcription factor binding sites', *Nucleic Acids Res* 32(Web Server issue): W217-21.
- Lopez-Rios, J., Speziale, D., Robay, D., Scotti, M., Osterwalder, M., Nusspamer, G., Galli, A., Holländer, G. A., Kmita, M. and Zeller, R. (2012) 'GLI3 Constrains Digit Number by Controlling Both Progenitor Proliferation and BMP-Dependent Exit to Chondrogenesis', *Developmental Cell* 22: 837-848.
- Lopez-Rovira, T., Chalaux, E., Massague, J., Rosa, J. L. and Ventura, F. (2002) 'Direct binding of Smad1 and Smad4 to two distinct motifs mediates bone morphogenetic protein-specific transcriptional activation of Id1 gene', *J Biol Chem* 277(5): 3176-85.
- Lu, P., Weaver, V. M. and Werb, Z. (2012) 'The extracellular matrix: a dynamic niche in cancer progression', *J Cell Biol* 196(4): 395-406.
- Luna-Zurita, L., Prados, B., Grego-Bessa, J., Luxan, G., del Monte, G., Benguria, A., Adams, R. H., Perez-Pomares, J. M. and de la Pompa, J. L. (2010) 'Integration of a Notch-dependent mesenchymal gene program and Bmp2-driven cell invasiveness regulates murine cardiac valve formation', *J Clin Invest* 120(10): 3493-507.
- Lyons, I., Parsons, L. M., Hartley, L., Li, R., Andrews, J. E., Robb, L. and Harvey, R. P. (1995) 'Myogenic and morphogenetic defects in the heart tubes of murine embryos lacking the homeo box gene Nkx2-5', *Genes & development* 9(13): 1654-1666.
- Ma, L., Lu, M. F., Schwartz, R. J. and Martin, J. F. (2005) 'Bmp2 is essential for cardiac cushion epithelial-mesenchymal transition and myocardial patterning', *Development* 132(24): 5601-11.
- MacQuarrie, K. L., Fong, A. P., Morse, R. H. and Tapscott, S. J. (2011) 'Genome-wide transcription factor binding: beyond direct target regulation', *Trends Genet* 27(4): 141-8.
- Männer, J., Pérez-Pomares, J., Macías, D. and Muñoz-Chápuli, R. (2001) 'The origin, formation and developmental significance of the epicardium: a review', *Cells Tissues Organs* 169(2): 89-103.
- Marinic, M., Aktas, T., Ruf, S. and Spitz, F. (2013) 'An integrated holo-enhancer unit defines tissue and gene specificity of the Fgf8 regulatory landscape', *Dev Cell* 24(5): 530-42.
- Martin-Puig, S., Wang, Z. and Chien, K. R. (2008) 'Lives of a heart cell: tracing the origins of cardiac progenitors', *Cell Stem Cell* 2(4): 320-31.
- Massari, M. and Murre, C. (2000) 'Helix-loop-helix proteins: regulators of transcription in eucaryotic organisms.', *Mol Cell Biol* 20(2): 429-40.
- Massie, C. E. and Mills, I. G. (2008) 'ChIPping away at gene regulation', *EMBO Rep* 9(4): 337-43.
- May, D., Blow, M. J., Kaplan, T., McCulley, D. J., Jensen, B. C., Akiyama, J. A., Holt, A., Plajzer-Frick, I., Shoukry, M., Wright, C. et al. (2012) 'Large-scale discovery of enhancers from human heart tissue', *Nat Genet* 44(1): 89-93.

- Maynard, T. M., Jain, M. D., Balmer, C. W. and LaMantia, A. S. (2002) 'High-resolution mapping of the Gli3 mutation extra-toes reveals a 51.5-kb deletion', *Mamm Genome* 13(1): 58-61.
- McCulley, D. J., Kang, J. O., Martin, J. F. and Black, B. L. (2008) 'BMP4 is required in the anterior heart field and its derivatives for endocardial cushion remodeling, outflow tract septation, and semilunar valve development', *Dev Dyn* 237(11): 3200-9.
- McFadden, D., Charité, J., Richardson, J., Srivastava, D., Firulli, A. and Olson, E. (2000) 'A GATA-dependent right ventricular enhancer controls dHAND transcription in the developing heart', *Development* 127(24): 5331-41.
- McFadden, D. G., Barbosa, A. C., Richardson, J. A., Schneider, M. D., Srivastava, D. and Olson, E. N. (2005) 'The Hand1 and Hand2 transcription factors regulate expansion of the embryonic cardiac ventricles in a gene dosage-dependent manner', *Development* 132(1): 189-201.
- McLean, C. Y., Bristor, D., Hiller, M., Clarke, S. L., Schaar, B. T., Lowe, C. B., Wenger, A. M. and Bejerano, G. (2010) 'GREAT improves functional interpretation of cis-regulatory regions', *Nat Biotechnol* 28(5): 495-501.
- Meilhac, S., Kelly, R., Rocancourt, D., Eloy-Trinquet, S., Nicolas, J. and Buckingham, M. (2003) 'A retrospective clonal analysis of the myocardium reveals two phases of clonal growth in the developing mouse heart', *Development* 130(16): 3877-3889.
- Meilhac, S., Esner, M., Kelly, R., Nicolas, J. and Buckingham, M. (2004) 'The Clonal Origin of Myocardial Cells in Different Regions of the Embryonic Mouse Heart', *Dev Cell* 6(5): 685-98.
- Mendez, M. G., Kojima, S. and Goldman, R. D. (2010) 'Vimentin induces changes in cell shape, motility, and adhesion during the epithelial to mesenchymal transition', *FASEB J* 24(6): 1838-51.
- Menke, D. B., Guenther, C. and Kingsley, D. M. (2008) 'Dual hindlimb control elements in the Tbx4 gene and region-specific control of bone size in vertebrate limbs', *Development* 135(15): 2543-53.
- Mesbah, K., Harrelson, Z., Theveniau-Ruissy, M., Papaioannou, V. E. and Kelly, R. G. (2008) 'Tbx3 is required for outflow tract development', *Circ Res* 103(7): 743-50.
- Mesbah, K., Rana, M. S., Francou, A., van Duijvenboden, K., Papaioannou, V. E., Moorman, A. F., Kelly, R. G. and Christoffels, V. M. (2012) 'Identification of a Tbx1/Tbx2/Tbx3 genetic pathway governing pharyngeal and arterial pole morphogenesis', *Hum Mol Genet* 21(6): 1217-29.
- Michos, O., Panman, L., Vintersten, K., Beier, K., Zeller, R. and Zuniga, A. (2004) 'Gremlin-mediated BMP antagonism induces the epithelial-mesenchymal feedback signaling controlling metanephric kidney and limb organogenesis', *Development* 131(14): 3401-10.
- Milgrom-Hoffman, M., Harrelson, Z., Ferrara, N., Zelzer, E., Evans, S. M. and Tzahor, E. (2011) 'The heart endocardium is derived from vascular endothelial progenitors', *Development* 138(21): 4777-87.
- Minguillon, C., Gibson-Brown, J. J. and Logan, M. P. (2009) 'Tbx4/5 gene duplication and the origin of vertebrate paired appendages', *Proc Natl Acad Sci U S A* 106(51): 21726-30.
- Misfeldt, A. M., Boyle, S. C., Tompkins, K. L., Bautch, V. L., Labosky, P. A. and Baldwin, H. S. (2009) 'Endocardial cells are a distinct endothelial lineage derived from Flk1+ multipotent cardiovascular progenitors', *Dev Biol* 333(1): 78-89.
- Misra, C. and Garg, V. (2013) 'Compacting the heart with Notch', *Nat Med* 19(2): 133-4.
- Mjaatvedt, C., Yamamura, H., Capehart, A., Turner, D. and Markwald, R. (1998) 'The Cspg2 Gene, Disrupted in the hdf Mutant, Is Required for Right Cardiac Chamber and Endocardial Cushion Formation', *Dev Biol* 202(1): 56-66.

- Mjaatvedt, C. H., Nakaoka, T., Moreno-Rodriguez, R., Norris, R. A., Kern, M. J., Eisenberg, C. A., Turner, D. and Markwald, R. R. (2001) 'The outflow tract of the heart is recruited from a novel heart-forming field', *Dev Biol* 238(1): 97-109.
- Molkentin, J. D., Lin, Q., Duncan, S. A. and Olson, E. N. (1997) 'Requirement of the transcription factor GATA4 for heart tube formation and ventral morphogenesis', *Genes & development* 11(8): 1061-1072.
- Montavon, T., Soshnikova, N., Mascrez, B., Joye, E., Thevenet, L., Splinter, E., de Laat, W., Spitz, F. and Duboule, D. (2011) 'A regulatory archipelago controls Hox genes transcription in digits', *Cell* 147(5): 1132-45.
- Moorman, A. and Christoffels, V. (2003) 'Cardiac Chamber Formation: Development, Genes, and Evolution', *Physiol Rev* 83(4): 1223-67.
- Moretti, A., Caron, L., Nakano, A., Lam, J. T., Bernshausen, A., Chen, Y., Qyang, Y., Bu, L., Sasaki, M., Martin-Puig, S. et al. (2006) 'Multipotent embryonic isl1+ progenitor cells lead to cardiac, smooth muscle, and endothelial cell diversification', *Cell* 127(6): 1151-65.
- Morikawa, M., Koinuma, D., Tsutsumi, S., Vasilaki, E., Kanki, Y., Heldin, C. H., Aburatani, H. and Miyazono, K. (2011) 'ChIP-seq reveals cell type-specific binding patterns of BMP-specific Smads and a novel binding motif', *Nucleic Acids Res* 39(20): 8712-27.
- Morikawa, Y., D'Autreaux, F., Gershon, M. D. and Cserjesi, P. (2007) 'Hand2 determines the noradrenergic phenotype in the mouse sympathetic nervous system', *Dev Biol* 307(1): 114-26.
- Morikawa, Y. and Cserjesi, P. (2008) 'Cardiac neural crest expression of Hand2 regulates outflow and second heart field development', *Circ Res* 103(12): 1422-9.
- Moskowitz, I. P., Wang, J., Peterson, M. A., Pu, W. T., Mackinnon, A. C., Oxburgh, L., Chu, G. C., Sarkar, M., Berul, C., Smoot, L. et al. (2011) 'Transcription factor genes Smad4 and Gata4 cooperatively regulate cardiac valve development. [corrected]', *Proc Natl Acad Sci U S A* 108(10): 4006-11.
- Munshi, N. V. (2012) 'Gene regulatory networks in cardiac conduction system development', *Circ Res* 110(11): 1525-37.
- Murray, S. A. and Gridley, T. (2006) 'Snail family genes are required for left-right asymmetry determination, but not neural crest formation, in mice', *Proc Natl Acad Sci U S A* 103(27): 10300-4.
- Murray, S. A., Oram, K. F. and Gridley, T. (2007) 'Multiple functions of Snail family genes during palate development in mice', *Development* 134(9): 1789-97.
- Narlikar, L., Sakabe, N. J., Blanski, A. A., Arimura, F. E., Westlund, J. M., Nobrega, M. A. and Ovcharenko, I. (2010) 'Genome-wide discovery of human heart enhancers', *Genome research* 20(3): 381-92.
- Nelson, A. C. and Wardle, F. C. (2013) 'Conserved non-coding elements and cis regulation: actions speak louder than words', *Development* 140(7): 1385-95.
- Niessen, K., Fu, Y., Chang, L., Hoodless, P. A., McFadden, D. and Karsan, A. (2008) 'Slug is a direct Notch target required for initiation of cardiac cushion cellularization', *J Cell Biol* 182(2): 315-25.
- Nishii, K. and Shibata, Y. (2006) 'Mode and determination of the initial contraction stage in the mouse embryo heart', *Anat Embryol (Berl)* 211(2): 95-100.
- Nissim, S., Hasso, S. M., Fallon, J. F. and Tabin, C. J. (2006) 'Regulation of Gremlin expression in the posterior limb bud', *Dev Biol* 299(1): 12-21.

- Nobrega, M., Ovcharenko, I., Afzal, V. and Rubin, E. (2003) 'Scanning Human Gene Deserts for Long-Range Enhancers', *Science* 302(5644): 413.
- Noonan, J. P. and McCallion, A. S. (2010) 'Genomics of long-range regulatory elements', *Annu Rev Genomics Hum Genet* 11: 1-23.
- Olivey, H. E. and Svensson, E. C. (2010) 'Epicardial-myocardial signaling directing coronary vasculogenesis', *Circ Res* 106(5): 818-32.
- Olson, E. N. (2006) 'Gene regulatory networks in the evolution and development of the heart', *Science* 313(5795): 1922-7.
- Ong, C. T. and Corces, V. G. (2011) 'Enhancer function: new insights into the regulation of tissue-specific gene expression', *Nat Rev Genet* 12(4): 283-93.
- Ong, C. T. and Corces, V. G. (2014) 'CTCF: an architectural protein bridging genome topology and function', *Nat Rev Genet* 15(4): 234-46.
- Osterwalder, M., Galli, A., Rosen, B., Skarnes, W. C., Zeller, R. and Lopez-Rios, J. (2010a) 'Dual RMCE for efficient re-engineering of mouse mutant alleles', *Nat Methods* 7(11): 893-5.
- Osterwalder, M., Lopez-Rios, J. and Zeller, R. (2010b) 'Next generation engineering of conditional mouse alleles with loxP and FRT sites by dual RMCE', *Nature Protocol Exchange*.
- Osterwalder, M., Speziale, D., Shoukry, M., Mohan, R., Ivanek, R., Kohler, M., Beisel, C., Wen, X., Scales, S. J., Christoffels, V. M. et al. (in press) 'HAND2 Targets Define a Network of Transcriptional Regulators that Compartmentalize the Early Limb Bud Mesenchyme', *Dev Cell*.
- Ovcharenko, I., Nobrega, M. A., Loots, G. G. and Stubbs, L. (2004) 'ECR Browser: a tool for visualizing and accessing data from comparisons of multiple vertebrate genomes', *Nucleic Acids Res* 32(Web Server issue): W280-6.
- Pandur, P., Läsche, M., Eisenberg, L. and Kühl, M. (2002) 'Wnt-11 activation of a non-canonical Wnt signalling pathway is required for cardiogenesis', *Nature* 418(6898): 636-41.
- Panman, L., Galli, A., Lagarde, N., Michos, O., Soete, G., Zuniga, A. and Zeller, R. (2006) 'Differential regulation of gene expression in the digit forming area of the mouse limb bud by SHH and gremlin 1/FGF-mediated epithelial-mesenchymal signalling', *Development* 133(17): 3419-28.
- Park, E. J., Ogden, L. A., Talbot, A., Evans, S., Cai, C. L., Black, B. L., Frank, D. U. and Moon, A. M. (2006) 'Required, tissue-specific roles for Fgf8 in outflow tract formation and remodeling', *Development* 133(12): 2419-33.
- Park, E. J., Watanabe, Y., Smyth, G., Miyagawa-Tomita, S., Meyers, E., Klingensmith, J., Camenisch, T., Buckingham, M. and Moon, A. M. (2008) 'An FGF autocrine loop initiated in second heart field mesoderm regulates morphogenesis at the arterial pole of the heart', *Development* 135(21): 3599-610.
- Park, P. J. (2009) 'ChIP-seq: advantages and challenges of a maturing technology', *Nat Rev Genet* 10(10): 669-80.
- Peacock, J. D., Lu, Y., Koch, M., Kadler, K. E. and Lincoln, J. (2008) 'Temporal and spatial expression of collagens during murine atrioventricular heart valve development and maintenance', *Dev Dyn* 237(10): 3051-8.
- Peacock, J. D., Levay, A. K., Gillaspie, D. B., Tao, G. and Lincoln, J. (2010) 'Reduced sox9 function promotes heart valve calcification phenotypes in vivo', *Circ Res* 106(4): 712-9.

- Petrykowska, H. M., Vockley, C. M. and Elnitski, L. (2008) 'Detection and characterization of silencers and enhancer-blockers in the greater CFTR locus', *Genome research* 18(8): 1238-46.
- Pettitt, S. J., Liang, Q., Rairdan, X. Y., Moran, J. L., Prosser, H. M., Beier, D. R., Lloyd, K. C., Bradley, A. and Skarnes, W. C. (2009) 'Agouti C57BL/6N embryonic stem cells for mouse genetic resources', *Nat Methods* 6(7): 493-5.
- Phan, D., Rasmussen, T. L., Nakagawa, O., McAnally, J., Gottlieb, P. D., Tucker, P. W., Richardson, J. A., Bassel-Duby, R. and Olson, E. N. (2005) 'BOP, a regulator of right ventricular heart development, is a direct transcriptional target of MEF2C in the developing heart', *Development* 132(11): 2669-78.
- Phillips-Cremins, J. E. and Corces, V. G. (2013) 'Chromatin insulators: linking genome organization to cellular function', *Mol Cell* 50(4): 461-74.
- Pignatti, E., Zeller, R. and Zuniga, A. (2014) 'To BMP or not to BMP during vertebrate limb bud development', *Semin Cell Dev Biol* 32C: 119-127.
- Plageman, T. F., Jr. and Yutzey, K. E. (2005) 'T-box genes and heart development: putting the "T" in heart', *Dev Dyn* 232(1): 11-20.
- Puceat, M. (2013) 'Embryological origin of the endocardium and derived valve progenitor cells: from developmental biology to stem cell-based valve repair', *Biochim Biophys Acta* 1833(4): 917-22.
- Qin, H., Chan, M. W., Liyanarachchi, S., Balch, C., Potter, D., Souriraj, I. J., Cheng, A. S., Agosto-Perez, F. J., Nikonova, E. V., Yan, P. S. et al. (2009) 'An integrative ChIP-chip and gene expression profiling to model SMAD regulatory modules', *BMC Syst Biol* 3: 73.
- Rada-Iglesias, A., Bajpai, R., Swigut, T., Brugmann, S. A., Flynn, R. A. and Wysocka, J. (2011) 'A unique chromatin signature uncovers early developmental enhancers in humans', *Nature* 470(7333): 279-83.
- Rajamannan, N. M., Subramaniam, M., Rickard, D., Stock, S. R., Donovan, J., Springett, M., Orszulak, T., Fullerton, D. A., Tajik, A. J., Bonow, R. O. et al. (2003) 'Human aortic valve calcification is associated with an osteoblast phenotype', *Circulation* 107(17): 2181-4.
- Rana, M. S., Christoffels, V. M. and Moorman, A. F. (2013) 'A molecular and genetic outline of cardiac morphogenesis', *Acta Physiol (Oxf)* 207(4): 588-615.
- Ranger, A., Grusby, M., Hodge, M., Gravallesse, E., de la Brousse, F., Hoey, T., Mickanin, C., Baldwin, H. and Glimcher, L. (1998) 'The transcription factor NF-ATc is essential for cardiac valve formation', *Nature* 392(6672): 186-190.
- Reecy, J., Li, X., Yamada, M., DeMayo, F., Newman, C., Harvey, R. and Schwartz, R. (1999) 'Identification of upstream regulatory regions in the heart-expressed homeobox gene Nkx2-5', *Development* 126(4): 839-849.
- Reese, D., Mikawa, T. and Bader, D. (2002) 'Development of the Coronary Vessel System', *Circ Res* 91(9): 761-768.
- Rivera-Feliciano, J., Lee, K. H., Kong, S. W., Rajagopal, S., Ma, Q., Springer, Z., Izumo, S., Tabin, C. J. and Pu, W. T. (2006) 'Development of heart valves requires Gata4 expression in endothelial-derived cells', *Development* 133(18): 3607-18.
- Rivera-Feliciano, J. and Tabin, C. J. (2006) 'Bmp2 instructs cardiac progenitors to form the heart-valve-inducing field', *Dev Biol* 295(2): 580-8.

- Rochais, F., Dandonneau, M., Mesbah, K., Jarry, T., Mattei, M. and Kelly, R. (2009a) 'Hes1 is expressed in the second heart field and is required for outflow tract development', *PLoS One* 4(7): e6267.
- Rochais, F., Mesbah, K. and Kelly, R. G. (2009b) 'Signaling pathways controlling second heart field development', *Circ Res* 104(8): 933-42.
- Roebroek, A., Umans, L., Pauli, I., Robertson, E., van Leuven, F., Van de Ven, W. and DB., C. (1998) 'Failure of ventral closure and axial rotation in embryos lacking the proprotein convertase Furin', *Development* 125(24): 4863-4876.
- Roy, A., Kucukural, A. and Zhang, Y. (2010) 'I-TASSER: a unified platform for automated protein structure and function prediction', *Nat Protoc* 5(4): 725-38.
- Rozowsky, J., Euskirchen, G., Auerbach, R. K., Zhang, Z. D., Gibson, T., Bjornson, R., Carriero, N., Snyder, M. and Gerstein, M. B. (2009) 'PeakSeq enables systematic scoring of ChIP-seq experiments relative to controls', *Nat Biotechnol* 27(1): 66-75.
- Runyan, R. B. and Markwald, R. R. (1983) 'Invasion of mesenchyme into three-dimensional collagen gels: a regional and temporal analysis of interaction in embryonic heart tissue', *Dev Biol* 95(1): 108-14.
- Rutenberg, J. B., Fischer, A., Jia, H., Gessler, M., Zhong, T. P. and Mercola, M. (2006) 'Developmental patterning of the cardiac atrioventricular canal by Notch and Hairy-related transcription factors', *Development* 133(21): 4381-90.
- Ryckebusch, L., Wang, Z., Bertrand, N., Lin, S. C., Chi, X., Schwartz, R., Zaffran, S. and Niederreither, K. (2008) 'Retinoic acid deficiency alters second heart field formation', *Proc Natl Acad Sci U S A* 105(8): 2913-8.
- Sauka-Spengler, T. and Bronner-Fraser, M. (2008) 'A gene regulatory network orchestrates neural crest formation', *Nat Rev Mol Cell Biol* 9(7): 557-68.
- Scherz, P. J., Harfe, B. D., McMahon, A. P. and Tabin, C. J. (2004) 'The limb bud Shh-Fgf feedback loop is terminated by expansion of former ZPA cells', *Science* 305(5682): 396-9.
- Scherz, P. J., Huisken, J., Sahai-Hernandez, P. and Stainier, D. Y. (2008) 'High-speed imaging of developing heart valves reveals interplay of morphogenesis and function', *Development* 135(6): 1179-87.
- Schilham, M., Oosterwegel, M., Moerer, P., Ya, J., de Boer, P., van de Wetering, M., Verbeek, S., Lamers, W., Kruisbeek, A., Cumano, A. et al. (1996) 'Defects in cardiac outflow tract formation and pro-B-lymphocyte expansion in mice lacking Sox-4', *Nature* 380(6576): 711-4.
- Schindler, Y. L., Garske, K. M., Wang, J., Firulli, B. A., Firulli, A. B., Poss, K. D. and Yelon, D. (2014) 'Hand2 elevates cardiomyocyte production during zebrafish heart development and regeneration', *Development* 141(16): 3112-22.
- Schwenk, F., Baron, U. and Rajewsky, K. (1995) 'A cre-transgenic mouse strain for the ubiquitous deletion of loxP-flanked gene segments including deletion in germ cells', *Nucleic Acids Res* 23(24): 5080-1.
- Searcy, R., Vincent, E., Liberatore, C. and Yutzey, K. (1998) 'A GATA-dependent nkx-2.5 regulatory element activates early cardiac gene expression in transgenic mice', *Development* 125(22): 4461-4470.
- Sefton, M., Sánchez, S. and Nieto, M. (1998) 'Conserved and divergent roles for members of the Snail family of transcription factors in the chick and mouse embryo', *Development* 125(16): 3111-3121.

- Shelton, E. L. and Yutzey, K. E. (2008) 'Twist1 function in endocardial cushion cell proliferation, migration, and differentiation during heart valve development', *Dev Biol* 317(1): 282-95.
- Shen, L., Li, X., Shen, A., Wang, Q., Liu, C., Guo, Y., Song, Z. and Li, Z. (2010) 'Transcription factor HAND2 mutations in sporadic Chinese patients with congenital heart disease', *Chin Med J* 123(13): 1623-7.
- Shen, T., Aneas, I., Sakabe, N., Dirschinger, R. J., Wang, G., Smemo, S., Westlund, J. M., Cheng, H., Dalton, N., Gu, Y. et al. (2011) 'Tbx20 regulates a genetic program essential to adult mouse cardiomyocyte function', *J Clin Invest* 121(12): 4640-54.
- Shen, Y., Yue, F., McCleary, D. F., Ye, Z., Edsall, L., Kuan, S., Wagner, U., Dixon, J., Lee, L., Lobanenkov, V. V. et al. (2012) 'A map of the cis-regulatory sequences in the mouse genome', *Nature* 488(7409): 116-20.
- Sheth, R., Gregoire, D., Dumouchel, A., Scotti, M., Pham, J. M., Nemecek, S., Bastida, M. F., Ros, M. A. and Kmita, M. (2013) 'Decoupling the function of Hox and Shh in developing limb reveals multiple inputs of Hox genes on limb growth', *Development* 140(10): 2130-8.
- Shirai, M., Imanaka-Yoshida, K., Schneider, M. D., Schwartz, R. J. and Morisaki, T. (2009) 'T-box 2, a mediator of Bmp-Smad signaling, induced hyaluronan synthase 2 and Tgfbeta2 expression and endocardial cushion formation', *Proc Natl Acad Sci U S A* 106(44): 18604-9.
- Shu, W., Chen, H., Bo, X. and Wang, S. (2011) 'Genome-wide analysis of the relationships between DNase I HS, histone modifications and gene expression reveals distinct modes of chromatin domains', *Nucleic Acids Res* 39(17): 7428-43.
- Singh, M. K., Christoffels, V. M., Dias, J. M., Trowe, M. O., Petry, M., Schuster-Gossler, K., Burger, A., Ericson, J. and Kispert, A. (2005) 'Tbx20 is essential for cardiac chamber differentiation and repression of Tbx2', *Development* 132(12): 2697-707.
- Singh, R., Horsthuis, T., Farin, H. F., Grieskamp, T., Norden, J., Petry, M., Wakker, V., Moorman, A. F., Christoffels, V. M. and Kispert, A. (2009) 'Tbx20 interacts with smads to confine tbx2 expression to the atrioventricular canal', *Circ Res* 105(5): 442-52.
- Singh, R. and Kispert, A. (2010) 'Tbx20, Smads, and the atrioventricular canal', *Trends Cardiovasc Med* 20(4): 109-14.
- Singh, R., Hoogaars, W. M., Barnett, P., Grieskamp, T., Rana, M. S., Buermans, H., Farin, H. F., Petry, M., Heallen, T., Martin, J. F. et al. (2012) 'Tbx2 and Tbx3 induce atrioventricular myocardial development and endocardial cushion formation', *Cell Mol Life Sci* 69(8): 1377-89.
- Sirard, C., de la Pompa, J. L., Elia, A., Itie, A., Mirtsos, C., Cheung, A., Hahn, S., Wakeham, A., Schwartz, L., Kern, S. E. et al. (1998) 'The tumor suppressor gene Smad4/Dpc4 is required for gastrulation and later for anterior development of the mouse embryo', *Genes & development* 12(1): 107-19.
- Skarnes, W. C., Rosen, B., West, A. P., Koutourakis, M., Bushell, W., Iyer, V., Mujica, A. O., Thomas, M., Harrow, J., Cox, T. et al. (2011) 'A conditional knockout resource for the genome-wide study of mouse gene function', *Nature* 474(7351): 337-42.
- Smemo, S., Campos, L. C., Moskowitz, I. P., Krieger, J. E., Pereira, A. C. and Nobrega, M. A. (2012) 'Regulatory variation in a TBX5 enhancer leads to isolated congenital heart disease', *Hum Mol Genet* 21(14): 3255-63.
- Song, W., Jackson, K. and McGuire, P. G. (2000) 'Degradation of type IV collagen by matrix metalloproteinases is an important step in the epithelial-mesenchymal transformation of the endocardial cushions', *Dev Biol* 227(2): 606-17.

Soshnikova, N., Montavon, T., Leleu, M., Galjart, N. and Duboule, D. (2010) 'Functional analysis of CTCF during mammalian limb development', *Dev Cell* 19(6): 819-30.

Spitz, F. and Duboule, D. (2008) 'Global control regions and regulatory landscapes in vertebrate development and evolution', *Adv Genet* 61: 175-205.

Spitz, F. and Furlong, E. E. (2012) 'Transcription factors: from enhancer binding to developmental control', *Nat Rev Genet* 13(9): 613-26.

Srivastava, D., Thomas, T., Lin, Q., Kirby, M., Brown, D. and Olson, E. (1997) 'Regulation of cardiac mesodermal and neural crest development by the bHLH transcription factor, dHAND', *Nat Genet* 16(2): 154-60.

Srivastava, D. and Olson, E. N. (2000) 'A genetic blueprint for cardiac development', *Nature* 407(6801): 221-6.

Srivastava, D. (2006) 'Making or breaking the heart: from lineage determination to morphogenesis', *Cell* 126(6): 1037-48.

Srivastava, D., Cserjeesi, P., Olson, E.N. (1995) 'A subclass of bHLH proteins required for cardiac morphogenesis', *Science* 270(5244): 1995-9.

St-Jacques, B., Dassule, H. R., Karavanova, I., Botchkarev, V. A., Li, J., Danielian, P. S., McMahon, J. A., Lewis, P. M., Paus, R. and McMahon, A. P. (1998) 'Sonic hedgehog signaling is essential for hair development', *Curr Biol* 8(19): 1058-68.

Stennard, F. A., Costa, M. W., Lai, D., Biben, C., Furtado, M. B., Solloway, M. J., McCulley, D. J., Leimena, C., Preis, J. I., Dunwoodie, S. L. et al. (2005) 'Murine T-box transcription factor Tbx20 acts as a repressor during heart development, and is essential for adult heart integrity, function and adaptation', *Development* 132(10): 2451-62.

Stennard, F. A. and Harvey, R. P. (2005) 'T-box transcription factors and their roles in regulatory hierarchies in the developing heart', *Development* 132(22): 4897-910.

Stieber, J., Herrmann, S., Feil, S., Loster, J., Feil, R., Biel, M., Hofmann, F. and Ludwig, A. (2003) 'The hyperpolarization-activated channel HCN4 is required for the generation of pacemaker action potentials in the embryonic heart', *Proc Natl Acad Sci U S A* 100(25): 15235-40.

Strehle, E. M., Yu, L., Rosenfeld, J. A., Donkervoort, S., Zhou, Y., Chen, T. J., Martinez, J. E., Fan, Y. S., Barbouth, D., Zhu, H. et al. (2012) 'Genotype-phenotype analysis of 4q deletion syndrome: proposal of a critical region', *Am J Med Genet A* 158A(9): 2139-51.

Sun, Y., Liang, X., Najafi, N., Cass, M., Lin, L., Cai, C. L., Chen, J. and Evans, S. M. (2007) 'Islet 1 is expressed in distinct cardiovascular lineages, including pacemaker and coronary vascular cells', *Dev Biol* 304(1): 286-96.

Susan-Resiga, D., Essalmani, R., Hamelin, J., Asselin, M. C., Benjannet, S., Chamberland, A., Day, R., Szumska, D., Constam, D., Bhattacharya, S. et al. (2011) 'Furin is the major processing enzyme of the cardiac-specific growth factor bone morphogenetic protein 10', *J Biol Chem* 286(26): 22785-94.

Takaku, K., Oshima, M., Miyoshi, H., Matsui, M., Seldin, M. F. and Taketo, M. M. (1998) 'Intestinal tumorigenesis in compound mutant mice of both Dpc4 (Smad4) and Apc genes', *Cell* 92(5): 645-56.

Takeuchi, J. K., Mileikovskaia, M., Koshiba-Takeuchi, K., Heidt, A. B., Mori, A. D., Arruda, E. P., Gertsenstein, M., Georges, R., Davidson, L., Mo, R. et al. (2005) 'Tbx20 dose-dependently regulates transcription factor networks required for mouse heart and motoneuron development', *Development* 132(10): 2463-74.

- Tanaka, M., Wechsler, S., Lee, I., Yamasaki, N., Lawitts, J. and Izumo, S. (1999) 'Complex modular cis-acting elements regulate expression of the cardiac specifying homeobox gene *Csx/Nkx2.5*', *Development* 126(7): 1439-1450.
- Tao, G., Levay, A. K., Gridley, T. and Lincoln, J. (2011) 'Mmp15 is a direct target of Snai1 during endothelial to mesenchymal transformation and endocardial cushion development', *Dev Biol* 359(2): 209-21.
- Tao, G., Kotick, J. D. and Lincoln, J. (2012) 'Heart valve development, maintenance, and disease: the role of endothelial cells', *Curr Top Dev Biol* 100: 203-32.
- Tao, G., Miller, L. J. and Lincoln, J. (2013) 'Snai1 is important for avian epicardial cell transformation and motility', *Dev Dyn* 242(6): 699-708.
- te Welscher, P., Fernandez-Teran, M., Ros, M. A. and Zeller, R. (2002) 'Mutual genetic antagonism involving GLI3 and dHAND prepatterns the vertebrate limb bud mesenchyme prior to SHH signaling', *Genes & development* 16(4): 421-6.
- Tesson, L., Heslan, J. M., Menoret, S. and Anegon, I. (2002) 'Rapid and accurate determination of zygosity in transgenic animals by real-time quantitative PCR', *Transgenic research* 11(1): 43-8.
- Thattaliyath, B., Firulli, B. and Firulli, A. (2002) 'The Basic-Helix-Loop-Helix Transcription Factor HAND2 Directly Regulates Transcription of the Atrial Naturetic Peptide Gene', *J Mol Cell Cardiol* 34(10): 1335-44.
- Thiery, J. P., Acloque, H., Huang, R. Y. and Nieto, M. A. (2009) 'Epithelial-mesenchymal transitions in development and disease', *Cell* 139(5): 871-90.
- Timmerman, L. A., Grego-Bessa, J., Raya, A., Bertran, E., Perez-Pomares, J. M., Diez, J., Aranda, S., Palomo, S., McCormick, F., Izpisua-Belmonte, J. C. et al. (2004) 'Notch promotes epithelial-mesenchymal transition during cardiac development and oncogenic transformation', *Genes & development* 18(1): 99-115.
- Tirosh-Finkel, L., Zeisel, A., Brodt-Ivenshitz, M., Shamai, A., Yao, Z., Seger, R., Domany, E. and Tzahor, E. (2010) 'BMP-mediated inhibition of FGF signaling promotes cardiomyocyte differentiation of anterior heart field progenitors', *Development* 137(18): 2989-3000.
- Togi, K., Yoshida, Y., Matsumae, H., Nakashima, Y., Kita, T. and Tanaka, M. (2006) 'Essential role of Hand2 in interventricular septum formation and trabeculation during cardiac development', *Biochem Biophys Res Commun* 343(1): 144-51.
- Tsanov, K. M., Nishi, Y., Peterson, K. A., Liu, J., Baetscher, M. and McMahon, A. P. (2012) 'An embryonic stem cell-based system for rapid analysis of transcriptional enhancers', *Genesis* 50(5): 443-50.
- Tsuchihashi, T., Maeda, J., Shin, C. H., Ivey, K. N., Black, B. L., Olson, E. N., Yamagishi, H. and Srivastava, D. (2011) 'Hand2 function in second heart field progenitors is essential for cardiogenesis', *Dev Biol* 351(1): 62-9.
- Tzahor, E. and Evans, S. M. (2011) 'Pharyngeal mesoderm development during embryogenesis: implications for both heart and head myogenesis', *Cardiovasc Res* 91(2): 196-202.
- Uslu, V. V., Petretich, M., Ruf, S., Langenfeld, K., Fonseca, N. A., Marioni, J. C. and Spitz, F. (2014) 'Long-range enhancers regulating Myc expression are required for normal facial morphogenesis', *Nat Genet* 46(7): 753-8.

- van den Boogaard, M., Wong, L., Tessadori, F., Bakker, M., Dreizehnter, L., Wakker, V., Bezzina, C., 't Hoen, P., Bakkers, J., Barnett, P. et al. (2012) 'Genetic variation in T-box binding element functionally affects SCN5A/SCN10A enhancer', *J Clin Invest* 122(7): 2519-30.
- van Weerd, J. H., Badi, I., van den Boogaard, M., Stefanovic, S., van de Werken, H. J., Gomez-Velazquez, M., Badia-Careaga, C., Manzanares, M., de Laat, W., Barnett, P. et al. (2014) 'A large permissive regulatory domain exclusively controls tbx3 expression in the cardiac conduction system', *Circ Res* 115(4): 432-41.
- VanDusen, N. J. and Firulli, A. B. (2012) 'Twist factor regulation of non-cardiomyocyte cell lineages in the developing heart', *Differentiation* 84(1): 79-88.
- VanDusen, N. J., Vincentz, J. W., Firulli, B. A., Howard, M. J., Rubart, M. and Firulli, A. B. (2014) 'Loss of Hand2 in a population of Periostin lineage cells results in pronounced bradycardia and neonatal death', *Dev Biol* 388(2): 149-58.
- Verheyden, J. M. and Sun, X. (2008) 'An Fgf/Gremlin inhibitory feedback loop triggers termination of limb bud outgrowth', *Nature* 454: 638-641.
- Vestweber, D. (2008) 'VE-cadherin: the major endothelial adhesion molecule controlling cellular junctions and blood vessel formation', *Arterioscler Thromb Vasc Biol* 28(2): 223-32.
- Vincent, S. and Buckingham, M. (2010) 'How to Make a Heart', *Curr Top Dev Biol* 90: 1-41.
- Vincentz, J. W., Barnes, R. M., Rodgers, R., Firulli, B. A., Conway, S. J. and Firulli, A. B. (2008) 'An absence of Twist1 results in aberrant cardiac neural crest morphogenesis', *Dev Biol* 320(1): 131-9.
- Vincentz, J. W., Barnes, R. M. and Firulli, A. B. (2011) 'Hand factors as regulators of cardiac morphogenesis and implications for congenital heart defects', *Birth Defects Res A Clin Mol Teratol* 91(6): 485-94.
- Visel, A., Minovitsky, S., Dubchak, I. and Pennacchio, L. A. (2007) 'VISTA Enhancer Browser--a database of tissue-specific human enhancers', *Nucleic Acids Res* 35(Database issue): D88-92.
- Visel, A., Blow, M. J., Li, Z., Zhang, T., Akiyama, J. A., Holt, A., Plajzer-Frick, I., Shoukry, M., Wright, C., Chen, F. et al. (2009a) 'ChIP-seq accurately predicts tissue-specific activity of enhancers', *Nature* 457(7231): 854-8.
- Visel, A., Rubin, E. M. and Pennacchio, L. A. (2009b) 'Genomic views of distant-acting enhancers', *Nature* 461(7261): 199-205.
- Vo, N., Dalton, R., Liu, N., Olson, E. and Goodman, R. (2010) 'Affinity purification of microRNA-133a with the cardiac transcription factor, Hand2', *Proc Natl Acad Sci U S A* 107(45): 19231-6.
- Vokes, S. A., Ji, H., Wong, W. H. and McMahon, A. P. (2008) 'A genome-scale analysis of the cis-regulatory circuitry underlying sonic hedgehog-mediated patterning of the mammalian limb', *Genes & development* 22(19): 2651-63.
- von Both, I., Silvestri, C., Erdemir, T., Lickert, H., Walls, J. R., Henkelman, R. M., Rossant, J., Harvey, R. P., Attisano, L. and Wrana, J. L. (2004) 'Foxh1 is essential for development of the anterior heart field', *Dev Cell* 7(3): 331-45.
- von Gise, A. and Pu, W. T. (2012) 'Endocardial and epicardial epithelial to mesenchymal transitions in heart development and disease', *Circ Res* 110(12): 1628-45.
- Vrljicak, P., Cullum, R., Xu, E., Chang, A. C., Wederell, E. D., Bilenky, M., Jones, S. J., Marra, M. A., Karsan, A. and Hoodless, P. A. (2012) 'Twist1 transcriptional targets in the developing atrio-ventricular canal of the mouse', *PLoS One* 7(7): e40815.

- Waldo, K., Kumiski, D., Wallis, K., Stadt, H., Hutson, M., Platt, D. and Kirby, M. (2001) 'Conotruncal myocardium arises from a secondary heart field', *Development* 128(16): 3179-88.
- Wamstad, J. A., Wang, X., Demuren, O. O. and Boyer, L. A. (2014) 'Distal enhancers: new insights into heart development and disease', *Trends Cell Biol* 24(5): 294-302.
- Wang, D., Chang, P., Wang, Z., Sutherland, L., Richardson, J., Small, E., Krieg, P. and Olson, E. (2001) 'Activation of Cardiac Gene Expression by Myocardin, a Transcriptional Cofactor for Serum Response Factor', *Cell* 105(7): 851-862.
- Wang, Y., Wu, B., Chamberlain, A., Lui, W., Koirala, P., Susztak, K., Klein, D., Taylor, V. and Zhou, B. (2013) 'Endocardial to myocardial notch-wnt-bmp axis regulates early heart valve development.', *PLoS One* 8(4): e60244.
- Wang, Z., Wang, D. Z., Pipes, G. C. and Olson, E. N. (2003) 'Myocardin is a master regulator of smooth muscle gene expression', *Proc Natl Acad Sci U S A* 100(12): 7129-34.
- Watanabe, Y., Miyagawa-Tomita, S., Vincent, S. D., Kelly, R. G., Moon, A. M. and Buckingham, M. E. (2010) 'Role of mesodermal FGF8 and FGF10 overlaps in the development of the arterial pole of the heart and pharyngeal arch arteries', *Circ Res* 106(3): 495-503.
- Watanabe, Y., Zaffran, S., Kuroiwa, A., Higuchi, H., Ogura, T., Harvey, R. P., Kelly, R. G. and Buckingham, M. (2012) 'Fibroblast growth factor 10 gene regulation in the second heart field by Tbx1, Nkx2-5, and Islet1 reveals a genetic switch for down-regulation in the myocardium', *Proc Natl Acad Sci U S A* 109(45): 18273-80.
- Wilczynski, B. and Furlong, E. E. (2010) 'Dynamic CRM occupancy reflects a temporal map of developmental progression', *Mol Syst Biol* 6: 383.
- Wills, A. A., Holdway, J. E., Major, R. J. and Poss, K. D. (2008) 'Regulated addition of new myocardial and epicardial cells fosters homeostatic cardiac growth and maintenance in adult zebrafish', *Development* 135(1): 183-92.
- Wren, C., Irving, C. A., Griffiths, J. A., O'Sullivan, J. J., Chaudhari, M. P., Haynes, S. R., Smith, J. H., Hamilton, J. R. and Hasan, A. (2012) 'Mortality in infants with cardiovascular malformations', *Eur J Pediatr* 171(2): 281-7.
- Wu, B., Wang, Y., Lui, W., Langworthy, M., Tompkins, K. L., Hatzopoulos, A. K., Baldwin, H. S. and Zhou, B. (2011) 'Nfatc1 coordinates valve endocardial cell lineage development required for heart valve formation', *Circ Res* 109(2): 183-92.
- Wu, B., Zhang, Z., Lui, W., Chen, X., Wang, Y., Chamberlain, A. A., Moreno-Rodriguez, R. A., Markwald, R. R., O'Rourke, B. P., Sharp, D. J. et al. (2012) 'Endocardial cells form the coronary arteries by angiogenesis through myocardial-endocardial VEGF signaling', *Cell* 151(5): 1083-96.
- Wu, S., Dong, X., Regan, J., Su, C. and Majesky, M. (2013) 'Tbx18 regulates development of the epicardium and coronary vessels', *Dev Biol* 383(2): 307-320.
- Wu, S. M., Fujiwara, Y., Cibulsky, S. M., Clapham, D. E., Lien, C. L., Schultheiss, T. M. and Orkin, S. H. (2006) 'Developmental origin of a bipotential myocardial and smooth muscle cell precursor in the mammalian heart', *Cell* 127(6): 1137-50.
- Xin, M., Olson, E. N. and Bassel-Duby, R. (2013) 'Mending broken hearts: cardiac development as a basis for adult heart regeneration and repair', *Nat Rev Mol Cell Biol* 14(8): 529-41.
- Xiong, W., He, F., Morikawa, Y., Yu, X., Zhang, Z., Lan, Y., Jiang, R., Cserjesi, P. and Chen, Y. (2009) 'Hand2 is required in the epithelium for palatogenesis in mice', *Dev Biol* 330(1): 131-41.

- Xu, H., Morishima, M., Wylie, J. N., Schwartz, R. J., Bruneau, B. G., Lindsay, E. A. and Baldini, A. (2004) 'Tbx1 has a dual role in the morphogenesis of the cardiac outflow tract', *Development* 131(13): 3217-27.
- Yamada, M., Revelli, J. P., Eichele, G., Barron, M. and Schwartz, R. J. (2000) 'Expression of chick Tbx-2, Tbx-3, and Tbx-5 genes during early heart development: evidence for BMP2 induction of Tbx2', *Dev Biol* 228(1): 95-105.
- Yamagishi, H., Yamagishi, C., Nakagawa, O., Harvey, R. P., Olson, E. N. and Srivastava, D. (2001) 'The combinatorial activities of Nkx2.5 and dHAND are essential for cardiac ventricle formation', *Dev Biol* 239(2): 190-203.
- Yamamura, H., Zhang, M., Markwald, R. R. and Mjaatvedt, C. H. (1997) 'A heart segmental defect in the anterior-posterior axis of a transgenic mutant mouse', *Dev Biol* 186(1): 58-72.
- Yanagisawa, H., Clouthier, D., Richardson, J., Charité, J. and Olson, E. (2003) 'Targeted deletion of a branchial arch-specific enhancer reveals a role of dHAND in craniofacial development', *Development* 130(6): 1069-1078.
- Yanez-Cuna, J. O., Dinh, H. Q., Kvon, E. Z., Shlyueva, D. and Stark, A. (2012) 'Uncovering cis-regulatory sequence requirements for context-specific transcription factor binding', *Genome research* 22(10): 2018-30.
- Yang, X., Li, C., Herrera, P. L. and Deng, C. X. (2002) 'Generation of Smad4/Dpc4 conditional knockout mice', *Genesis* 32(2): 80-1.
- Yao, T. P., Oh, S. P., Fuchs, M., Zhou, N. D., Ch'ng, L. E., Newsome, D., Bronson, R. T., Li, E., Livingston, D. M. and Eckner, R. (1998) 'Gene dosage-dependent embryonic development and proliferation defects in mice lacking the transcriptional integrator p300', *Cell* 93(3): 361-72.
- Yelbuz, T., Waldo, K., Kumiski, D., Stadt, H., Wolfe, R., Leatherbury, L. and Kirby, M. (2002) 'Shortened Outflow Tract Leads to Altered Cardiac Looping After Neural Crest Ablation', *Circulation* 106(4): 504-510.
- Yelon, D., Baruch, T., Halpern, M. E., Ruvinsky, I., Ho, R. K., Silver, L. M. and Stainier, D. Y. R. (2000) 'The bHLH transcription factor Hand2 plays parallel roles in zebrafish heart and pectoral fin development', *Development* 127: 2573-2582.
- Yin, C., Kikuchi, K., Hochgreb, T., Poss, K. D. and Stainier, D. Y. (2010) 'Hand2 regulates extracellular matrix remodeling essential for gut-looping morphogenesis in zebrafish', *Dev Cell* 18(6): 973-84.
- Zaffran, S. and Frasch, M. (2002) 'Early Signals in Cardiac Development', *Circ Res* 91(6): 457-469.
- Zaffran, S., Kelly, R. G., Meilhac, S. M., Buckingham, M. E. and Brown, N. A. (2004) 'Right ventricular myocardium derives from the anterior heart field', *Circ Res* 95(3): 261-8.
- Zang, M. X., Li, Y., Wang, H., Wang, J. B. and Jia, H. T. (2004) 'Cooperative interaction between the basic helix-loop-helix transcription factor dHAND and myocyte enhancer factor 2C regulates myocardial gene expression', *J Biol Chem* 279(52): 54258-63.
- Zeller, R. and Zuniga, A. (2007) 'Shh and Gremlin1 chromosomal landscapes in development and disease', *Curr Opin Genet Dev* 17(5): 428-34.
- Zeller, R., Lopez-Rios, J. and Zuniga, A. (2009) 'Vertebrate limb bud development: moving towards integrative analysis of organogenesis', *Nat Rev Genet* 10(12): 845-58.

- Zhang, L., Nomura-Kitabayashi, A., Sultana, N., Cai, W., Cai, X., Moon, A. and Cai, C. (2014) 'Mesodermal Nkx2.5 is necessary and sufficient for early second heart field development', *Dev Biol* 390(1): 68-79.
- Zhang, W., Chen, H., Wang, Y., Yong, W., Zhu, W., Liu, Y., Wagner, G. R., Payne, R. M., Field, L. J., Xin, H. et al. (2011) 'Tbx20 transcription factor is a downstream mediator for bone morphogenetic protein-10 in regulating cardiac ventricular wall development and function', *J Biol Chem* 286(42): 36820-9.
- Zhang, X., Guo, C., Chen, Y., Shulha, H. P., Schnetz, M. P., LaFramboise, T., Bartels, C. F., Markowitz, S., Weng, Z., Scacheri, P. C. et al. (2008a) 'Epitope tagging of endogenous proteins for genome-wide ChIP-chip studies', *Nat Methods* 5(2): 163-5.
- Zhang, Y., Liu, T., Meyer, C. A., Eeckhoute, J., Johnson, D. S., Bernstein, B. E., Nusbaum, C., Myers, R. M., Brown, M., Li, W. et al. (2008b) 'Model-based analysis of ChIP-Seq (MACS)', *Genome Biol* 9(9): R137.
- Zhao, Y., Samal, E. and Srivastava, D. (2005) 'Serum response factor regulates a muscle-specific microRNA that targets Hand2 during cardiogenesis', *Nature* 436(7048): 214-20.
- Zhou, W., Lin, L., Majumdar, A., Li, X., Zhang, X., Liu, W., Etheridge, L., Shi, Y., Martin, J., Van de Ven, W. et al. (2007) 'Modulation of morphogenesis by noncanonical Wnt signaling requires ATF/CREB family-mediated transcriptional activation of TGFbeta2', *Nat Genet* 39(10): 1225-1234.
- Zuniga, A., Haramis, A. P., McMahon, A. P. and Zeller, R. (1999) 'Signal relay by BMP antagonism controls the SHH/FGF4 feedback loop in vertebrate limb buds', *Nature* 401(6753): 598-602.
- Zuniga, A., Michos, O., Spitz, F., Haramis, A. P., Panman, L., Galli, A., Vintersten, K., Klasen, C., Mansfield, W., Kuc, S. et al. (2004) 'Mouse limb deformity mutations disrupt a global control region within the large regulatory landscape required for Gremlin expression', *Genes & development* 18(13): 1553-64.
- Zuniga, A., Laurent, F., Lopez-Rios, J., Klasen, C., Matt, N. and Zeller, R. (2012) 'Conserved cis-regulatory regions in a large genomic landscape control SHH and BMP-regulated Gremlin1 expression in mouse limb buds', *BMC Dev Biol* 12(1): 23.

12. Appendixes

12.1. Generation of *Smad4*^{3xFLAG} mice using dRMCE

12.1.1. Testing three epitope-tagged versions of SMAD4 in ES cells

The first attempt to generate a mouse with an epitope tag fused in frame in the *Smad4* coding sequence was done using dRMCE. This technique is based on dual recombination of the *loxP* and *FRT* sites present in numerous conditional alleles available as ES cell lines, for example from the EUCOMM and IKMC consortium (Osterwalder et al., 2010a). The co-electroporation of the pDIRE vector coding for the iCre and FLPo recombinases together with a pDREV targeting vector is designed to insert an epitope tag, a mutation or a reporter in a specific floxed locus at much higher efficiencies than homologous recombination (Osterwalder et al., 2010a).

Several epitope-tagged versions of SMAD4 had been generated and used mainly for *in-vitro* expression studies in various cell lines over the past decades, without a consistent position of the epitope tag relative to the N-term or the C-term extremities of the protein. The choice of the epitope tag and its positions are important points to avoid potential interference with the physiological function of the target transcription factor. We thus took advantage of the high targeting efficiency with dRMCE to test three different epitope tags and assess their sensitivity and specificity before deciding which one using to generate a *Smad4* epitope-tagged mouse strain. The three different epitope tags (FLAG, HA and V5) were inserted in frame of the C-terminal part of SMAD4 and multimerized (3x) to increase detection sensitivity (3xFLAG, 3xHA and 3xV5). *In silico* comparison of SMAD4 3D structure with the predicted 3D structures of the three different versions of the SMAD4^{3xTAG} protein using I-TASSER (Roy et al., 2010) did not show significant alteration in the conformation of the epitope tagged protein (data not shown). Overexpression of the three versions of the SMAD4^{3xTAG} protein in HEK293 cells showed that the three epitope tags are efficiently detected with high sensitivity using specific antibodies (data not shown).

For dRMCE mediated cassette exchange, we used an existing floxed *Smad4* knockout-first tm1a allele generated by IKMC. This allele encodes a promotorless gene-trap selection cassette flanked by FRT sites, which is followed by loxP sites flanking *Smad4* exon 9 (*S4*^{EC} allele, Fig.30A).

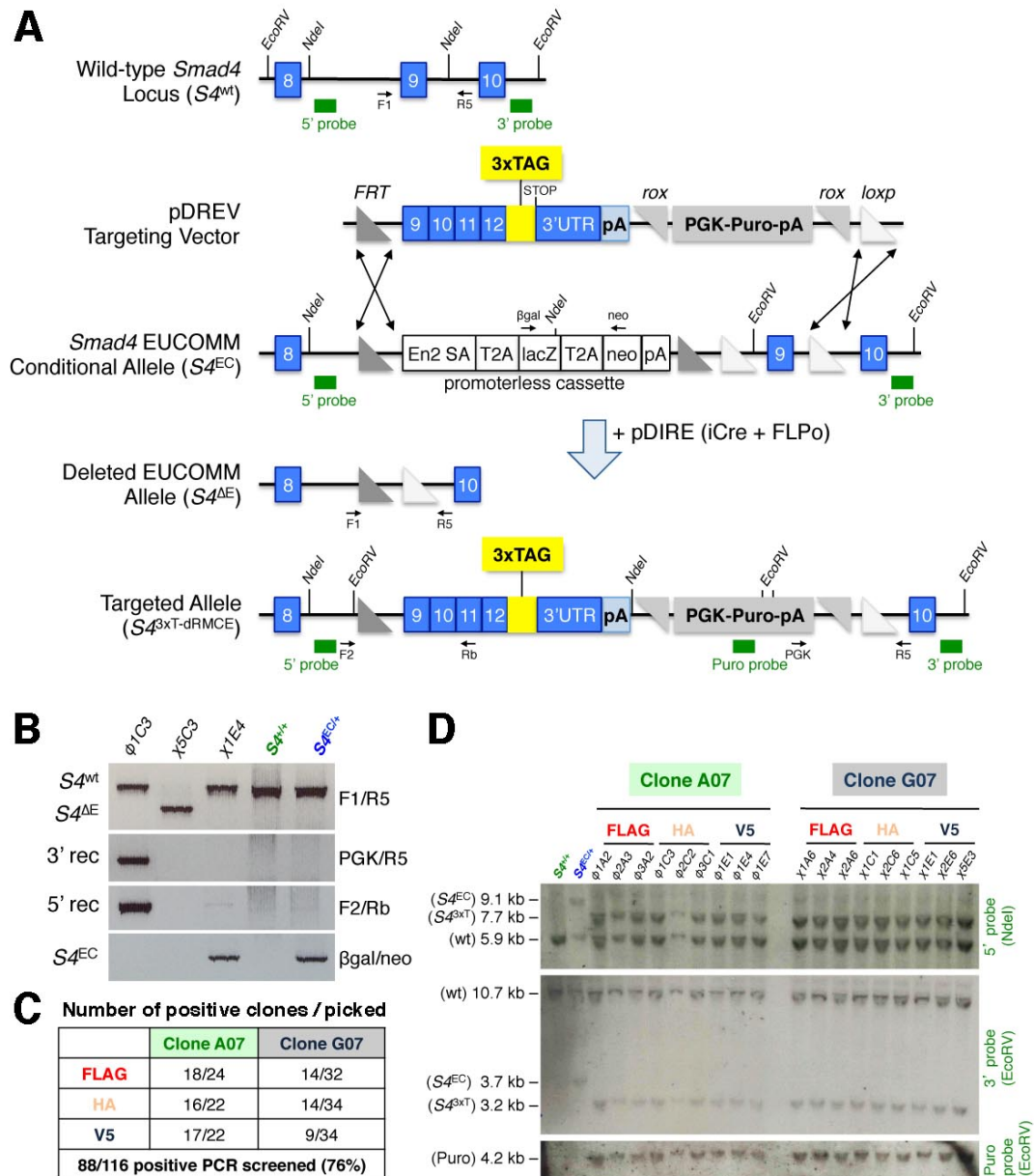


Figure 30. Dual recombinase-mediated cassette exchange in mouse ES cells to engineer a *Smad4*^{3xTAG} allele

(A) dRMCE targeting strategy. From top to bottom: the *Smad4* wild-type allele ($S4^{wt}$). The pDREV targeting vector containing a *FRT* site, *Smad4* exons 9-12, 3 different versions of a 3x epitope tag (3xFLAG, 3xHA or 3xV5) fused in frame to *Smad4* exon 12, a STOP codon, *Smad4* 3'UTR, SV40 pA signal, a Puromycin selection cassette flanked by *rox* sites, and a *loxP* site. The *Smad4* EUCOMM conditional allele with a promoterless cassette flanked by *FRT* sites and *Smad4* exon 9 flanked by *loxP* sites ($S4^{EC}$). The *Smad4* deleted EUCOMM allele following double iCre and FLPo recombination without insertion of a targeting element ($S4^{AE}$). The *Smad4* targeted allele with dRMCE-mediated insertion of the targeting element from pDREV between the *FRT* and *loxP* sites ($S4^{3xT-dRMCE}$). The primers for PCR screening are indicated with arrows. The restriction sites used for Southern Blot are indicated in italics, and the Southern Blot probes are shown as green boxes. (B) PCR screening analysis of all *Smad4* alleles. Primers used for each reaction are indicated on the right. For the $S4^{3xT-dRMCE}$ allele, the screening was performed both on the 3' and on the 5' sides. Clone Φ 1C3 is a

positively targeted clone, χ 5C3 is a $S4^{\Delta E/+}$ clone, and χ 1E4 a parental $S4^{EC/+}$ clone. $S4^{+/+}$ (green) and $S4^{EC/+}$ (blue) ES cells were used as controls. (C) Table showing the number of PCR positive clones in relation to the total number of clones picked. In total, 116 of 168 ES cell clones were screened by PCR. 88 ES cell clones were correctly targeted on both 3' and 5' sides. (D) Southern Blot analysis for three ES cell clones of each replacement. $S4^{+/+}$ (green) and $S4^{EC/+}$ (blue) ES cells were used as controls. Top panel: ES cells DNA was digested with NdeI and blotted with the 5' probe shown in (A). The sizes of the expected $S4^{wt}$, $S4^{EC}$ or $S4^{3xT-dRMCE}$ bands are indicated on the left. Middle panel: EcoRV digestion in combination with the 3' probe. Lower panel: detection of the Puro cassette after EcoRV digestion.

Two ES cell clones of this EUCOMM conditional allele were used and targeted in parallel (A07 and G07). The targeting vector was designed to replace the promoterless cassette and exon 9 of the $S4^{EC}$ allele with the coding sequence of exon 9-12 with an in frame 3x epitope TAG, a STOP codon, the endogenous *Smad4* 3'UTR and a polyadenylation site from SV40. These modifications are followed by a Puromycin selection cassette that is flanked by *rox* sites (Fig.30A). Following electroporation and Puromycin selection, 168 ES cell clones were picked (together with M.Osterwalder). Screening of positively targeted clones was done by PCR to discriminate between the different possible recombination events and the parental allele (Fig.30A,B). For the six conditions (two ES cell clones and three different tags), 76% of the 116 screened ES cell clones were correctly exchanged (Fig.30C). This percentage is very close to the 69% obtained in a previous targeting of the $S4^{EC}$ allele (Osterwalder et al., 2010a). Southern Blot analysis using probes for both the 5' and 3' arms of the exchanged region and a probe detecting the Puro cassette confirmed correct recombination and single insertion of the targeting construct in all tested clones (Fig.30D). For each condition, three clones with normal karyotypes were analyzed further (data not shown).

The three versions of the epitope-tagged SMAD4 proteins were detected in ES cells using specific antibodies. This showed that tagged SMAD4 was best detected by using the 3xFLAG and 3xV5 epitope tags (Fig.31A). As the *Hand2*^{3xFLAG} allele had produced high quality ChIP-Seq data from limb buds (Osterwalder et al., in press), we selected the *Smad4*^{3xFLAG} allele for further analysis. As immunoprecipitation is the crucial step in the ChIP-Seq process, we used the anti-FLAG M2 antibody to establish its ability to IPP the SMAD4^{3xFLAG} protein (Fig.31B).

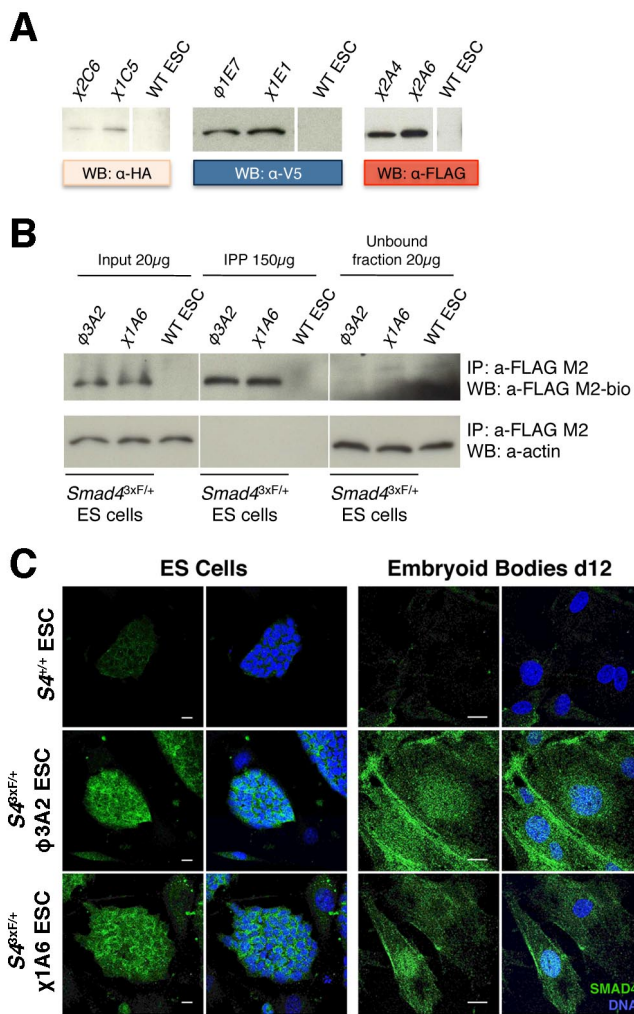


Figure 31. Detection tests of SMAD4^{3xTAG} in ES cells

(A) Western Blot detection of SMAD4^{3xHA} (left), SMAD4^{3xV5} (middle) and SMAD4^{3xFLAG} (right) in protein extracts of two different S4^{3xT-dRMCE/+} ES cell clones each. Wild-type ES cells were included as controls. SMAD4^{3xTAG} size: ~63kDa. (B) Immunoprecipitation using the anti-FLAG M2 antibody on two S4^{3xF-dRMCE/+} ES cell clones and wild-type cells. The top panel is blotted with a biotinylated anti-FLAG antibody and the lower panel with an anti-Actin antibody (size: 42kDa). On the left, 20 μ g of protein extracts were loaded as input controls. In the middle, the whole immunoprecipitate from 150 μ g of total proteins (1 μ g/ μ l) was loaded. On the right, 20 μ l of the unbound fraction after the IPP were loaded. The SMAD4^{3xFLAG} protein is detected in the input and IPP samples of the S4^{3xF-dRMCE/+} clones. All SMAD4^{3xFLAG} protein was immunoprecipitated as revealed by its absence in the unbound fraction (top right panel). ACTIN was used as a loading control and is present in similar amounts in all samples. (C) Immunofluorescence detection of the

SMAD4^{3xFLAG} protein in undifferentiated ES cells (left panels) and after twelve days of differentiation into embryoid bodies (right panels). Two different S4^{3xF-dRMCE/+} ES cell clones were analyzed together with wild-type controls. Green: SMAD4^{3xFLAG}. Blue: Hoechst: Scale bar: 20 μ m.

Finally, as SMAD4 is shuttling between cytoplasm and nucleus following activation of BMP signal transduction, immunocytochemistry was used to assess its cellular localization. In undifferentiated ES cells, the SMAD4^{3xFLAG} protein was detected both in the cytoplasm and in the nuclei (Fig.31C, left panel). Previous studies had shown that BMP signaling and consequential phosphorylation and nuclear translocation of SMAD1/5 are higher in differentiated ES cells (Fei et al., 2010; Galvin et al., 2010; James et al., 2005). Therefore, the SMAD4^{3xFLAG} protein distribution was assessed in embryoid bodies after 12 days of differentiation, at which *Smad4* transcripts levels are the highest (M.O., unpublished result). Consistent with activation of BMP signal transduction in differentiating ES cells, we observed an increase in nuclear

SMAD4^{3xFLAG} proteins in comparison to undifferentiated ES cells (Fig.31C, right panel). We thus concluded that the SMAD4^{3xFLAG} protein was functional.

12.1.2. Embryonic lethality of *Smad4*^{3xFLAG} homozygous embryos

Three different *Smad4*^{3xFLAG/+} ES cells clones (C57BL/6 background) were injected into BALB/c blastocysts at the Transgenic Mouse Core Facility (TMCF, Basel). Only one 80% chimeric male was obtained from clone Φ 3A2 and no chimeras were obtained from the other two clones. This chimeric male was mated to C57BL/6 females and germline transmission was observed in 6% of the offspring and confirmed by PCR genotyping (see primers F2/R2 in Fig.32F). As *Smad4* is ubiquitously expressed, we could efficiently detect the SMAD4^{3xFLAG} protein from various embryonic tissues by Western Blot analysis of heterozygous embryos (E11.5, Fig.32A). Anti-FLAG immunoprecipitation from embryonic forelimbs of *S4*^{3xFLAG/+} also established highly efficient and clear IP of SMAD4^{3xFLAG} proteins (E11.5, Fig.32B).

Next, we wanted to assess a candidate direct target of SMAD4 by ChIP-qPCR in limb buds using the *Smad4*^{3xFLAG} allele. A good candidate is the BMP Responsive Element (BRE) located in the proximal promoter of *Id1*. The expression of *Id1* is cleared from *Smad4* ^{Δ/Δ} limb buds (E.P, unpublished result), and SMAD4 interacts *in vitro* with this BRE (Korchynskiy and ten Dijke, 2002; Lopez-Rovira et al., 2002; Katagiri et al., 2002). This conserved BRE overlaps with a DNase HS region (ENCODE/UW) and a p300 ChIP-Seq peak in forelimb buds (E11.5) (Visel et al., 2009a) (Fig.32C, left panel). Therefore, we assessed if the SMAD4^{3xFLAG} protein was interacting *in vivo* with this BRE by ChIP-qPCR from pooled wild-type and *Smad4*^{3xFLAG/+} embryonic limb buds versus wild-type limb buds (E11.75, Fig.32C, right panel). We observed a small ~3x fold enrichment of *Id1* BRE in the FLAG sample.

In parallel, we attempted to generate homozygous *Smad4*^{3xFLAG/3xFLAG} mice. However, we observed that this was not possible due to early embryonic lethality similar to the lethality of *Smad4* ^{Δ/Δ} embryos at E7.5 (Fig.32D, (Sirard et al., 1998). The likely explanation for this lethality is that the *S4*^{3xFLAG-dRMCE} allele was somehow damaged and its expression reduced to low levels. Indeed, quantification of the expression of *Smad4* by RT-qPCR in embryonic limb buds showed that this was the case (E11.0, Fig.32E).

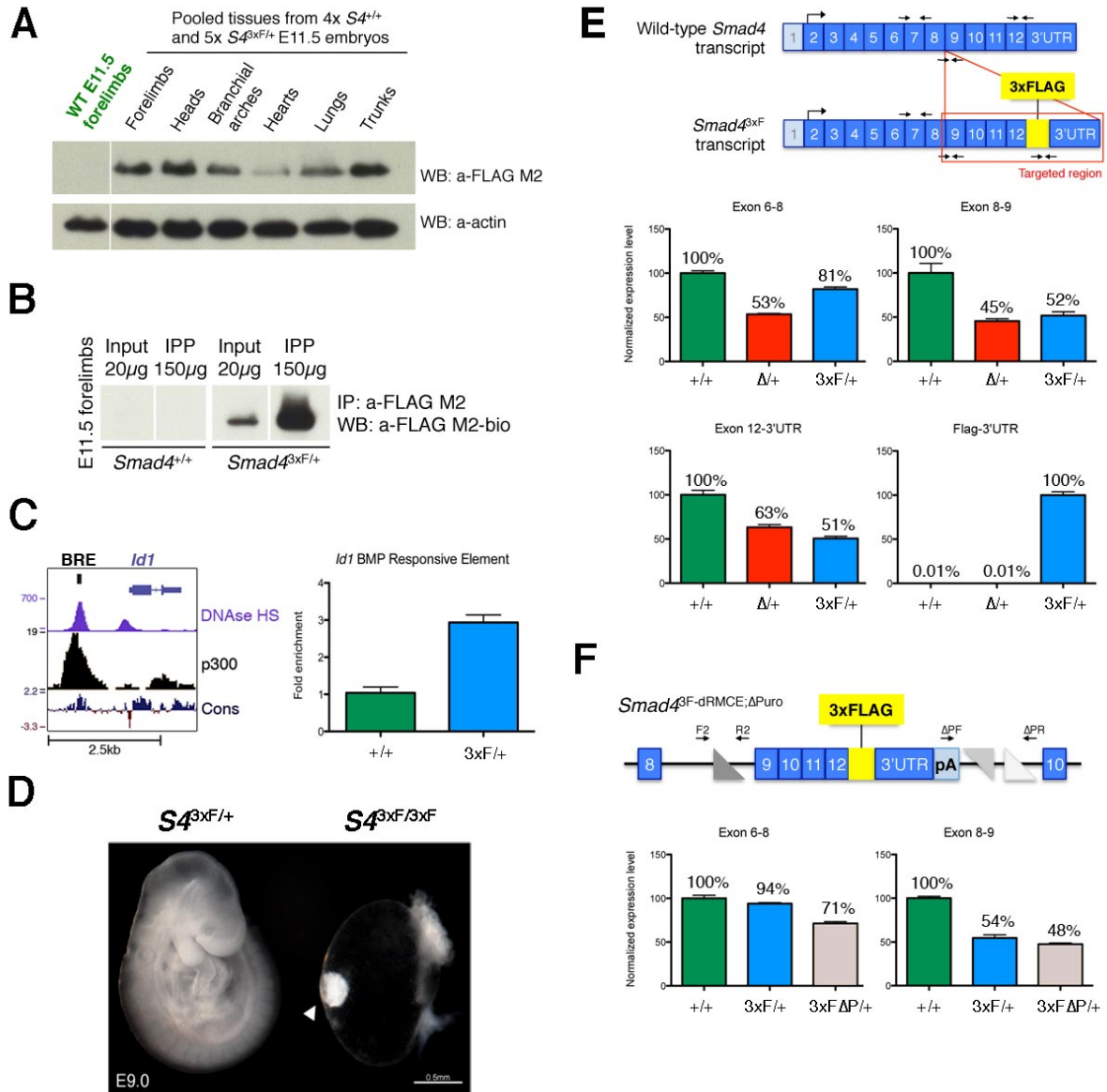


Figure 32. Expression of the $Smad4^{3xFLAG}$ allele in mouse embryos

(A) Western Blot detection of SMAD4^{3xFLAG} (top panel) and Actin (lower panel) from protein extracts of various embryonic tissues from a pool of $S4^{+/+}$ and $S4^{3xFLAG/+}$ embryos at E11.5. Protein extracts from wild-type forelimbs at E11.5 were used as a control (green). (B) Immunoprecipitation analysis from forelimb buds at E11.5. (C) Anti-FLAG ChIP from $S4^{+/+}$ and $S4^{3xFLAG/+}$ E11.75 forelimbs. Left panel: UCSC browser window representing the BMP Responsive Element (BRE) located -1.1kb from $Id1$ TSS (black box). DNase HS and p300 ChIP-Seq profile from E11.5 limb buds are displayed above the placental mammal conservation (Cons) plot. Right panel: ChIP-qPCR for $Id1$ BRE in $S4^{+/+}$ (green) and $S4^{3xFLAG/+}$ (blue) samples. Mean \pm SD (n=2) is shown. (D) Bright-field pictures of a $S4^{3xFLAG/+}$ embryo at E9.0 (left) and dead $S4^{3xFLAG/3xFLAG}$ embryo (right, white arrow). Scale bar: 0.5mm. (E) RT-qPCR analysis of $Smad4$ transcripts in limb buds at E11.0. Top panel: schematic representation of the $Smad4^{wt}$ and $Smad4^{3xFLAG}$ transcripts with the qPCR primers indicated by arrows. The area indicated by the red box in the $Smad4^{3xFLAG}$ transcript corresponds to the targeted region introduced by the pDREV vector. RT-qPCR amplification probed transcripts containing exons 6-8 (top left graph), exons 8-9 (top right graph), exon 12-3'UTR (bottom left graph) and Flag-3'UTR (bottom right graph) from the following genotypes: $S4^{+/+}$ (green), $S4^{\Delta/+}$ (red) and $S4^{3xFLAG/+}$ (blue). The normalized fold expression is indicated

above each bar relative to the $S4^{3xFL/+/}$ embryos (bottom right graph) or wild-type control. (F) *Smad4* transcripts levels following removal of the Puro cassette. Top panel: schematic representation of the $Smad4^{3xFL-dRMCE;\Delta Puro}$ allele obtained by mating $S4^{3xFL/+/}$ females with $Dre^{tg/+}$ males. F2/R2: primers used to genotype $Smad4^{3xFLAG}$ versus $Smad4^{wt}$ allele. $\Delta PF/\Delta PR$: primers used to genotype $Smad4^{3xFL-dRMCE;\Delta Puro}$ allele. Bottom panel: RT-qPCR in limb buds at E11.75 to detect *Smad4* transcripts encoding exons 6-8 (left) and exons 8-9 (right). The following genotypes were used: $S4^{+/+}$ (green), $S4^{3xFL/+/}$ (blue) and $S4^{3xFL-\Delta P/+}$ (grey). Normalized fold expression levels are indicated above each bar relative to the wild-type control.

Assessing *Smad4* expression at the junction between exons 6-8 (i.e. outside of the targeted region) and at the exons 8-9 junction (i.e. in the targeted region) showed that $Smad4^{\Delta/+}$ embryos (Fig.32E, red) have ~50% of transcripts in comparison to $Smad4^{+/+}$ embryos (Fig.32E, green). While the expression of coding exons 6-8 in $Smad4^{3xFLAG/+}$ embryos was reduced to 81% (Fig.32E, top left panel, blue), the expression of exons 8-9 dropped to 52% in $Smad4^{3xFLAG/+}$ embryos, similar to $Smad4^{\Delta/+}$ embryos (Fig.32E, top right panel, blue). These results and others established that the $S4^{3xFLAG-dRMCE}$ allele is severely hypomorphic, as the majority of the $S4^{3xFLAG-dRMCE}$ transcripts appear truncated in the crucial 3' part. The small fraction of full-length transcripts is sufficient to produce SMAD4^{3xFLAG} proteins at levels detectable by Western Blot and IP analysis (Fig.32A and Fig.32B), but not sufficient to sustain the viability of homozygous embryos (Fig.32D).

As the presence of the neighboring Puromycin selection cassette in the $S4^{3xFLAG-dRMCE}$ allele (Fig.30A) could account for this reduction in transcription (Lewandoski, 2007), we used *Dre*-recombinase expressing mice to remove the *rox*-flanked PGK-Puro cassette (Anastassiadis et al., 2009). However, RT-qPCR analysis showed that the deletion of the Puro cassette did not rescue the expression levels of the $S4^{3xFLAG-dRMCE}$ allele and embryonic lethality of homozygous embryos (Fig.32F and data not shown).

The reduced transcription level in the targeted region of the locus is thus likely due to a defect in the $S4^{3xFLAG-dRMCE}$ allele itself. As the whole targeted region was fully sequenced and no mutation was detected, we suspect that the parental IKMC knockout-first conditional allele ($S4^{EC}$) could have already been damaged. The automated, computer-assisted design of the targeting vector used to generate IKMC

alleles could introduce errors that cannot be detected until the knockout-first conditional allele is tested (Skarnes et al., 2011). In particular, we realized that the FRT-promoterless cassette-loxP is inserted in *Smad4* intron 8-9 close to the 5' end of exon 9. Thus, the presence of the remaining FRT site in this intron in the targeted allele may affect the correct splicing of this region. Such incorrectly spliced transcripts could be eliminated by nonsense-mediated RNA decay, resulting in the observed reduction in the amount of transcripts coding exons 8-9 (not shown) and 9-10 (Fig.32E). Alternatively, the presence of the FRT site in intron 8-9 could have generated a cryptic polyA signal, leading to a majority of transcripts truncated after exon 8. These two possibilities have not been investigated further but provide potential explanations for the observed severe hypomorphic phenotype.

As the *Smad4*^{3xFLAG-dRMCE} allele is not expressed at wild-type levels, we tested another cassette exchange strategy. We introduced the whole coding sequence and endogenous promoter of *Smad4* with the 3xFLAG epitope tag in the non-essential *Rosa26* locus using ES cells previously engineered for efficient RMCE (Tsanov et al., 2012). The resulting *Smad4*^{3xFLAG-R26} allele was expressed at levels lower than the *Smad4*^{3xFLAG-dRMCE} allele in ES cells (data not shown), and we decided to resort to conventional homologous recombination to generate a normally expressed *Smad4*^{3xFLAG} allele (see chapter 6.1.5).

12.2. Additional methods relative to the dRMCE targeting

12.2.1. Construction of the pcDNA3 *Smad4*^{3xTag} expression vectors

The *Smad4* coding sequence (CS) was first amplified by PCR using primers to introduce an *Asp718* and *NarI* restriction sites at the 5'- and 3'- ends, respectively. A Kozak sequence (GCCGCCACC) was introduced as part of the 5' primer between the *Asp718* site and *Smad4* ATG codon to enhance translation. This *Asp718-Smad4* CS-*NarI* fragment was inserted into a pBluescript II KS (pBSK, Stratagene) backbone vector previously constructed by J.Lopez-Rios (unpublished data) in frame with an epitope tag followed by a STOP codon. Two versions of this vector were used, one carrying a 3xFLAG and one with a 3xHA epitope tag. The whole *Smad4* CS-3xTag-STOP fragments from the pBSK-*Smad4*^{3xFLAG} and pBSK-*Smad4*^{3xHA} plasmids were then transferred into the pcDNA3 (Invitrogen) mammalian expression vector as an

Asp718-EcoRI fragment. This resulted in the pcDNA3 *Smad4*^{3xFLAG} and pcDNA3 *Smad4*^{3xHA} expression vectors (Fig.33). A pcDNA3 vector expressing *Smad4* with 3xV5 epitope tag was also constructed (see below).

12.2.2. Construction of the pDREV *Smad4*^{3xTag} targeting vectors for dRMCE

Three versions of the pDREV targeting vector for dRMCE were constructed using the three different epitope tags (3xFLAG, 3x HA and 3xV5). All were designed to target the promoterless cassette of the knockout first *Smad4*^{tm1a(EUCOMM)Wtsi} allele in ES cells by dual Recombinase Mediated Cassette Exchange (dRMCE, see (Osterwalder et al., 2010a)). First, a synthetic fragment containing a part of *Smad4* intron 9/10, the cDNA of coding exons 9-12, an in frame 3xV5 tag and a STOP codon was synthesized by GeneArt in the pMA vector (pMA-Tag). This fragment was flanked by *BstBI* restriction site on the 5' end and by a *EcoRI-MfeI-NdeI-PacI* polylinker on the 3' end. Subsequently, a *BamHI-EcoRI* fragment containing part of exon 12 and the 3xV5 tag was released from the pMA-Tag vector and introduced into the pcDNA3 expression vectors containing the *Smad4* CS to replace the 3xFLAG tag with the 3xV5 (pcDNA3-*Smad4*^{3xV5} expression vector). In addition, *BamHI-EcoRI* fragments containing part of exon 12 and the 3xFLAG or 3xHA epitope tags were released from the pBSK-*Smad4*^{3xTag} vectors and introduced into the pMA-Tag to replace the 3xV5 *BamHI-EcoRI* fragment. A PCR fragment encoding *Smad4* 3'UTR was amplified from cDNA with primers introducing *MfeI* and *NdeI* restriction sites on the 5'- and 3'- ends respectively. The *Smad4* 3'UTR was then cloned into the three different pMA-Tag vectors as an *MfeI-NdeI* fragment. Finally, a *BstBI-PacI* fragment containing the 3' part of *Smad4* coding sequence, the epitope tag and the 3'UTR was released from the three pMA-Tag vectors and transferred into the pDREV-0 targeting vector (Osterwalder et al., 2010a). These pDREV-*Smad4*^{3xTag} vectors were the ones used for dRMCE (Fig.33).

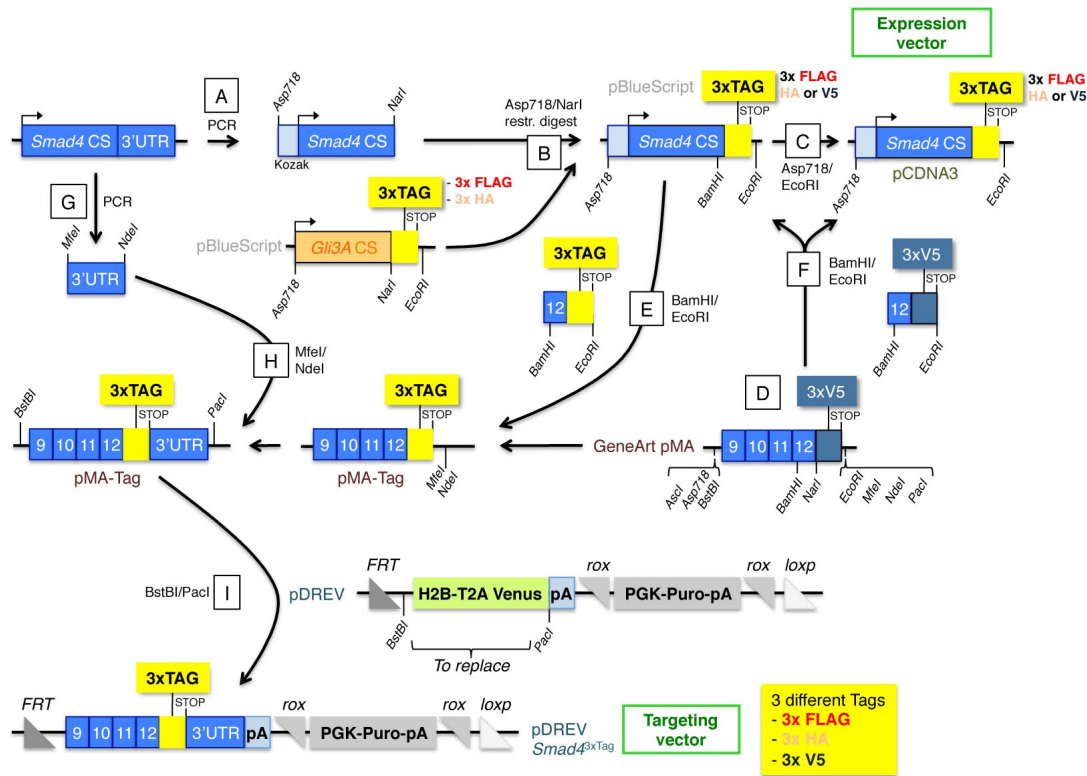


Figure 33. Generation of the pDREV-*Smad4*^{3xTag} targeting vectors for dRMCE and pCDNA3-*Smad4*^{3xTag} expression vectors

(A) The *Smad4* coding sequence was amplified by PCR and (B) inserted in the pBSK vector containing either a 3xFLAG or 3xHA epitope tag. (C) The expression vectors were generated by subcloning *Smad4* CS^{3xTag} into pCDNA3. (D) A synthetic fragment containing the 3' end of *Smad4* CS and a 3xV5 epitope tag was assembled by GeneArt in the pMA vector. (E) The fragments containing the 3xFLAG or 3xHA epitope tags were released from pBSK *Smad4* CS^{3xTag} and exchanged with the equivalent 3xV5 fragment in the pMA vector. (F) The *Smad4* CS^{3xV5} expression vector was generated by exchanging the 3xFLAG fragment with the 3xV5 fragment in the pCDNA3 vector. (G) The *Smad4* 3'UTR was amplified by PCR and (H) inserted in the three different types of pMA-Tag templates. (I) The fragment containing the 3' end of *Smad4* CS, the epitope tag and the 3'UTR was recovered from the three versions of pMA-Tag templates and introduced into the pDREV-0 targeting vector by replacing the H2B-T2A Venus cassette. See main text for details.

12.2.3. Transfection of HEK-293T cells

Human Embryonic Kidney 293T cells (HEK-293T) were cultured in DMEM containing 4.5g/l Glucose, 10% FCS, 100U-0.1mg/ml Pen Strep, 2mM L-Glutamine, 1x Non-essential Amino Acids, 1mM Sodium Pyruvate at 37°C with 5% CO₂. The pCDNA3-*Smad4*^{3xTag} expression vectors were transfected into 60-80% confluent HEK-293T cells grown in 6-well plates using the FuGENE[®]6 Transfection Reagent (Promega). The pEGFP vector was co-transfected to assess the transfection efficiency, and the

empty pCDNA3 vector was transfected as negative control. HEK-293T cells were collected for protein extraction 24hrs after transfection.

12.2.4. dRMCE: ES cells electroporation, selection and screening

Two clones of the JM8.F6 ES cells carrying the *Smad4* knockout first allele tm1a(EUCOMM)Wtsi (EUCOMM project ID 29509, called hereafter *Smad4* EUCOMM Conditional ($S4^{EC}$)) were targeted in parallel with the three versions of the pDREV-*Smad4*^{3xTag} vector. ES cells were cultured and expanded for electroporation as described in the chapter 9.2.3 (see also ((Osterwalder et al., 2010b)). Briefly, $S4^{EC/+}$ cells were co-electroporated with both a pDREV-*Smad4*^{3xTag} vector and the pDIRE vector, which encodes the iCre and Flpo recombinases for dRMCE (Osterwalder et al., 2010a). ES cells were selected for 9-11 days in 0.5 μ g/ml of Puromycin (Sigma P9620). After picking ES cell clones and expanding them in 48 well plates, a part of the ES cells were collected to isolate DNA while the remainder was further expanded. The ES cell clones were screened by PCR and negative or mixed clones were eliminated. Positive clones were expanded into 10cm dishes and frozen in aliquots.

The PCR screening strategy was designed to discriminate between the endogenous *Smad4* wild-type allele ($S4^{wt}$, primers F1/R5), the *Smad4* EUCOMM conditional allele ($S4^{EC}$, primers β gal/neo), the deleted EUCOMM allele ($S4^{\Delta E}$, primers F1/R5) and positively targeted *Smad4*^{3xTag-dRMCE} allele both on both sides of the cassette exchange (primers PGK/R5 and F2/Rb). Correct targeting of the *Smad4* locus was confirmed by Southern Blot analysis using both 5' and 3' probes and the Puromycin selection cassette. See Fig.30A for the location of the screening primers and Southern Blot probes; and chapter 12.2.6 for their sequences.

12.2.5. Differentiation of ES cells to embryoid bodies

Smad4^{3xFLAG-dRMCE/+} ES cells into embryoid bodies were differentiated using the protocol developed by (Kurosawa et al., 2003). 2×10^4 ES cells were resuspended in ES cell medium containing no LIF in order to induce differentiation and incubated at 37°C in low-adherence conical 1.5ml screw cap micro tube (Starstedt) for 5 days. The embryoid bodies were transferred to μ -Slide 8 well (Ibidi) and cultured for up to

two weeks. The medium was changed every second day, and differentiated embryoid bodies were fixed for immunocytochemical analysis.

12.2.6. dRMCE primers table

Smad4 dRMCE targeting - cloning primers				
Target	Primer		Used for	
S4_CS_Asp718	5'-ATAGGTACC GCCGCCACC ATG G GACAATATGTCTATAAC-3'		Forward for S4 CS with 5' Asp718 , Kozak , ATG	
S4_CS_NarI	5'-TAT GGCGCC GTCTAAAGGCTGTGGGTCC-3'		Reverse for S4 CS with 3' NarI	
S4_3UTR_MfeI	5'-TAT CAATTG GATCTCACACCACGGA-3'		Forward for S4 3'UTR with 5' MfeI	
S4_3UTR_NdeI	5'-TCG CATATG TTCGTATAGTGA CTCAG -3'		Reverse for S4 3'UTR with 3' NdeI	
Smad4 dRMCE targeting - screening primers				
Locus	Forward primer	Reverse primer	Size	Allele
<i>Smad4</i> F1-R5	5'-ACTAACTCTGTGTT CAGAGCCCCG -3'	5'-GCTGCCCAAATCAATAGCCA-3'	1265bp	<i>Smad4</i> Wt
<i>Smad4</i> F1-R5	5'-ACTAACTCTGTGTT CAGAGCCCCG -3'	5'-GCTGCCCAAATCAATAGCCA-3'	559bp	<i>Smad4</i> Δ EUCOMM
<i>Smad4</i> PGK-R5	5'-GCAAAACCAAATTAAGGGCCA-3'	5'-GCTGCCCAAATCAATAGCCA-3'	456bp	S4-3xTag 3' rec
<i>Smad4</i> F2-Rb	5'-GCAATCCAAACCAAGCATTGTC-3'	5'-CAGACAGACTGATGGCTGGA-3'	1395bp	S4 -3xTag 5' rec
bgal-neo	5'-AGCAGAGCGGGTAAACTGGC-3'	5'-GCATCAGAGCAGCCGATTGTC-3'	557bp	S4 EUCOMM conditional
Smad4 dRMCE targeting - Southern Blot probes primers				
Probe	Forward primer	Reverse primer	Size	
5' probe	5'-ATGCAAAAAAAAAAGCTTAAGGGG-3'	5'-TTATAGGCAAGAGTCAACTCAAAGA-3'	475bp	
3' probe	5'-GAGCACCACCACGGCAAAGT-3'	5'-TGTTGCCTGCTGGTAAGGAA-3'	487bp	
Puro probe	5'-GCAAAACCAAATTAAGGGCCA-3'	5'-GGCCTTCCATCTGTTGCTGC-3'	334bp	
Smad4 dRMCE - mice genotyping primers				
Locus	Forward primer	Reverse primer	Size	Allele
<i>Smad4</i>	5'-AACTAACTCTGTGTT CAGAGCCCCG -3'	5'-CAGGTGGATTTCATGAGATAGGC-3'	429bp + 536bp	Wt + 3xFlag
<i>Dre</i>	5'-TGCTGTTCCCTCCTATCCAC-3'	5'-CGGAGTCCATCAGCCTAGAG-3'	300bp	Tg
<i>Puromycin</i>	5'-GCAAAACCAAATTAAGGGCCA-3'	5'-GCTGCCCAAATCAATAGCCA-3'	456bp	Puro'
<i>S4-ΔPuro</i>	5'GGTTTGTCCAAACTCATCAATG-3'	5'GCTAAAACACAGCCTTGTTAAC-3'	498bp	ΔPuro

12.3. Manuscripts in preparation

“Mammalian NDR kinases are essential for cardiac development and impact on the Notch pathway”

Debora Schmitz-Rohmer¹, Simone Probst², Alexander Hergovich^{1,4}, Zhong-Zhou Yang³, Frédéric Laurent², Rolf Zeller² and Brian A. Hemmings¹

¹ Friedrich Miescher Institut for Biomedical Research, Maulbeerstrasse 66, CH-4058 Basel, Switzerland

² Department Biomedizin, Mattenstrasse 28, CH-4058 Basel, Switzerland

³ Model Animal Research Center of NanJing University, 12 Xue-Fu Road, Pukou District, NanJing, P.R. China 210061

⁴ current address: UCL Cancer Institut, University College London, London WC1E 6BT, United Kingdom

The aim of this project is to understand the roles of NDR1 and NDR2 kinases during mouse embryonic development by generating double knockout animals. Among other phenotypes, the heart tube of *Ndr*-deficient embryos does not loop and is filled with cells that obstruct the cardiac lumen and prevent blood flow. *Ndr*-deficient embryos die by E10.0 from cardiac insufficiency. I contributed to thy project by performing Optical Projection Tomography (OPT) analysis of wild-type and *Ndr*-deficient embryos at E7.75-E8.0. Analysis of virtual sections from 3D reconstructed embryos allowed better visualization of the cardiac obstruction phenotype observed in *Ndr*-deficient embryos.

“Generation of a bone organ *in vivo* through endochondral ossification by adipose-derived stromal cells”

Rik Osinga^{1,2}, Nunzia di Maggio², Nima Allafi¹, Andrea Barbero², Frédéric Laurent³, Dirk J. Schaefer¹, Ivan Martin², Arnaud Scherberich²

¹ Department of Plastic, Reconstructive, Aesthetic and Hand Surgery, University Hospital of Basel

² Laboratory of Tissue Engineering, Department of Surgery, University Hospital of Basel and Department of Biomedicine, University of Basel, Basel, Switzerland

³ Department of Biomedizin, Mattenstrasse 28, CH-4058 Basel, Switzerland

In this project, adipose-derived stromal cells (ASC) from human tissues were cultured in micromasses or on collagen scaffolds and implanted subcutaneously in nude mice to investigate their potential to form bone tissues by endochondral ossification. These pellets and scaffolds were harvested after a few weeks and sectioned for histological analysis. I performed *in situ* hybridization on some of these sections for the chondrocyte differentiation marker *Indian Hedgehog*.

12.4. Curriculum vitae

FREDERIC LAURENT

Date and place of birth 17th December 1984, Meyrin, Switzerland
Origin Fey (VD), Switzerland
Nationality Swiss, French and Italian
Address Florastrasse 25, 4057 Basel, Switzerland
Phone number +41 (0)79 718 55 61
E-mail frederic.laurent@unibas.ch

EDUCATION AND DIPLOMAS

- 2010 – 2014 University of Basel, Department of Biomedicine, Developmental Genetics group
PhD in Genetics
- 2007 – 2009 University of Lausanne, Faculty of Biology and Medicine, School of Biology
Master of Science in Genomics and Experimental Biology
- 2004 – 2007 University of Lausanne, Faculty of Biology and Medicine, School of Biology
Bachelor of Science in Biology
- 2000 – 2003 High school of Nyon – Matura School in Biology and Chemistry
Matura work: “Can we learn by role playing games?” – Grade excellent
Bachelor and Matura Certificate

RESEARCH EXPERIENCE

- 06/2010 – 09/2014 **PhD in Genetics**
Supervisor: Prof. Dr Rolf Zeller
Department of Biomedicine, University of Basel
“Identification of cis-regulatory modules in mouse embryonic limb buds and heart using endogenous epitope-tagged transcription factors”
- 02/2008 – 01/2009 **Master Thesis**
Supervisor: Dr Elena Buetti
Institute of Microbiology, University Hospital of the canton of Vaud (CHUV)
“Analysis of signaling pathways involved in the transcription of the Mouse Mammary Tumor Virus using mutant PKC δ and Src kinases”
- 02/2008 – 05/2008 **Assistant-student for a scientific forest inventory** (“Bois de Chênes” reserve)
Institute of Terrestrial Ecosystems of Swiss Federal Institute of Technology, Zürich (ETH)
- 09/2007 – 12/2007 **Research introduction internship**
Supervisor: Dr Liliane Michalik
Center for Integrative Genomics, University of Lausanne
“Cell protection during skin repair: do Nrf2 and PPAR β combine their efforts?”
- 07/2007 – 09/2007 **Summer Research Program in Life Sciences** of the Swiss Federal Institute of Technology, Lausanne (EPFL)
Supervisor: Prof. Winship Herr
Center for Integrative Genomics, University of Lausanne
“Characterization of CeHCF-1 in RNAi in Caenorhabditis elegans”

PUBLICATIONS

A Zuniga, **F Laurent**, J Lopez-Rios, C Klasen, N Matt, R Zeller. *Conserved cis-regulatory regions in a large genomic landscape control SHH and BMP-regulated Gremlin1 expression in mouse limb buds.* BMC Developmental Biology, 2012,12:23.

JD Benazet, E Pignatti, A Nugent, E Unal, **F Laurent**, R Zeller. *Smad4 is required to induce digit ray primordia and to initiate the aggregation and differentiation of chondrogenic progenitors in mouse limb buds.* Development 139, 4250-4260 (2012)

CONFERENCES PARTICIPATION

2014 Weinstein Cardiovascular Development Conference, Madrid, Spain – Poster

2013 26th Mouse Molecular Genetics Meeting, Hinxton, UK – Selected speaker

2011 9th [BC]² Basel Computational Biology Conference, Basel, Switzerland – Poster

2007 Life Science Summer Research Program, EPFL, Lausanne, Switzerland – Poster

TECHNICAL SKILLS

Animal handling Mouse care, husbandry and colony management. Embryo collection, *in vivo* wound healing experiments

Molecular biology DNA and RNA extraction, PCR, RT-qPCR, molecular cloning with plasmids and BACs, chromatin immunoprecipitation, whole-mount *in situ* hybridization, Southern Blot, Western Blot

Cell culture HEK293, mouse embryonic stem cells. Gene targeting by cassette exchange and homologous recombination, immunocytochemistry, karyotyping, transfection, viral transduction, luciferase reporter assays

Histology Tissue preparation and sectioning with microtome and cryostat, immunohistochemistry, section *in situ* hybridization, TUNEL assay, hematoxylin/eosin and alcian blue stainings

Microscopy Light, fluorescent and confocal microscopy, optical projection tomography

PROFESSIONALS AND SOFT SKILLS

- Creativity
- Initiative
- Flexibility/adaptability
- Highly organized
- Work well under pressure
- Problems solving skills
- Team building and leadership
- Project management
- Event planning

ASSOCIATIONS MEMBERSHIP

Department of Biomedicine PhD Club, Basel

2011 – 2014 Co-founder. Organization of scientific retreats, career days and social events for the PhD, MD-PhD and Master students of the Department

Association of Biology students, University of Lausanne

2006 – 2008 Responsible for events and animation for Bachelor and Master students

Scout group « Groupe de la Harpe », Rolle-Aubonne (VD)

1994 – 2008 Organization of weekly outdoors activities, weekends and summer camps for 7-11 kids

TEACHING EXPERIENCE

- 2011-2013 Assistant in Developmental Biology practical for medicine students, University of Basel
- 2014 Supervision of a 1st year PhD student regarding mouse colony management and molecular biology

SWISS MILITARY SERVICE

- Rank First Lieutenant
Function Platoon leader in Medical Logistics
Corps Cp EM hôp 2
- 2009 **School of Logistics Officers 1/10 (Bern)**
Developing personal skills in management and leadership. Learning military techniques and tactics specifically applied to the army medical and logistics corps
- 2009 – 2010 **Practical job as platoon leader, School of Hospital Recruits 41/3 (Moudon, VD)**
Organizing and teaching basic military training for a platoon of medical soldiers
- 2004 **School of Hospital Recruits 41/1 (Moudon, VD)**
Basic military training as a medical soldier with specialization in emergency room

ADDITIONAL TRAININGS AND DIPLOMAS

- 2013 Leadership Level 1 Diploma – Swiss Managers Organization
Group animation and dynamics, adult pedagogy, giving feedback, stress management, oral communication techniques, work techniques, ethics, co-workers motivation
- 2011 Optical Projection Tomography training in MRC Technology, Edinburgh, Scotland
- 2010 Certificate “Managing my time at the group/team level” – Swiss association for the Training of Executives (SVF-ASFC)
- 2009 Military sport instructor certificate
- 2007 Laboratory animal science course – Swiss Veterinary Office of canton of Vaud
Legislation, ethical principles, biology and handling of laboratory animals, anesthesia, blood sampling and microsurgery
- 2004 Diploma of Health Care Assistant – Swiss Red Cross
- 2003 JV base training
Health promotion and addictions prevention in youth associations of canton of Vaud
- 2002 Instructor license in trekking and sports camps – Youth + Sports (J+S), Swiss Federal Office of Sports
- 2002 Rescuer Certificate

AWARDS AND FELLOWSHIPS

- 2009 **Honorary Certificate** – Prof. Nicole Galland, School of Biology Director, University of Lausanne
For active involvement as member of the committee of the association of students
- 2007 **Summer Research Fellowship** – School of Life Sciences, EPFL
For the participation to the Summer Research Program in Life Sciences

LANGUAGES

- | | | | |
|----------------|---------------|---------------|---------------|
| French | Mother tongue | German | Scholar level |
| English | Fluent | | |

